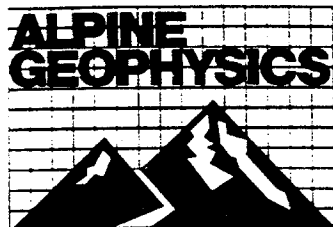


FINAL REPORT



Atmospheric & Hydrologic Sciences

EVALUATION OF THE UAM-IV AND  
CALGRID-IV PHOTOCHEMICAL MODELS WITH  
TWO SANTA BARBARA-VENTURA OZONE EPISODES

ARB Agreement No. A974-212

AG-90/TS14

Prepared for

Dr. Kit Wagner  
California Air Resources Board  
Technical Support Division  
P.O. Box 2815  
Sacramento, CA 95812

Prepared by

T. W. Tesche  
Alpine Geophysics  
Post Office Box 2059  
Crested Butte, CO 81224

and

Dennis E. McNally  
Alpine Geophysics  
16225 W. 74th Dr.  
Golden, CO 80403

1 October, 1992



TABLE OF CONTENTS

LIBRARY  
 CALIFORNIA AIR RESOURCES BOARD  
 P.O. BOX 2815  
 SACRAMENTO, CA 95812

List of Illustrations .....	vi
List of Tables .....	xiv
Abstract .....	A-1
<b>1. INTRODUCTION .....</b>	<b>1-1</b>
1.1 Overview .....	1-1
1.2 Study Objectives .....	1-1
1.3 Report Structure .....	1-2
<b>2. THE 1984 SCCCAMP FIELD STUDY .....</b>	<b>2-1</b>
<b>3. DESCRIPTION OF THE MODELS .....</b>	<b>3-1</b>
3.1 The UAM-IV Model .....	3-1
3.1.1 Processes Treated by the UAM-IV .....	3-1
3.1.2 Theoretical Formulation .....	3-3
3.1.3 Numerical Implementation .....	3-6
3.1.4 Implementation of the CBM-IV Chemistry in the UAM-IV .....	3-8
3.1.5 Operational Features .....	3-9
3.1.6 Computational Requirements .....	3-9
3.1.7 Documentation .....	3-10
3.2 The CALGRID-IV Model .....	3-13
3.2.1 Processes Treated by CALGRID-IV .....	3-13
3.2.2 Theoretical Formulation .....	3-14
3.2.3 Numerical Implementation .....	3-15
3.2.4 Implementation of the CBM-IV Chemistry in CALGRID-IV .....	3-15
3.2.5 Operational Features .....	3-15
3.2.6 Computational Requirements .....	3-15
3.2.7 Documentation .....	3-16
<b>4. PREPARATION OF MODEL INPUTS .....</b>	<b>4-1</b>
4.1 The 1984 SCCCAMP Data Base .....	4-1
4.2 Emissions Estimates .....	4-1
4.3 Scalar Inputs .....	4-2
4.4 Meteorological Inputs .....	4-2
4.4.1 Windfields .....	4-2
4.4.2 Temperature Fields .....	4-2
4.4.3 Mixing Heights .....	4-3

4.4.4	Short Wave Radiation .....	4-3
4.4.5	PGT Stability Class .....	4-3
4.4.6	Surface Station Parameters .....	4-3
4.5	Initial and Boundary Conditions .....	4-3
4.6	Modeling Region Definition .....	4-4
<b>5.</b>	<b>MODEL EVALUATION PROCEDURES .....</b>	<b>5-1</b>
5.1	Base Case Evaluation Procedures .....	5-1
5.1.1	Statistical Measures .....	5-1
5.1.2	Graphical Procedures .....	5-5
5.2	Comparative Evaluation Procedures .....	5-9
<b>6.</b>	<b>BASE CASE SIMULATION RESULTS .....</b>	<b>6-1</b>
6.1	Previous UAM Performance Evaluations with the 1984 SCCAMP Data Base .....	6-1
6.1.1	5-7 September, 1984 Episode .....	6-1
6.1.2	16-17 September, 1984 Episode .....	6-2
6.2	Base Case UAM-IV and CALGRID-IV Evaluations for the 5-7 September, 1984 Episode .....	6-2
6.2.1	Statistical Measures .....	6-2
6.2.2	Graphical Results .....	6-3
6.3	Base Case UAM-IV and CALGRID-IV Evaluations for the 16-17 September, 1984 Episode .....	6-8
6.3.1	Statistical Measures .....	6-8
6.3.2	Graphical Results .....	6-9
<b>7.</b>	<b>SENSITIVITY ANALYSES .....</b>	<b>7-1</b>
7.1	Objectives .....	7-1
7.2	Zero Emissions .....	7-2
7.3	Zero Initial Conditions .....	7-2
7.4	Zero Boundary Conditions .....	7-2
7.5	Zero Surface Deposition .....	7-3
<b>8.</b>	<b>DIAGNOSTIC ANALYSES .....</b>	<b>8-1</b>
8.1	Reactive CALGRID-IV Diagnostic Simulations .....	8-1

8.1.1	Short Time Step .....	8-1
8.1.2	Option C Grid Structure .....	3-2
8.1.3	18 Level Model .....	8-3
9.	SUMMARY AND RECOMMENDATIONS .....	9-1
9.1	Summary .....	9-1
9.1.1	Model Evaluation Results .....	9-1
9.1.2	Sensitivity Analysis Results .....	9-5
9.1.3	Diagnostic Experiments .....	9-6
9.1.4	Ease of Use of the UAM-VI and CALGRID-IV Models .....	9-7
9.1.5	Computational Requirements .....	9-8
9.1.6	Synthesis of Results .....	9-8
9.2	Recommendations .....	9-12
9.2.1	Continue the Evaluation Process of the CALGRID-IV Model .....	9-12
9.2.2	Upgrade the Photochemical Models .....	9-13
9.2.3	Implement Procedures to Reduce Bias in Photochemical Models .....	9-15
9.2.4	Treat the Transport Problem at the Boundaries of the SCCAB Model Domain .....	9-16
	REFERENCES .....	R-1

## LIST OF ILLUSTRATIONS

2-1.	Location of Air Monitoring Stations in the SCCCAB .....	2-3
3-1.	Urban Airshed Model Simulation Program with Input and Output Files .....	3-17
3-2.	CALGRID-IV Model Simulation Program with Input and Output Files .....	3-18
6-1a.	Measures of Peak Ozone Estimation Accuracy for the 5-7 September, 1984 Episode -- 5 September, 1984 .....	6-55
6-1b.	Measures of Peak Ozone Estimation Accuracy for the 5-7 September, 1984 Episode -- 6 September, 1984 .....	6-56
6-1c.	Measures of Peak Ozone Estimation Accuracy for the 5-7 September, 1984 Episode -- 7 September, 1984 .....	6-57
6-1d.	Maximum Estimated and Observed Ozone Concentrations and Station Accuracy Estimates for the 5-7 September, 1984 CALGRID-IV Simulation -- 6 September, 1984 .....	6-58
6-1e.	Maximum Estimated and Observed Ozone Concentrations and Station Accuracy Estimates for the 5-7 September, 1984 UAM-IV Simulation -- 6 September, 1984 .....	6-59
6-1f.	Maximum Estimated and Observed Ozone Concentrations and Station Accuracy Estimates for the 5-7 September, 1984 CALGRID-IV Simulation -- 7 September, 1984 .....	6-60
6-1g.	Maximum Estimated and Observed Ozone Concentrations and Station Accuracy Estimates for the 5-7 September, 1984 UAM-IV Simulation -- 7 September, 1984 .....	6-61
6-2a.	Normalized Bias in Ozone Estimation as a Function of Time Throughout the 5-7 September, 1984 Episode .....	6-62
6-2b.	Normalized Bias in Ozone Estimation as a Function of Observed Concentration Level for the 5-7 September, 1984 Episode -- 6 September, 1984 .....	6-63
6-2c.	Normalized Bias in Ozone Estimation as a Function of Observed Concentration Level for the 5-7 September, 1984 Episode -- 7 September, 1984 .....	6-64
6-3a.	Normalized Gross Error in Ozone Estimation as a	

	Function of Time Throughout the 5-7 September, 1984 Episode .....	6-65
6-3b.	Normalized Gross Error in Ozone Estimation as a Function of Observed Concentration Level for the 5-7 September, 1984 Episode -- 6 September, 1984 .....	6-66
6-3c.	Normalized Gross Error in Ozone Estimation as a Function of Observed Concentration Level for the 5-7 September, 1984 Episode -- 7 September, 1984 .....	6-67
6-4a.	Hourly Ozone Residuals as a Function of Concentration Throughout the 5-7 September, 1984 Episode -- 5 September, 1984 .....	6-68
6-4b.	Hourly Ozone Residuals as a Function of Concentration Throughout the 5-7 September, 1984 Episode -- 6 September, 1984 .....	6-70
6-4c.	Hourly Ozone Residuals as a Function of Concentration Throughout the 5-7 September, 1984 Episode -- 7 September, 1984 .....	6-71
6-5a.	Scatterplot of Hourly Ozone Concentration Residuals for the 5-7 September, 1984 Episode -- 5 September, 1984 .....	6-72
6-5b.	Scatterplot of Hourly Ozone Concentration Residuals for the 5-7 September, 1984 Episode -- 6 September, 1984 .....	6-73
6-5c.	Scatterplot of Hourly Ozone Concentration Residuals for the 5-7 September, 1984 Episode -- 7 September, 1984 .....	6-74
6-6a.	Scatterplot of Daily Maximum Ozone Concentration Residuals for the 5-7 September, 1984 Episode -- 5 September, 1984 .....	6-75
6-6b.	Scatterplot of Daily Maximum Ozone Concentration Residuals for the 5-7 September, 1984 Episode -- 6 September, 1984 .....	6-76
6-6c.	Scatterplot of Daily Maximum Ozone Concentration Residuals for the 5-7 September, 1984 Episode -- 7 September, 1984 .....	6-77
6-7.	Standard Deviation of Ozone Estimates and Observations as a Function of Time Throughout the 5-7 September, 1984 Episode .....	6-78

6-8.	Mean Value of Ozone Estimates and Observations as a Function of Time Throughout the 5-7 September, 1984 Episode .....	6-79
6-9.	Time Series of Hourly Estimated and Observed Ozone Concentrations for the 5-7 September, 1984 Episode .....	6-80
6-9.	Time Series of Hourly Estimated and Observed NO Concentrations for the 5-7 September, 1984 Episode .....	6-87
6-9.	Time Series of Hourly Estimated and Observed NO <sub>2</sub> Concentrations for the 5-7 September, 1984 Episode .....	6-93
6-10a.	Ground Level Ozone Isopleths of Hourly Ozone Concentrations for the 5-7 September, 1984 Episode -- 5 September, 1200 PST .....	6-98
6-10b.	Ground Level Ozone Isopleths of Hourly Ozone Concentrations for the 5-7 September, 1984 Episode -- 5 September, 1400 PST .....	6-99
6-10c.	Ground Level Ozone Isopleths of Hourly Ozone Concentrations for the 5-7 September, 1984 Episode -- 5 September, 1600 PST .....	6-100
6-10d.	Ground Level Ozone Isopleths of Hourly Ozone Concentrations for the 5-7 September, 1984 Episode -- 5 September, 1800 PST .....	6-101
6-10e.	Ground Level Ozone Isopleths of Hourly Ozone Concentrations for the 5-7 September, 1984 Episode -- 6 September, 1200 PST .....	6-102
6-10f.	Ground Level Ozone Isopleths of Hourly Ozone Concentrations for the 5-7 September, 1984 Episode -- 6 September, 1400 PST .....	6-103
6-10f-s1.	UAM-IV Vertical Ozone Isopleths Along East-West Transect for the 5-7 September, 1984 Episode -- 6 September, 1400 PST .....	6-104
6-10f-s2.	CALGRID-IV Vertical Ozone Isopleths Along East-West Transect for the 5-7 September, 1984 Episode -- 6 September, 1400 PST .....	6-105
6-10f-s3.	UAM-IV Vertical Ozone Isopleths Along North-South Transect for the 5-7 September, 1984 Episode --	

	6 September, 1400 PST .....	6-106
6-10f-s4.	CALGRID-IV Vertical Ozone Isopleths Along North-South Transect for the 5-7 September, 1984 Episode -- 6 September, 1400 PST .....	6-107
6-10g.	Ground Level Ozone Isopleths of Hourly Ozone Concentrations for the 5-7 September, 1984 Episode -- 6 September, 1600 PST .....	6-108
6-10h.	Ground Level Ozone Isopleths of Hourly Ozone Concentrations for the 5-7 September, 1984 Episode -- 6 September, 1800 PST .....	6-109
6-10i.	Ground Level Ozone Isopleths of Hourly Ozone Concentrations for the 5-7 September, 1984 Episode -- 7 September, 1200 PST .....	6-110
6-10j.	Ground Level Ozone Isopleths of Hourly Ozone Concentrations for the 5-7 September, 1984 Episode -- 7 September, 1400 PST .....	6-111
6-10j-s1.	UAM-IV Vertical Ozone Isopleths Along East-West Transect for the 5-7 September, 1984 Episode -- 7 September, 1400 PST .....	6-112
6-10j-s2.	CALGRID-IV Vertical Ozone Isopleths Along East-West Transect for the 5-7 September, 1984 Episode -- 7 September, 1400 PST .....	6-113
6-10j-s3.	UAM-IV Vertical Ozone Isopleths Along North-South Transect for the 5-7 September, 1984 Episode -- 7 September, 1400 PST .....	6-114
6-10j-s4.	CALGRID-IV Vertical Ozone Isopleths Along North-South Transect for the 5-7 September, 1984 Episode -- 7 September, 1400 PST .....	6-115
6-10k.	Ground Level Ozone Isopleths of Hourly Ozone Concentrations for the 5-7 September, 1984 Episode -- 7 September, 1600 PST .....	6-116
6-10l.	Ground Level Ozone Isopleths of Hourly Ozone Concentrations for the 5-7 September, 1984 Episode -- 7 September, 1800 PST .....	6-117
6-11a.	Maximum Daily Ozone Residual Plot (UAM-IV Minus	

	CALGRID-IV) for the 5-7 September, 1984 Episode -- 5 September, 1984 .....	6-118
6-11b.	Maximum Daily Ozone Residual Plot (UAM-IV Minus CALGRID-IV) for the 5-7 September, 1984 Episode -- 6 September, 1984 .....	6-119
6-11c.	Maximum Daily Ozone Residual Plot (UAM-IV Minus CALGRID-IV) for the 5-7 September, 1984 Episode -- 7 September, 1984 .....	6-120
6-12a.	Measures of Peak Ozone Estimation Accuracy for the 16-17 September, 1984 Episode -- 16 September, 1984 .....	6-121
6-12b.	Measures of Peak Ozone Estimation Accuracy for the 16-17 September, 1984 Episode -- 17 September, 1984 .....	6-122
6-12c.	Maximum Estimated and Observed Ozone Concentrations and Station Accuracy Estimates for the 16-17 September 1984 CALGRID-IV Simulation -- 16 September, 1984 .....	6-123
6-12d.	Maximum Estimated and Observed Ozone Concentrations and Station Accuracy Estimates for the 16-17 September 1984 UAM-IV Simulation -- 16 September, 1984 .....	6-124
6-12e.	Maximum Estimated and Observed Ozone Concentrations and Station Accuracy Estimates for the 16-17 September 1984 CALGRID-IV Simulation -- 17 September, 1984 .....	6-125
6-12f.	Maximum Estimated and Observed Ozone Concentrations and Station Accuracy Estimates for the 16-17 September 1984 UAM-IV Simulation -- 17 September, 1984 .....	6-126
6-13a.	Normalized Bias in Ozone Estimation as a Function of Time Throughout the 16-17 September, 1984 Episode .....	6-127
6-13b.	Normalized Bias in Ozone Estimation as a Function of Observed Concentration Level for the 16-17 September, 1984 Episode -- 16 September, 1984 .....	6-128
6-13c.	Normalized Bias in Ozone Estimation as a Function of Observed Concentration Level for the 16-17 September, 1984 Episode -- 17 September, 1984 .....	6-129
6-14a.	Normalized Gross Error in Ozone Estimation as a Function of Time Throughout the 16-17 September, 1984 Episode .....	6-130

6-14b.	Normalized Gross Error in Ozone Estimation as a Function of Observed Concentration Level for the 16-17 September, 1984 Episode -- 16 September, 1984 .....	6-131
6-14c.	Normalized Gross Error in Ozone Estimation as a Function of Observed Concentration Level for the 16-17 September, 1984 Episode -- 17 September, 1984 .....	6-132
6-15a.	Hourly Ozone Residuals as a Function of Concentration Throughout the 16-17 September, 1984 Episode -- 16 September, 1984 .....	6-133
6-15b.	Hourly Ozone Residuals as a Function of Concentration Throughout the 16-17 September, 1984 Episode -- 17 September, 1984 .....	6-134
6-16a.	Scatterplot of Hourly Ozone Concentration Residuals for the 16-17 September, 1984 Episode -- 16 September, 1984 .....	6-135
6-16b.	Scatterplot of Hourly Ozone Concentration Residuals for the 16-17 September, 1984 Episode -- 17 September, 1984 .....	6-136
6-17a.	Scatterplot of Daily Maximum Ozone Concentration Residuals for the 16-17 September, 1984 Episode -- 16 September, 1984 .....	6-137
6-17b.	Scatterplot of Daily Maximum Ozone Concentration Residuals for the 16-17 September, 1984 Episode -- 17 September, 1984 .....	6-138
6-18.	Standard Deviation of Ozone Estimates and Observations as a Function of Time Throughout the 16-17 September, 1984 Episode .....	6-139
6-19.	Mean Value of Ozone Estimates and Observations as a Function of Time Throughout the 16-17 September, 1984 Episode .....	6-140
6-20.	Time Series of Hourly Estimated and Observed Ozone Concentrations for the 16-17 September, 1984 Episode .....	6-141
6-20.	Time Series of Hourly Estimated and Observed NO Concentrations for the 16-17 September, 1984 Episode .....	6-149
6-20.	Time Series of Hourly Estimated and Observed NO <sub>2</sub>	

	Concentrations for the 16-17 September, 1984 Episode . . . . .	6-155
6-21a.	Ground Level Ozone Isopleths of Hourly Ozone Concentrations for the 16-17 September, 1984 Episode -- 16 September, 1200 PST . . . . .	6-160
6-21b.	Ground Level Ozone Isopleths of Hourly Ozone Concentrations for the 16-17 September, 1984 Episode -- 16 September, 1400 PST . . . . .	6-161
6-21c.	Ground Level Ozone Isopleths of Hourly Ozone Concentrations for the 16-17 September, 1984 Episode -- 16 September, 1600 PST . . . . .	6-162
6-21d.	Ground Level Ozone Isopleths of Hourly Ozone Concentrations for the 16-17 September, 1984 Episode -- 16 September, 1800 PST . . . . .	6-163
6-21e.	Ground Level Ozone Isopleths of Hourly Ozone Concentrations for the 16-17 September, 1984 Episode -- 17 September, 1200 PST . . . . .	6-164
6-21f.	Ground Level Ozone Isopleths of Hourly Ozone Concentrations for the 16-17 September, 1984 Episode -- 17 September, 1400 PST . . . . .	6-165
6-21f-s1.	UAM-IV Vertical Ozone Isopleths Along East-West Transect for the 16-17 September, 1984 Episode -- 17 September, 1400 PST . . . . .	6-166
6-21f-s2.	CALGRID-IV Vertical Ozone Isopleths Along East-West Transect for the 16-17 September, 1984 Episode -- 17 September, 1400 PST . . . . .	6-167
6-21f-s3.	UAM-IV Vertical Ozone Isopleths Along North-South Transect for the 16-17 September, 1984 Episode -- 17 September, 1400 PST . . . . .	6-168
6-21f-s4.	CALGRID-IV Vertical Ozone Isopleths Along North-South Transect for the 16-17 September, 1984 Episode -- 17 September, 1400 PST . . . . .	6-169
6-21g.	Ground Level Ozone Isopleths of Hourly Ozone Concentrations for the 16-17 September, 1984 Episode -- 17 September, 1600 PST . . . . .	6-170
6-21h.	Ground Level Ozone Isopleths of Hourly Ozone	

	Concentrations for the 16-17 September, 1984 Episode -- 17 September, 1800 PST .....	6-171
6-22a.	Maximum Daily Ozone Residual Plot (UAM-IV Minus CALGRID-IV) for the 16-17 September, 1984 Episode -- 16 September, 1984 .....	6-172
6-22b.	Maximum Daily Ozone Residual Plot (UAM-IV Minus CALGRID-IV) for the 16-17 September, 1984 Episode -- 17 September, 1984 .....	6-173
8-1.	Ozone Time Series At Santa Ynez Comparing the Effects of Option B (Base Case) and Option C Grid Specifications for the 5-7 September and 16-17 September, 1984 Episodes .....	8-15
8-2.	Ozone Time Series Comparing the Effects of Option B (Base Case) and Option C (18 Level Grid) Specifications for the 5-7 September, 1984 Episode .....	8-17

## LIST OF TABLES

2-1	Peak Ozone Concentrations During the Two 1984 SCCCAMP Episodes .....	2-4
4-1	Hourly NO <sub>2</sub> Photolysis Rates for the UAM-IV in the SCCAB .....	4-5
4-2	Hourly Short-Wave Radiation for the CALGRID-IV Modeling in the SCCAB .....	4-6
4-3	Respeciation of Initial and Boundary Concentrations of Hydrocarbons for Converting CBM-II Species to CBM-IV Species .....	4-7
6-1	Peak Ozone Concentrations for Three Urban Airshed Model Simulations of the 5-7 September, 1984 Episode .....	6-14
6-2	UAM Ozone Model Evaluation Statistics for three Simulations of the 5-7 September, 1984 Episode .....	6-17
6-3	Peak Ozone Concentrations for Two UAM Simulations of the 16-17 September, 1984 Episode .....	6-20
6-4	UAM Ozone Model Evaluation Statistics for Two Simulations of the 16-17 September, 1984 Episode .....	6-22
6-5	Peak NO Concentrations for the UAM-IV and CALGRID-IV Models for the 5-7 September, 1984 Episode .....	6-23
6-6	Peak NO <sub>2</sub> Concentrations for the UAM-IV and CALGRID-IV Models for the 5-7 September, 1984 Episode .....	6-26
6-7	Peak Ozone Concentrations for the UAM-IV and CALGRID-IV Models for the 5-7 September, 1984 Episode .....	6-29
6-8	UAM-IV and CALGRID-IV NO Model Evaluation Statistics for the 5-7 September, 1984 Episode .....	6-32
6-9	UAM-IV and CALGRID-IV NO <sub>2</sub> Model Evaluation Statistics for the 5-7 September, 1984 Episode .....	6-35
6-10	UAM-IV and CALGRID-IV Ozone Model Evaluation Statistics for the 5-7 September, 1984 Episode .....	6-38
6-11	Peak NO Concentrations for the UAM-IV and CALGRID-IV Models	

	for the 16-17 September, 1984 Episode .....	6-41
6-12	Peak NO <sub>2</sub> Concentrations for the UAM-IV and CALGRID-IV Models for the 16-17 September, 1984 Episode .....	6-43
6-13	Peak Ozone Concentrations for the UAM-IV and CALGRID-IV Models for the 16-17 September, 1984 Episode .....	6-47
6-14	UAM-IV and CALGRID-IV NO Model Evaluation Statistics for the 16-17 September, 1984 Episode .....	6-49
6-15	UAM-IV and CALGRID-IV NO <sub>2</sub> Model Evaluation Statistics for the 16-17 September, 1984 Episode .....	6-51
6-16	UAM-IV and CALGRID-IV Ozone Model Evaluation Statistics for the 16-17 September, 1984 Episode .....	6-53
7-1	Peak Ozone Concentrations for Four UAM-IV Sensitivity Simulations of the 5-7 September, 1984 Episode .....	7-4
7-2	Peak Ozone Concentrations for Four CALGRID-IV Sensitivity Simulations of the 5-7 September, 1984 Episode .....	7-7
7-3	Peak Ozone Concentrations for Four UAM-IV Sensitivity Simulations of the 16-17 September, 1984 Episode .....	7-10
7-4	Peak Ozone Concentrations for Four CALGRID-IV Sensitivity Simulations of the 16-17 September, 1984 Episode .....	7-12
7-5	UAM-IV Ozone Model Sensitivity Results for the 5-7 September, 1984 Episode .....	7-14
7-6	CALGRID-IV Ozone Model Sensitivity Results for Four Simulations of the 5-7 September, 1984 Episode .....	7-17
7-7	UAM-IV Ozone Model Sensitivity Results for Four Simulations of the 16-17 September, 1984 Episode .....	7-20
7-8	CALGRID-IV Ozone Model Sensitivity Results for Four Simulations of the 16-17 September, 1984 Episode .....	7-22
8-1	Peak Ozone Concentrations for Three CALGRID-IV Diagnostic Simulations for the 5-7 September, 1984 Episode .....	8-5
8-2	CALGRID-IV Ozone Statistics for Three Diagnostic Simulations of the 5-7 September, 1984 Episode .....	8-8

8-3	Peak Ozone Concentrations for Three CALGRID-IV Diagnostic Simulations for the 16-17 September, 1984 Episode . . . . .	8-11
8-4	CALGRID-IV Ozone Statistics for Three Diagnostic Simulations of the 16-17 September, 1984 Episode . . . . .	8-13
9-1	CPU Time Requirements for the CALGRID-IV and UAM-IV Models in the SCCAB on an IBM RS/6000 Model 530 Workstation . . . . .	9-8

## ABSTRACT

### Overview

The goal of this study was to establish the usefulness and reliability of the CALGRID photochemical model as an air quality planning tool in California. We approached this task through a step-wise model performance evaluation using two well-documented, multiple-day ozone modeling data bases developed in the South Central Coast Air Basin (Tesche and McNally, 1991). Specific objectives were to: (1) carry out a detailed evaluation of CALGRID in the South Central Coast Air Basin (SCCAB), (2) compare the level of performance of CALGRID with that of the Urban Airshed Model (UAM-IV), (3) evaluate the adequacy of the model CALGRID model and users documentation, and (4) make recommendations pertaining to additional model refinement and evaluation needs.

Originally, the evaluation was to be carried out using the version of CALGRID developed by Sigma Research Corporation (Yamartino et al., 1989; Scire et al., 1989). This version incorporates the SAPRC chemical mechanism (Carter, 1988, 1990.) However, the ARB Project Officer later directed that a different version of CALGRID was to be evaluated instead. Specifically, we were supplied with a version of CALGRID with Carbon Bond IV (CBM-IV) chemistry. This code, revised by researchers at Carnegie Mellon University (CMU), is undergoing testing with the 26-28 August, 1987 Southern California Air Quality Study (SCAQS) data base. We refer to this version as CALGRID-IV.

The simulations of both models were performed on the an IBM RS/6000 model 530 workstation with 64 Mbytes of memory. Run times for the UAM-IV and CALGRID-IV models were 4 hours and 6 hours, respectively for the 5-7 September episode and 4 hours for the 16-17 September episode.

### Findings

For both episodes, the UAM-IV and CALGRID-IV significantly underestimated the maximum measured hourly NO concentrations. Both models also underestimated NO<sub>2</sub> concentrations, although the UAM-IV peak estimates of NO<sub>2</sub> were nearly 50% larger than those for CALGRID-IV. On the 7th, above approximately 9 pphm, both models underestimate ozone concentrations. This negative bias is nearly double for CALGRID-IV compared with the UAM-IV. The UAM-IV's ozone gross errors are approximately 50% to 60% less than CALGRID-IV's on the 7th, particularly during the afternoon high-ozone period. The systematic bias in CALGRID-IV and UAM-IV hourly ozone estimates on the 17th are -16% and -14%, respectively. Gross errors for both models are approximately the same (27% and 29%, respectively). On the 17th, both models produce nearly identical negative bias-concentration plots for ozone levels above

4 pphm. From 8 to 13 pphm, the bias is nearly constant for both models at approximately -30%.

Four sensitivity runs were carried out with the two models for both episodes. These runs involved reducing to zero the: (a) emissions inventory, (b) initial conditions, (c) boundary conditions, and (e) surface dry deposition. The sensitivity simulation results indicate that the two models respond similarly to gross changes in major inputs. In particular, boundary conditions and emissions play the dominant roles in station peak and hourly ozone concentrations, with boundary conditions being by far the most influential. Surface dry deposition has little influence on peak ozone levels but for hourly values, the UAM-IV appears to be somewhat more sensitive than CALGRID-IV. Emissions appear to produce an ozone contribution somewhat smaller than that of naturally occurring background levels.

Three diagnostic model simulations were made with the CALGRID-IV model for the two September episodes. These runs involved: (a) reducing the integration time step from 20 minutes to 6 minutes, (b) use of a temporally-invariant vertical grid structure, and (c) use of an 18-level vertical grid structure. Reducing the integration time step has little effect on the base case ozone results for the episodes studied. Fixing the four grid levels at 20 m, 250 m, 500 m, and 1000 m reduced the average of the station peak ozone concentrations on the 6th, 7th, and 17th from the base case values by 0.5 pphm, 0.4 pphm, and 0.4 pphm, respectively. The fixed layer model produces somewhat lower gross errors compared with the base case, yet the magnitudes of the biases tend to increase very slightly. Running CALGRID-IV with 18 vertical layers systematically produces lower average peak ozone levels for both episodes. The overall bias and error statistics are degraded somewhat from the base cases.

The user interface to the UAM-IV and CALGRID-IV models are very different. The UAM-IV model provides an extensive preprocessor network to assist in preparing inputs but it is fairly inflexible. CALGRID-IV does not include preprocessors to help prepare model inputs but is more flexible in which files are necessary to run the model. CALGRID-IV was designed assuming that the CALMET model would be used to prepare meteorological inputs. If other meteorological models are used, a fairly complicated processor must be written.

### Synthesis

Based on the collection of statistical measures and graphical tools applied to the base case model results for both episodes, the UAM-IV has performed somewhat better than CALGRID-IV in simulating hourly NO, NO<sub>2</sub>, and ozone concentrations for the two September episodes. These findings do not confirm superiority of the UAM-IV over CALGRID-IV as an ozone assessment tool, however. First, the September episode modeling files were tailored to the specific requirements and limitations of the UAM system. These data bases are therefore not optimal for fully testing CALGRID-IV's

capabilities. Second, the time and resource constraints of this study only allowed for an "operational" evaluation of the two models. It has not been possible to explore the modeling results more fully to reveal the causes for the various differences seen in the performance results. Diagnostic analyses of the model differences are needed to clarify whether the differences stem from model flaws in UAM-IV, CALGRID-IV or both, or are instead the result of data base limitations. Finally, a comparative evaluation of the two models using two episodes in one air basin is insufficient to draw firm conclusions regarding which is the better overall model. Both models should be exercised with episodes drawn from other regions possessing higher quality data bases (e.g., SCAQS, SARMAP, LMOS).

### Applications Issues

Two important model applications issues are raised by the results of this evaluation. The first issue arises because both models exhibit negative bias in estimating ozone concentrations. The second issue arises by virtue of our finding that both models are very sensitive to (uncertain) boundary conditions in the SCCAB.

Bias in Estimation Bias refers to the inaccurate estimation of pollutant concentrations. A minor degree of bias is tolerable; a larger degree testifies to significant flaws or weaknesses in the model or input data. It is essential that an effort be made to reduce substantive bias to insignificance using appropriate and justifiable procedures. Of principal concern is the current practice nationwide of accepting a model for application despite the fact that it is found to be deficient (e.g., biased). Should a biased model be used to evaluate multi-billion dollar ozone control plans? Questions that California regulatory agencies involved in ozone attainment planning should address include:

- > How should current ozone modeling practice be modified to minimize both the existence of bias and the risk of inaccurate estimation that attends its presence? Also, under what circumstances should a model be deemed acceptable?
- > What procedures should be adopted to compensate for the presence of residual bias?

Addressing the Issue of Boundary Condition Sensitivity Boundary conditions to the UAM-IV and CALGRID-IV are critical inputs. They represent a continuous emissions source at the upwind boundary, injecting pollutants at a rate that is well above 50-75% of the emissions rate within the model domain. Boundary conditions are important in the SCCAB because: (a) the intensity of emissions (number of sources, emissions rates) upwind is high, (b) pollutants from the study area recirculate, leaving the region to return later, (c) pollutants are either held or transported aloft into the area of interest and later mixed down to the surface, (d) vertical motions are likely to be

significant and the top of the modeling region is limited in height. Compounding the problem is that when anthropogenic emissions are reduced significantly in future years, the influence will be even greater. Thus, efforts should be undertaken to improve the reliability of the boundary conditions to the UAM-IV and CALGRID-IV models in the SCCAB.

### Recommendations

Four general recommendations are derived from this study.

1. Given the generally similar model evaluation results found in this study, the evaluation of the CALGRID-IV model should continue. Three specific investigations are recommended:
  - > Diagnostic efforts should be undertaken to provide explanations for the different surface and aloft ozone patterns generated by UAM-IV and CALGRID-IV for both episodes. This analysis, if carried out, may reveal potential flaws in either the UAM-IV, in CALGRID-IV, in both models, or perhaps inherent weaknesses in the September, 1984 data bases.
  - > The comparative evaluation of the UAM-IV and CALGRID-IV models should be extended to other urban areas. Alpine Geophysics is performing such an effort with the 23-25 June, 1987 and 26-28 August, 1987 SCAQS data bases in the South Coast Air Basin. Similar exercises should be considered for the SARMAP and LMOS episodes.
  - > Model inputs to future CALGRID-IV performance evaluations should be constructed directly, rather than "mapping" UAM-IV input data bases onto the CALGRID-IV structure. This will provide a more reliable test of those formulation and implementation features of CALGRID-IV that are closer to the current state-of-science than the UAM-IV's.
2. The UAM-IV model should be upgraded if it is to be relied upon for evaluating ozone attainment strategies. If the UAM-IV is to be used in California for designing multi-billion dollar emissions control programs, a number of upgrades should be implemented to bring the model closer to the current state-of-science. Needed improvements to the UAM-IV fall in the categories of model formulations, emissions estimation, meteorology, chemistry, and numerical methods.
3. Procedures should be developed to reduce bias in the UAM-IV and CALGRID-IV models. Because both models exhibit a tendency to underestimate ozone concentration levels. Efforts to remove bias in the UAM-IV and CALGRID-IV model results for the September episodes should be mounted along several lines,

particularly improving model formulation and, perhaps more importantly, improving model inputs.

4. Procedures should be developed to treat the significant transport uncertainties on the boundaries of the SCCAB model domain. In particular, consideration should be given to (a) expanding the modeling regions, where feasible, sufficiently far upwind to include major source areas and thus diminish the magnitude and importance of upwind determinations, (b) adopting the use of a nested-grid regional scale model applied to a much larger, more encompassing geographical area to generate boundary conditions through simulation, and (c) supporting data collection programs to provide detailed information on the inflow boundaries of the model domain.

## 1.0 INTRODUCTION

### 1.1 Overview

The California Air Resources Board (ARB) plays a central role in the development, evaluation, and application of state-of-the-art photochemical grid models. The need for this leadership has intensified in recent years with the passage of the California Clean Air Act (Health and Safety Code 39609). The CCAA requires, in part, that the ARB periodically report to the state legislature on the feasibility of using air quality models to aid decision-makers in dealing with ozone, NO<sub>2</sub>, CO and SO<sub>2</sub> attainment problems in the state. Components of this feasibility assessment include critical reviews of existing photochemical models, aerometric and emissions data bases, and results of model performance evaluations.

Urban- and mesoscale photochemical models represent an important tool for state and local decision-makers facing difficult air quality planning issues. Among these issues are (1) the role of interbasin transport of ozone and its precursors on local pollution levels, (2) the potential benefits associated with the use of reformulated gasolines or alternative fuels, (3) the tradeoffs between ROG and NO<sub>x</sub> control, and (4) the usefulness of alternative measures of air quality improvement such as population dosage and exposure. In response to these planning requirements, the ARB has sponsored a vigorous program of mathematical model development, emissions inventory development, and aerometric data collection all aimed at improving the reliability of models in the decision making process. As one component of this overall program of model development and evaluation, the Technical Support Division contracted with Alpine Geophysics to carry out a detailed performance evaluation of the CALGRID model, developed by Sigma Research Corporation (Yamartino et al., 1992). This report describes the results of our evaluation.

### 1.2 Study Objectives

The goal of this study was to establish the usefulness and reliability of the CALGRID photochemical model as an air quality planning tool in California. We approached this task through a step-wise model performance evaluation using two well-documented, multiple-day ozone modeling data bases developed in the South Central Coast Air Basin (Tesche and McNally, 1991). Specific objectives were to: (1) carry out a detailed evaluation of CALGRID in the South Central Coast Air Basin (SCCAB), (2) compare the level of performance of CALGRID with that of the Urban Airshed Model (UAM-IV), (3) evaluate the adequacy of the model CALGRID model and users documentation, and (4) make recommendations pertaining to additional model refinement and evaluation needs.

Originally, the evaluation was to be carried out using the version of CALGRID developed by Sigma Research Corporation (Yamartino et al., 1989; Scire et al., 1989).

This version incorporates the SAPRC chemical mechanism (Carter, 1988, 1990.) However, the ARB Project Officer later directed that a different version of CALGRID was to be evaluated instead. Specifically, we were supplied with a version of CALGRID with Carbon Bond IV (CMB-IV) chemistry. This code, revised by researchers at Carnegie Mellon University (CMU), is undergoing testing with the 26-28 August, 1987 Southern California Air Quality Study (SCAQS) data base. Hereafter, we refer to this version as CALGRID-IV.

### 1.3 Structure of Report

Chapter 2 of this report summarizes the 1984 SCCCAMP Exploratory Field Study that collected the aerometric data sets used in this study. In chapter 3 we discuss the theoretical formulations and operational features of the UAM-IV and CALGRID-IV models. Preparation of model inputs for the two September base cases is presented in chapter 4. In Chapter 5 we describe the statistical measures and graphical procedures used to compare the two models and to analyze the sensitivity and diagnostic simulations. The principal results of the comparative evaluation of the UAM-IV and CALGRID-IV models are given in chapter 6. Chapters 7 and 8 present the results of several sensitivity and diagnostic experiments to extend the results of the comparative evaluation and to identify areas warranting further investigation with CALGRID-IV. Chapter 10 summarizes the key evaluation results and our observations on the adequacy of the CALGRID-IV coding and documentation. We also summarize the computational requirements of both models on scientific workstations. Our recommendations are also contained in Chapter 9.

Appendix A, prepared by Systems Applications, Int. contains the results of an inert tracer analysis of CALGRID-IV using the inputs derived in this study for the 5-7 September and 16-17 September, 1984 SCCCAMP episodes.

## 2.0 THE 1984 SCCAMP FIELD STUDY

Five different multi-day modeling episodes have been developed in recent years in the South Central Coast Air Basin using routine and intensive data collected from the 1984 and 1985 SCCAMP field programs. Based on the air quality and meteorological characteristics of the 5-7 September and 16-17 September, 1984 episodes and the results of UAM model performance evaluations for these periods, these episodes have been the principal focus for emissions control strategy development and modeling research in the Ventura-Santa Barbara region. This section summarizes the main features of the 1984 field study.

The 1984 SCCAMP Exploratory Field Study consisted of continuous aerometric monitoring and intensive measurements specifically designed to test sampling techniques and to provide the basis for more refined experiments the following year (Dabberdt, 1984). These experiments included enhanced measurements of surface and upper level winds,  $\text{NO}_x$  and ROG speciation, aircraft soundings, and chemical species sampling. Following the field work, SCCAMP sponsored an analysis of the 1984 data (Tesche et al., 1985) to strengthen the design of the 1985 measurement program and to assess the suitability of the 1984 data base for photochemical modeling. The first activity aided in formulating the 1985 SCCAMP monitoring program study design and experimental protocol (Reynolds et al., 1985; Dabberdt and Viezee, 1987) while the second activity led to a conceptual model of the meteorology and air quality during the sampling period.

The September 1984 data indicated that surface winds in the SCCAB follow a diurnal pattern composed of two major regimes: an afternoon-evening sea-breeze flow; and a nighttime-morning drainage flow. The sea-breeze influence is strongest over the Oxnard plain, which is directly exposed to the westerly wind flow across the Santa Barbara channel. Some of this westerly flow is deflected south of the Santa Monica Mountains toward Los Angeles. Although onshore winds influence the flow regimes in mountain areas, an upper-level southeasterly flow was dominant during this study period above 750 meters msl. Drainage winds were an order of magnitude weaker than their onshore counterparts, and were most pronounced in channeling situations, such as in the Santa Clara River valley. Lack of data from the Santa Barbara channel area limited characterization of the nocturnal counter-clockwise eddy over the northern half of the channel. Similarly, data are needed in the vicinity of Gaviota Pass to reveal more clearly the formation of eddies by winds rounding Pt. Conception. Still, there is evidence in the 1984 data of a nocturnal counter-clockwise eddy circulation over the northern portion of the Santa Monica Bay.

Upper level air flow at six stations (except Platform C) during September, 1984 is dominated by easterly to southeasterly winds above 750-1000 meters. Below 500-750 meters, winds at all stations are affected by diurnal offshore-onshore flows. Strong onshore flows appear to push the lower level of the southeasterlies upward, creating a sharply-defined shear zone within the boundary layer.

The timing of sea-breeze episodes varies daily but, typically, the sea breeze peaks over the Oxnard plain at about 1500 PST. This timing does not appear to be a function of distance from the coast. During the 5-7 September episode, winds were generally light and there was considerable air mass stagnation over the Santa Barbara channel area and coastal regions. The 16-17 September ozone episode was preceded by two days of strong offshore (east-to-southeasterly) winds aloft; sea-breeze episodes were weak. A subsidence inversion kept vertical mixing to a minimum. On the afternoon of the 17th, the sea breeze strengthened slightly and the inversion weakened, allowing previously stagnant air to move inland and a limited amount of mixing with the upper air to occur.

Hourly-averaged ozone measurements were performed during September 1984 at sixteen monitoring stations (See Figure 2-1). For the two episodes modeled here, the six highest stations and their respective ozone maxima are listed in Table 2-1. Both episodes exhibit widespread ozone levels above the federal one-hour standard (12 pphm). The 5-7 September episode not only has the higher ozone maximum (18 pphm at Casitas on the 7th) but the overall ozone concentrations for this period are greater than for 16-17 September. Both episodes coincide with peaks in the morning 850 mb temperature, a strong indicator of high ozone formation potential in southern California. During the 5-7 September period, the region of maximum afternoon ozone was shifted westward from the eastern basin on the 6th (near Simi) to a mid-basin location (Casitas) on the 7th. High ozone levels are reported in Santa Barbara county on this day. A similar westerly shift does not appear on the 16-17th of September.

Although adequate performance results were achieved with the UAM-II using the 5-7 September and 16-17 September, 1984 data bases (Tesche and McNally, 1991), there are some important data limitations that need to be considered for the present comparative evaluation of UAM-IV and CALGRID-IV. To begin, there are very little upper air data for use in evaluating the performance of elevated wind patterns or mixing height estimates or for verifying the concentrations of ozone and precursor species aloft. No speciated hydrocarbon sampling was performed during the early part of SCCCAMP-84, but some speciated measurements, as well as detailed aircraft measurements, are available for the 16-17 September period. Reactive hydrocarbon measurements were made at six onshore monitoring stations in Santa Barbara County, but none are available in Ventura County. Although  $\text{NO}_x$  concentrations were measured at 11 monitoring stations, the levels were typically quite low. Thus, this data base has important limitations with respect to its ability to support multi-species comparisons, and mechanistic evaluations of the wind and mixing height estimates.

In summary, the 1984 SCCCAMP data base, though not ideal, is nevertheless useful in supporting a comparative evaluation of UAM-IV and CALGRID-IV models. In the following chapter the two photochemical models are reviewed.

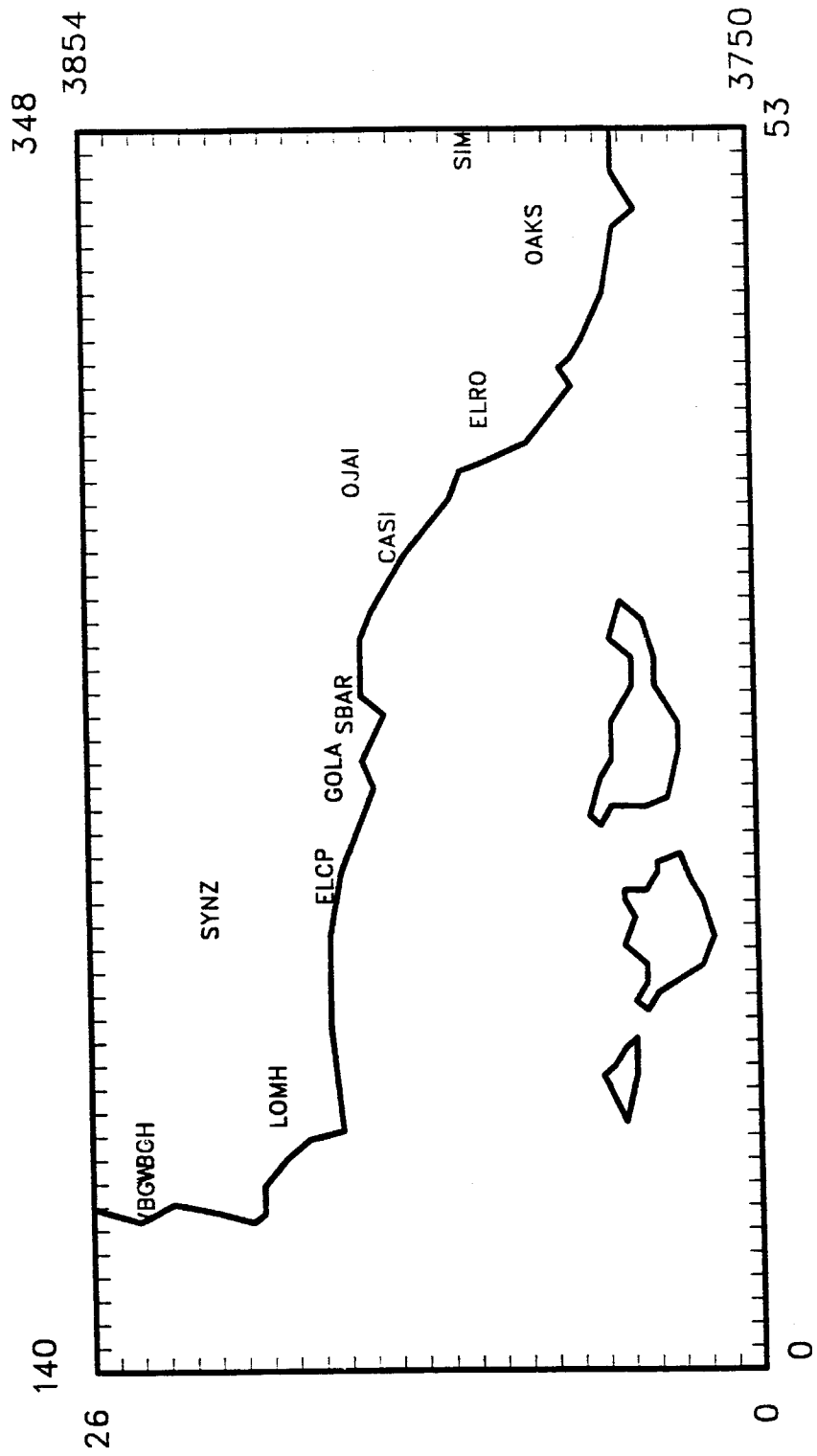


Figure 2-1. Location of Air Monitoring Stations in the South Central Coast Air Basin.

Table 2-1. Peak Ozone Concentrations (pphm) During the Two 1984 SCCAMP Episodes.

5 September, 1984		6 September, 1984		7 September, 1984		16 September, 1984		17 September, 1984	
Max	Station	Max	Station	Max	Station	Max	Station	Max	Station
10	Casitas	17	Simi	18	Casitas	11	Simi	14	Casitas
9	Simi	16	Piru	15	Goleta	9	Oaks	13	Simi
8	Gaviota	16	Oaks	15	Santa Barb	8	Ojai	12	Oaks
7	Oaks	13	Ojai	13	Simi	8	Casitas	12	Santa Barb
7	Ojai	13	Casitas	13	Ojai	7	Ventura	12	Ojai
		10	El Capitan	11	El Capitan, Oaks	6	Piru	11	Goleta

### 3.0 DESCRIPTION OF THE MODELS

This chapter compares the theoretical basis, operational features and computational characteristics of the UAM-IV and CALGRID-IV models. The models share many common features in formulation and implementation. Included is a brief overview of the user documentation currently available for each modeling system.

#### 3.1 The UAM-IV Model

The following description of the UAM-IV model is derived from the recent study by Tesche, Roth, Reynolds, and Lurmann (1992). Further details on the UAM-IV and recommendations for upgrading it to a state-of-science model are presented in that report.

##### 3.1.1 Processes Treated by the UAM-IV

Pollutant Advection. The primary mode of pollutant transport over urban and regional scales is horizontal advection by the mean wind. Horizontal advection is treated by specifying  $u$  and  $v$  wind components each hour, which transport pollutant mass at each integration time step, usually 0.1 hours (h) in duration. Vertical advection is controlled by the vertical wind component,  $w$ , which is not directly input to the model. Rather,  $w$  is computed internally in the UAM by integrating the mass continuity equation. All three wind components are assumed to be constant over an hour's interval.

Because the UAM employs a terrain-following grid system rather than one based on mean sea level coordinates, the  $u$ ,  $v$ , and  $w$  wind components may occasionally differ from the true cartesian values referenced to sea level. Therefore, the user must exercise caution when "mapping" winds for regions of strong terrain relief, such as mountainous areas, from meteorological models referenced to sea level onto the UAM grid mesh.

Considerable research has been carried out to determine the appropriate numerical methods for treating horizontal advection. The grid-based formulation of the model introduces errors in the calculation of advection; these are commonly referred to as "numerical diffusion" because they produce artificial spreading of pollutant distributions. The current version of the UAM employs the Smolarkiewicz (1983) scheme because it helps minimize artificial horizontal diffusion; in addition, it does not generate negative concentrations, and it is computationally efficient.

Turbulent Diffusion. Pollutant transport by turbulent diffusion (i.e., the random motions in the atmosphere) is treated using so-called K-theory, which assumes that the turbulent flux of material is proportional to the gradient in the concentration field. This "first-order closure" approach essentially defines a property of the flow referred to as the turbulent eddy diffusivity. In the atmosphere, the eddy diffusivity varies in all three

spatial directions and is a function of time as well. In the UAM, the diffusion process is considerably simplified. A constant horizontal eddy diffusivity is assumed, equal to  $50 \text{ m}^2/\text{sec}$ . The exact value is probably immaterial, however, because the undesirable effects of numerical diffusion are significantly greater than this nominal value. The problem may be mitigated somewhat because horizontal transport occurring by advection is much greater than that occurring by turbulent diffusion. This is not the case for vertical turbulent transport.

Turbulent diffusion is frequently the dominating vertical transport process. For neutral and unstable atmospheric conditions, the vertical eddy diffusivity is based on a detailed set of numerical experiments that used a planetary boundary layer model to simulate turbulent atmospheric flows (Lamb et al., 1977). The turbulence levels simulated by this complex flow model were used to derive "optimal" vertical eddy diffusivities for unstable conditions. For stable conditions, the diffusivity relationships developed by Businger and Arya (1974) are used.

Solar Radiation. Several chemical reactions in the UAM are driven by solar ultraviolet (UV) radiation, most notably the photolysis of  $\text{NO}_2$ . The photolytic rates are based on clear sky actinic fluxes calculated by Peterson and Flowers (1976) for typical urban conditions. Appreciable quantities of aerosols in the atmosphere can cause light scattering that alters the intensity of UV radiation. This, in turn, can lower the effective photolysis rate constants near the ground by 30% or more from those at the top of the modeling domain (of the order of 1-2 km). The UAM provides for linearly attenuating the effective photolysis rates near the ground on the basis of model-estimated aerosol concentrations. This option is rarely employed, however. There is no provision for treating horizontal variability of the UV radiation distribution over the modeling region, attributable to coastal fog or stratus clouds, for example. To date, solar radiation processes have received limited attention relative to the other meteorological processes treated in the UAM.

Chemical Transformation. The UAM contains the Carbon Bond IV (CBM-IV) mechanism, a condensed chemical scheme consisting of over 80 reactions and 30 species. The CBM-IV, described by Gery et al. (1988), employs "carbon bond" lumping to aggregate organic species according to bond types (for example, as single carbon bonds, double carbon bonds, or carbonyl bonds). This structural lumping technique groups the reactions of similar carbon bonds, as opposed to the molecular lumping approach that groups the reactions of entire molecules. With the carbon bond approach, fewer surrogate categories are needed to represent bond groups than are needed for molecular surrogate mechanisms, resulting in fewer species to be modeled and a concomitant savings in central processing unit (CPU) time.

The CBM-IV treats the following reactive organic gas species groupings: paraffins, olefins, toluene, xylene, formaldehyde, higher aldehydes, ethylene, and isoprene. Its performance has been tested (and calibrated) against 170 experiments

conducted in three different environmental (smog) chambers. These experiments included  $\text{NO}_x$ -air irradiations of individual organic compounds as well as a number of simple and complex organic mixtures. The CBM-IV is "hard-wired" into the UAM code, that is, the chemical mechanism and chemical solver are merged with one another. Although this results in a computationally efficient code, it significantly reduces the ease with which alternative chemical mechanisms can be substituted into the UAM.

### Emissions.

The UAM-IV treats emissions of primary pollutant species derived from both anthropogenic and natural sources. Pollutants from anthropogenic sources can be released from either a point at the ground or aloft, from surface or elevated line segments (e.g., a roadway or an inclined aircraft takeoff or landing pattern), from a small, reasonably homogeneous area or large areas. The rate of emission can vary temporally as well as spatially: some sources emit pollutants at a nearly continuous rate, whereas others may be intermittent or may exhibit significant variations over time. Emissions from natural sources, which consist principally of geogenic and biogenic sources, can also be released from either point or area sources, and they can vary temporally as well. For example, emissions from lightning, a potentially large, though infrequent, source of natural emissions of  $\text{NO}_x$ , are highly variable in both time and space. In contrast,  $\text{NO}_x$  emissions from a base-loaded electric generating station may be nearly constant. Moreover, the thermodynamic character of the emitted materials, principally the release temperature and specific humidity relative to ambient conditions, plays an important role in the initial assimilation of pollutants into the atmosphere. Emissions of principal concern include  $\text{NO}$ ,  $\text{NO}_2$ ,  $\text{CO}$ , and a wide range of VOCs. In addition,  $\text{SO}_2$ , fine particulate (PM-10), and total suspended particulates (TSP) may be important in situations in which the mass loading of these materials, or their oxidation products, is sufficient to produce significant attenuation of incoming UV solar radiation. With the exception of PM-10 and TSP, all of these are gaseous pollutants.

Surface Removal. Many pollutants, including  $\text{NO}_2$ ,  $\text{O}_3$ , and sulfur dioxide ( $\text{SO}_2$ ), can be removed from the atmosphere by chemical reaction, adsorption, or absorption at various surfaces. The UAM uses a simple resistance methodology to calculate the removal of gaseous pollutants by surface sinks. A two-step process is assumed: transport to the surface, followed by uptake by the surface. A resistance to mass transport and a resistance to surface removal are defined. The transport resistance is estimated from theoretical considerations of turbulent transfer in the atmospheric boundary layer, and the surface resistance is obtained from experimental data on the uptake of pollutants by various types of surfaces (Killus et al., 1977).

### **3.1.2 Theoretical Formulation**

The basis of the UAM is the atmospheric diffusion (or species continuity) equation. This equation represents a mass balance in which each of the relevant emission,

transport, chemical reaction, and removal processes is expressed in mathematical terms. To solve the equation, it is necessary to employ numerical procedures; therefore, the atmospheric diffusion equation is spatially and temporally averaged. Omitting chemical effects resulting from subgrid-scale concentration variations yields the following governing equation for the model:

$$\begin{aligned} & \frac{\partial c_i}{\partial t} + \frac{\partial uc_i}{\partial x} + \frac{\partial vc_i}{\partial y} + \frac{\partial wc_i}{\partial z} \\ &= \frac{\partial}{\partial x} \left( K_h \frac{\partial c_i}{\partial x} \right) + \frac{\partial}{\partial y} \left( K_h \frac{\partial c_i}{\partial y} \right) + \frac{\partial}{\partial z} \left( K_z \frac{\partial c_i}{\partial z} \right) \\ & \quad + R_i + S_i - L_i \end{aligned}$$

where

$c_i$  is the concentration of pollutant  $i$ ;

$u, v, w$  are the mean wind velocity components in the  $x, y,$  and  $z$  directions, respectively;

$K_h$  and  $K_z$  are the horizontal and vertical turbulent diffusivities, respectively;

$R_i$  is the net rate of production of pollutant  $i$  by chemical reactions;

$S_i$  is the rate of emissions of species  $i$  from sources; and

$L_i$  is the rate of removal of pollutant  $i$  by surface uptake processes.

The governing equations are defined over the region,  $x_w \leq x \leq x_e, y_s \leq y \leq y_n, h(x,y) \leq z \leq H(x,y,t)$ , where  $x_w, x_e, y_s,$  and  $y_n$  are the west, east, south, and north boundaries of the airshed,  $h(x,y)$  is the ground elevation above sea level at  $(x,y)$ , and  $H(x,y,t)$  is the height of the top of the modeling region.

The initial conditions for the governing equations require that the mean concentration for each pollutant be specified at the starting time of the simulation ( $t_0$ ) at all locations, that is,

$$c_i(x,y,z,t_0) = f_i(x,y,z)$$

The vertical boundary conditions are:

1. At  $z = h(x,y)$ ,

$$-K \nabla c_i \cdot n_h = Q_i(x,y,t)$$

where  $K$  is the eddy diffusivity tensor,  $n_h$  is the unit vector normal to the terrain directed into the atmosphere, and  $Q_i$  is the mass flux of species  $i$  at the surface.

2. At  $z = H(x,y,t)$ ,

$$\begin{aligned} (Wc_i - K \nabla c_i) \cdot n_H &= [Wg_i(x,y,z,t)] \cdot n_H && \text{if } W \cdot n_H \leq 0 \\ \nabla c_i \cdot n_H &= 0 && \text{if } W \cdot n_H > 0 \end{aligned}$$

where  $W$  is the advective velocity of pollutants relative to the top of the modeling region,  $n_H$  is the outwardly directed unit vector normal to the surface defined by the top of the modeling region, and  $g_i$  is the mean concentration of species  $i$  aloft (just above the top of the modeling region).

The condition  $W \cdot n_H \leq 0$  at the top of the modeling region applies when material is transported into the modeling region from above the region. The condition simply states that the normal component of the mass flux is continuous across the upper boundary. The condition  $W \cdot n_H > 0$  applies when pollutants are transported upward through the top of the region. Basically, this condition allows pollutants to be advected through the top of the region.

The horizontal boundary conditions are

$$\begin{aligned} (Uc_i - K \nabla c_i) \cdot n &= U[g_i(x,y,z,t)] \cdot n && \text{if } U \cdot n \leq 0 \\ -K \nabla c_i \cdot n &= 0 && \text{if } U \cdot n > 0 \end{aligned}$$

where  $U = u_i + v_j$ ,  $n$  is the outwardly directed unit vector normal to the horizontal boundary, and  $g_i$  is the concentration of species  $i$  just outside the airshed boundary. The first condition is, as before, a statement of the continuity of mass flux across the boundary when the flow is directed into the airshed. The second condition specifies that the diffusive component of the total mass flux is set equal to zero when the wind is directed out of the airshed. This condition is equivalent to that conventionally employed at the exit of a tubular chemical reactor (Wehner and Wilhelm, 1956), though the conditions prevailing at the boundary of the region are not precisely the same as those at the exit of such a reactor. As noted earlier, because the horizontal advective component of the mass flux generally dominates the horizontal diffusive component, the error incurred as a result of this approximation is small.

### 3.1.3 Numerical Implementation

Because the governing equations are nonlinear, an analytical solution is not possible. Thus, numerical integration procedures are employed to develop approximate solutions. To facilitate the application of finite difference methods, a change of variables is introduced to normalize the vertical dimension by the distance between the bottom and the top of the region. This is accomplished by defining a new independent variable  $\rho$  as follows:

$$\rho = \frac{z - H_b(x,y,t)}{H_t(x,y,t) - H_b(x,y,t)}$$

where  $H_b$  and  $H_t$  are the elevations of the bottom and top of the region, respectively. Note that the vertical dimension of the modeling region can be segmented into two subregions: (1) from the ground to the base of the elevated inversion layer (the diffusion break), and (2) from the diffusion break to the top of the region. Upon performing this change of variables and neglecting small cross-derivative turbulent diffusion terms, the governing equations become

$$\begin{aligned} & \frac{\partial}{\partial t}(\Delta H c_i) + \frac{\partial}{\partial x}(u \Delta H c_i) + \frac{\partial}{\partial y}(v \Delta H c_i) + \frac{\partial}{\partial \rho}(W c_i) \\ &= \frac{\partial}{\partial x} \left( K_h \Delta H \frac{\partial c_i}{\partial x} \right) + \frac{\partial}{\partial y} \left( K_h \Delta H \frac{\partial c_i}{\partial y} \right) + \frac{\partial}{\partial \rho} \left( \frac{K_z}{\Delta H} \frac{\partial c_i}{\partial \rho} \right) \\ &+ R_i \Delta H + S_i \Delta H - L_i \Delta H \end{aligned}$$

where

$$W = w - u \left( \frac{\partial H_b}{\partial x} + \rho \frac{\partial \Delta H}{\partial x} \right) - v \left( \frac{\partial H_b}{\partial y} + \rho \frac{\partial \Delta H}{\partial y} \right) - \rho \frac{\partial \Delta H}{\partial t}$$

and

$$\Delta H = H_t(x,y,t) - H_b(x,y,t)$$

The UAM can segment the modeling region into one or two groups of grid cells. A single group might be employed, for example, to perform calculations in the mixed layer only. Thus, the modeling region would be subdivided into several equally spaced cells<sup>1</sup> in the vertical direction bounded by the terrain and the base of the inversion. To facilitate the calculation of pollutant concentrations above the mixed layer, a second

---

<sup>1</sup>The cells are equally spaced in the  $\rho$  coordinate system.

group of equally spaced cells can be added to the modeling region that is bounded (for example) by the base and top of the inversion layer. These provisions may be important in performing multiple-day simulations to account for the proper vertical placement and subsequent transport, reaction, and entrainment into the mixed layer of emissions injected from tall stacks.

Special consideration must be given to the application of finite difference methods to multidimensional problems. The UAM employs the method of fractional steps. Applying this technique to the solution of the governing equations results in the following four-step numerical integration procedure:

Step 1:

$$\frac{\partial}{\partial t}(\Delta H c_i) + \frac{\partial}{\partial x}(u \Delta H c_i) = \frac{\partial}{\partial x} \left( K_H \Delta H \frac{\partial c_i}{\partial x} \right)$$

Step 2:

$$\frac{\partial}{\partial t}(\Delta H c_i) + \frac{\partial}{\partial y}(v \Delta H c_i) = \frac{\partial}{\partial y} \left( K_H \Delta H \frac{\partial c_i}{\partial y} \right)$$

Step 3:

$$\frac{\partial}{\partial t}(\Delta H c_i) + \frac{\partial}{\partial \rho}(W \Delta H c_i) = \frac{\partial}{\partial \rho} \left( \frac{K_V}{\Delta H} \frac{\partial c_i}{\partial \rho} \right) + S_i \Delta H - L_i \Delta H$$

Step 4:

$$\frac{\partial}{\partial t}(\Delta H c_i) = R_i \Delta H$$

If the modeling region is segmented into two layers, two sets of equations differing only in the definition of  $\Delta H$  will be used. The numerical integration of the full governing equations for one time interval is approximated in the method of fractional steps by the sequential integration of Steps 1 through 4 for one time interval. The temporal variation of each pollutant concentration in each grid cell is developed by carrying out this four-step procedure for several time intervals.

Steps 1 and 2 treat horizontal transport due to advection and turbulent diffusion. Step 1 integrates the x-direction components of the pollutant transport terms, and Step

2 integrates the y-direction terms. These one-dimensional advection-diffusion equations are solved using an integration technique developed by Smolarkiewicz (1983).

Step 3 entails the integration of the vertical advection and diffusion terms as well as pollutant emissions and deposition. The equation is solved using an implicit finite difference technique to eliminate stability constraints on the size of the time step that might otherwise arise if the vertical grid spacing becomes relatively small at some point in the simulation.

Step 4 treats the contributions of chemical reactions through use of a Crank-Nicolson difference scheme, which yields a set of nonlinear algebraic equations. These equations are solved using a Newton iterative procedure.

### 3.1.4 Implementation of the CBM-IV Chemistry in the UAM-IV

The CBM-IV mechanism is generally sound for estimating urban- and regional-scale ozone concentrations (Tesche et al., 1992). However, the implementation of the mechanism into the UAM-IV includes numerous approximations that are worth mentioning. Although most are valid, concern exists regarding the treatment of  $\text{NO}_3$  and  $\text{N}_2\text{O}_5$  at night. In urban environments where significant amounts of  $\text{NO}_2$  and ozone exist prior to sunset, the nighttime  $\text{NO}_x$  chemistry is quite active and important. Significant amounts of  $\text{NO}_3$  and  $\text{N}_2\text{O}_5$  are formed after sunset and are converted to nitric acid. Because of fast forward and backward reactions occurring in the  $\text{NO-NO}_2\text{-NO}_3\text{-N}_2\text{O}_5$  system,  $\text{NO}_3$  and  $\text{N}_2\text{O}_5$  are numerically stiff whenever  $\text{NO}_2$  and ozone are both present at night. The UAM does not explicitly integrate these species at night; rather, it integrates the sum of  $\text{NO}_3$  and  $\text{N}_2\text{O}_5$  in a species called NOXY. The latter approach significantly reduces the numerical stiffness of the differential equations which, in turn, allows the UAM to run very fast at night. However, the evaluation of the rate of change of NOXY requires estimates of the individual species concentrations, which the UAM accomplishes by partitioning the NOXY into  $\text{NO}_3$  and  $\text{N}_2\text{O}_5$  using the steady-state approximation. Unfortunately, the approximation is not always valid for urban conditions and, in addition, its use can cause significant numerical errors in the solution of the nighttime chemistry.

The formaldehyde photolysis rates implemented in the UAM and those used for testing the mechanism are inconsistent. This is a concern because the formaldehyde photolysis rates are one of the most important parameters in photochemical mechanisms. At the time the CBM-IV was developed, significant uncertainty existed regarding the formaldehyde absorption cross sections. The performance evaluation was carried out using formaldehyde photolysis rates based on the absorption cross sections reported by Bass et al. (1980). At about the time the CBM-IV evaluation was completed, several sets of new data became available indicating that the absorption cross sections developed by Moortgat et al. (1980), rather than those of Bass et al., were correct. Moortgat's data produce photolysis rates that are about 30% higher than those obtained using Bass's

data. Rather than reevaluating the mechanism with the new data, the developers simply incorporated the CBM-IV into the UAM using the Moortgat rates. The mechanism was never tested against the chamber data using these rates.

Species assignment procedures also are inconsistent. The assignments of acetone, methyl ethyl ketone, neopentane, and iso-octane in the UAM documentation differ from those of the mechanism development report. These inconsistencies are minor; nevertheless, they should be corrected.

Neither the UAM nor its UAM preprocessing program calculate photolysis rates from basic data (i.e., from solar actinic fluxes, absorption cross sections, and quantum yields). This is a shortcoming of the UAM software, not the CBM-IV mechanism. However, the solar actinic fluxes on which the UAM's default photolytic rates are based are apparently undocumented. The absorption cross sections and quantum yields are documented, but the actinic fluxes are unavailable.

### 3.1.5 Operational Features

The UAM is actually one component of a larger system of FORTRAN model codes and pre- and postprocessor programs. Figure 3-1 depicts the information flow into and out of the model. (Note that the naming convention for the various subroutines varies slightly from that used in this report.) The role of the pre- and postprocessor programs is briefly described below. Further details can be obtained from the "Users Guide for the Urban Airshed Model" (Morris et al., 1990e).

As indicated in Figure 3-1, 13 data files provide information to the UAM. Generally, separate files are created for each full or partial day of a simulation. All the files are required. These files are unformatted (binary). Their content is described in Tesche et al., (1992).

### 3.1.6 Computational Requirements

When the UAM was first developed, its computational requirements far exceeded the memory capabilities of computers existing at that time. To circumvent this limitation, the code was written in FORTRAN IV with several innovative programming techniques (i.e., segmentation) that allowed large problems to be run on computers having limited memory. In particular, the model was segmented so as to require only 170,000 octal words of memory; arrays were overlain to reduce storage requirements. Much of the early developmental work was carried out on the CDC 6600 and 7600 machines at Lawrence Berkeley Laboratory. With the advent of significantly greater memory and the introduction of minicomputers and scientific workstations in the 1980s, many of these limitations disappeared. Segmentation of model runs is no longer necessary. However, the structure of the UAM-IV code retains much of the original, and now archaic, architecture; in addition, the code does not readily take advantage of

several of the speed enhancement features of current computers. The UAM-IV, as currently written, is designed to run on scalar computers, which today still constitute nearly 90% of the available systems. If the model is to be run efficiently on vector or parallel computers, the entire code should be restructured.

The computational requirements of the UAM system fall into two categories: computer speed and mass storage. Computer run times vary according to many factors, such as the size of the modeling domain, the number and size of the grid cells, the number of vertical grid layers, the maximum wind speed each hour, the number of species simulated, and so on. Typical CPU requirements from recent applications of the UAM-IV in different cities may prove informative. For example, a three-day (56-h) simulation of the 45 x 40 x 5 modeling region in Dallas-Ft. Worth required (1) 23 hours on a SPARCstation1 with 24 mb memory, (2) 9 hours on the Multiflow/TRACE 7/300, and (3) 7.5 hours on the IBM RISC/6000 Model 530. In San Diego, for a 40 x 35 x 5 grid, a 48-h simulation required 1.5 hours of RISC/6000 time; and the 26-28 August 1987 (60-h) simulation in the SoCAB (65 x 36 x 5) required 7 hours of RISC/6000 time.

Although the minimum disk storage requirements can be as small as 150 mb, for practical purposes, a minimum of 750 mb to 1.0 gigabyte is more reasonable. Even though the output files (AVERAGE, DEPN, and INSTANT) may be only of the order of 60-80 mb per simulation day, the directories containing the preprocessor programs, ASCII and binary input files, data bases, and graphics programs may require as much as 10 times more disk space just to accommodate the adaptation and performance evaluation activities. When developing and evaluating multiple emissions control scenarios, the storage requirements for the numerous emissions and results files can easily require several hundred megabytes.

### 3.1.7 Documentation

The five-volume series of documents describing the UAM-IV that were released by the EPA in mid-1990 are the following.

- ▶ "User's Guide for the Urban Airshed Model -- Volume I: User's Manual for UAM(CB-IV)," by R. E. Morris, T. C. Myers, and J. L. Haney, 1990. Systems Applications, Inc., SYSAPP 90/018a, San Rafael, CA.

Volume I summarizes the historical development of the model and provides a general technical description of model formulation. This volume also presents the file structures of the UAM and describes the input and output data files.

- ▶ "User's Guide for the Urban Airshed Model -- Volume II: Preprocessors and Postprocessors for the UAM Modeling System," by R. E. Morris, T. C. Myers, E. L. Carr, M. C. Causley, S. G. Douglas, and J. L. Haney, 1990. Systems Applications, Inc., SYSAPP 90/018b, San Rafael, CA.

Volume II introduces and describes the use of various preprocessor programs developed over the past decade to assist in preparing air quality, emissions, and meteorological inputs. The general technical assumptions underlying the preprocessor programs are presented, and examples of the input file requirements and output results from each preprocessor are described.

- ▶ "User's Guide for the Urban Airshed Model -- Volume III: User's Manual for the Diagnostic Wind Model (Version 1.1)," by S. G. Douglas, R. C. Kessler, and E. L. Carr, 1990. Systems Applications, Inc., SYSAPP 90/018c, San Rafael, CA.

Volume III describes the theory and applications requirements of a specific windfield generator, the Diagnostic Wind Model (DWM). This volume presents the DWM's theoretical formulation, input requirements, and example output. The volume also includes recommended default values of various parameters.

- ▶ "User's Guide for the Urban Airshed Model -- Volume IV: User's Guide for the Emissions Preprocessor System," by M. C. Causely, J. L. Fieber, M. Jimenez, and L. Gardner, 1990. Systems Applications, Inc., SYSAPP 90/018d, San Rafael, CA.

The Emissions Preprocessor System (EPS), describes a family of emissions data processing codes intended to supply point and area source emissions estimates. The EPS includes both anthropogenic and biogenic sources. Each emissions module code is briefly described, and examples of module input and output files structures are given. The EPS, as currently designed, is intended to process emissions data sets from the National Emissions Data Systems (NEDS) or the National Acid Precipitation Assessment Program (NAPAP).

- ▶ "User's Guide for the Urban Airshed Model -- Volume V: Description and Operation of the ROM-UAM Interface Program System," by R. T. Tang, S. C. Gerry, J. S. Newsom, A. R. Van Meter, and R. A. Wayland, 1990. Computer Sciences Corporation, Research Triangle Park, NC.

Volume V describes the program designed to generate UAM input files from the inputs and outputs provided by the EPA Regional Oxidant Model (ROM).

Collectively, Volumes I through IV should be sufficient to guide new users through the various data analysis, model input preparation, and computer simulation steps involved in a routine application of the UAM. However, users may also find it helpful to consult certain other reports and users' guides that were prepared prior to the release of the UAM-IV. These include

- ▶ "An Introduction to the Airshed Model and Its Usage," by S. D. Reynolds, T. W. Tesche, and L. E. Reid, Systems Applications, Inc., 1979. (updated 1985), SYSAPP EF79-31, San Rafael, CA.
- ▶ "SAI Airshed Model Operations Manuals. Volume I -- User's Manual," by J. Ames, T. C. Myers, L. E. Reid, D. C. Whitney, S. H. Golding, S. R. Hayes, and S. D. Reynolds, Systems Applications, Inc., 1985. EPA-600/8-85-007a, San Rafael, CA.
- ▶ "SAI Airshed Model Operations Manuals. Volume II -- System's Manual," by J. Ames, S. R. Hayes, T. C. Myers, and D. C. Whitney, Systems Applications, Inc., 1985. EPA-600/8-85-007a, San Rafael, CA.
- ▶ "Guideline for Applying the Airshed Model to Urban Areas," by D. E. Leyland, 1980, U.S. Environmental Protection Agency, Office of Air Quality Planning and Standards, EPA-450/4-80-020, Research Triangle Park, NC.

These reports provide additional background information on UAM model theory, implementation, and application (though several of the older model descriptions have been replaced by newer techniques).

None of the reports described here discusses the way in which a detailed model performance evaluation should be performed using the UAM and its supporting modules (e.g., emissions and meteorology) or the way in which the UAM should be used in control strategy design and testing. The ARB and EPA has recently published generic guidelines (ARB, 1992; EPA, 1991) on these two important subjects.

## 3.2 The CALGRID-IV Model

A description of the CALGRID model is given by Yamartino et al., (1992) and Scire et al., (1989). As a brief overview, CALGRID-IV is formulated to treat essentially the same physical and chemical processes as the UAM-IV. Important distinctions between the models exist more in terms of how the various processes are represented mathematically and calculated via numerical algorithms than in conceptual differences in the basic processes. In general, the process representations in CALGRID-IV are closer to the current state-of-science. For example, the treatment of vertical mixing in the UAM-IV employs the antiquated "mixing-height" concept to distinguish between mixing pollutants below and above an elevated temperature inversion. CALGRID-IV does not rely on the mixing height concept; instead, the user is provided several options for prescribing vertical grid structure that are not constrained by the mixing height concept. This improvement allows the user, for example, to prescribe several layers of minimal thickness near the ground where resolution is needed; aloft, less resolution is possible, unless one needs to track elevated point source plumes. CALGRID-IV's computational requirements are comparable to those of the UAM-IV.

### 3.2.1 Processes Treated by CALGRID-IV

Pollutant Advection. CALGRID-IV treats pollutant advection by the mean wind by specifying u and v wind components each hour. As with the UAM-IV, the model employs a terrain-following grid system; therefore, winds from an external meteorological model (e.g., interpolative, diagnostic, or prognostic) must be mapped onto the CALGRID-IV grid mesh.

Turbulent Diffusion. The description of turbulent diffusion in CALGRID-IV attempts to take into account recent advances in boundary layer theory. Turbulent diffusion is modeled according to K-theory. Horizontal diffusion is prescribed using the simple Smagorinsky (1963) formulation while vertical diffusion is parameterized following recent semi-empirical relationships developed by Holtslag and Nieuwstadt (1986), Wyngaard (1985, 1988), Businger (1982), and Tennekes (1982).

Chemical Transformation. The version of CALGRID used in this study employs the Carbon Bond IV (CBM-IV) mechanism, described by Gery et al. (1988). Implementation of the CBM-IV mechanism was carried out by Carnegie Mellon University (Kumar et al., 1992) under contract to the ARB.

#### Emissions.

CALGRID-IV treats the same emissions sources of primary pollutant species derived from both anthropogenic and natural sources as the UAM-IV.

Dry Deposition. CALGRID-IV treats the dry deposition of NO, NO<sub>2</sub>, O<sub>3</sub>, sulfur dioxide (SO<sub>2</sub>), nitrogeous species and other pollutants via a full resistance-based model that includes geophysical parameters (e.g., surface roughness, composition of the surface and the type, amount, and physiological state of surface vegetation), meteorological conditions (e.g., stability, turbulence intensity), and pollutant characteristics (e.g., molecular diffusivity, solubility, and reactivity).

### 3.2.2 Theoretical Formulation

As with the UAM-IV, CALGRID-IV is based on the species continuity equation. Central to the model is the concept of operator splitting (Marchunk, 1975) and use of the method of fractional steps. As described by Yamartino (1992), the time-dependent species conservation equation is written as:

$$\begin{aligned} & \frac{\partial c_i}{\partial t} + \frac{\partial uc_i}{\partial x} + \frac{\partial vc_i}{\partial y} + \frac{\partial wc_i}{\partial z} \\ &= \frac{\partial}{\partial x} \left( K_h \rho \frac{\partial(c_i / \rho)}{\partial x} \right) + \frac{\partial}{\partial y} \left( K_h \rho \frac{\partial(c_i / \rho)}{\partial y} \right) + \frac{\partial}{\partial z} \left( K_z \rho \frac{\partial(c_i / \rho)}{\partial z} \right) \\ &+ R_i \end{aligned}$$

where  $c/\rho$  is the dimensionless mixing ratio based on the atmospheric density,  $\rho$  and  $R_i$  is the net rate of production of pollutant  $i$  by chemical reactions. As discussed below, the terms  $S_i$  and  $L_i$  in the UAM-IV's governing equation (the rate of emissions the rate of removal of pollutant  $i$  by surface uptake processes) are treated as boundary conditions in CALGRID-IV.

The CALGRID-IV equations are defined over the region,  $x_w \leq x \leq x_E$ ,  $y_S \leq y \leq y_N$ ,  $h(x,y) \leq z \leq H(x,y,t)$ , where  $x_w$ ,  $x_E$ ,  $y_S$ , and  $y_N$  are the west, east, south, and north boundaries of the airshed,  $h(x,y)$  is the ground elevation above sea level at  $(x,y)$ , and  $H(x,y,t)$  is the height of the top of the modeling region.

The initial conditions for CALGRID-IV are specified at the starting time of the simulation ( $t_0$ ) at all locations, that is:

$$c_i(x,y,z,t_0) = f_i(x,y,z)$$

The lower level boundary conditions account for emissions and surface removal by dry deposition and are given by:

$$v_{gi} c_i - K \nabla c_i \cdot n_h = E_i(x,y,t)$$

where  $K$  is the eddy diffusivity tensor,  $n_h$  is the unit vector normal to the terrain directed into the atmosphere, and  $E_i$  is the emissions mass flux of species  $i$  at the surface. The term  $v_{gi}$  is the dry deposition of species  $i$ .

At the top of the model domain, i.e., at  $z = H(x,y,t)$ :

$$c_i(x,y,H) = c_H(x,y)$$

where  $c_H$  is the two-dimensional concentration field at the top of the model grid.

### 3.2.3 Numerical Implementation

A significant effort was spent in the CALGRID model development to study alternative numerical schemes for solving the horizontal advection problem. CALGRID-IV currently allows the user to select either a chapeau-function-based scheme or a modified cubic spline-based technique for solving the horizontal advection-diffusion equations. Integration of the vertical diffusion equation is accomplished by a hybrid solver that is stability dependent. Under conditions of small or moderate vertical diffusion, a Crank-Nicholson scheme is used, while under strongly convective conditions (e.g., during the afternoon periods) a fully implicit scheme is employed.

### 3.2.4 Implementation of the CBM-IV Chemistry in CALGRID-IV

A description of the CBM-IV implementation in the CALGRID-IV model is given by Kumar et al., (1992) and thus will not be presented here.

### 3.2.5 Operational Features

CALGRID-IV, like most large Eulerian photochemical models, consists of a large system of FORTRAN model codes and pre- and postprocessor programs. Figure 3-2 depicts the information flow into and out of the model. Further details can be obtained from the CALGRID Users Guide (Scire et al., 1989).

### 3.2.6 Computational Requirements

We have found that the computational requirements (e.g., disk storage, memory requirements, CPU times) of CALGRID-IV are similar to those for the UAM-IV. This subject is addressed briefly in Chapter 9 where we give comparisons of the storage and CPU requirements for CALGRID-IV simulations of the 5-7 September and 16-17 September, 1984 SCCAB episodes.

### 3.2.7 Documentation

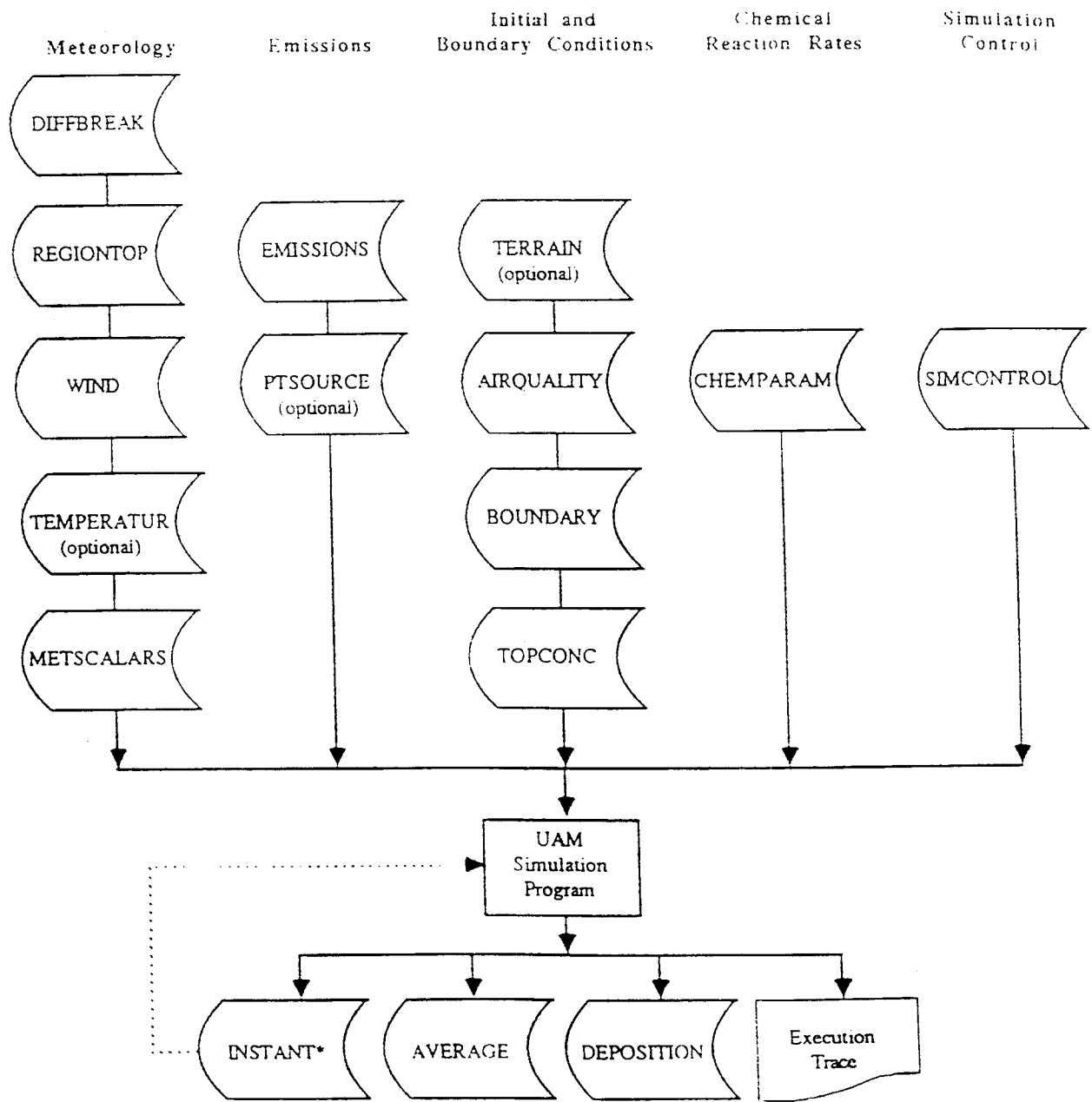
Two documents describe the CALGRID model:

- ▶ "CALGRID: A Mesoscale Photochemical Grid Model: Volume 1: Model Formulation," by R. J. Yamartino, J. S. Scire, S. R. Hanna, G. R. Carmichael, and Y. S. Chang, 1989. Sigma Research Corporation, Final Report on Contract A6-215-74 for the California Air Resources Board.

Volume I summarizes the theoretical formulation and numerical implementation of the model.

- ▶ "CALGRID: A Mesoscale Photochemical Grid Model: Volume 2: User's Guide," by J. S. Scire, R. J. Yamartino, G. R. Carmichael, and Y. S. Chang, 1989. Sigma Research Corporation, Final Report on Contract A6-215-74 for the California Air Resources Board.

Volume II introduces and describes the CALGRID file structures, the input and output data files, use of various preprocessor programs, and brief technical descriptions of the assumptions underlying the preprocessor programs. Examples of the input and output files are described.



\* Can be used as initial condition file to restart model (replaces AIRQUALITY)

Figure 3-1. UAM-IV Simulation Program with Input and Output Files (Source: Morris et al., 1990).

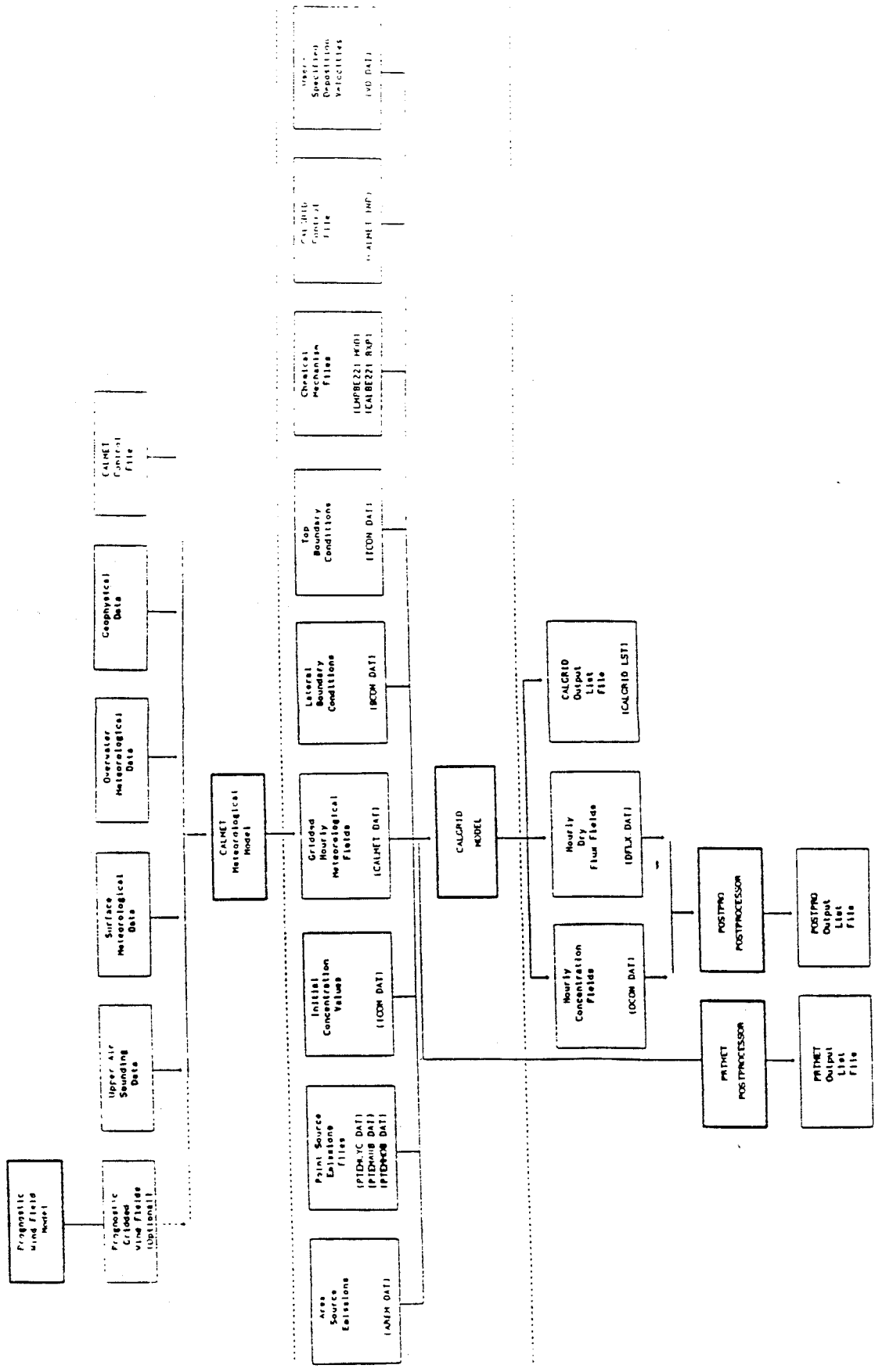


Figure 3-2. CALGRID-IV Model Simulation Program with Input and Output Files  
 (Source: Scire et al., 1989).

## 4.0 PREPARATION OF MODEL INPUTS

The procedures used to generate the Urban Airshed Model (UAM) model inputs for the two September, 1984 episodes are described in detail in project reports (Tesche et. al., 1988a,b; Tesche and McNally, 1991). Below we describe briefly the available data sets and the modifications to the input preparation procedures required to carry out this study. The modifications principally involved converting UAM-II model (using Carbon Bond II chemistry) inputs to UAM-IV files and converting UAM-IV files to CALGRID-IV inputs.

### 4.1 The 1984 SCCAMP Data Base

The 1984 SCCAMP Exploratory Field Study provided a data base that was significantly richer than that afforded by the routine monitoring activities in the basin. Surface wind data, collected hourly, were available from 17 onshore sites and from 3 offshore oil production platforms. Upper level wind monitoring was performed at 5 sites, supplementing the routine data collection at Pt. Mugu and Vandenberg AFB. Twelve surface temperature stations were in operation and vertical temperature profiles were available twice daily at Vandenberg and three times daily at Pt. Mugu. In addition, during the 16-17 September episode, 25 vertical aircraft soundings were performed over land and water for upper air characterization. During the period 10-22 September, a total of 15 aircraft flights were performed over strategic portions of the basing, documenting the vertical and horizontal extent of temperature, humidity, turbulence,  $\text{NO}_x$ , ozone, and b-scat fields. This intensive measurement set combined with the information from the routine surface aerometric data base represented the available data base with which UAM-IV inputs for the September episodes were prepared.

### 4.2 Emissions Estimates

The UAM-IV requires emissions estimates for all relevant anthropogenic and natural sources in the modeling region. The emission used in this study were resolved on a 4 km grid, temporally allocated (i.e. hourly emissions estimates), and disaggregated according to  $\text{NO}_x$  and reactive organic gas (ROG) chemical species. Emissions rates for all sources in the region were constructed from baseline estimates for TOG,  $\text{NO}_x$ , PM,  $\text{SO}_2$ , and CO.

The emissions estimation process was carried out by the California Air Resources Board and the two local air pollution control districts. It involved the following steps: (a) source identification; (b) source and process characterization; (c) source activity level determination; (d) emission factor estimation; (e) emission rate calculation; and (f) emission gridding, temporal splitting and species allocation. Day specific emission information were not used in preparing the emissions for this project. Following ARB

directives, emissions estimates for 6 September were used for all days in both the UAM-IV and CALGRID-IV models.

### 4.3 Scalar Inputs

The UAM-IV requires a number of scalar quantities to calculate the atmospheric stabilities, turbulent diffusivities, surface deposition rates, plume rise, and so on. Available meteorological observations were used with boundary layer parameterization schemes (Holtslag and van Ulden, 1983; van Ulden and Holtslag, 1985; Wilczak and Phillips, 1986) to calculate the surface turbulent heat flux, friction velocity, Monin-Obukov length, turbulence intensity, friction velocity, and the temperature scale for turbulent heat transfer. These parameters were calculated hourly based on terrain elevations, surface roughness and vegetation factors, and estimates of local surface wind speed and direction, early morning temperature soundings, surface albedo, and soil moisture content.

The only changes made to the scalar fields in converting from UAM-II to UAM-IV was to re-estimate the hourly  $\text{NO}_2$  photolysis rates using the SUNFUNC processor distributed with the UAM-IV code. Hourly specific  $\text{NO}_2$  photolysis rates are presented in Table 4.1.

### 4.4 Meteorological Inputs

The meteorological input requirements of the UAM-II and UAM-IV are identical. The only changes in converting the meteorological fields from UAM-II to UAM-IV was to rerun the meteorological preprocessors. However, the meteorological fields required by CALGRID-IV are significantly different. In performing the conversion from UAM-IV to CALGRID-IV, no additional observational data were used. It is possible that the inclusion of additional data would have improved the CALGRID-IV performance.

#### 4.4.1 Windfields

Wind fields were converted from the UAM-IV vertical grid which varies in time and space into the fixed CALGRID-IV meteorological structure using a vertical averaging scheme. The averaging scheme was weighted by the amount of overlap between UAM-II and CALGRID-IV layers. After mapping the winds from the UAM-IV to CALGRID-IV grid structures, the vertical wind components were calculated using a central difference divergence routine.

#### 4.4.2 Temperature Fields

CALGRID-IV requires a three-dimensional temperature field. This field was calculated using the gridded surface temperatures from the UAM-IV model and the temperature gradient from the UAM-IV meteorological scalar file.

#### 4.4.3 Mixing Heights

The UAM-IV mixing height fields were converted unchanged into CALGRID-IV format.

#### 4.4.4 Short-Wave Radiation

Because the UAM-IV model does not input short-wave solar radiation directly, its values had to be specified. Hourly short-wave radiation values estimated from the available surface measurements are presented in Table 4.2.

#### 4.4.5 PGT Stability Class

PGT stability class was calculated using the same routine as is used in the UAM-IV point source preprocessor. This method relates the wind speed and exposure class (from the UAM-IV meteorological scalars file) to the PGT stability.

#### 4.4.6 Surface Station Parameters

The CALGRID-IV model requires station specific parameters for temperature, cloud cover and surface pressure. Temperature and surface pressure were calculated from UAM-IV values. Surface temperature was taken to be the mean surface temperature throughout the domain. Surface pressure was taken from the UAM-IV meteorological scalars file. Cloud cover was assumed to be one-tenth throughout the simulation.

### 4.5 Initial and Boundary Conditions

Initial and boundary conditions required processing in a two step process. First the original Carbon Bond II initial and boundary files were modified for use in the UAM-IV. Then, the UAM-IV initial and boundary condition files were converted into CALGRID-IV format.

Hydrocarbon data were respecified using formulas presented in Table 4.3. These respeciation factors were previously determined for use in the South Central Coast Air Basin by Myers (1990). Ozone and NO<sub>x</sub> concentrations were not changed in converting to UAM-IV inputs. Reactive intermediate species were set to a lower bound concentration of 10<sup>-13</sup> ppm. The original UAM-II modeling grid excluded large regions in the south-west and north-east portions of the domain. Because the CALGRID-IV model does not allow for excluding grid cells, the computational boundaries were extended to within two grid cells of the domain for both the UAM-IV and CALGRID-IV simulations.

UAM-IV initial and boundary conditions were converted into the CALGRID-IV vertical grid structure using the same methodology as was used for the wind fields. The

concentrations were vertically averaged, weighted by the degree of overlap between UAM-IV and CALGRID-IV levels.

#### 4.6 Modeling Region Definition

The modeling region consists of a 53 x 26 grid domain with 4 km horizontal resolution. Use of finer grid resolution, useful in resolving transport processes occurring near the coastline and mountain slopes, was impractical since the emissions grid, previously developed by state and local agencies, was fixed at 4 km. The vertical grid structure was based upon analysis of the windfields, mixing heights, aircraft measurements, and emissions source heights in the basin. The vertical grid definition consists of four vertical levels with two above the inversion and two below. A modeling domain height was set at 1000 meters.

As with previous UAM-IV simulations, four vertical levels were used. Two levels below the diffusion break and two levels above. For the CALGRID-IV model base case simulations, vertical grid option B was used. This option specifies a log-like profile of a specific number of grid cells below the diffusion break and a log-like profile above the diffusion break with the depth of the first level fixed at 20 meters. With only two levels below the diffusion break and with the first level fixed at twenty meters, the second level extended throughout the rest of the mixed layer. Thus, below the mixed layer this option is as close to the UAM-IV vertical grid structure as was possible. Use of a log-like profile above the diffusion break provided more resolution near the ground. Thus, option B was the best choice of vertical grid structure maintaining compatibility with the UAM-IV structure.

TABLE 4.1. HOURLY NO<sub>2</sub> PHOTOLYSIS RATES FOR UAM-IV IN THE SCCAB (per min).

Hour	5 Sept. 1984	6 Sept. 1984	7 Sept. 1984	16 Sept. 1984	17 Sept. 1984
0000	0.0	0.0	0.0	0.0	0.0
0100	0.0	0.0	0.0	0.0	0.0
0200	0.0	0.0	0.0	0.0	0.0
0300	0.0	0.0	0.0	0.0	0.0
0400	0.0	0.0	0.0	0.0	0.0
0500	0.0	0.0	0.0	0.0	0.0
0600	0.055	0.053	0.051	0.034	0.032
0700	0.237	0.235	0.233	0.213	0.211
0800	0.391	0.389	0.388	0.373	0.371
0900	0.488	0.487	0.486	0.474	0.472
1000	0.549	0.548	0.547	0.536	0.534
1100	0.584	0.583	0.581	0.569	0.568
1200	0.594	0.592	0.591	0.578	0.577
1300	0.581	0.579	0.578	0.563	0.561
1400	0.543	0.541	0.539	0.522	0.514
1500	0.477	0.475	0.473	0.450	0.448
1600	0.373	0.370	0.367	0.336	0.333
1700	0.210	0.206	0.202	0.161	0.157
1800	0.031	0.027	0.023	0.0	0.0
1900	0.0	0.0	0.0	0.0	0.0
2000	0.0	0.0	0.0	0.0	0.0
2100	0.0	0.0	0.0	0.0	0.0
2200	0.0	0.0	0.0	0.0	0.0
2300	0.0	0.0	0.0	0.0	0.0

TABLE 4.2. HOURLY SHORT-WAVE RADIATION FOR THE CALGRID-IV MODELING IN THE SCCAB (watts/sq meter).

Hour	5 Sept. 1984	6 Sept. 1984	7 Sept. 1984	16 Sept. 1984	17 Sept. 1984
0000	0.	0.	0	0	0.
0100	0.	0.	0.	0.	0.
0200	0.	0.	0.	0.	0.
0300	0.	0.	0.	0.	0.
0400	0.	0.	0.	0.	0.
0500	0.	0.	0.	0.	0.
0600	55.	53.	51.	34.	32.
0700	237.	235.	232.	213.	211.
0800	391.	389.	388.	373.	371.
0900	488.	487.	486.	474.	472.
1000	549.	548.	547.	536.	534.
1100	584.	583.	582.	569.	568.
1200	594.	592.	591.	578.	577.
1300	581.	579.	577.	563.	561.
1400	543.	541.	539.	522.	519.
1500	477.	475.	473.	450.	448.
1600	373.	370.	367.	336.	333.
1700	210.	206.	201.	161.	157.
1800	31.	25.	18.	10.	7.
1900	0.	0.	0.	0.	0.
2000	0.	0.	0.	0.	0.
2100	0.	0.	0.	0.	0.
2200	0.	0.	0.	0.	0.
2300	0.	0.	0.	0.	0.

TABLE 4.3. RESPECIATION OF INITIAL AND BOUNDARY CONCENTRATIONS OF HYDROCARBONS FOR CONVERTING CBMII SPECIES TO CBMIV SPECIES.

CBM-IV SPECIES	AS A FUNCTION OF CBM-II SPECIES
OLE	OLE
PAR	PAR - ARO * 0.432 - ARO * 2 * 0.568
TOL	ARO * 0.432
XYL	ARO * 0.568
FORM	CARB * 0.288
ALD2	CARB * 0.712
ETH	ETH
CRES	$1.0 \times 10^{-13}$
MGLY	$1.0 \times 10^{-13}$
OPEN	$1.0 \times 10^{-13}$

## 5.0 MODEL EVALUATION PROCEDURES

Through photochemical model performance evaluation, one seeks to ascertain how well the peak concentrations and spatial and temporal distributions of ozone and its precursor species are simulated throughout the study area under the episodic conditions of interest. These features are revealed by comparison of hourly-averaged concentration measurements with corresponding model estimates. In this section, we define the specific statistical measures and graphical procedures to be used in evaluating the UAM-IV and CALGRID-IV models with the September, 1984 data sets. We refer to this activity as the base case model performance evaluation. We also present the procedures to be used in the comparative evaluation of the two model's responses to similar changes in inputs (e.g., sensitivity analyses).

The statistical and graphical procedures used in this study are produced by Alpine Geophysics' Model Performance Evaluation, Analysis, and Plotting Software (MAPS) system. This package was developed for urban- and regional-scale model evaluations in San Diego, Los Angeles, Lower Lake Michigan (LMOS), and the San Joaquin Valley (SARMAP). The MAPS system embodies all of the recommended statistical and graphical model testing methods for photochemical and meteorological models suggested by Tesche et al., (1990) and subsequently adopted by the ARB and EPA in their photochemical modeling guidance documents (ARB, 1992; EPA, 1991). MAPS also contains statistical and graphical tools for analyzing emissions model output.

MAPS consists of a set of special-purpose FORTRAN codes, the National Center for Supercomputer Applications (NCSA) Hierarchical Data Format (HDF) data management libraries (ported to SUN SPARCStation and IBM RS/6000 platforms) and National Center for Atmospheric Research (NCAR) Graphics, Version 3.01. Details of the MAPS statistical and graphical procedures are presented in the SARMAP Model Evaluation Protocol (Tesche, 1992).

### 5.1 Base Case Evaluation Procedures

A wide variety of procedures have been developed over the years for quantifying photochemical grid model performance. For the base case performance evaluations of the UAM-IV and CALGRID-IV models, we use a subset of statistical procedures and graphical displays suggested by Tesche et al., (1990) and ARB (ARB, 1992).

#### 5.1.1 Statistical Measures

The principal statistical measures to be used for base case performance evaluation include the mean normalized bias, the normalized gross error, the ratio of the peak model estimate to peak measured value, and three measures of accuracy in simulating

the calculated peak concentrations. These measures, computed for NO, NO<sub>2</sub> and ozone are defined as follows:

Mean Normalized Bias. The mean normalized bias, D, is given by

$$D = \frac{1}{N} \sum_{i=1}^N \frac{(c_e(x_i, t) - c_o(x_i, t))}{c_o(x_i, t)}$$

where N equals the number of hourly estimate-observation pairs drawn from all valid monitoring station data on the simulation day of interest. The subscripts e and o refer to modeled concentration estimates and measured concentrations, respectively. Here,  $x_i$  is the  $i^{\text{th}}$  monitoring station location. Mathematically, the bias is derived from the average signed deviation of the concentration residuals and is calculated using all pairs of estimates and observations above the cutoff level. Arbitrary cutoff levels of 4-6 pphm for ozone and 2 pphm for NO<sub>2</sub> are frequently used to reduce the influence of low estimated or observed concentrations (often occurring at night or on the upwind boundaries) on the bias statistics. In the base case performance evaluation, we use a cutoff of 4 pphm for ozone and 1 pphm for NO and NO<sub>2</sub>. We will examine the model's bias and error statistics as a function of observed concentration levels using graphical means.

Bias estimates indicate the degree to which simulated 1-h concentrations are over- or underestimated. Based on the ensemble of estimate-observation pairs, this measure reveals the presence of systematic deviation from observed concentrations. Although bias estimates help identify systematic errors in the model's temporal or spatial response, this measure provides little insight into problems that may occur in a subregion or within specific time periods during the diurnal cycle. In fact, low estimates may conceal significant local bias. For example, a model simulation may exhibit strong overestimation in one region and strong underestimation in another. On average, the regionwide bias estimate could be zero, yet significant local biases would still remain.

Normalized Gross Error. The normalized gross error,  $E_d$ , is given by

$$E_d = \frac{1}{N} \sum_{i=1}^N \frac{|c_e(x_i, t) - c_o(x_i, t)|}{c_o(x_i, t)}$$

The gross error quantifies the mean absolute deviation of the concentration residuals. It indicates the average unsigned discrepancy between hourly estimates and observations and is calculated for all pairs above the cutoff level. Gross error is one of the more useful single measures for comparing model simulations. Gross error is a robust measure of overall model performance and provides a basis for comparing simulations across different air basins or ozone episodes. Unless calculated for specific locations or

time intervals, however, it provides no direct information about subregional errors or large discrepancies occurring within portions of the diurnal cycle.

Maximum Ratio. The maximum ratio is defined as the quotient of the maximum one-hour averaged model estimated concentration and the maximum hourly-averaged measurement, i.e.,

$$R_{\max} = \frac{c_e(x, t)}{c_o(\hat{x}, \hat{t})}$$

where  $c_e$  is the estimated one-hour averaged pollutant concentration,  $c_o$  is the observed hourly averaged concentration,  $\hat{x}$  refers to the peak monitoring station location,  $\hat{t}$  is the time of the peak observation. The caret,  $\hat{\quad}$ , denotes the time or location of the maximum observed concentration. There is no requirement that the maximum estimated and observed concentrations be paired in either time or space but for this measure we require that the maximum modeled concentration be taken from a monitoring station.

Accuracy Measures. Several accuracy measures are used because there are different, informative, and plausible ways of comparing the peak measurement on a given day with model estimates. Five accuracy measures provide complimentary tests of the model's performance. When applied to ozone simulations, they are particularly useful from a regulatory perspective since they deal with peak ozone (or precursor) concentration levels. The methods we use here consist of comparing the measured concentration at a given monitoring station with peak concentration that are paired in time and space, paired in space, paired in time, or unpaired. The first accuracy measure -- matching estimates and observations in time and space -- is the most stringent test that is typically applied to an ozone air quality model. The unpaired in time accuracy estimate, a more commonly used measure, is consistent with the form of the federal ambient ozone standard. The third measure provides a more general indication of the model's ability to simulate peak concentrations across the domain. (Here the model estimates are paired in space, but not in time). The five accuracy measures are defined mathematically as follows.

Paired Peak Estimation Accuracy. The paired peak estimation accuracy,  $A_{ps}$ , is given by:

$$A_{ps} = \frac{c_e(\hat{x}, \hat{t}) - c_o(\hat{x}, \hat{t})}{c_o(\hat{x}, \hat{t})} 100\%$$

$A_{ps}$  quantifies the discrepancy between the magnitude of the peak one-hour average concentration measurement at a monitoring station,  $c_o(\hat{x}, \hat{t})$ , and the estimated

concentration at the same location,  $\hat{x}$ , and at the same time,  $\hat{t}$ . Model estimates and observations are thus "paired in time and space." The paired peak estimation accuracy is a stringent model evaluation measure. It quantifies the model's ability to reproduce, at the same time and location, the highest observed concentration during each day of the episode. The model-estimated concentration used in all comparisons with observations is derived from bi-linear interpolation of the four ground level grid cells nearest the monitoring station.

$A_{ts}$  is very sensitive to spatial and temporal misalignments between the estimated and observed concentration fields. These space and time offsets may arise from spatial displacements in the transport fields resulting from biases in wind speed and direction, problems with the "timing" of photochemical oxidation and removal processes, or subgrid-scale phenomena (e.g., ozone titration by local  $\text{NO}_x$  emission sources) that are not intended to be resolvable by the Eulerian models such as UAM-IV and CALGRID-IV.

Temporally-Paired Peak Estimation Accuracy. The temporally-paired peak estimation accuracy,  $A_t$ , is given by:

$$A_t = \frac{c_e(x, \hat{t}) - c_o(\hat{x}, \hat{t})}{c_o(\hat{x}, \hat{t})} \quad 100 \%$$

$A_t$  quantifies the discrepancy between the highest concentration measurement at a monitoring station and the highest model estimate at the same station or any other grid cell within a distance of, say, 25 km. This measure examines the model's ability to reproduce the highest observed concentration in the same subregion at the correct hour.

Spatially-Paired Peak Estimation Accuracy. The spatially-paired peak estimation accuracy,  $A_s$ , is given by:

$$A_s = \frac{c_e(\hat{x}, t) - c_o(\hat{x}, \hat{t})}{c_o(\hat{x}, \hat{t})} \quad 100 \%$$

$A_s$  quantifies the discrepancy between the magnitude of the peak one-hour average concentration measurement at a monitoring station and the highest estimated concentration at the same monitor, within 3 hours (before or after) the peak hour.

Unpaired Peak Estimation Accuracy. The unpaired peak estimation accuracy,  $A_u$ , is given by:

$$A_u = \frac{c_e(x, t) - c_o(\hat{x}, \hat{t})}{c_o(\hat{x}, \hat{t})} \quad 100 \%$$

$A_u$  quantifies the difference between the magnitude of the peak one-hour average measured concentration and the highest estimated value in the modeling domain, whether this occur at a monitoring station or not. The unpaired peak estimation accuracy tests the model's ability to reproduce the highest observed concentration anywhere in the region. This is the least stringent of the above four peak estimation measures introduced thus far. It is a weak comparison relative to the previous ones but is useful in coarse screening for model failures. This measure quickly identifies situations where the model produces maximum ozone concentrations in the air basin that significantly exceed the highest observed values within the network.

Average Station Peak Estimation Accuracy. The average station peak estimation accuracy,  $\bar{A}$ , is given by:

$$\bar{A} = \frac{1}{N} \sum_{i=1}^N |A_{si}|$$

where:

$$A_{si} = \frac{c_e(\hat{x}_i, \hat{t}) - c_o(\hat{x}, \hat{t})}{c_o(\hat{x}, \hat{t})} \quad 100 \%$$

Here,  $x_i$  is the  $i$ th monitoring station location.  $\bar{A}$  is calculated by first determining the spatially-paired peak estimation accuracy,  $A_{si}$ , at each monitoring station. Thus, the average station peak estimation accuracy is simply the mean of the absolute value of the  $A_{si}$  scores, where the temporal offset between estimated and observed maxima at any monitoring station does not exceed three hours.

Although other statistical measures that can be calculated are, in many cases, useful in assessing model performance, the bias, error, ratio, and accuracy statistics are the measures that have most consistently been reported in the literature and they are the measures upon which our base case performance analysis of UAM-IV and CALGRID-IV is based.

### 5.1.2 Graphical Procedures

The main graphical tools used to analyze the base case UAM-IV and CALGRID-IV model results include:

- > The relationships between different accuracy measures;
- > The temporal correlation between estimates and observations;
- > The spatial distribution of estimated concentration fields;

- > The correlation among hourly pairs of estimates, observations and residuals;
- > The variation in bias and error estimates as functions of time and space, and;
- > The degree of mismatch between volume estimates and point measurements.

Brief discussions of these plotting methods are presented below.

### Accuracy Plots

The accuracy plotting method used in this study depicts relationships between the peak five accuracy measures while the other plot summarizes the peak estimation accuracy at all monitoring stations, revealing the presence of subregional estimation bias if it occurs. The plot consists of a histogram that displays the calculated values of  $A_{1s}$ ,  $A_v$ ,  $A_s$ ,  $A_w$ , and  $A$ . In addition, we also plot the maximum estimated and observed ozone concentrations and the quantity  $A_s$  at each monitoring station. This latter plotting method provides a quick overall comparison between the results of two model simulations.

### Time Series Plots

Probably the most useful graphical procedure for depicting air quality model results is the time series plot. Developed for each monitoring station for which observed concentrations are available, this plot presents the hourly estimates and observations throughout the simulation period. The time series plot consists of the hourly averaged observations (asterisks) and the hourly averaged estimates, the latter being fitted by a smooth continuous line.

Conventional time series plots do not reveal situations where the model estimates concentrations comparable in magnitude to the observations a short distance away from the monitoring station. In this study, we use so-called a "spatial time series plots". These plots provide information about the degree to which model discrepancies result from the procedure for selecting the estimated values. There is no a priori reason to select the four-cell bi-linear average estimate over the estimate in the specific grid cell containing the monitor (i.e., the "cell value"), or perhaps the grid cell estimate within any of the four adjacent cells that is closest in magnitude to the observed value (i.e. the "best" estimate). Spatial time series plots are constructed for each monitoring station by plotting the hourly observations together with an envelope defined by the highest and lowest grid cell estimate within one cell of the monitoring station.

The spatial time series plots provide diagnostic information about the "steepness" of the concentration gradients in the simulated fields. A small envelope indicates relatively flat concentration gradients. Conversely, steep gradients may produce a fairly large envelope. Ideally, the measurement points will fall within the envelope. Spatial time series plots are one method of revealing the correspondence or "commensurability" between volume-averaged model estimates and point measurements.

### Ground Level Isopleths

Ground-level ozone isopleths are developed for each hour of the episode to display the spatial distribution of estimated concentration fields. The isopleth plots are developed by computer-contouring the hourly, gridded ozone estimates. The information content of these plots are enhanced by including the following:

- > A base map identifying significant geophysical and political boundaries;
- > Locations of air monitoring stations;
- > The observed concentrations at each monitoring station by a bold numeral; and
- > The location of local modeled maxima or minima (signified by the letter H or L asterisk).

Ground-level isopleths are also constructed based on the daily maximum concentration estimate in each grid cell. These "maximum" ozone isopleths supply direct information about the magnitude and location of pollutant concentrations and help to identify situations where sub-regional biases may be attributed to spatial misalignment of the estimated and observed concentration fields.

### Scatterplots of Estimates and Observations

Scatterplots are a useful means of visually assessing the extent of bias and error in hourly ozone estimate-observation pairs. Hourly scatterplots are developed by plotting all hourly-averaged estimate-observation pairs for which the observed concentration exceeds the cutoff value. Similarly, daily maximum scatterplots are developed from the pairs of maximum hourly estimated and observed values at each monitoring station. The estimated maximum is the highest value simulated within three hours of the observed maximum. In these plots, the solid diagonal line with 1:1 slope will be used to identify the perfect correlation line and the dashed lines enclose the region wherein estimates and observations agree to within a factor of two. The lines of agreement can be made more stringent if desired.

The scatterplot is used to give a quick visual indication of the extent of over- or underestimation in the hourly estimates and whether there appear to be strong nonlinearities in model estimates and observations over the concentration range studied. Bias is indicated by the preponderance of data points falling above or below the perfect correlation line. The dispersion (spread) of points provides a visual indication of the general error pattern in the simulation. Scatterplots help identify outlier estimate-observation pairs, i.e., a seemingly discrepant estimate-observation pair that may result from erroneous data, a fundamental flaw in the model, or some other cause that requires investigation. These plots provide little diagnostic information about sub-regional performance problems, temporal or spatial misalignments, or other inadequacies in the simulation. In addition, scatterplots mask the temporal correlation between various estimate-observation pairs.

#### Bias Stratified by Concentration

Bias-concentration plots are derived from the residual distribution to depict the degree of systematic bias in hourly-averaged model estimates (paired in time and space) as a function of observed concentration level. This plot (and the companion error-concentration plot) aids in model diagnosis. The observed concentration range is divided into several equal-sized concentration bins and the normalized bias within each bin is calculated and plotted as a function of concentration level. A smooth line is then fitted through the bin-averaged values. The bias-concentration plot is used to reveal the existence of under- or over-estimation throughout the concentration range.

#### Gross Error Stratified by Concentration

Gross error-concentration plots is derived from the residual distribution to depict the error in model estimation (paired in time and space) as a function of observed concentration level. The observed concentration range is divided into several equal-sized concentration bins. Then, the average value of the normalized gross error within each bin is calculated and the bin averages are plotted as a function of the observed concentration level. MAPS will display the mean normalized gross error on the plot for easy reference.

The gross error-concentration plot is used to reveal the variation in model error at various intervals throughout the concentration range. The plot must be interpreted carefully, however, remembering that the concentration residual is normalized by the observed value.

#### Bias Stratified by Time

Bias-time plots are developed to help identify specific time periods within the photochemical simulation when systematic patterns of under- or overestimation occur. The bias-time plot is constructed in a manner similar to the bias-concentration plot,

except that the simulation period is discretized into a number of time intervals, usually 1-2 hours in duration. Systematic bias in model estimates during specific periods within the diurnal cycle may have several causes: biases in vertical mixing or wind transport; "timing" problems with the chemistry; non-representative temporal distributions assumed in the emissions inventory, and so on. While the bias-time plots may not clearly pinpoint the causes of bias, they may be helpful in defining the time intervals when the bias is most apparent. This helps focus subsequent diagnostic investigations.

### Gross Error Stratified by Time

Gross error-time plots are developed to help identify specific time periods when gross errors in the model estimates may be a problem. This plot is constructed in a similar manner as the error-concentration plot, except that the simulation period is discretized into a number of time intervals, usually 1-2 hours in duration. When interpreting the gross error-time and bias-time plots, one must remember that the concentration levels of all pollutants vary throughout the diurnal cycle.

## 5.2 Comparative Evaluation Procedures

The comparative evaluation of UAM-IV and CALGRID-IV consists of exercising both models with similar sets of inputs and comparing the model's responses. This evaluation has two components: (1) sensitivity analysis, and (2) diagnostic analysis. The statistical and graphical tools are the same for each. The statistical measures presented below are used to quantify the influence on model response to changes in inputs. These measures are mathematically similar to those discussed previously for the base case evaluation. The specific measures we focus on are:

Mean Normalized Deviation. The normalized signed deviation,  $D_s$ , is given by

$$D_s = \frac{1}{N} \sum_{i=1}^N \frac{(c_s(x_i, t) - c_b(x_i, t))}{c_b(x_i, t)}$$

where N equals the number of hourly estimate-observation pairs drawn from all valid monitoring station data on the simulation day of interest. The subscripts s and b refer to the modeled base case and sensitivity case concentration estimates, respectively. Here,  $x_i$  is the  $i^{\text{th}}$  monitoring station location. Mathematically, this measure is identical to the mean normalized bias except the base case model estimates are substituted for the observations at each monitoring station. For the comparative evaluation, we use a cutoff of 1 pphm for NO, NO<sub>2</sub>, and ozone.

Normalized Absolute Deviation. The normalized absolute deviation,  $E_s$ , is given by

$$E_s = \frac{1}{N} \sum_{i=1}^N \frac{|c_s(x_i, t) - c_b(x_i, t)|}{c_b(x_i, t)}$$

$E_s$  quantifies the mean absolute deviation of the concentration residuals derived from base case and sensitivity simulations. It indicates the average unsigned change between hourly base case and sensitivity estimates and is calculated for all pairs above the cutoff level.

Sensitivity Ratio. The sensitivity ratio is defined as the quotient of the maximum one-hour averaged model estimated concentration from the sensitivity simulation and the maximum hourly-averaged model estimate in the base case, i.e.,

$$R_s = \frac{c_s(x, t)}{c_b(\hat{x}, \hat{t})}$$

where  $c_s$  is the estimated one-hour averaged pollutant concentration in the sensitivity simulation,  $c_b$  is the maximum hourly-averaged concentration in the base case,  $\hat{x}$  refers to the peak station location in the base case,  $\hat{t}$  is the time of the peak base case estimate. The caret,  $\hat{\cdot}$ , denotes the time or location of the maximum base case concentration. There is no requirement that the maximum concentrations be paired in either time or space but for this measure we require that the maximum modeled concentrations be taken from a monitoring station.

Paired Peak Estimate Change. The paired peak estimate change,  $C_{is}$  is given by:

$$C_{is} = \frac{c_s(\hat{x}, \hat{t}) - c_b(\hat{x}, \hat{t})}{c_b(\hat{x}, \hat{t})} 100\%$$

$C_{is}$  quantifies the change between the magnitude of the base case peak concentration at a monitoring station,  $c_b(\hat{x}, \hat{t})$ , and the estimated concentration at the same location,  $\hat{x}$ , and at the same time,  $\hat{t}$ , in the sensitivity simulation. Both model estimates are "paired in time and space."

Unpaired Peak Estimate Change. The unpaired peak estimation accuracy,  $C_u$  is given by:

$$C_u = \frac{c_s(\lambda, t) - c_b(\hat{x}, \hat{t})}{c_b(\hat{x}, \hat{t})} 100\%$$

$C_u$  quantifies the difference between the magnitude of the base case peak concentration and the highest estimated value in the modeling domain, whether this occur at a monitoring station or not.

Average Peak Estimate Change. The average peak estimate change,  $C$ , is given by:

$$\bar{C} = \frac{1}{N} \sum_{i=1}^N |C_{si}|$$

where:

$$C_{si} = \frac{c_s(\hat{x}_i, t) - c_b(\hat{x}_i, \hat{t})}{c_b(\hat{x}_i, \hat{t})} \quad 100 \%$$

Here,  $x_i$  is the  $i$ th monitoring station location.  $C$  is calculated by first determining the spatially-paired peak estimation accuracy,  $C_{si}$ , is given by:

$$C_s = \frac{c_s(\hat{x}, t) - c_b(\hat{x}, \hat{t})}{c_b(\hat{x}, \hat{t})} \quad 100 \%$$

$C_s$  quantifies the discrepancy between the magnitude of the peak one-hour average concentration in the base case (at a monitoring station) and the highest estimated concentration at the same monitor in the sensitivity run, within 3 hours (before or after) the peak hour.

## 6.0 BASE CASE SIMULATION RESULTS

This chapter summarizes the results of the base case simulations of the 5-7 September, 1984 and 16-17 September, 1984 episodes using the UAM-IV and CALGRID-IV models. We begin by comparing the current UAM-IV ozone results with those from previously reported evaluations of UAM-II (Tesche and McNally, 1991) and UAM-IV (Myers, 1990). Then, statistical and graphical results from the UAM-IV and CALGRID-IV base case simulations are presented and discussed briefly. To aid the reader, all tables and figures referred to in this chapter are presented at the end of the text.

### 6.1 Previous UAM Performance Evaluations with the 1984 SCCAMP Data Base

#### 6.1.1 5-7 September, 1984 Episode

Tesche and McNally (1991) and Myers (1990) evaluated different versions of the UAM with essentially the same aerometric data base developed for the SCCAB (Tesche et al., 1989a,b). The principal difference between the two sets of simulations was in the re-Myers' re-speciation of the point and area source emissions files and the initial conditions, the boundary conditions used by Tesche and McNally. This was necessary to accommodate the UAM-IV. Table 6-1 lists the peak observed and modeled ozone concentrations at 14 monitoring stations for these two earlier UAM simulations of the 5-7 September, 1984 episode. Included are the present base case simulation results.

In view of the modifications made to the emissions inputs and the re-speciation of the initial and boundary files, the three simulations are quite comparable when examining the maximum one-hour ozone estimates. Generally, the UAM-IV simulations produced slightly higher basin-wide peak ozone values compared with UAM-II. With the exception of Myer's 7 September ozone peak, all UAM-IV simulations overestimated the maximum observed value for all three days as did the UAM-II. Considering the average (over all stations) of the modeled ozone peaks, the UAM-IV results tend to be slightly higher than those from the UAM-II. Here also, the modeled mean of the station peak values are marginally higher than the observed means for the three days.

Estimates of mean normalized deviation (bias) and mean absolute normalized deviation (error) for the three UAM base cases are presented in Table 6-2 along with other statistical measures of interest. As noted in Chapter 5, these measures are based on the ensemble of estimate-observations pairs above the cutoff level of 4 pphm. Considering all three simulation days, the models tend to overestimate ozone concentrations (from 4% to 23%) more frequently than they are underestimated (from -3% to -10%). The average bias in the current UAM-IV simulation over the three days is -2% compared with 13% for Myer's simulations and 3% for the UAM-II base case. For gross error, a slightly different ranking appears. The UAM-II gives the lowest gross error averaged over all three days (31%) compared with Myer's results (34%) and the

present UAM-IV base case (37%). These differences in bias and error estimates between the three simulations are minor.

### 6.1.2 16-17 September, 1984 Episode

Tables 6-3 and 6-4 compare the UAM-II results with those of the current study for the 16-17 September episode. (This is the first simulation of the 16-17 September episode with the UAM-IV). Both versions of UAM tend to overestimate the basin-wide maximum and mean station peak concentrations on the 16th and to underestimate these measures on the 17th. The UAM-II performance in simulating the peak values appears to be slightly better than that for UAM-IV. This trend is also evident by examining the paired and unpaired accuracy measures given in Table 6-4. On the 16th, the bias and error results for the two model runs are roughly the same, but on the 17th, the UAM-IV bias increases to -14% compared with -5% for UAM-II. The gross errors for the two models in the second day are 29% and 26%, respectively.

## 6.2 Base Case UAM-IV and CALGRID-IV Evaluations for the 5-7 September, 1984 Episode

This section begins with a presentation of the results of the UAM-IV and CALGRID-IV base case simulations for the 5-7 September episode. Statistical performance measures of accuracy, bias and error are given for NO, NO<sub>2</sub>, and ozone in order to compare the ability of the two models to simulate primary and secondary species. Comparisons for other species such as PAN and individual VOC species (or species groupings) is not possible given the lack of sufficient measurements. Subsequently, we present a variety of graphical results (e.g., time series plots, concentration isopleths, bias and error plots, scatterplots) to augment the statistical measures. The graphical comparisons primarily emphasize ozone since this is the species of greatest regulatory interest. Graphical results for NO and NO<sub>2</sub> are also added in the form of spatial time series plots.

### 6.2.1 Statistical Measures

UAM-IV and CALGRID-IV both significantly underestimated the maximum hourly NO concentrations at the eleven monitoring stations in operation during the 5-7 September, 1984 episode. From Table 6-5, the 11-station average of the peak NO observations were 8.1 pphm, 5.1 pphm, and 4.5 pphm for the three days, respectively. The UAM-IV produced overall averages of 1.6 pphm, 1.2 pphm, and 0.9 pphm while CALGRID-IV gave averages of 0.9 pphm, 0.8 pphm, and 0.6 pphm for the three days. Both models significantly underestimated the peak one-hour values on all three days. For example, on the 6th, the maximum observed NO was 19 pphm at Simi. CALGRID-IV produced a peak of 2.1 pphm at Simi while UAM-IV gave 2.8 pphm. In general, the UAM-IV produced NO peaks approximately 30% higher than CALGRID-IV for this episode.

The NO<sub>2</sub> results for both models (Table 6-6) agree somewhat better with observations than the NO comparisons. Both models also underestimate NO<sub>2</sub> concentration; the UAM-IV NO<sub>2</sub> peaks are in better agreement with observations than those from CALGRID-IV. For example, the average peak NO<sub>2</sub> UAM-IV estimates over the 10 stations were 2.5 pphm and 2.5 pphm for the 6th and 7th, compared with 1.7 pphm and 1.7 pphm for CALGRID-IV. The averages of the peak observations were 4.4 and 4.9 pphm, respectively. Overall, the UAM-IV peak estimates of NO<sub>2</sub> were nearly 50% larger than those for CALGRID-IV.

Both models tended to overestimate the peak one-hour ozone concentrations (averaged over the 14 monitoring stations) during the 5-7 September episode (Table 6-7). UAM-IV and CALGRID-IV overestimated the average station peak ozone values by 1.5 to 2 pphm on the first two days; in the 7th, the agreement between both models and the observed average was less than 1 pphm. For all three days, the UAM-IV's estimates of the average station peak ozone value was slightly better than those for CALGRID-IV.

Tables 6-8 through 6-10 present overall accuracy, bias and error results for the three days. CALGRID's NO estimates (above the 1 pphm cutoff threshold) are systematically underestimated by -83% to -85% for the three days while the UAM's NO estimates are similarly underestimated, ranging from -77% to -81%. Both models give peak one hour NO estimates (at a monitoring station) that are no more than about one fifth (1/5) to one tenth (1/10) of the maximum observed values. For NO<sub>2</sub>, CALGRID-IV underestimates hourly concentrations by -55% to -70%. The degree of systematic bias (i.e., underestimation) by UAM-IV is less, ranging between -40% to -49%. Both model's give gross errors in the 60% to 70% percent range with the UAM's average discrepancy being slightly less. Both model's estimates of the peak one-hour NO<sub>2</sub> concentrations are only about 1/2 of the observed values for the three days.

The systematic bias in both models hourly ozone estimates (equal to or greater than 4 pphm) is roughly comparable over all three days. On the three days, the biases are approximately -3%, -10%, and  $\pm 4\%$  for the two models. Gross errors range from 29% to 46%. Both models have the same gross error on the 6th (36%) while on the 7th, the UAM-IV's error (29%) is slightly lower than CALGRID-IV's (34%).

## 6.2.2 Graphical Results

Figures 6-1 through 6-11 contain highlights of the graphical analyses carried out for the two models with the 5-7 September data base. In the brief presentations the follow, we devote primary attention to the results on the 6th and 7th, days less influenced by uncertainties in the prescription of initial model fields.

## Accuracy of Peak Estimation

Figures 6-1a through 6-1c present summaries of the five different measures of model "accuracy" in estimating peak one-hour ozone concentrations on the three simulation days. For the 6th and 7th, the two models produce generally similar values of the five measures although, of course, there are some differences. For example, on the 6th, three of the five CALGRID-IV accuracy measures tend to be slightly better than those for the UAM-IV. On the 7th, all CALGRID-IV accuracy measures are systematically poorer than the UAM-IV's, typically be 10% to 20%.

Figures 6-1d through 6-1g depict the accuracy of peak estimation at each of the monitoring stations in operation during the 5-7 September episode. The monitoring stations are presented in the figures (from left to right) as they exist in the SCCAB moving from the coast inland (i.e., west to east). These plots give both the maximum observed and estimated values at each station and the accuracy estimates ( $A_S$ ) at each station. On the 6th, CALGRID-IV produces lower ozone maxima in the western basin relative to the UAM-IV; elsewhere, the peaks from the two models are roughly similar. On the 7th, the two models produce similar peaks on the extreme west and east ends of the basin, but in the central region, from Gaviota to El Rio (a total of eight stations), the CALGRID-IV ozone maxima are systematically lower than the UAM-IV's. UAM-IV's estimates of peak ozone is uniformly better than CALGRID-IV's on the 7th at those stations with maxima exceeding 6 pphm.

## Bias and Error as Functions of Time and Concentration Level

Figures 6-2 and 6-3 depict model bias and error in hourly ozone estimates (equal to or greater than 4 pphm) as functions of time throughout the three-day episode and as functions of observed concentration level. The bias time series (Figure 6-2a) are generally similar for both models on the 6th and 7th but there are some noteworthy differences. Specifically, during the early morning hours CALGRID-IV appears to exhibit higher negative bias (i.e., underestimation) than UAM-IV. Mid-day, CALGRID-IV overestimates ozone (positive bias) by a greater amount than UAM-IV. From early afternoon on, both models bias estimates goes from positive to negative; late in evening on both models tend to underestimate ozone. CALGRID-IV's underestimation is more pronounced than UAM-IV's.

Figures 6-2b and 6-2c display the bias in ozone estimation as functions of observed concentration level for both models in the 6th and 7th. On the 6th, the bias-concentration plots are similar for both models, although the CALGRID-IV estimates appear to be slightly more negatively biased. On the 7th, for concentrations above 9 pphm, both models underestimate ozone concentrations but this bias is nearly double for CALGRID-IV compared with the UAM-IV.

The error times series plots (Figure 6-3a) show that the CALGRID-IV and UAM-IV errors have similar diurnal patterns over the 6th; indeed, from Table 6-10b, the daily gross errors for the two models are identical -- 36.4%). On the 7th, the UAM-IV's gross errors are less than CALGRID-IV's, particularly during the early morning hours and during the afternoon high-ozone period.

Figures 6-3b and 6-3c display the error in ozone estimation as functions of observed concentration level for both models in the 6th and 7th. The UAM-IV's gross errors on the 6th tend to be slightly less than CALGRID-IV's on the 6th but on the 7th, above 9 pphm, the errors are approximately 50% to 60% of CALGRID-IV's.

#### Ozone Residuals as Functions of Concentration

Figure 6-4 contains the residual estimates for the two models as a function of ozone concentration level. The dispersion patterns of the residuals are similar for each model. On the 6th, the residuals tend to increase (either positively or negatively) above 8 pphm while in the 7th, the dispersion of the residuals appears to be independent of observed concentration level.

#### Scatterplots of Modeled and Observed Ozone Concentrations

The correlation between hourly pairs of modeled and observed ozone values ( $\geq 4$  pphm) is presented in Figure 6-5. On the 6th, above 9 pphm essentially all of the model estimates are within a factor of two of the observations. Below 9 pphm, both models underestimate some of the observations by factors larger than 2. On the 7th, the correlation of hourly pairs produced by the UAM-IV is better than for CALGRID-IV, where several pairs above 9 pphm are outside the factor of 2 agreement envelope.

The correlation between daily maximum modeled and observed ozone values at the monitoring stations is presented in Figure 6-6. On the 6th, both models produce the same number of overestimated (5) and underestimated (4) stations. On the 7th, two thirds (8) of the maximum estimate-observation pairs are underestimated for CALGRID-IV, while for the UAM-IV they are evenly distributed (in number) about the perfect correlation line. For both simulation days, all but one maximum estimate-observation pairs fall within a factor of 2 agreement.

#### Mean and Standard Deviation of Ozone Concentrations

Figure 6-7 presents the standard deviation of measured and observed hourly ozone concentrations as a function of time throughout the three day episode. The modeled and observed deviations agree well on the 6th, particularly during midday. In the early morning and late evening hours, both models exhibit less variability in the hourly values (compared with the hourly means) than the measurements. In contrast,

on the 7th, the models give the largest variability around midday whereas the measurement variability reached its greatest level in mid- to late-afternoon.

The mean hourly measured and observed ozone concentrations (averaged over all monitoring stations) is shown in Figure 6-8. For both the 6th and 7th, CALGRID-IV hourly means are slightly less than those for the UAM-IV and the peak values for CALGRID-IV occur 2 and 1 hours earlier than those for the UAM-IV on the two days. The UAM-IV reproduces the hourly averages on the 7th quite well.

### Time Series

Hourly time series plots of estimated and observed ozone, NO, and NO<sub>2</sub> concentrations over the three day episode are presented in Figure 6-9. The solid line represents the UAM-IV results and the dotted line corresponds to CALGRID-IV. The asterisks represent the measured values. The stations are presented in order proceeding from west to east across the SCCAB.

On the western end of the basin (e.g., Vandenburg, Lompoc, Santa Ynez) the observed ozone levels are fairly low with measured peaks in the 5-7 pphm range. Both models systematically overestimate ozone in this region throughout the episode and the CALGRID-IV's overestimation is slightly larger than that for the UAM-IV. At the El Capitan, Goleta, and Santa Barbara monitors, the UAM-IV captures the general buildup of ozone levels from the 6th into the 7th fairly well; CALGRID-IV does not reproduce this buildup pattern. The UAM-IV tends to underestimate the peak ozone in this region on the 7th by about 2 pphm (see the Goleta and Santa Barbara plots) and the modeled peak is "narrower" (in time) compared with the observed time series.

Mid-basin, both models poorly replicate the observed ozone peaks at Casitas on the 6th and 7th and CALGRID-IV produces maximum ozone levels several hours earlier on the 7th compared with UAM-IV. At Ojai, better agreement in the estimated and observed time series is obtained, with the UAM-IV producing better agreement with the elevated afternoon ozone levels than CALGRID-IV, especially on the 7th. At El Rio, where the observed peaks are in the 6-7 pphm range on the 6th and 7th, both models match the magnitudes of the peaks quite well. The UAM-IV slightly overestimates the peaks while CALGRID-IV slightly underestimates them. CALGRID-IV simulates peak ozone at the El Rio monitor 2-3 hours earlier than UAM-IV.

In the eastern basin (e.g., Thousand Oaks, Piru, and Simi), both models reproduce the general buildup of ozone levels from the 5th to the 6th but neither adequately captures the reduction in peak ozone that occurred at these monitors on the 7th. At Thousand Oaks and Piru, both models simulate the peak value to within 2 pphm at about the correct time. CALGRID-IV ozone estimates at Piru are systematically higher than the UAM-IV values for most of the daylight period. At Piru and Simi on the 7th,

both models significantly overestimate the peak observed values of 10 pphm and 13 pphm, respectively.

### Horizontal and Vertical Ozone Distributions

Figure 6-10 contains a number of ozone plots depicting the time-evolution of the surface and upper-level ozone distributions produced by the models during the 5-7 September, 1984 episode. Ground-level ozone fields are given for each day on a 2-hour interval basis between 1200 and 1800. In addition, vertical ozone isopleths along east-west and north-south transect of the basin are given at 1400 to provide some indication of the differences and similarities of the upper-level ozone distributions produced by the two models. (The ozone isopleths are contoured in units of pphm). The location of the observation site is underneath the first letter of the name.

On the 6th, ozone levels in the western basin are in the 6-8 pphm range; in the eastern basin they vary from 10 to 20 pphm or more. In both models the region of high ozone appears as a cloud whose western boundary has a primarily north-south orientation (see Figure 6-10e). From 1400 to 1800, an east-west oriented band of high surface ozone is simulated by the UAM-IV extending from the Santa Barbara-Ventura county line eastward. This feature is only weakly evident in the CALGRID-IV results. Both models produce small regions of ozone exceeding 20 pphm in the extreme eastern portion of the modeling domain between 1200 and 1400.

During mid-afternoon (1400) on the 6th, the vertical ozone distributions from the two models (Figures 6-10f-s1 through 6-10f-s4) reveal the presence of a large volume of ozone in the northeast portion of the domain approximately 250 meters above the surface extending to the top of the model domain (1000 meters). The western and southern boundaries of this "elevated ozone cloud" is located near Piru. Generally, the vertical ozone distributions produced by UAM-IV and CALGRID-IV at this hour are quite similar.

The afternoon ozone distributions on the 7th (Figures 6-10i through 6-10l) are similar to those of the 6th. The UAM-IV again simulates an east-west band of high surface ozone, now beginning offshore Goleta and extending inland to Piru. This feature is noticeably absent in the CALGRID-IV simulation. Aloft, an elevated ozone cloud is again simulated in the northeastern portion of the domain by both models. The cloud (arbitrarily defined by the 20 pphm contour) is approximately 250 meters above ground and extends up to the top of the model domain. Both models produce similar results in the vertical distribution of this cloud and in the magnitude of the peak concentrations aloft. For example, along the east-west transect at 1400, CALGRID-IV produces a peak ozone value aloft 29.5 pphm, compared with 27.5 pphm for the UAM-IV.

## Maximum Daily Ozone Isopleths

Figure 6-11 is a maximum daily ozone residual plot that is constructed by subtracting the peak gridded CALGRID-IV ozone estimates from the UAM-IV peak estimates and contouring the residuals. Thus, for example, solid isopleths represent subregions where the UAM-IV produced maximum daily ozone values exceeding those from CALGRID-IV, irrespective of time of occurrence. Recall from the ozone time series plots presented earlier that the CALGRID-IV peaks tend to be an hour or so earlier than the UAM-IV's.

On the 6th, the UAM-IV simulates 2-3 pphm more ozone than CALGRID-IV over the Santa Barbara channel region, along a thin east-west band north of the city of Santa Barbara, and in the vicinity of Simi. CALGRID-IV estimates more ground level ozone than UAM-IV in two areas: north of a line connecting Ojai and Piru, and north of Santa Ynez and north of Simi. The largest difference between the two models over the full domain is 3.9 pphm northeast of Ojai. This general pattern is reproduced on the 7th but the extent of differences between the two model's peak estimates is much larger. Specifically, over the Santa Barbara channel, the UAM-IV estimates ozone levels as much as 7.5 pphm higher than CALGRID-IV. North of Santa Ynez and in the northeast portion of the domain, the maximum CALGRID-IV ozone levels are as much as 4.6 pphm larger than those from the UAM-IV.

### 6.3 Base Case UAM-IV and CALGRID-IV Evaluations for the 16-17 September, 1984 Episode

#### 6.3.1 Statistical Measures

As with the 5-7 September, episode, UAM-IV and CALGRID-IV both significantly underestimated the maximum hourly NO concentrations during the 16-17 September, 1984 episode. From Table 6-11 the 10-station average of the peak NO observations was 3.6 pphm on both days. The UAM-IV produced overall averages of 1.9 pphm and 1.3 pphm while CALGRID-IV gave averages of 0.9 pphm and 0.6 pphm for the two days. Both models significantly underestimated the peak one-hour values on both days. For example, on the 17th, the maximum observed NO was 11 pphm at the Simi and Santa Barbara monitors. CALGRID-IV produced a peak of 1.8 pphm at Santa Barbara while UAM-IV gave 5.3 pphm at Ventura. In general, the UAM-IV produced NO peaks approximately double those for CALGRID-IV during this episode.

The NO<sub>2</sub> results for both models (Table 6-12) again agree somewhat better with observations than the NO comparisons. Both models underestimate NO<sub>2</sub> concentration; the UAM-IV NO<sub>2</sub> peaks are in better agreement with observations than those from CALGRID-IV. For example, the average peak NO<sub>2</sub> UAM-IV estimates over the 10 stations on the 17th was 2.0 pphm compared with 1.2 pphm for CALGRID-IV. The average measured peak NO<sub>2</sub> was 3.5 pphm.

Both models tended to underestimate the peak one-hour ozone concentrations (averaged over the 15 monitoring stations) on the 17th (Table 6-13). UAM-IV and CALGRID-IV underestimated the average station peak ozone value of 9.3 pphm by -22% and -24%, respectively. On the 16th, the UAM-IV's estimates of the average station peak ozone value was slightly poorer than those for CALGRID-IV.

Tables 6-14 through 6-16 present overall accuracy, bias and error results for the three days. CALGRID's NO estimates are systematically underestimated by -83%, essentially the same negative bias as in the 5-7 September, episode. The UAM-IV's NO estimates are also underestimated, ranging from -58% to -74%. Both models give peak one hour NO estimates that are no more than about 32% (CALGRID-IV) to 48% (UAM-IV) of the maximum one-hour observed peaks. For NO<sub>2</sub>, CALGRID-IV underestimates hourly concentrations by -40% to -69%. The degree of systematic bias (i.e., underestimation) by UAM-IV is less, ranging between -22% to -49%. Both model's give gross errors in the 50% to 70% percent range with the UAM's average discrepancy being slightly less. Both model's tend to underestimate the peak one-hour NO<sub>2</sub> concentrations. However, on the 16th, the UAM-IV overestimated the peak one hour value of 5.0 pphm at Santa Barbara by 0.2 pphm.

The systematic bias in CALGRID-IV and UAM-IV hourly ozone estimates on the 17th are -16% and -14%, respectively as indicated in Table 6-16. Gross errors for both models are approximately the same (27% and 29%, respectively). UAM-IV's estimate of the maximum measured ozone concentration during the 16-17 September episode (14.0 pphm at Casitas) is 11.6 pphm (at Ojai). CALGRID-IV produced a maximum of 10.0 pphm at Ojai.

### 6.3.2 Graphical Results

Figures 6-12 through 6-22 contain the graphical analyses carried out for the two models with the 16-17 September data base. As before, we devote primary attention to the results on the second day of the simulation, i.e., 17 September, 1984, but many of the graphics are presented for the 16th.

#### Accuracy of Peak Estimation

Figures 6-12a and 6-12b present summaries of the five different measures of model "accuracy" in estimating peak one-hour ozone concentrations on the two simulation days. On the 17th, the two models produce generally similar values of the five measures; the UAM-IV accuracy measure are slightly better than those for CALGRID-IV. This finding is consistent with the trend seen in the 5-7 September simulation results.

Figures 6-12c and 6-12f present the accuracy of peak estimation at each of the monitoring stations during the 16-17 September episode. On the 16th, CALGRID-IV

systematically produces lower ozone peaks at the monitoring stations compared with the UAM-IV, whereas on the 17th, both models produce approximately similar peaks at the various stations. From Figures 6-12e and 6-12f, we see that the temporally-unpaired peak ozone estimates for the UAM-IV tend to be better across nearly all of the monitoring stations compared with CALGRID-IV.

#### Bias and Error as Functions of Time and Concentration

Figures 6-13 and 6-14 depict model bias and error in hourly ozone estimates (equal to or greater than 4 pphm) as functions of time throughout the two-day episode and as a function of observed concentration level. The bias time series (Figure 6-13a) on the 17th are generally similar for both models. However, during the early morning through mid-day hours, the UAM-IV underestimates ozone levels substantially more than does CALGRID-IV. In the afternoon of the 17th, however, the UAM-IV bias is very close to zero while CALGRID-IV underestimates by 10 to 20%. After sunset, the underestimation problem with both models increases again.

The bias results for the 17th are somewhat different than for the 7th (presented in section 6.2.2). Recall that during the early morning hours of the 7th CALGRID-IV gave larger underestimation than UAM-IV; the opposite occurs on the 17th. Also, CALGRID-IV does not overestimate ozone midday on the 17th as it did during the 6th and 7th.

Figures 6-13b and 6-13c display the bias in ozone estimation as functions of observed concentration level for both models in the 16th and 17th. On the 16th, the UAM-IV tends to overestimate ozone concentrations (relative to CALGRID-IV) from 4-6 pphm and above 9 pphm the UAM-IV's degree of underestimation is slightly less than that for CALGRID-IV. On the 17th, both models produce nearly identical negative bias-concentration plots for ozone levels above 4 pphm. From 8 to 13 pphm, the bias is nearly constant for both models at approximately -30%.

The error time series plots (Figure 6-14a) show that the CALGRID-IV and UAM-IV errors have similar patterns on the 17th after approximately 1200. However, from midnight to noon on the 17th, the UAM-IV exhibits substantially larger error than CALGRID-IV. After 1200, the UAM-IV's errors are less than CALGRID-IV's but, because of the large UAM-IV errors before noon, the overall gross error for UAM-IV in the 17th (29%) exceeds that for CALGRID-IV (27%). Figure 6-14a amply demonstrates the principal that reliance on overall statistics such as daily gross error or bias may mask important variations occurring within the diurnal cycle. In the present instance we see that the UAM-IV performs better than CALGRID-IV during the high afternoon ozone period of the 17th while CALGRID-IV provides much smaller errors during the morning and pre-noon hours when ozone levels are moderate.

Figures 6-14b and 6-14c display the gross error in ozone estimation as functions of observed concentration level for both models in the 16th and 17th. Above 5 pphm

on the 16th, the UAM-IV's gross errors are systematically smaller than CALGRID-IV's while on the 17th the error-concentration plots are roughly comparable.

### Ozone Residuals as Functions of Concentration

Figure 6-15b contains the residual estimates for the two models as a function of ozone concentration level on the 17th. While the dispersion patterns of the residuals are similar for each model, at every concentration level, the dispersion of the CALGRID-IV residuals is less than (or equal to) that of the UAM-IV. Both models exhibit the tendency to underestimate as concentration levels increase.

### Scatterplots of Modeled and Observed Ozone Concentrations

The correlation between hourly pairs of modeled and observed ozone values is presented in Figure 6-16. On the 17th, CALGRID-IV produces fewer estimates that are outside factor of 2 agreement than UAM-IV. This is the opposite of the 7 September results where correlation of hourly pairs produced by the UAM-IV was better than CALGRID-IV. The scatterplot of daily maximum modeled and observed ozone values at the monitoring stations is presented in Figure 6-17. On the 17th, both models produce the same number of overestimated (3) and underestimated (12) stations. For both models, all maximum estimate-observation pairs fall within a factor of 2 agreement.

### Mean and Standard Deviation of Ozone Concentrations

Figure 6-18 presents the standard deviation of measured and observed hourly ozone concentrations as a function of time throughout the two day episode. The modeled and observed deviations show much less agreement on the 17th than was shown on the 6th and 7th (Figure 6-7). Neither model reproduces the variability in hourly ozone concentrations particularly well, especially during midday. In the late afternoon hours, the UAM-IV begins to replicate the variability in the measurements but it is still underestimated.

The mean hourly measured and observed ozone concentrations (averaged over all monitoring stations) is shown in Figure 6-19. On the 17th, both models underestimate the domain mean ozone levels from around 1000 to 1800. Otherwise, the modeled and observed mean hourly ozone values are well replicated over the full two-day period.

### Time Series

Hourly time series concentration plots of ozone, NO, and NO<sub>2</sub> for the 16th-17th are presented in Figure 6-20. On the western end of the basin (e.g., Vandenburg, Lompoc, Santa Ynez, and Gaviota) the observed ozone levels are fairly low with measured peaks in the 5-6 pphm range. Both models replicate the diurnal trends

in the hourly ozone measurements in this region throughout the episode. At the Vandenburg stations, CALGRID-IV tends to produce slightly higher ozone than the UAM-IV while the converse is true at Santa Ynez. At night, the UAM-IV gives nearly twice the amount of ozone (4-6 pphm) as CALGRID-IV while the measured values are near zero.

At the El Capitan, Goleta, and Santa Barbara monitors, both models fail to capture the buildup to the peak mid-afternoon ozone concentrations. In particular, at Goleta and Santa Barbara, the models underestimate the peak values by 4-5 pphm. The extent of the underestimation in this subregion is roughly twice as great for the 17th as for the 6th and 7th (Figure 6-9). CALGRID-IV captures the timing of the ozone peak exactly; the UAM-IV peaks at these stations are 1 to 4 hours late.

Mid-basin, both models again poorly replicate the ozone peaks at Casitas (14 pphm) that was the highest observation during this episode. As with the earlier episode, at Ojai, better agreement in the estimated and observed time series is obtained, with the UAM-IV producing slightly better correspondence with the peak (11.6 pphm) than CALGRID-IV (10.0 pphm). Both models are late by 2 to 3 hours in estimating the time of the peak. At El Rio, where the observed peak on the 17th was 10 pphm, both models underestimate this value by roughly 35% to 50%.

In the eastern basin (e.g., Thousand Oaks, Piru, and Simi), neither model reproduces well the general buildup of ozone levels from the 16th to the 17th. At Thousand Oaks and Simi, both models significantly underestimate (i.e., by 3-4 pphm) the magnitude of the broad ozone peaks that lasted for as much as 4-5 hours after noon. CALGRID-IV continues to produce ozone maxima a few hours earlier than UAM-IV. Both models slightly underestimate the 10 pphm peak at Piru on the 17th.

#### Horizontal and Vertical Ozone Distributions

Figure 6-21 contains a number of ozone plots depicting the time-evolution of the surface and upper-level ozone distributions produced by the models during the 16-17 September, 1984 episode. Ground-level ozone fields are given for each day on a 2-hour interval basis between 1200 and 1800. In addition, vertical ozone isopleths along east-west and north-south transect of the basin are given at 1400 on the 17th.

On the 17th, ozone levels over the western basin are approximately 6 pphm in both models; in the eastern basin they vary from 10 to 12 pphm or more. Unlike the 5-7 September episodes, in both models the region of high ozone appears as a cloud that is aligned along a northwest-south east axis for the UAM-IV and along a southwest-northeast axis for CALGRID-IV. (Recall in the earlier episode the ozone cloud covered much of the eastern model domain). From 1400 to 1800, a region of moderately high ozone (8 to 12 pphm) forms in the northeastern portion of the CALGRID-IV simulation and appears to drift out of the modeling domain toward the end of the day. In contrast,

in the UAM-IV simulation, the ozone cloud is narrower and migrates southeast from Ojai (around 1400) toward Simi by 1800. The regions of high ozone in the two simulations do not overlap to any appreciable extent.

The mid-afternoon (1400) vertical ozone distributions from the two models (Figures 6-21f-s1 through 6-21f-s4) do not provide a direct explanation for the reason(s) why the two model's ozone plumes move in different directions. Along the east-west transect, the vertical ozone fields are quite similar. The north-south transect provides some information. It appears that the ozone plume in the CALGRID-IV model is a surface feature, that is, the area of high ozone is confined to the lowest layer in the model. At an elevation of approximately 200 meters above ground, the ozone levels drop off to a "background" level of 6 pphm. In the UAM-IV calculation, concentrations aloft are also 6 pphm or less.

#### Maximum Daily Ozone Isopleths

Figure 6-22 contains the daily ozone residual plots based on the differences between maximum gridded ozone concentrations produced by the two models. Recall that solid isopleths represent subregions where the UAM-IV produced maximum daily ozone values exceeding those from CALGRID-IV.

On the 17th, the UAM-IV simulates as much as 5.5 pphm more ozone than CALGRID-IV in the region just west of Piru. As in the 5-7 September simulation, CALGRID-IV estimates 4 to 6 pphm or more ground level ozone than UAM-IV in two areas: north of Piru and north of Santa Ynez. The largest difference between the two models over the full domain is 5.5 pphm near Piru. Comparing Figures 6-11c and 6-22b, we find that CALGRID-IV consistently produces high ozone levels relative to the UAM-IV in the northeastern portion of the domain.

Table 6-1. Peak Ozone Concentrations for Three UAM Simulations of the 5-7 September, 1984 Episode. (Concentrations in pphm).

(a) 5 September, 1984

Monitoring Station	Maximum Observed O <sub>3</sub>	UAM-II (Tesche and McNally; 1991)	UAM-IV (Myers; 1990)	UAM-IV Present Study
ELRO	4.0	7.3	6.7	6.3
SIMI	9.0	10.0	12.7	11.5
SBAR	5.0	9.2	8.1	8.3
CASI	10.0	12.0	11.2	10.7
PIRU	6.0	8.7	9.8	11.9
OJAI	7.0	7.0	8.0	7.0
OAKS	7.0	8.2	8.3	8.5
ELCP	5.0	6.5	6.5	7.0
GOLA	7.0	6.7	6.9	6.9
VBGH	3.0	4.1	--	3.7
VBGW	4.0	3.8	--	3.8
SYNZ	6.0	8.3	--	7.9
LOMH	3.0	5.6	--	5.5
GAVI	8.0	6.3	--	6.3
AVG	6.0	7.4	8.7	7.5

Table 6-1. Continued.

(b) 6 September, 1984

Monitoring Station	Maximum Observed O <sub>3</sub>	UAM-II (Tesche and McNally; 1991)	UAM-IV (Myers; 1990)	UAM-IV Present Study
ELRO	6.0	8.2	7.4	7.1
SIMI	17.0	16.3	18.3	23.1
SBAR	4.0	11.5	10.2	8.7
CASI	13.0	9.9	12.71	7.5
PIRU	16.0	15.5	19.3	14.6
OJAI	13.0	15.2	16.2	11.0
OAKS	16.0	16.3	15.2	17.9
ELCP	10.0	6.2	6.8	6.8
GOLA	8.0	9.0	8.4	8.5
VBGH	3.0	4.9	—	5.0
VBGW	4.0	4.8	—	4.9
SYNZ	4.0	7.1	7.9	8.0
LOMH	3.0	6.8	—	6.9
GAVI	6.0	6.5	—	7.0
AVG	8.8	9.4	12.7	9.8

Table 6-1. Concluded.

(c) 7 September, 1984

Monitoring Station	Maximum Observed O <sub>3</sub>	UAM-II (Tesche and McNally; 1991)	UAM-IV (Myers; 1990)	UAM-IV Present Study
ELRO	7.0	8.2	8.0	7.9
SIMI	13.0	13.7	15.1	20.4
SBAR	15.0	16.5	12.9	12.9
CASI	18.0	12.6	9.8	9.0
PIRU	10.0	10.5	12.8	16.3
OJAI	13.0	18.1	14.3	12.0
OAKS	11.0	10.0	10.7	16.9
ELCP	11.0	13.4	14.0	11.1
GOLA	15.0	14.2	13.9	12.9
VBGH	6.0	5.7	-	6.3
VBGW	6.0	6.0	-	6.7
SYNZ	8.0	7.7	8.9	8.1
LOMH	6.0	7.1	-	6.8
GAVI	13.0	10.3	-	7.8
AVG	10.9	11.0	12.4	11.1

Table 6-2. UAM Ozone Model Evaluation Statistics for Three Simulations of the 5-7 September, 1984 Episode. (Concentrations in pphm).

(a) 5 September, 1984 (Cutoff = 4 pphm)

Performance Attribute	UAM-II (Tesche and McNally, 1991)	UAM-IV (Myers;1990)	UAM-IV Present Study
Maximum modeled concentration at a station	12.0 (Casitas)	12.7 (Simi)	11.9 (Piru)
Maximum observed concentration at a station	10.0 (Casitas)	10.0 (Casitas)	10.0 (Casitas)
Ratio of maximum estimated to observed concentration	1.201	1.273	1.190
Accuracy of peak estimation (paired)	20%	12%	1%
Accuracy of peak estimation (unpaired)	20%	27%	34%
Mean normalized deviation (bias)	0.108	0.225	-0.032
Mean absolute normalized deviation (gross error)	0.377	0.388	0.456

Table 6-2. Continued.

(b) 6 September, 1984 (Cutoff = 4 pphm)

Performance Attribute	UAM-II (Tesché and McNally, 1991)	UAM-IV (Myers;1990)	UAM-IV Present Study
Maximum modeled concentration at a station	16.3 (Simi)	19.3 (Piru)	23.1 (Simi)
Maximum observed concentration at a station	17.0 (Simi)	17.0 (Simi)	17.0 (Simi)
Ratio of maximum estimated to observed concentration	0.961	1.133	1.359
Accuracy of peak estimation (paired)	-4%	8%	-25%
Accuracy of peak estimation (unpaired)	-4%	14%	63%
Mean normalized deviation (bias)	-0.056	0.063	-0.091
Mean absolute normalized deviation (gross error)	0.324	0.337	0.364

Table 6-2. Concluded.

(c) 7 September, 1984 (Cutoff = 4 pphm)

Performance Attribute	UAM-II (Tesche and McNally, 1991)	UAM-IV (Myers;1990)	UAM-IV Present Study
Maximum modeled concentration at a station	18.1 (Ojai)	15.1 (Simi)	20.4 (Simi)
Maximum observed concentration at a station	18.0 (Casitas)	18.0 (Casitas)	18.0 (Casitas)
Ratio of maximum estimated to observed concentration	1.004	0.836	1.133
Accuracy of peak estimation (paired)	-30%	-46%	-50%
Accuracy of peak estimation (unpaired)	-30%	-16%	22%
Mean normalized deviation (bias)	0.036	0.094	0.046
Mean absolute normalized deviation (gross error)	0.234	0.293	0.288

Table 6-3. Peak Ozone Concentrations for Two UAM Simulations of the 16-17 September, 1984 Episode. (Concentrations in pphm).

(a) 16 September, 1984

Monitoring Station	Maximum Observed O <sub>3</sub>	UAM-II (Tesche and McNally; 1991)	UAM-IV Present Study
ELRO	6.0	7.5	8.3
SIMI	11.0	10.9	9.2
SBAR	5.0	6.8	7.8
CASI	8.0	7.6	7.8
PIRU	8.0	11.6	12.0
OJAI	8.0	10.2	8.3
OAKS	9.0	7.5	7.3
ELCP	6.0	6.1	7.5
GOLA	6.0	6.5	7.7
VBGH	6.0	5.3	5.5
VBGW	5.0	5.0	5.0
SYNZ	5.0	6.8	7.9
LOMH	5.0	5.9	6.2
GAVI	4.0	4.8	5.6
VENT	7.0	7.9	7.6
AVG	6.6	7.4	7.6

Table 6-3. Concluded.

(b) 17 September, 1984

Monitoring Station	Maximum Observed O <sub>3</sub>	UAM-II (Tesche and McNally; 1991)	UAM-IV Present Study
ELRO	10.0	8.4	6.5
SIMI	13.0	10.7	10.2
SBAR	12.0	11.1	7.4
CASI	14.0	11.5	8.3
PIRU	10.0	12.3	8.5
OJAI	12.0	12.5	11.5
OAKS	12.0	9.3	7.3
ELCP	6.0	6.8	6.8
GOLA	11.0	8.6	7.8
VBGH	6.0	5.3	5.4
VBGW	6.0	5.1	5.1
SYNZ	6.0	6.5	7.1
LOMH	4.0	5.5	5.8
GAVI	7.0	5.5	6.0
VENT	10.0	8.0	6.4
AVG	9.3	8.5	7.3

Table 6-4. UAM Ozone Model Evaluation Statistics for Two Simulations of the 16-17 September, 1984 Episode. (Concentrations in pphm).

(a) 16 September, 1984 (Cutoff = 4 pphm)

Performance Attribute	UAM-II (Tesche and McNally, 1991)	UAM-IV Present Study
Maximum modeled concentration at a station	11.0 (Piru)	12.0 (Piru)
Maximum observed concentration at a station	11.0 (Simi)	11.0 (Simi)
Ratio of maximum estimated to observed concentration	1.000	1.090
Accuracy of peak estimation (paired)	0%	-16%
Accuracy of peak estimation (unpaired)	0%	12%
Mean normalized deviation (bias)	0.093	0.106
Mean absolute normalized deviation (gross error)	0.264	0.294

(b) 17 September, 1984 (Cutoff = 4 pphm)

Performance Attribute	UAM-II (Tesche and McNally, 1991)	UAM-IV Present Study
Maximum modeled concentration at a station	12.5 (Ojai)	11.6 (Ojai)
Maximum observed concentration at a station	14.0 (Casitas)	14.0 (Casitas)
Ratio of maximum estimated to observed concentration	0.891	0.829
Accuracy of peak estimation (paired)	18%	-41%
Accuracy of peak estimation (unpaired)	11%	-11%
Mean normalized deviation (bias)	-0.046	-0.142
Mean absolute normalized deviation (gross error)	0.262	0.293

Table 6-5. Peak NO Concentrations for the UAM-IV and CALGRID-IV Models for the 5-7 September, 1984 Episode. (Concentrations in pphm).

(a) 5 September, 1984

Monitoring Station	Maximum Observed NO	CALGRID-IV	UAM-IV
ELRO	7.0	2.1	3.6
SIMI	21.0	1.3	1.5
VENT	8.0	1.2	2.3
SBAR	18.0	1.8	3.5
CASI	2.0	1.3	2.0
ELCP	7.0	0.4	1.2
VBGH	1.0	0.3	0.6
VBGW	0.0	0.1	0.1
LOMH	5.0	0.2	0.3
MOLI	10.0	1.0	2.1
GAVI	10.0	0.3	0.5
AVG	8.1	0.9	1.6

Table 6-5. Continued.

(b) 6 September, 1984

Monitoring Station	Maximum Observed NO	CALGRID-IV	UAM-IV
ELRO	5.0	1.6	3.9
SIMI	19.0	2.1	2.8
VENT	11.0	0.8	1.9
SBAR	4.0	2.0	1.8
CASI	1.0	0.9	1.1
ELCP	3.0	0.3	0.6
VBGH	1.0	0.2	0.2
VBGW	0.0	0.1	0.0
LOMH	4.0	0.0	0.1
MOLI	4.0	0.5	0.3
GAVI	4.0	0.1	0.1
<b>AVG</b>	<b>5.1</b>	<b>0.8</b>	<b>1.2</b>

Table 6-5. Concluded.

(c) 7 September, 1984

Monitoring Station	Maximum Observed NO	CALGRID-IV	UAM-IV
ELRO	4.0	0.7	2.0
SIMI	10.0	1.5	1.4
VENT	11.0	1.4	2.6
SBAR	4.0	1.5	1.7
CASI	1.0	0.9	0.9
ELCP	3.0	0.1	0.3
VBGH	1.0	0.1	0.2
VBGW	3.0	0.1	0.1
LOMH	6.0	0.0	0.0
MOLI	4.0	0.3	0.2
GAVI	2.0	0.2	0.4
<b>AVG</b>	<b>4.5</b>	<b>0.6</b>	<b>0.9</b>

Table 6-6. Peak NO<sub>2</sub> Concentrations for the UAM-IV and CALGRID-IV Models for the 5-7 September, 1984 Episode. (Concentrations in pphm).

(a) 5 September, 1984

Monitoring Station	Maximum Observed NO <sub>2</sub>	CALGRID-IV	UAM-IV
SBAR	5.0	2.2	2.6
ELCP	3.0	1.9	1.9
VBGH	3.0	1.8	2.0
VBGW	1.0	1.8	2.0
LOMH	2.0	2.0	1.9
MOLI	4.0	2.1	2.2
GAVI	4.0	2.1	2.2
<b>AVG</b>	3.1	2.0	2.1

Table 6-6. Concluded.

(b) 6 September, 1984

Monitoring Station	Maximum Observed NO <sub>2</sub>	CALGRID-IV	UAM-IV
ELRO	7.0	4.3	5.2
SIMI	8.0	3.8	3.8
VENT	2.0	1.2	2.3
SBAR	5.0	3.3	5.9
ELCP	5.0	0.7	2.3
VBGH	9.0	0.5	0.9
VBGW	1.0	0.4	0.9
LOMH	1.0	0.2	0.6
MOLI	3.0	1.5	1.4
GAVI	3.0	1.2	1.6
<b>AVG</b>	<b>4.4</b>	<b>1.7</b>	<b>2.5</b>

Table 6-6. Concluded.

(c) 7 September, 1984

Monitoring Station	Maximum Observed NO <sub>2</sub>	CALGRID-IV	UAM-IV
ELRO	5.0	4.5	5.5
SIMI	7.0	3.2	3.7
VENT	6.0	2.4	3.8
SBAR	9.0	3.2	4.8
ELCP	5.0	0.6	2.5
VBGH	1.0	0.5	0.8
VBGW	2.0	0.4	1.1
LOMH	4.0	0.2	0.3
MOLI	6.0	1.1	1.2
GAVI	4.0	1.0	1.3
AVG	4.9	1.7	2.5

Table 6-7. Peak Ozone Concentrations for the UAM-IV and CALGRID-IV Models for the 5-7 September, 1984 Episode. (Concentrations in pphm).

(a) 5 September, 1984

Monitoring Station	Maximum Observed O <sub>3</sub>	CALGRID-IV	UAM-IV
ELRO	4.0	4.0	6.3
SIMI	9.0	14.7	11.5
SBAR	5.0	6.6	8.3
CASI	10.0	7.3	10.7
PIRU	6.0	13.7	11.9
OJAI	7.0	8.7	7.0
OAKS	7.0	10.5	8.5
ELCP	5.0	5.4	7.0
GOLA	7.0	6.0	6.9
VBGH	3.0	5.5	3.7
VBGW	4.0	4.8	3.8
SYNZ	6.0	14.3	7.9
LOMH	3.0	6.4	5.5
GAVI	8.0	8.2	6.3
AVG	6.0	8.3	7.5

Table 6-7. Continued

(b) 6 September, 1984

Monitoring Station	Maximum Observed O <sub>3</sub>	CALGRID-IV	UAM-IV
ELRO	6.0	6.4	7.1
SIMI	17.0	20.7	23.1
SBAR	4.0	8.9	8.7
CASI	13.0	8.1	7.5
PIRU	16.0	17.3	14.6
OJAI	13.0	9.3	11.0
OAKS	16.0	18.1	17.9
ELCP	10.0	6.0	6.8
GOLA	8.0	7.2	8.5
VBGH	3.0	6.7	5.0
VBGW	4.0	6.2	4.9
SYNZ	4.0	10.0	8.0
LOMH	3.0	7.2	6.9
GAVI	6.0	8.5	7.0
AVG	8.8	10.0	9.8

Table 6-7. Concluded.

(c) 7 September, 1984

Monitoring Station	Maximum Observed O <sub>3</sub>	CALGRID-IV	UAM-IV
ELRO	7.0	6.0	7.9
SIMI	13.0	18.9	20.4
SBAR	15.0	9.4	12.9
CASI	18.0	7.5	9.0
PIRU	10.0	20.1	16.3
OJAI	13.0	9.4	12.0
OAKS	11.0	17.5	16.9
ELCP	11.0	6.3	11.1
GOLA	15.0	8.6	12.9
VBGH	6.0	6.0	6.3
VBGW	6.0	5.5	6.7
SYNZ	8.0	9.8	8.1
LOMH	6.0	6.5	6.8
GAVI	13.0	8.3	7.8
AVG	10.9	10.0	11.1

Table 6-8. UAM-IV and CALGRID-IV NO Model Evaluation Statistics for the 5-7 September, 1984 Episode. (Concentrations in pphm).

(a) 5 September, 1984 (Cutoff = 1 pphm)

Performance Attribute	CALGRID-IV	UAM-IV
Maximum modeled concentration at a station	2.1 (El Rio)	3.6 (El Rio)
Maximum observed concentration at a station	21.0 (Simi)	21.0 (Simi)
Ratio of maximum estimated to observed concentration	0.100	0.171
Accuracy of peak estimation (paired)	-97%	-97%
Accuracy of peak estimation (unpaired)	-82%	-49%
Mean normalized deviation (bias)	-0.828	-0.774
Mean absolute normalized deviation (gross error)	0.840	0.842

Table 6-8. Continued.

(b) 6 September, 1984 (Cutoff = 1 pphm)

Performance Attribute	CALGRID-IV	UAM-IV
Maximum modeled concentration at a station	2.1 (Simi)	3.9 (El Rio)
Maximum observed concentration at a station	19.0 (Simi)	19.0 (Simi)
Ratio of maximum estimated to observed concentration	0.111	1.359
Accuracy of peak estimation (paired)	-94%	-98%
Accuracy of peak estimation (unpaired)	-75%	-72%
Mean normalized deviation (bias)	-0.849	-0.790
Mean absolute normalized deviation (gross error)	0.854	0.851

Table 6-8. Concluded.

(c) 7 September, 1984 (Cutoff = 1 pphm)

Performance Attribute	CALGRID-IV	UAM-IV
Maximum modeled concentration at a station	1.5 (Simi)	2.6 (Ventura)
Maximum observed concentration at a station	11.0 (Ventura)	11.0 (Ventura)
Ratio of maximum estimated to observed concentration	0.136	0.236
Accuracy of peak estimation (paired)	-99%	-100%
Accuracy of peak estimation (unpaired)	-63%	-47%
Mean normalized deviation (bias)	-0.870	-0.805
Mean absolute normalized deviation (gross error)	0.877	0.833

Table 6-9. UAM-IV and CALGRID-IV NO<sub>2</sub> Model Evaluation Statistics for the 5-7 September, 1984 Episode. (Concentrations in pphm).

(a) 5 September, 1984 (Cutoff = 1 pphm)

Performance Attribute	CALGRID-IV	UAM-IV
Maximum modeled concentration at a station	2.2 (Santa Barb)	2.6 (Santa Barb)
Maximum observed concentration at a station	5.0 (Santa Barb)	5.0 (Santa Barb)
Ratio of maximum estimated to observed concentration	0.440	0.520
Accuracy of peak estimation (paired)	-66%	-60%
Accuracy of peak estimation (unpaired)	20%	109%
Mean normalized deviation (bias)	-0.554	-0.430
Mean absolute normalized deviation (gross error)	0.651	0.603

Table 6-9. Continued.

(b) 6 September, 1984 (Cutoff = 1 pphm)

Performance Attribute	CALGRID-IV	UAM-IV
Maximum modeled concentration at a station	4.3 (El Rio)	5.9 (Santa Barb)
Maximum observed concentration at a station	8.0 (Simi)	8.0 (Simi)
Ratio of maximum estimated to observed concentration	0.538	0.738
Accuracy of peak estimation (paired)	-96%	-94%
Accuracy of peak estimation (unpaired)	-21%	7%
Mean normalized deviation (bias)	-0.577	-0.404
Mean absolute normalized deviation (gross error)	0.640	0.593

Table 6-9. Concluded.

(c) 7 September, 1984 (Cutoff = 1 pphm)

Performance Attribute	CALGRID-IV	UAM-IV
Maximum modeled concentration at a station	4.5 (El Rio)	5.5 (El Rio)
Maximum observed concentration at a station	9.0 (Santa Barb)	9.0 (Santa Barb)
Ratio of maximum estimated to observed concentration	0.500	0.611
Accuracy of peak estimation (paired)	-64%	-53%
Accuracy of peak estimation (unpaired)	9%	18%
Mean normalized deviation (bias)	-0.697	-0.494
Mean absolute normalized deviation (gross error)	0.725	0.635

Table 6-10. UAM-IV and CALGRID-IV Ozone Model Evaluation Statistics for the 5-7 September, 1984 Episode. (Concentrations in pphm).

(a) 5 September, 1984 (Cutoff = 4 pphm)

Performance Attribute	CALGRID-IV	UAM-IV
Maximum modeled concentration at a station	14.7 (Simi)	11.9 (Piru)
Maximum observed concentration at a station	10.0 (Casitas)	10.0 (Casitas)
Ratio of maximum estimated to observed concentration	1.470	1.190
Accuracy of peak estimation (paired)	-39%	1%
Accuracy of peak estimation (unpaired)	121%	34%
Mean normalized deviation (bias)	-0.037	-0.032
Mean absolute normalized deviation (gross error)	0.410	0.456

Table 6-10. Continued.

(b) 6 September, 1984 (Cutoff = 4 pphm)

Performance Attribute	CALGRID-IV	UAM-IV
Maximum modeled concentration at a station	20.7 (Simi)	23.1 (Simi)
Maximum observed concentration at a station	17.0 (Simi)	17.0 (Simi)
Ratio of maximum estimated to observed concentration	1.176	1.359
Accuracy of peak estimation (paired)	-29%	-25%
Accuracy of peak estimation (unpaired)	48%	63%
Mean normalized deviation (bias)	-0.116	-0.091
Mean absolute normalized deviation (gross error)	0.364	0.364

Table 6-10. Concluded.

(c) 7 September, 1984 (Cutoff = 4 pphm)

Performance Attribute	CALGRID-IV	UAM-IV
Maximum modeled concentration at a station	20.1 (Simi)	20.4 (Simi)
Maximum observed concentration at a station	18.0 (Casitas)	18.0 (Casitas)
Ratio of maximum estimated to observed concentration	1.117	1.133
Accuracy of peak estimation (paired)	-72%	-50%
Accuracy of peak estimation (unpaired)	60%	22%
Mean normalized deviation (bias)	-0.041	0.046
Mean absolute normalized deviation (gross error)	0.340	0.288

Table 6-11. Peak NO Concentrations for the UAM-IV and CALGRID-IV Models for the 16-17 September, 1984 Episode. (Concentrations in pphm).

(a) 16 September, 1984

Monitoring Station	Maximum Observed NO	CALGRID-IV	UAM-IV
ELRO	6.0	1.6	3.8
SIMI	6.0	0.4	0.4
VENT	8.0	2.9	7.8
SBAR	9.0	1.7	3.2
CASI	1.0	1.1	1.8
ELCP	2.0	0.2	0.5
VBGH	0.0	0.2	0.3
VBGW	1.0	0.1	0.2
LOMH	--	--	--
MOLI	3.0	0.6	0.6
GAVI	0.0	0.3	0.4
<b>AVG</b>	<b>3.6</b>	<b>0.9</b>	<b>1.9</b>

Table 6-11. Concluded.

(b) 17 September, 1984

Monitoring Station	Maximum Observed NO	CALGRID-IV	UAM-IV
ELRO	1.0	1.3	1.9
SIMI	11.0	0.4	0.3
VENT	7.0	1.0	5.3
SBAR	11.0	1.8	2.7
CASI	1.0	0.9	3.1
ELCP	4.0	0.2	0.3
VBGH	1.0	0.1	0.2
VBGW	1.0	0.1	0.1
LOMH	1.0	0.0	0.1
MOLI	2.0	0.6	0.4
GAVI	0.0	0.1	0.1
<b>AVG</b>	3.6	0.6	1.3

Table 6-12. Peak NO<sub>2</sub> Concentrations for the UAM-IV and CALGRID-IV Models for the 16-17 September, 1984 Episode. (Concentrations in pphm).

(a) 16 September, 1984

Monitoring Station	Maximum Observed NO <sub>2</sub>	CALGRID-IV	UAM-IV
ELRO	4.0	3.7	5.2
SIMI	4.0	3.0	3.3
VENT	4.0	3.2	2.8
SBAR	5.0	2.6	5.2
ELCP	2.0	2.4	2.6
VBGH	1.0	0.6	1.0
VBGW	1.0	0.4	0.8
MOLI	3.0	1.7	2.0
GAVI	3.0	1.2	1.2
AVG	3.0	2.1	2.7

Table 6-12. Concluded.

(b) 17 September, 1984

Monitoring Station	Maximum Observed NO <sub>2</sub>	CALGRID-IV	UAM-IV
ELRO	0.0	2.3	3.6
SIMI	7.0	1.1	0.9
VENT	5.0	2.4	4.5
SBAR	5.0	2.1	4.9
ELCP	3.0	0.6	1.0
VBGH	2.0	0.6	1.0
VBGW	2.0	0.3	0.9
LOMH	3.0	0.1	0.3
MOLI	4.0	1.5	1.8
GAVI	4.0	0.6	1.4
AVG	3.5	1.2	2.0

Table 6-12. Peak NO<sub>2</sub> Concentrations for the UAM-IV and CALGRID-IV Models for the 16-17 September, 1984 Episode. (Concentrations in pphm).

(a) 16 September, 1984

Monitoring Station	Maximum Observed NO <sub>2</sub>	CALGRID-IV	UAM-IV
ELRO	4.0	3.7	5.2
SIMI	4.0	3.0	3.3
VENT	4.0	3.2	2.8
SBAR	5.0	2.6	5.2
ELCP	2.0	2.4	2.6
VBGH	1.0	0.6	1.0
VBGW	1.0	0.4	0.8
MOLI	3.0	1.7	2.0
GAVI	3.0	1.2	1.2
AVG	3.0	2.1	2.7

Table 6-12. Concluded.

(b) 17 September, 1984

Monitoring Station	Maximum Observed NO <sub>2</sub>	CALGRID-IV	UAM-IV
ELRO	0.0	2.3	3.6
SIMI	7.0	1.1	0.9
VENT	5.0	2.4	4.5
SBAR	5.0	2.1	4.9
ELCP	3.0	0.6	1.0
VBGH	2.0	0.6	1.0
VBGW	2.0	0.3	0.9
LOMH	3.0	0.1	0.3
MOLI	4.0	1.5	1.8
GAVI	4.0	0.6	1.4
AVG	3.5	1.2	2.0

Table 6-13. Peak Ozone Concentrations for the UAM-IV and CALGRID-IV Models for the 16-17 September, 1984 Episode. (Concentrations in pphm).

(a) 16 September, 1984

Monitoring Station	Maximum Observed O <sub>3</sub>	CALGRID-IV	UAM-IV
ELRO	6.0	5.0	8.3
SIMI	11.0	8.9	9.2
VENT	7.0	4.8	7.6
SBAR	5.0	6.1	7.8
CASI	8.0	7.2	7.8
PIRU	8.0	10.0	12.0
OJAI	8.0	7.8	8.3
OAKS	9.0	6.6	7.3
ELCP	6.0	5.2	7.5
GOLA	6.0	5.6	7.7
VBGH	6.0	5.9	5.5
VBGW	5.0	5.8	5.0
SYNZ	5.0	6.1	7.9
LOMH	5.0	5.5	6.2
GAVI	4.0	5.3	5.6
AVG	6.6	6.4	7.6

Table 6-13. Concluded.

(b) 17 September, 1984

Monitoring Station	Maximum Observed O <sub>3</sub>	CALGRID-IV	UAM-IV
ELRO	10.0	5.0	6.5
SIMI	13.0	8.8	10.2
VENT	10.0	6.1	6.4
SBAR	12.0	8.0	7.4
CASI	14.0	7.0	8.3
PIRU	10.0	9.4	8.5
OJAI	12.0	10.0	11.5
OAKS	12.0	7.8	7.3
ELCP	6.0	6.1	6.8
GOLA	11.0	7.2	7.8
VBGH	6.0	5.4	5.4
VBGW	6.0	5.4	5.1
SYNZ	6.0	7.7	7.1
LOMH	4.0	5.7	5.8
GAVI	7.0	6.6	6.0
<b>AVG</b>	<b>0.3</b>	<b>7.1</b>	<b>7.3</b>

Table 6-14. UAM-IV and CALGRID-IV NO Model Evaluation Statistics for the 16-17 September, 1984 Episode. (Concentrations in pphm).

(a) 16 September, 1984 (Cutoff = 1 pphm)

Performance Attribute	CALGRID-IV	UAM-IV
Maximum modeled concentration at a station	2.9 (Ventura)	3.8 (EL Rio)
Maximum observed concentration at a station	9.0 (Santa Barb)	9.0 (Santa Barb)
Ratio of maximum estimated to observed concentration	0.322	0.422
Accuracy of peak estimation (paired)	-96%	-85%
Accuracy of peak estimation (unpaired)	-1%	177%
Mean normalized deviation (bias)	-0.827	-0.583
Mean absolute normalized deviation (gross error)	0.831	0.843

Table 6-14. Concluded.

(b) 17 September, 1984 (Cutoff = 1 pphm)

Performance Attribute	CALGRID-IV	UAM-IV
Maximum modeled concentration at a station	1.8 (Santa Barb)	5.3 (Ventura)
Maximum observed concentration at a station	11.0 (Santa Barb)	11.0 (Santa Barb)
Ratio of maximum estimated to observed concentration	0.164	0.482
Accuracy of peak estimation (paired)	-99%	-100%
Accuracy of peak estimation (unpaired)	-52%	68%
Mean normalized deviation (bias)	-0.827	-0.736
Mean absolute normalized deviation (gross error)	0.834	0.868

Table 6-15. UAM-IV and CALGRID-IV NO<sub>2</sub> Model Evaluation Statistics for the 16-17 September, 1984 Episode. (Concentrations in pphm).

(a) 16 September, 1984 (Cutoff = 1 pphm)

Performance Attribute	CALGRID-IV	UAM-IV
Maximum modeled concentration at a station	3.7 (El Rio)	5.2 (Santa Barb)
Maximum observed concentration at a station	5.0 (Santa Barb)	5.0 (Santa Barb)
Ratio of maximum estimated to observed concentration	0.740	1.040
Accuracy of peak estimation (paired)	-49%	-13%
Accuracy of peak estimation (unpaired)	33%	46%
Mean normalized deviation (bias)	-0.395	-0.217
Mean absolute normalized deviation (gross error)	0.573	0.478

Table 6-15. Concluded.

(b) 17 September, 1984 (Cutoff = 1 pphm)

Performance Attribute	CALGRID-IV	UAM-IV
Maximum modeled concentration at a station	2.4 (Ventura)	4.9 (Santa Barb)
Maximum observed concentration at a station	7.0 (Simi)	7.0 (Simi)
Ratio of maximum estimated to observed concentration	0.343	0.700
Accuracy of peak estimation (paired)	-84%	-92%
Accuracy of peak estimation (unpaired)	-11%	3%
Mean normalized deviation (bias)	-0.688	-0.488
Mean absolute normalized deviation (gross error)	0.719	0.612

Table 6-16. UAM-IV and CALGRID-IV Ozone Model Evaluation Statistics for the 16-17 September, 1984 Episode. (Concentrations in pphm).

(a) 16 September, 1984 (Cutoff = 4 pphm)

Performance Attribute	CALGRID-IV	UAM-IV
Maximum modeled concentration at a station	10.0 (Piru)	12.0 (Piru)
Maximum observed concentration at a station	11.0 (Simi)	11.0 (Simi)
Ratio of maximum estimated to observed concentration	0.909	1.090
Accuracy of peak estimation (paired)	-28%	-16%
Accuracy of peak estimation (unpaired)	17%	12%
Mean normalized deviation (bias)	-0.030	0.106
Mean absolute normalized deviation (gross error)	0.213	0.294

Table 6-16. Concluded.

(b) 17 September, 1984 (Cutoff = 4 pphm)

Performance Attribute	CALGRID-IV	UAM-IV
Maximum modeled concentration at a station	10.0 (Ojai)	11.6 (Ojai)
Maximum observed concentration at a station	14.0 (Casitas)	14.0 (Casitas)
Ratio of maximum estimated to observed concentration	0.714	0.829
Accuracy of peak estimation (paired)	-51%	-41%
Accuracy of peak estimation (unpaired)	28%	-11%
Mean normalized deviation (bias)	-0.163	-0.142
Mean absolute normalized deviation (gross error)	0.274	0.293

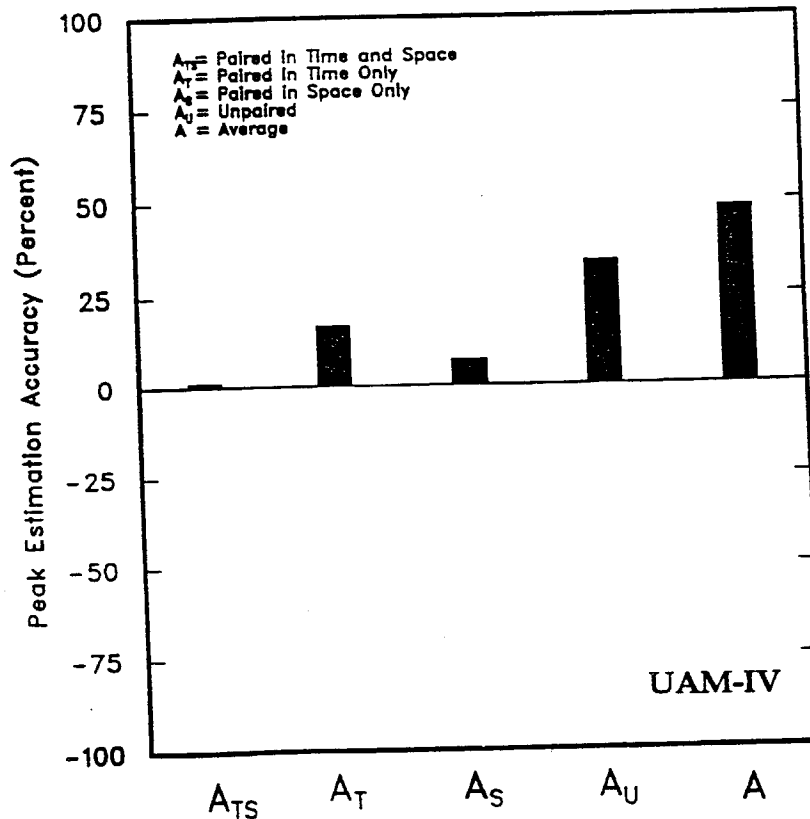
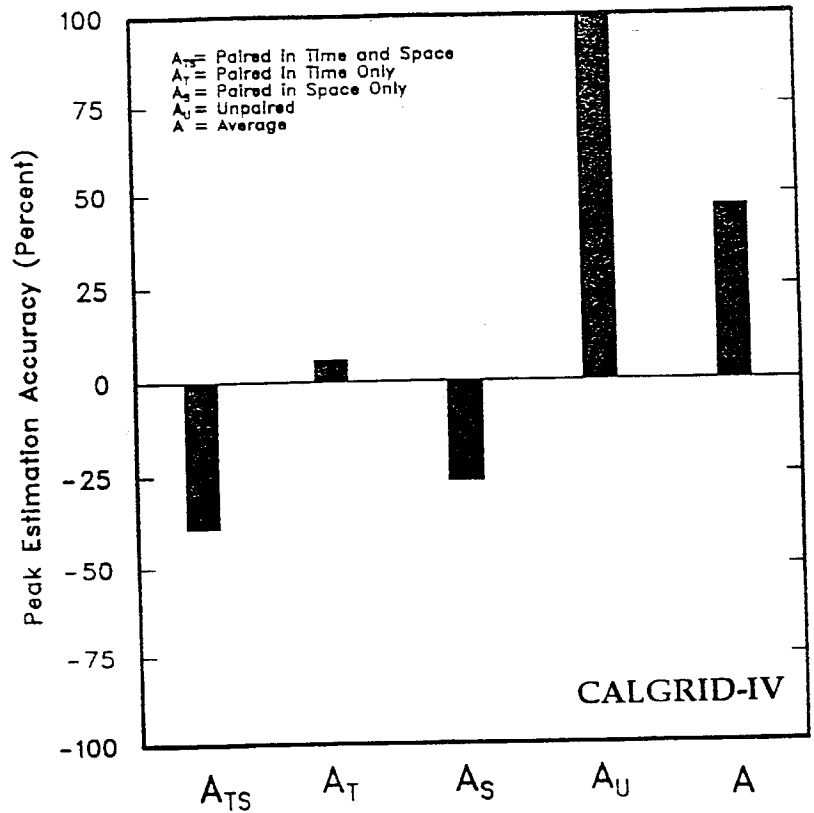


Figure 6-1a. Measures of Peak Ozone Estimation Accuracy for the 5-7 September, 1984 Episode -- 5 September, 1984.

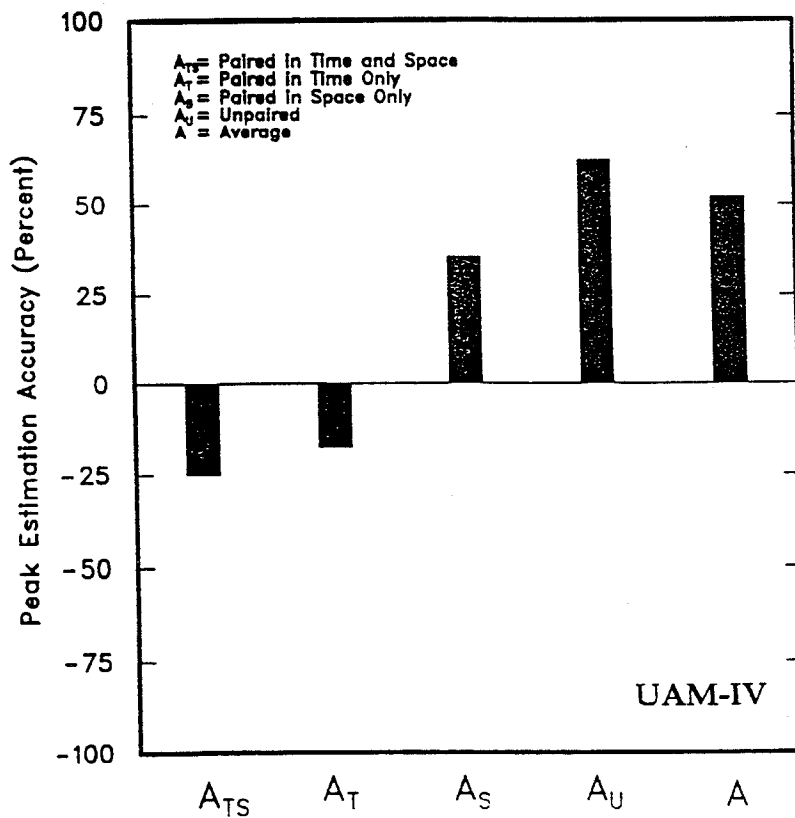
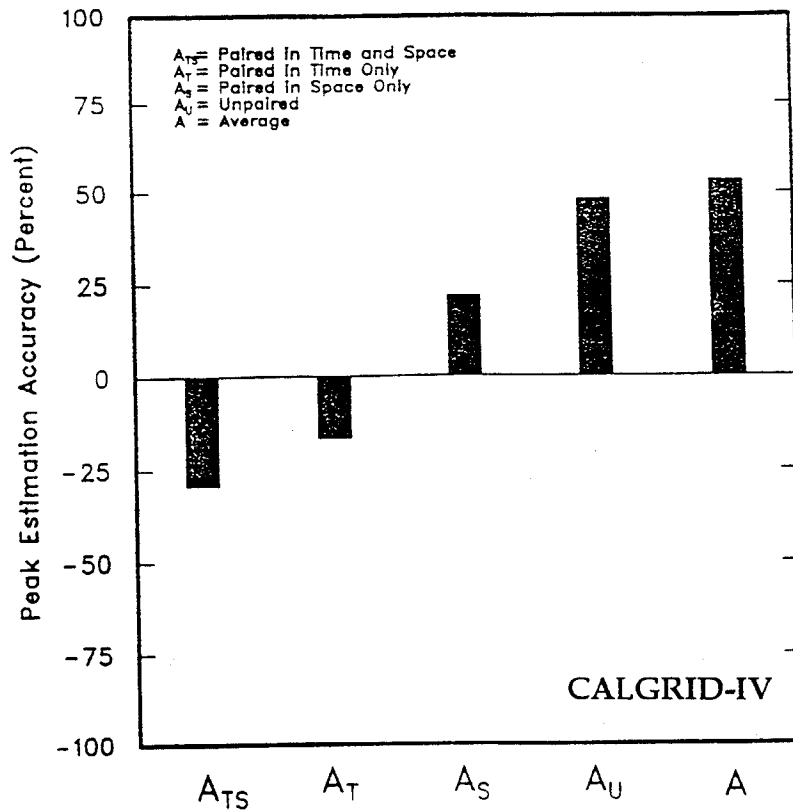


Figure 6-1b. Measures of Peak Ozone Estimation Accuracy for the 5-7 September, 1984 Episode -- 6 September, 1984.

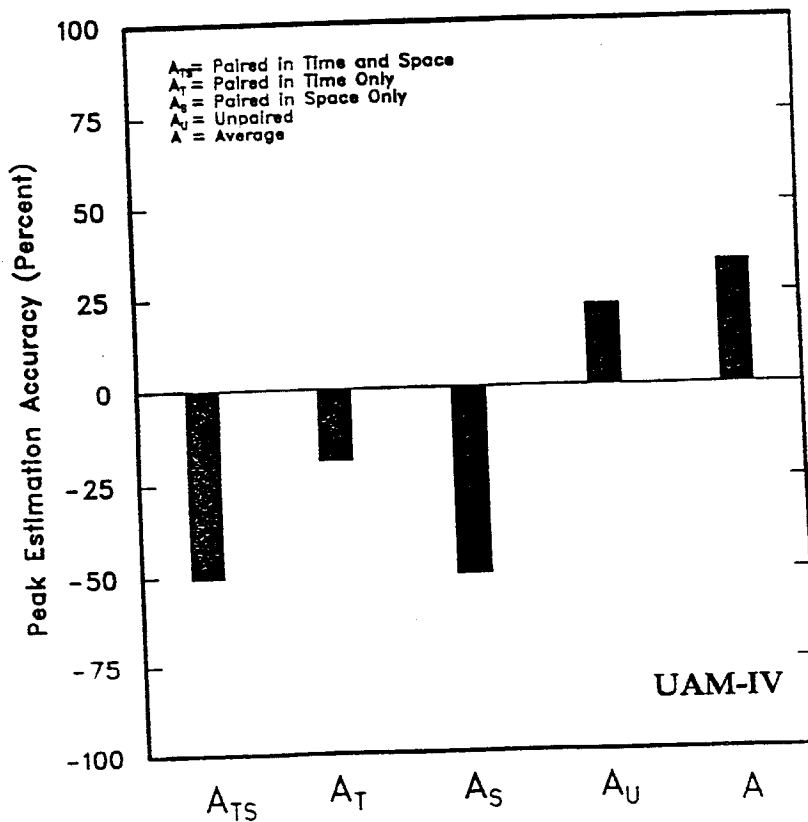
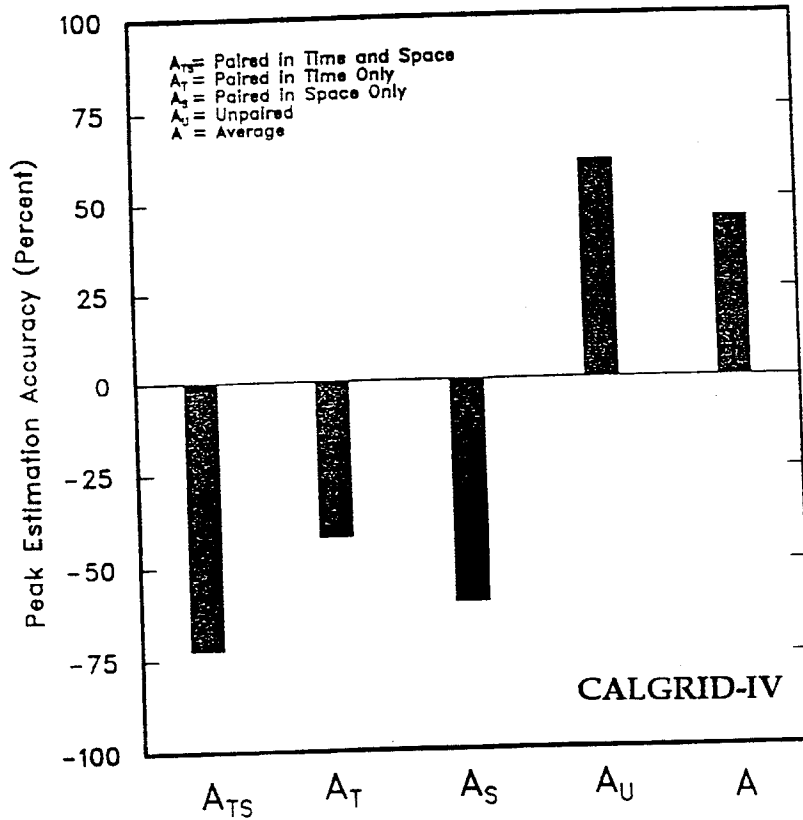


Figure 6-1c. Measures of Peak Ozone Estimation Accuracy for the 5-7 September, 1984 Episode -- 7 September, 1984.

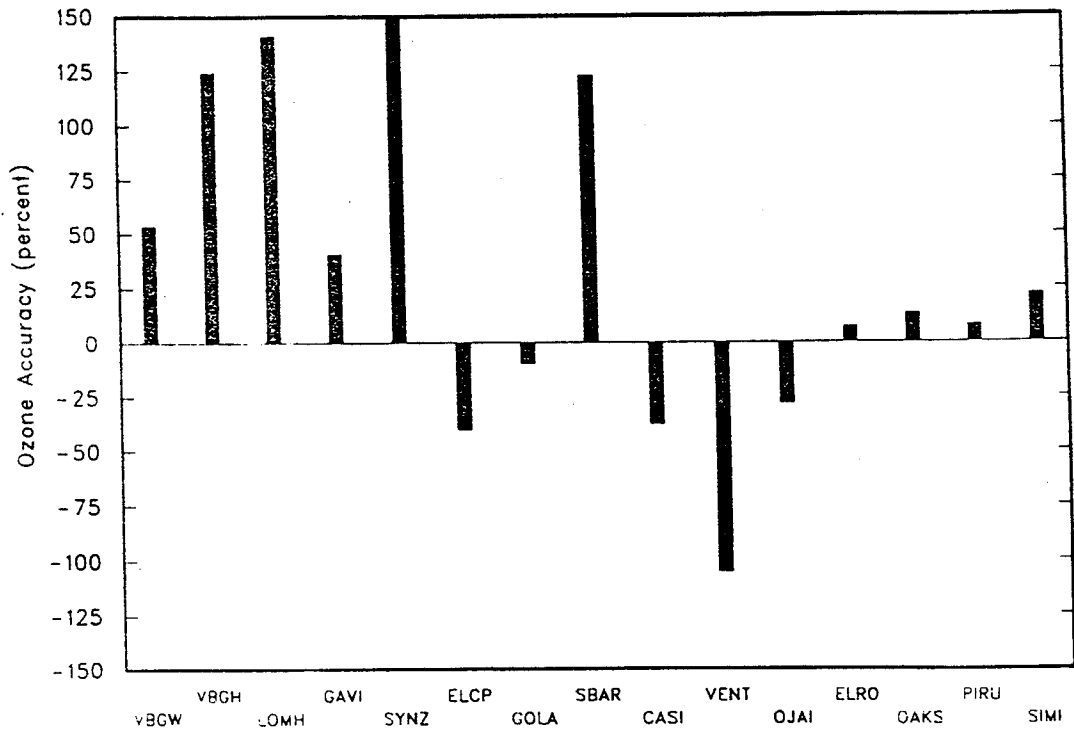
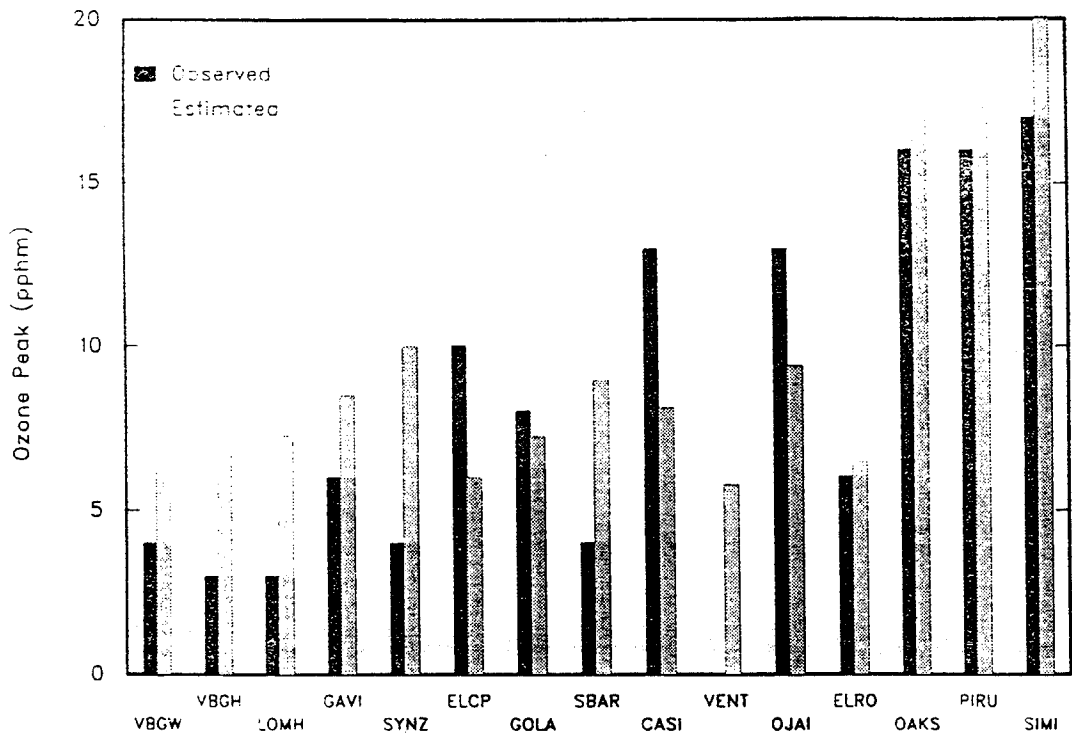


Figure 6-1d. Maximum Estimated and Observed Ozone Concentrations and Station Accuracy Estimates for the 5-7 September, 1984 CALGRID-IV Simulation -- 6 September, 1984.

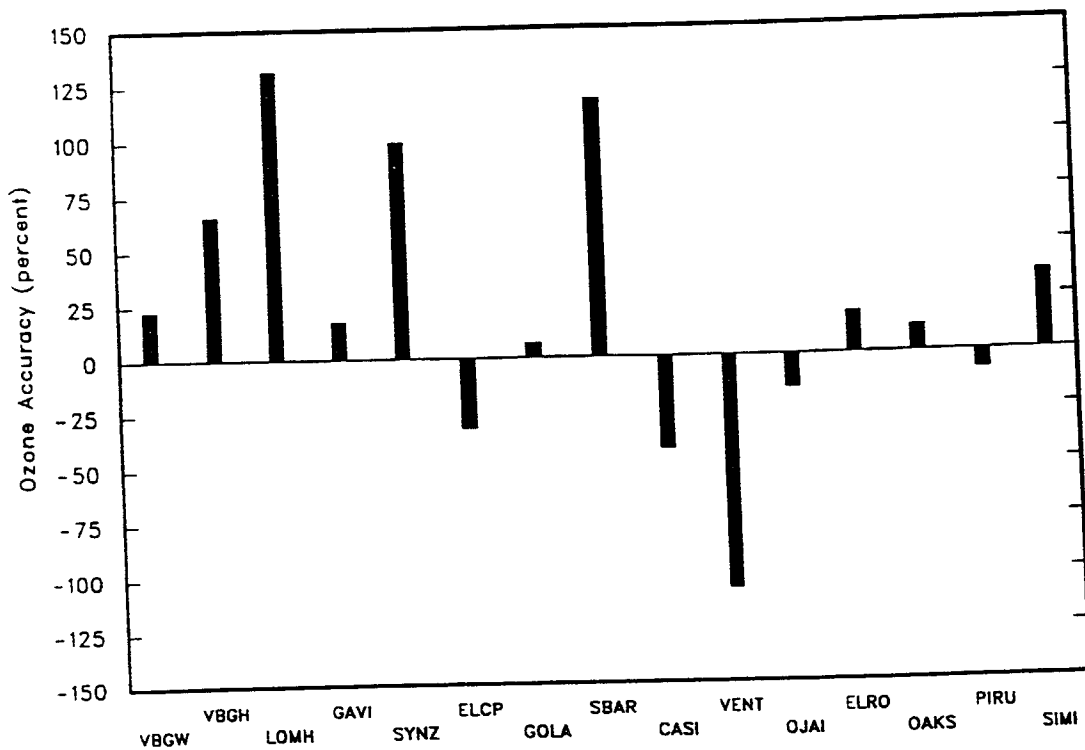
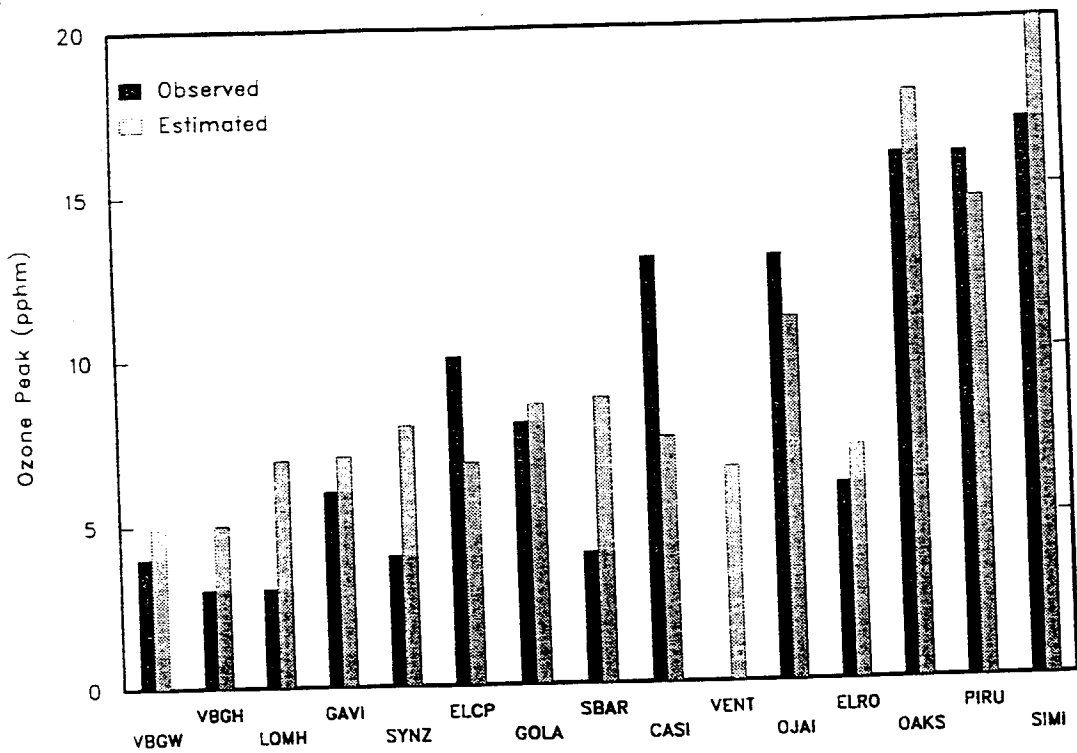


Figure 6-1e. Maximum Estimated and Observed Ozone Concentrations and Station Accuracy Estimates for the 5-7 September, 1984 UAM-IV Simulation -- 6 September, 1984.

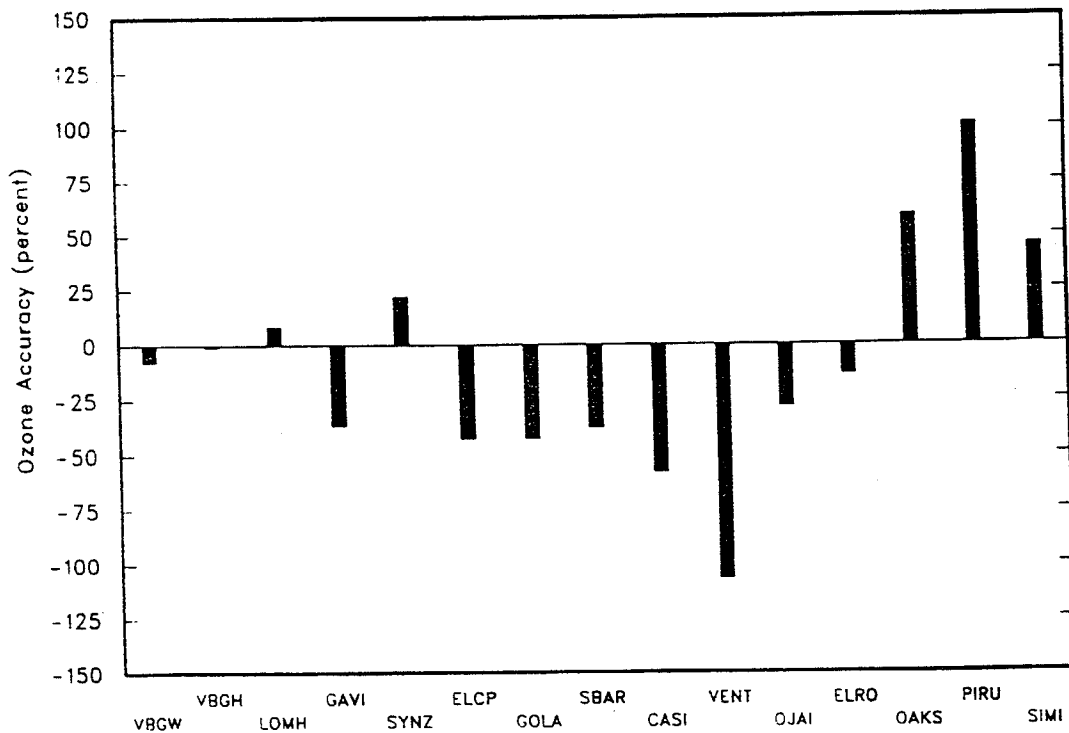
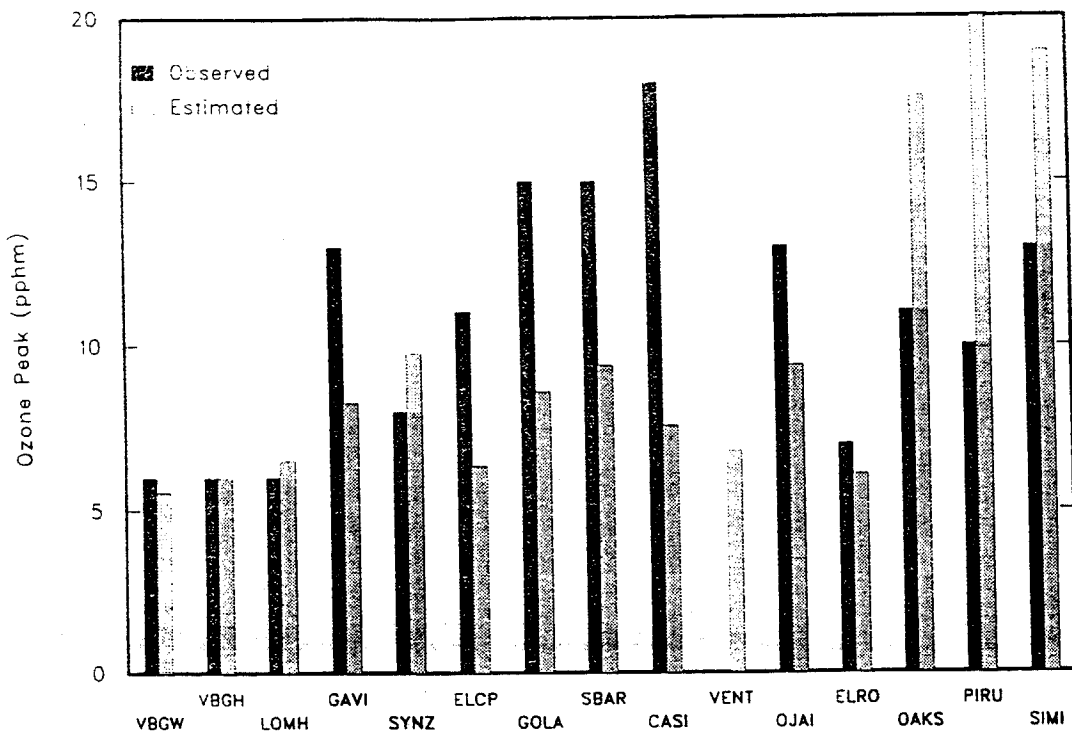


Figure 6-1f. Maximum Estimated and Observed Ozone Concentrations and Station Accuracy Estimates for the 5-7 September, 1984 CALGRID-IV Simulation -- 7 September, 1984.

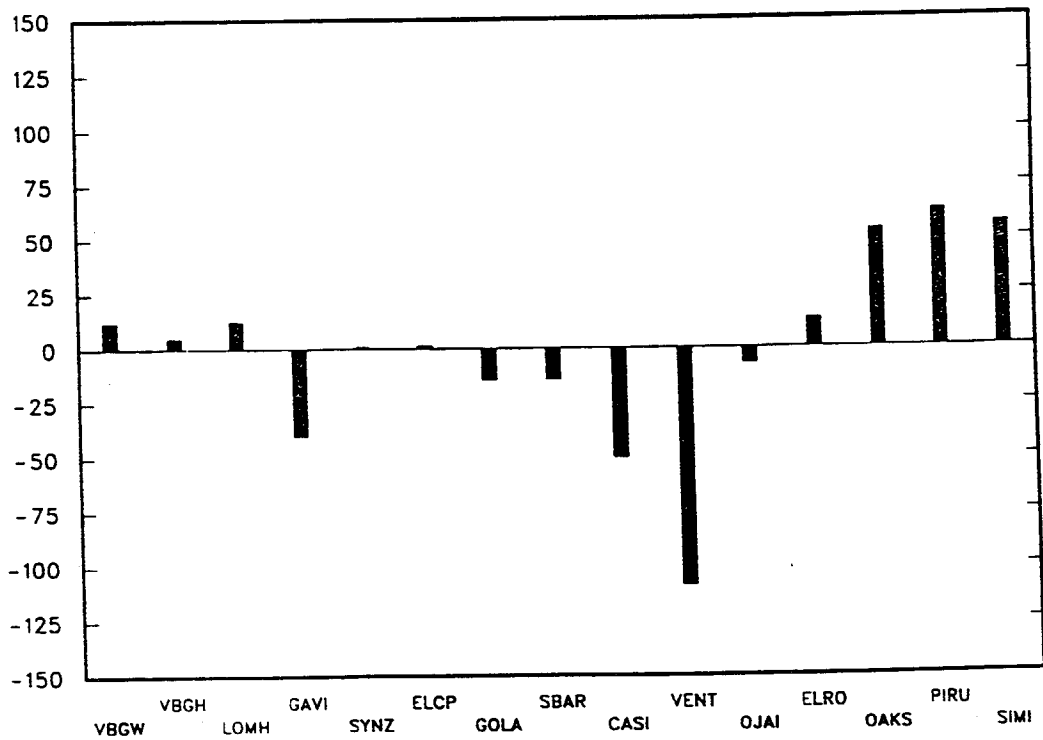
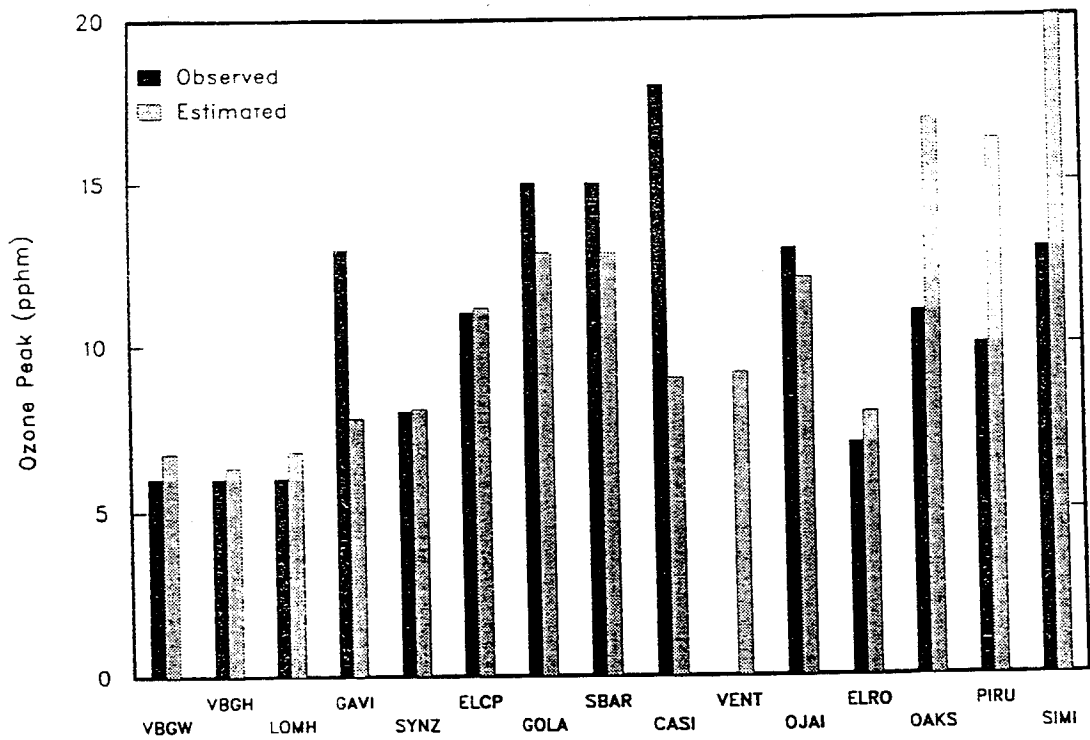


Figure 6-1g. Maximum Estimated and Observed Ozone Concentrations and Station Accuracy Estimates for the 5-7 September, 1984 UAM-IV Simulation -- 7 September, 1984.

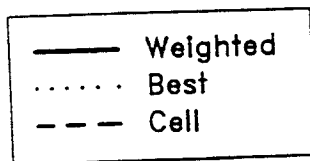
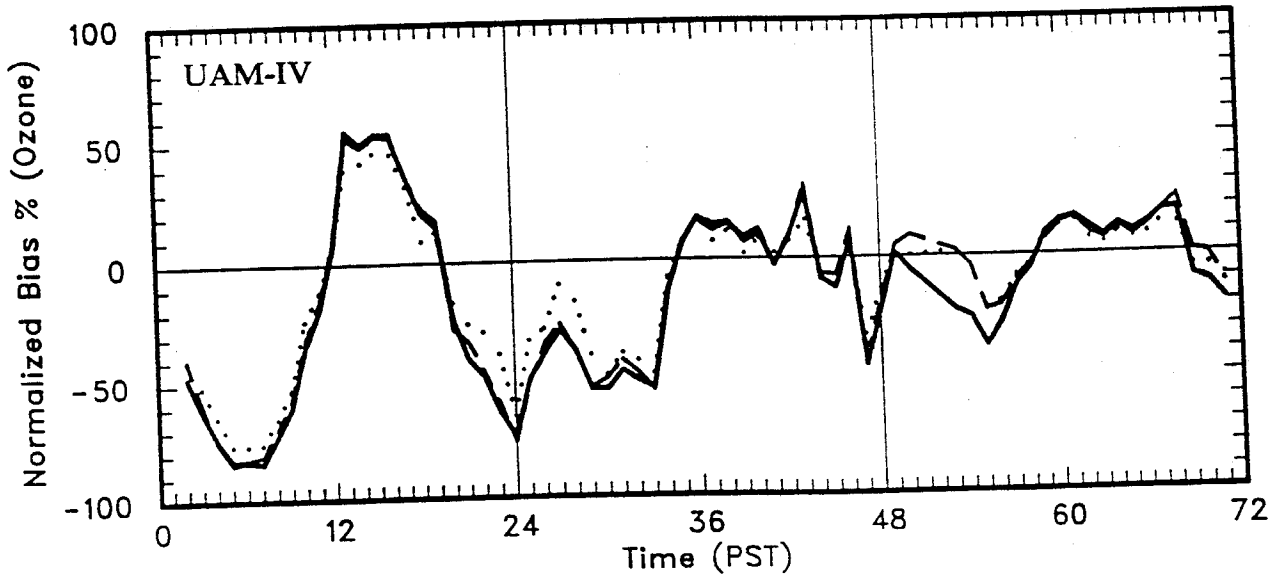
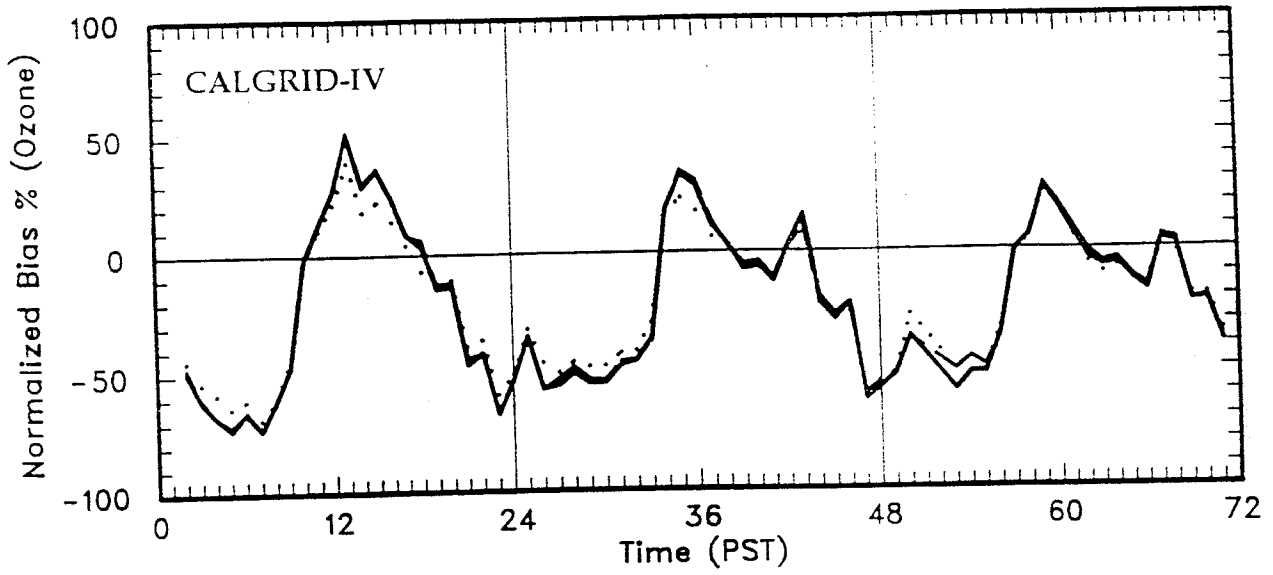


Figure 6-2. Normalized Bias in Ozone Estimation as a Function of Time Throughout the 5-7 September, 1984 Episode.

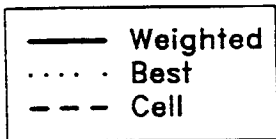
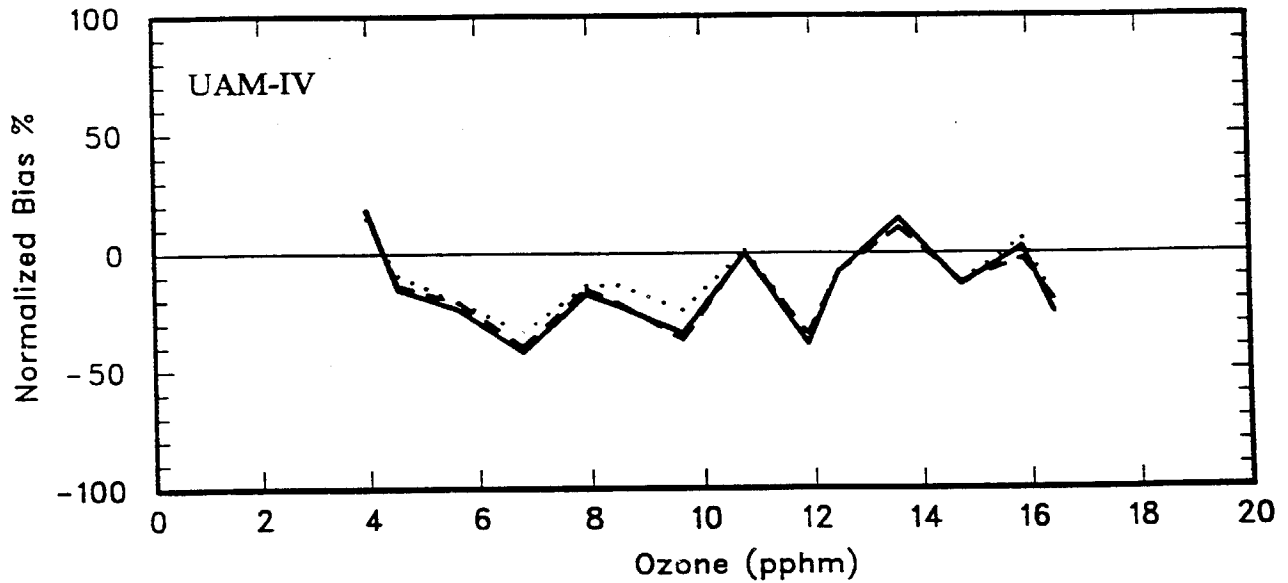
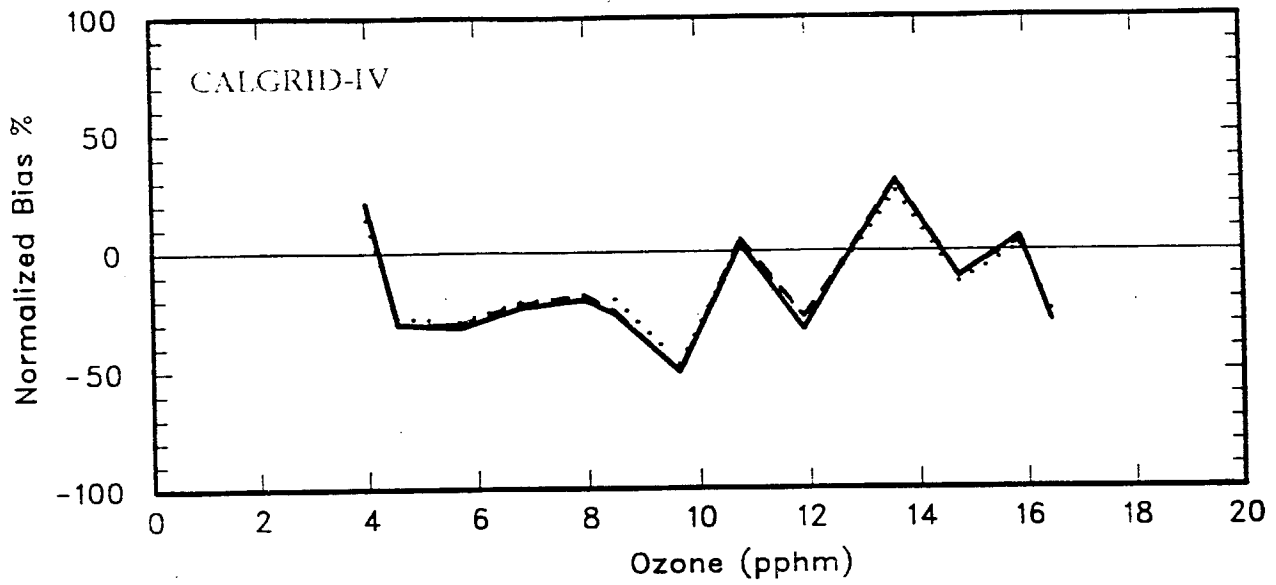


Figure 6-2b. Normalized Bias in Ozone Estimation as a Function of Observed Concentration Level for the 5-7 September, 1984 Episode -- 6 September, 1984.

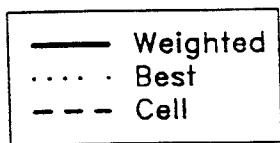
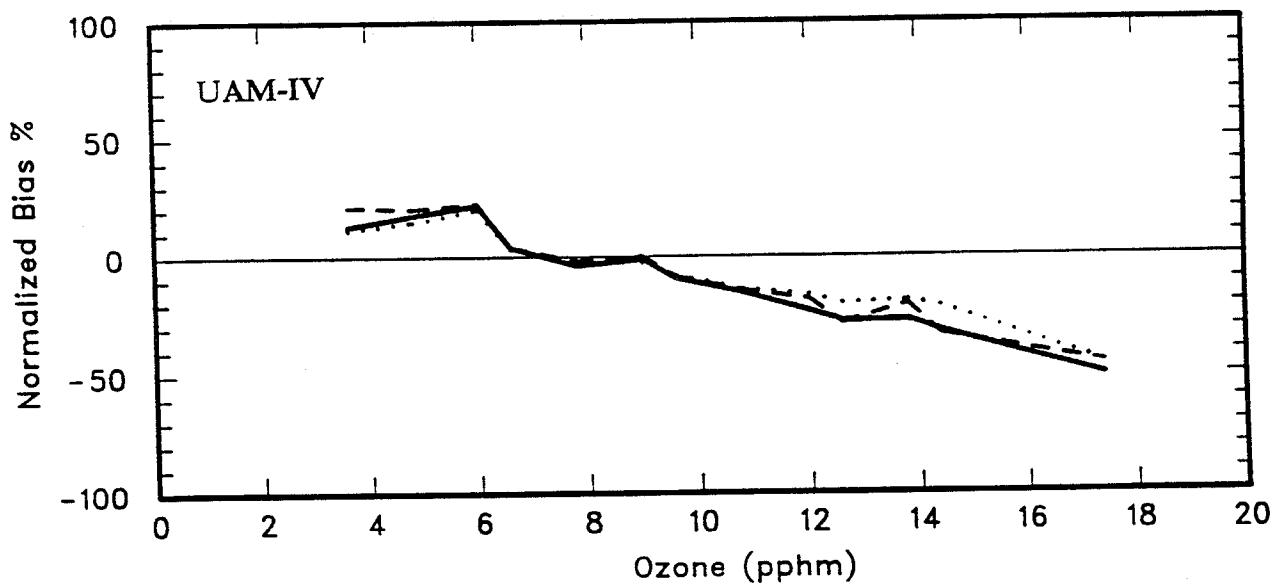
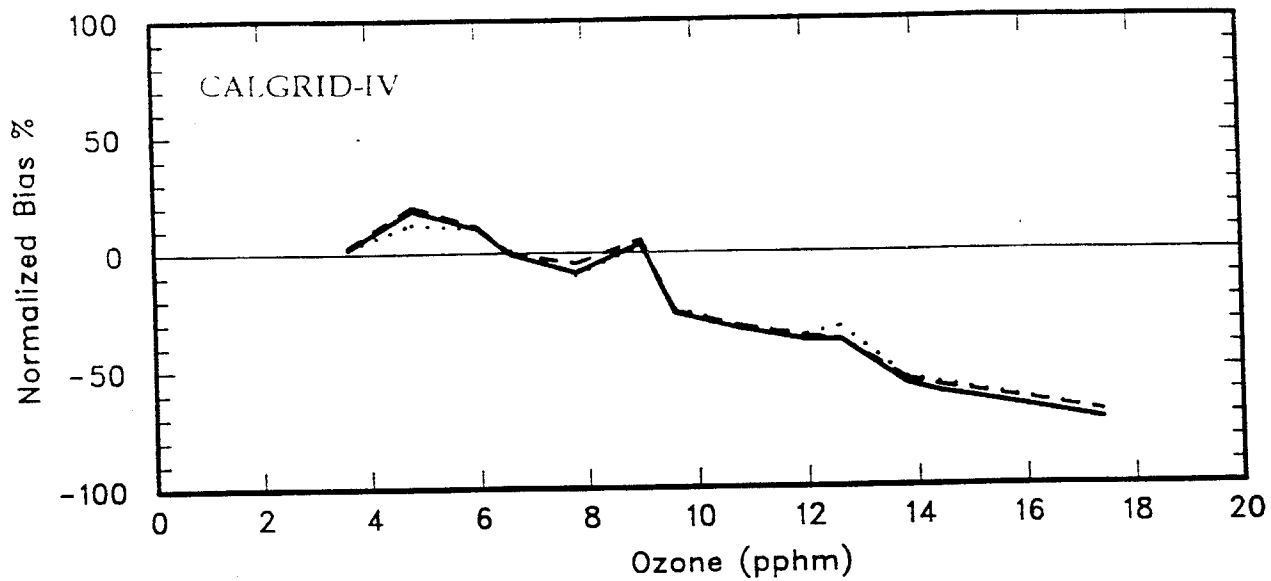


Figure 6-2c. Normalized Bias in Ozone Estimation as a Function of Observed Concentration Level for the 5-7 September, 1984 Episode -- 7 September, 1984.

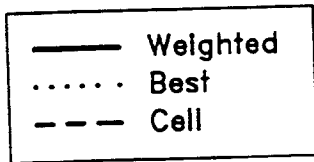
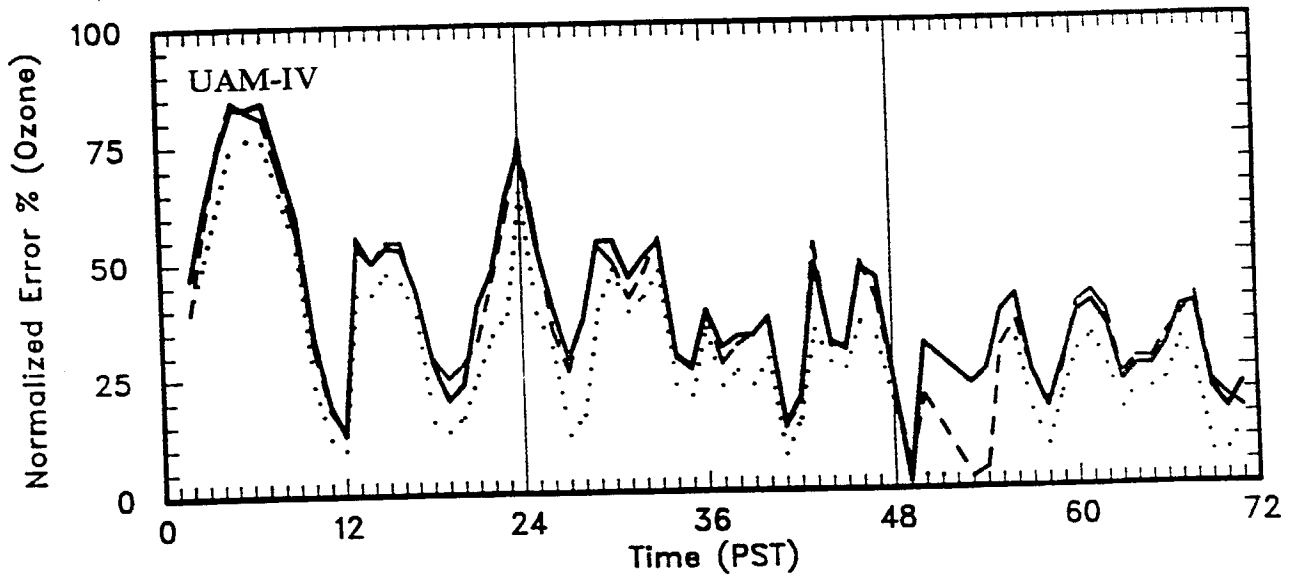
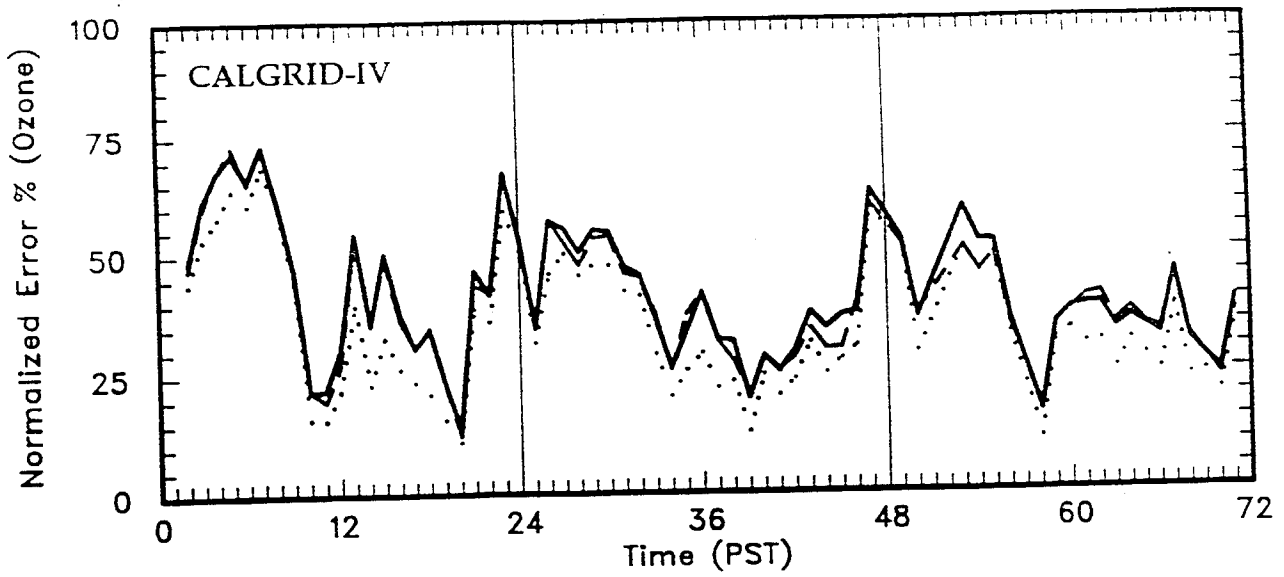


Figure 6-3. Normalized Gross Error in Ozone Estimations as a Function of Time Throughout the 5-7 September, 1984 Episode.

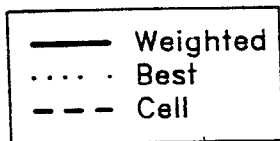
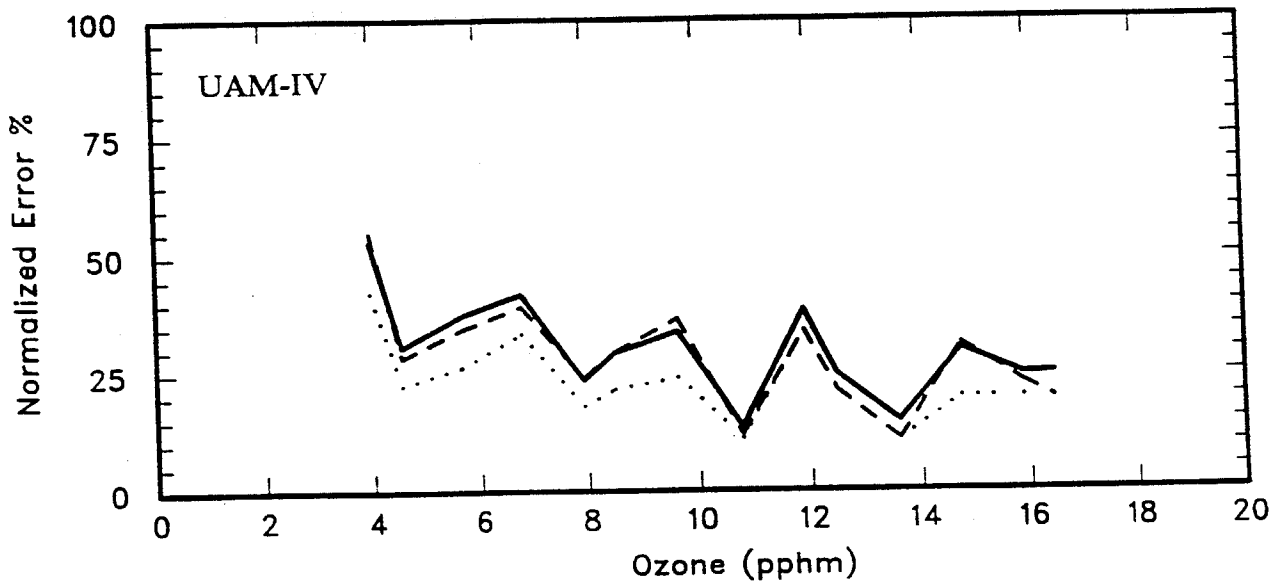
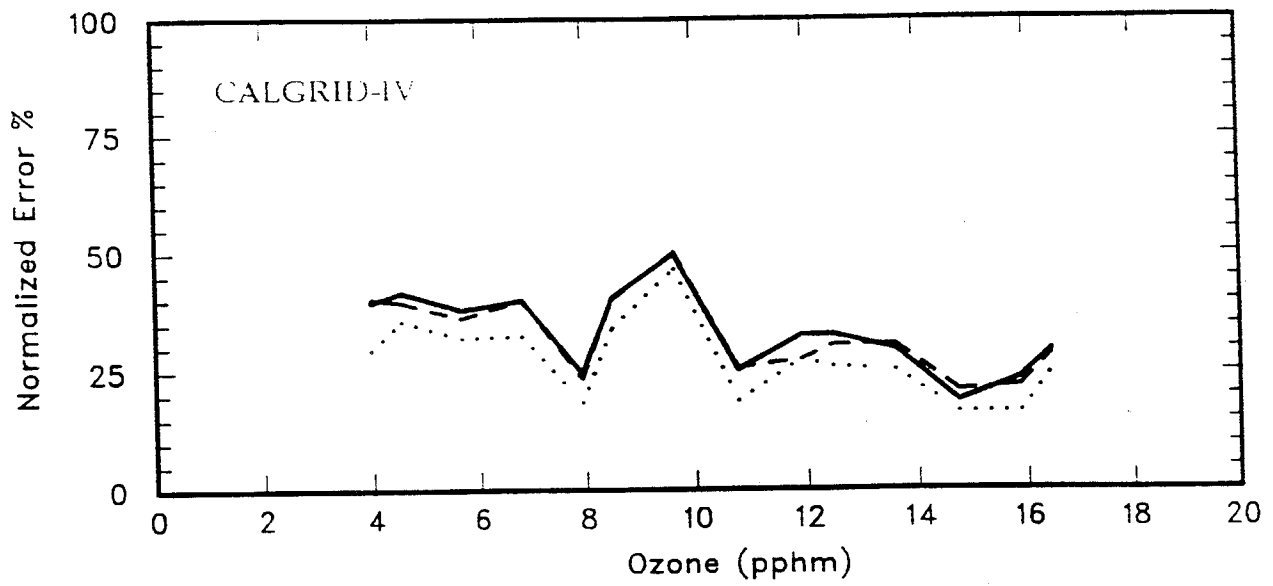


Figure 6-3b. Normalized Gross Error in Ozone Estimation as a Function of Observed Concentration Level for the 5-7 September, 1984 Episode -- 6 September, 1984.

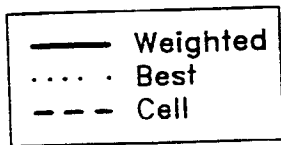
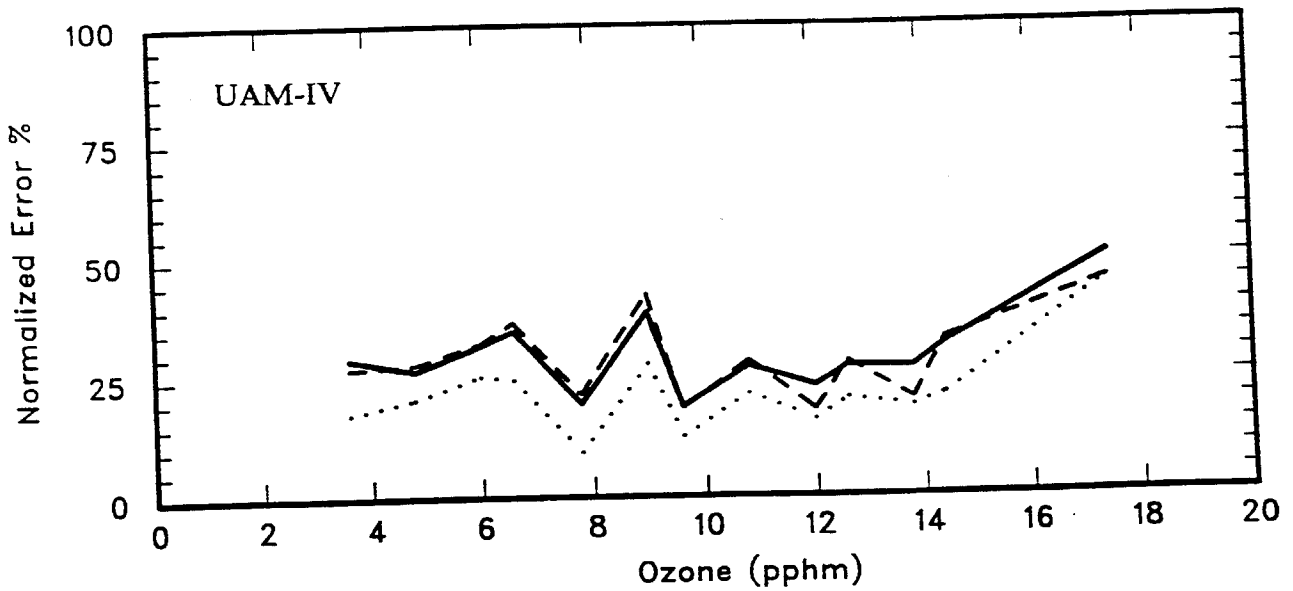
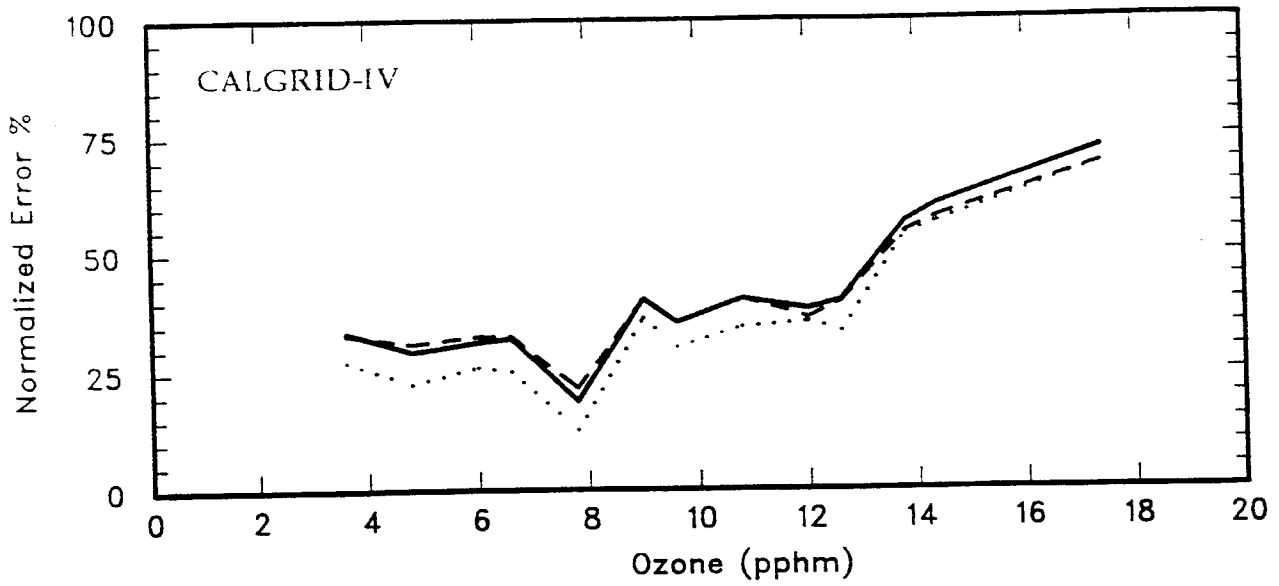
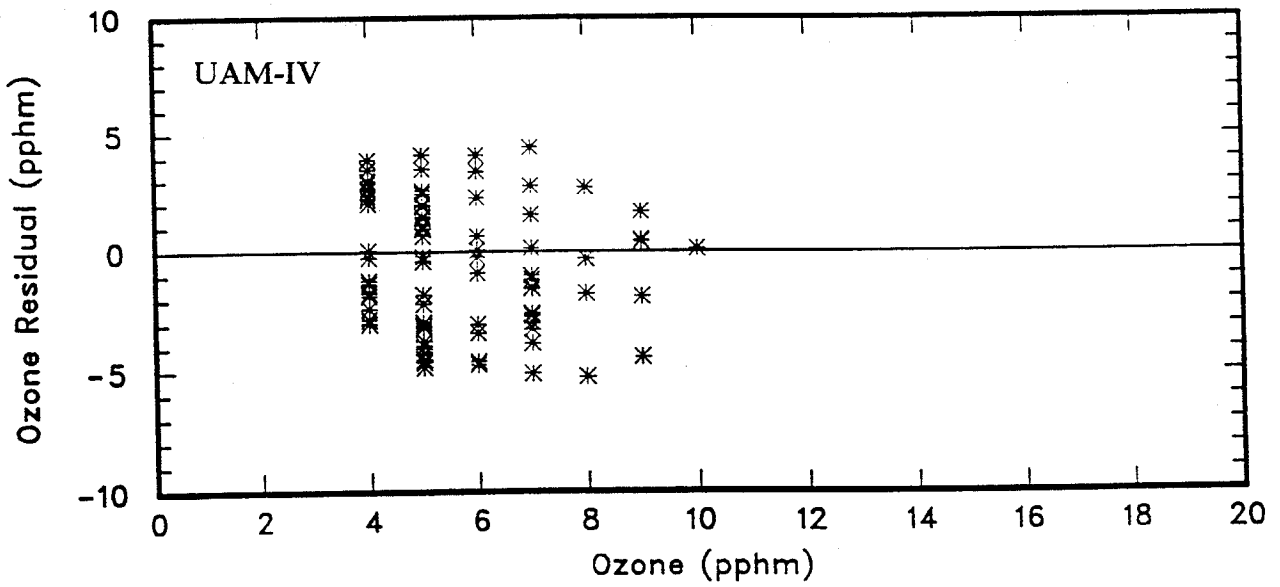
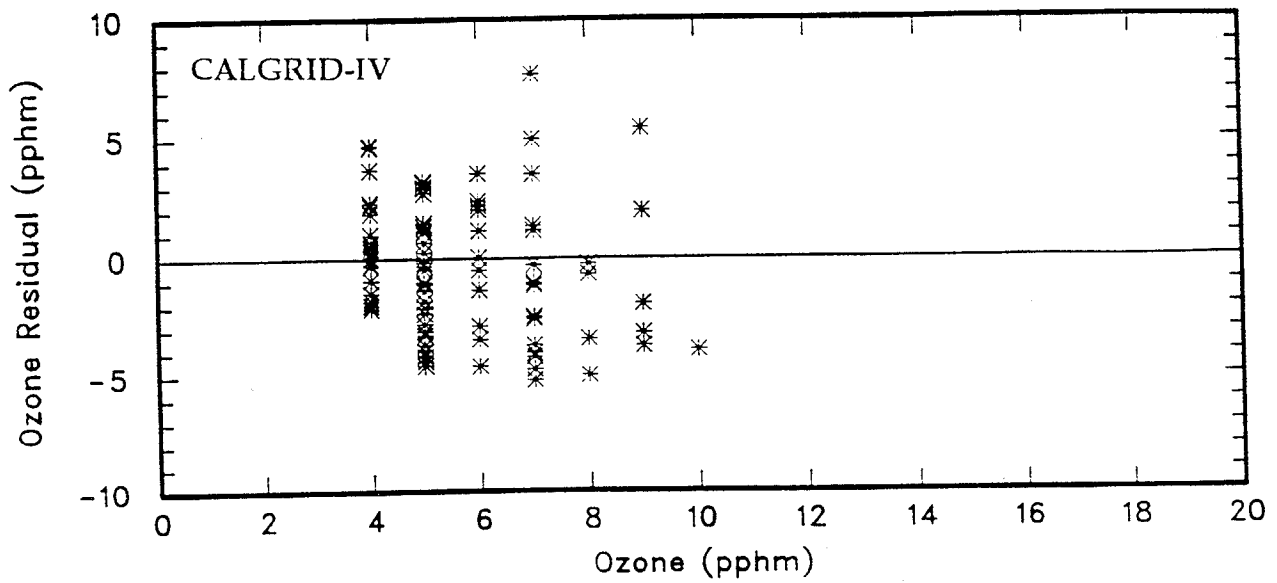
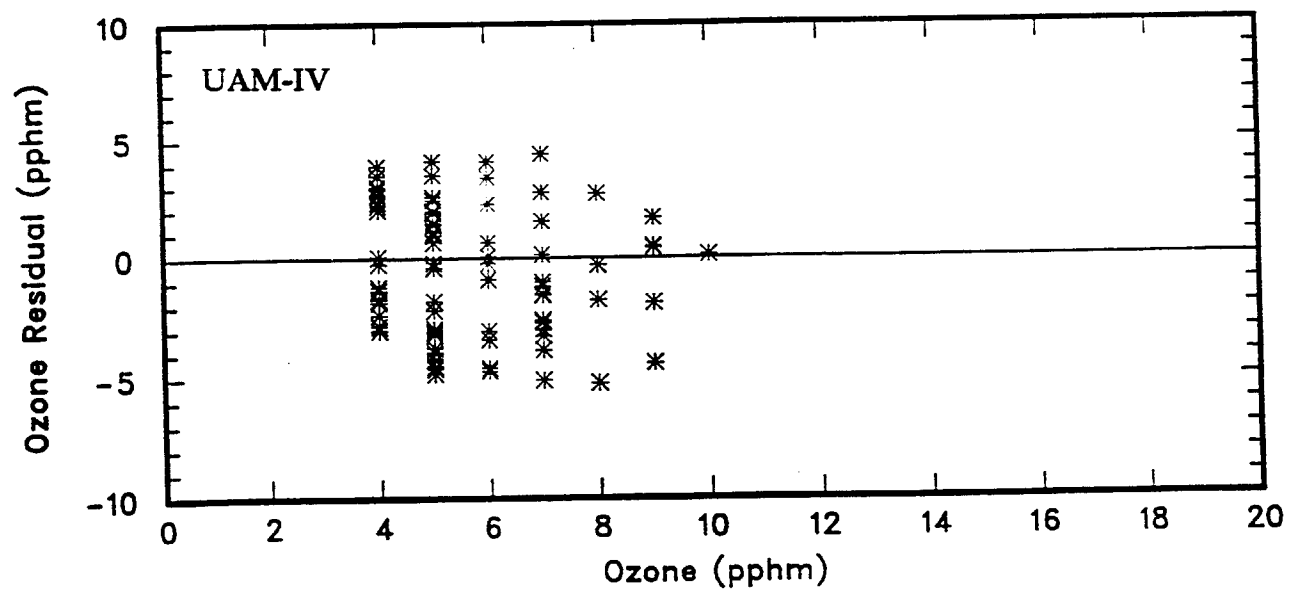
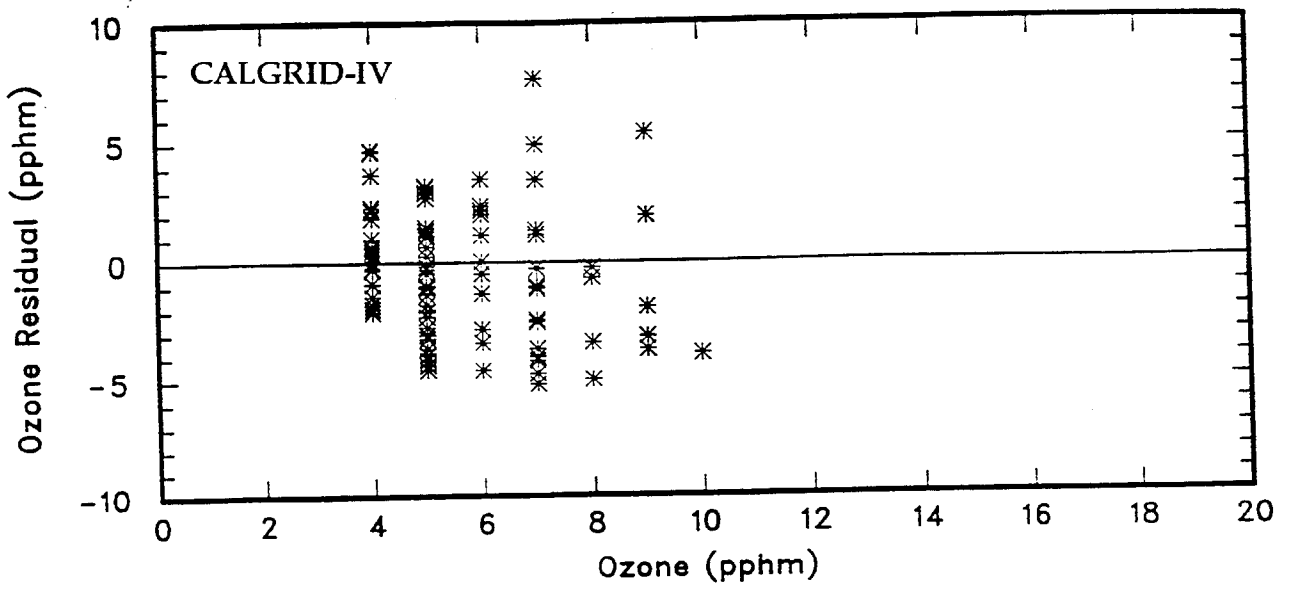


Figure 6-3c. Normalized Gross Error in Ozone Estimation as a Function of Observed Concentration Level for the 5-7 September, 1984 Episode – 7 September, 1984.



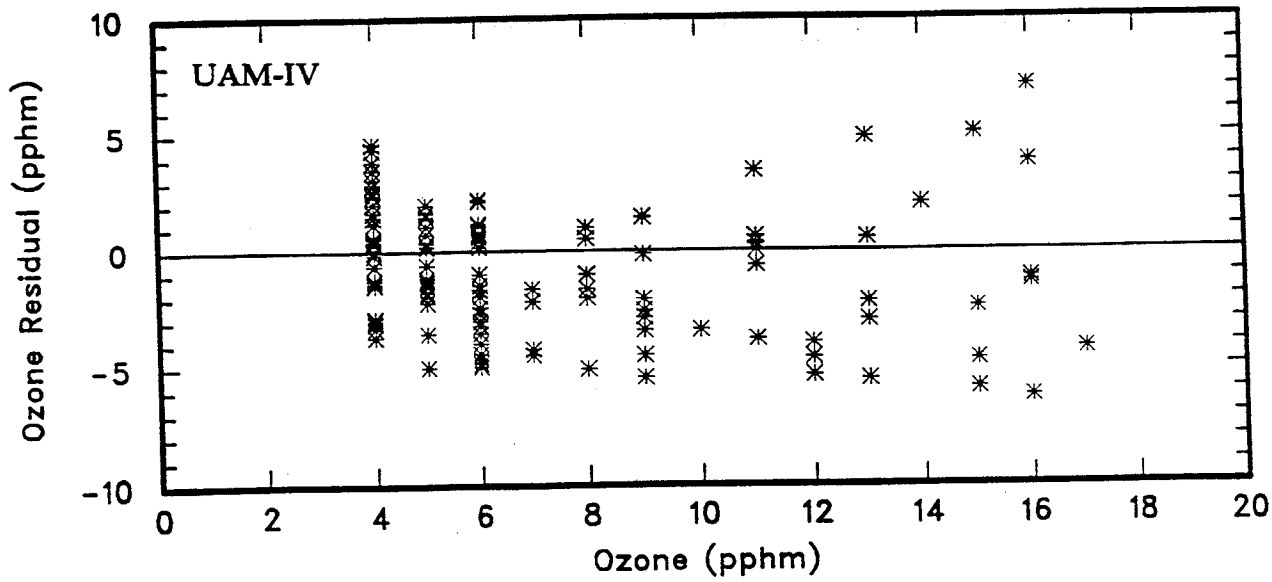
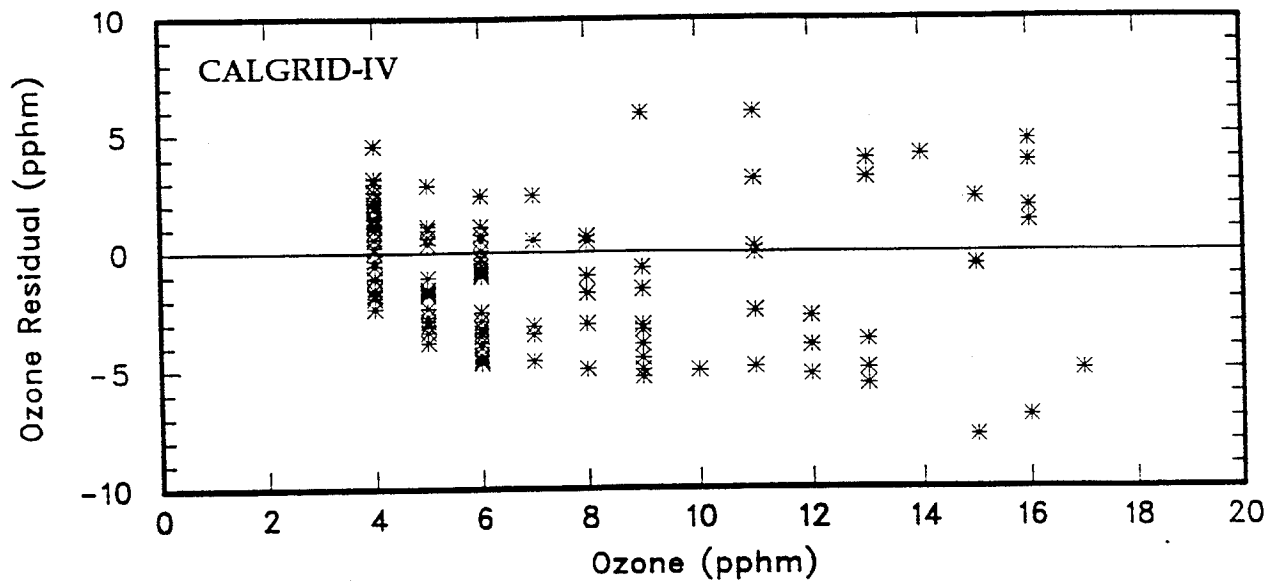
\* Residual = Estimated - Observed

Figure 6-4a. Hourly Ozone Residuals as a Function of Time Throughout the 5-7 September, 1984 Episode -- 5 September, 1984.



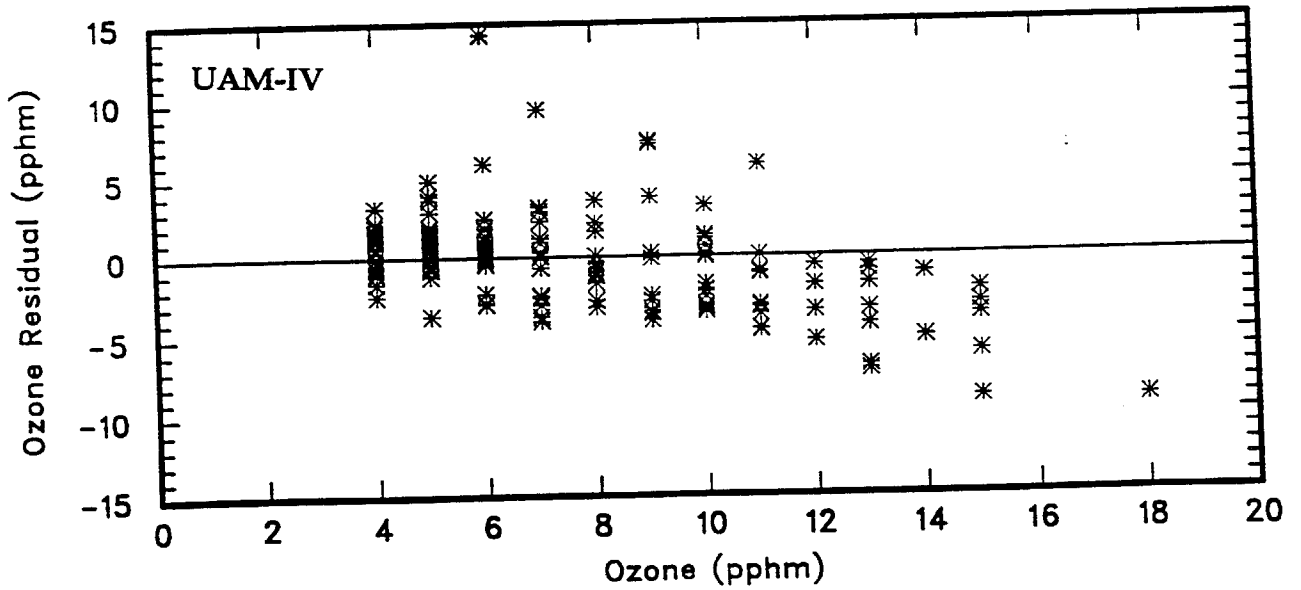
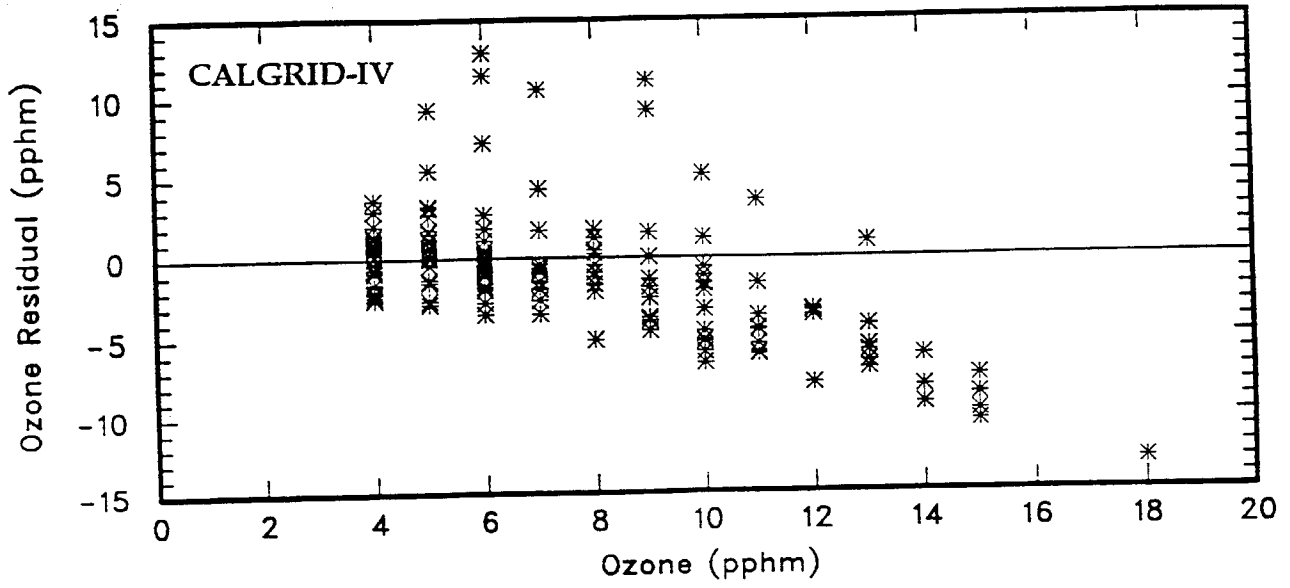
\* Residual = Estimated - Observed

Figure 6-4a. Hourly Ozone Residuals as a Function of Concentration Throughout the 5-7 September, 1984 Episode - 5 September, 1984.



\* Residual = Estimated - Observed

Figure 6-4b. Hourly Ozone Residuals as a Function of Concentration Throughout the 5-7 September, 1984 Episode - 6 September, 1984.



\* Residual = Estimated - Observed

Figure 6-4c. Hourly Ozone Residuals as a Function of Concentration Throughout the 5-7 September, 1984 Episode - 7 September, 1984.

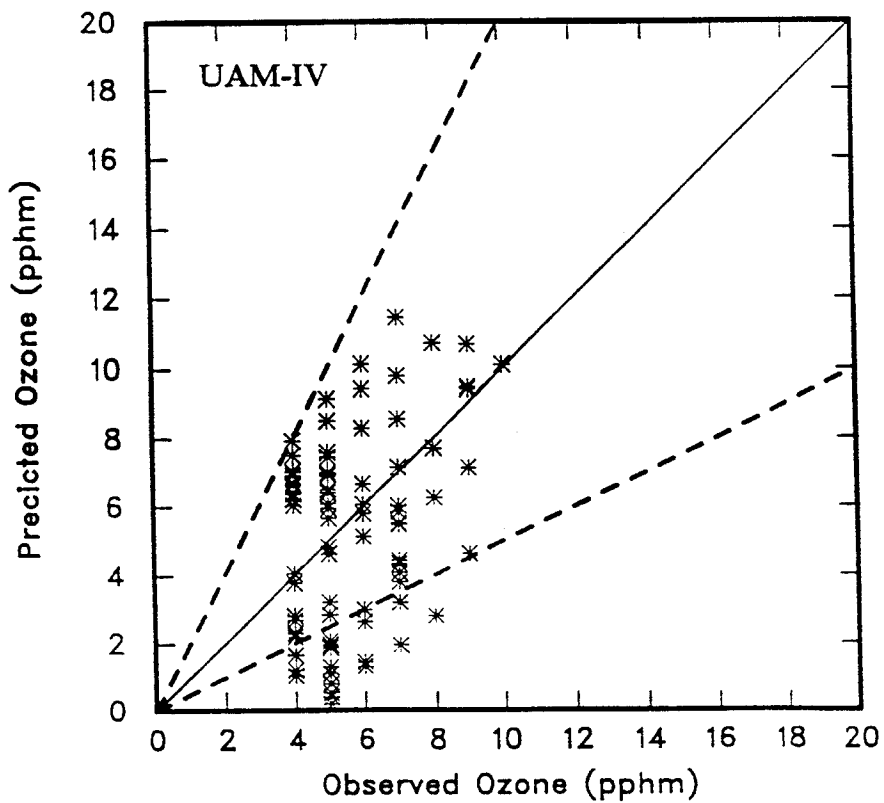
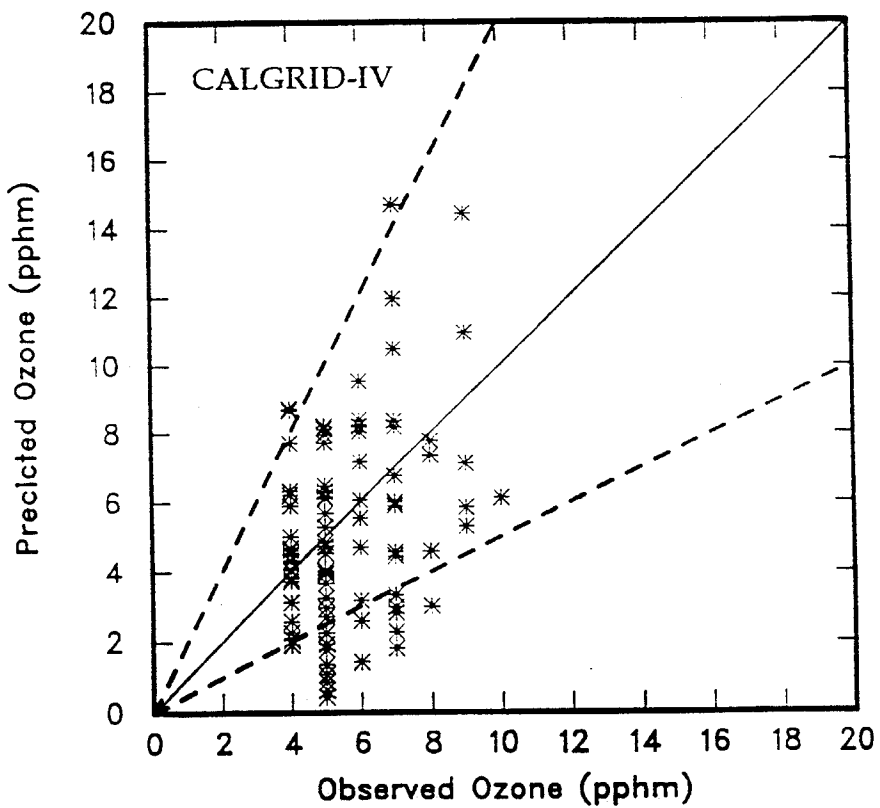


Figure 6-5a. Scatterplot of Hourly Ozone Concentration Residuals for the 5-7 September, 1984 Episode -- 5 September, 1984.

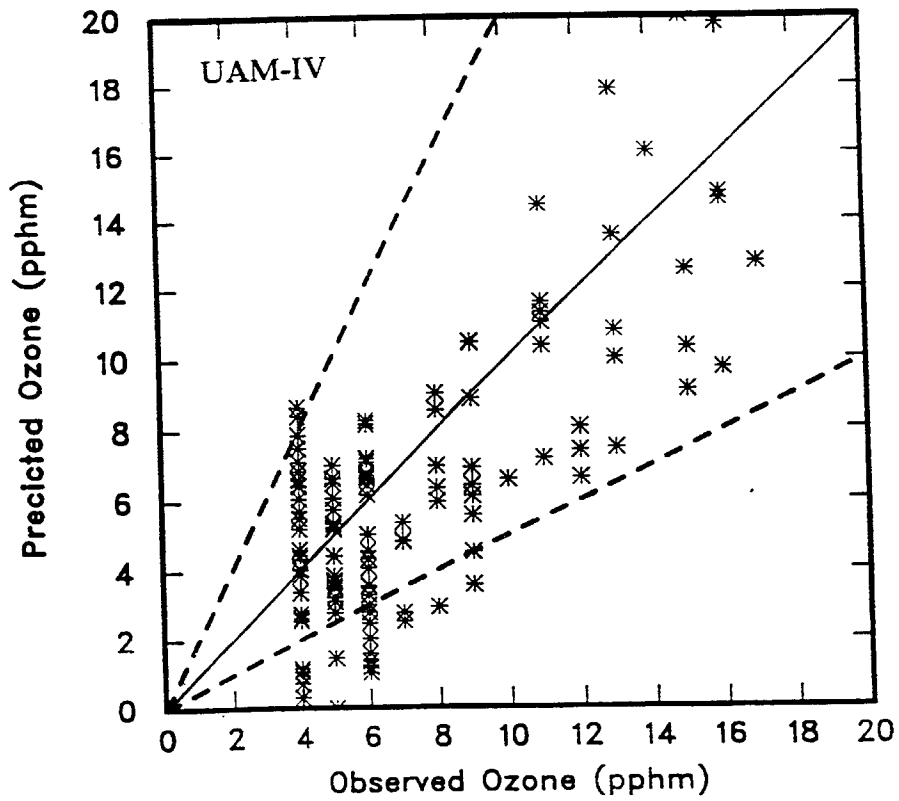
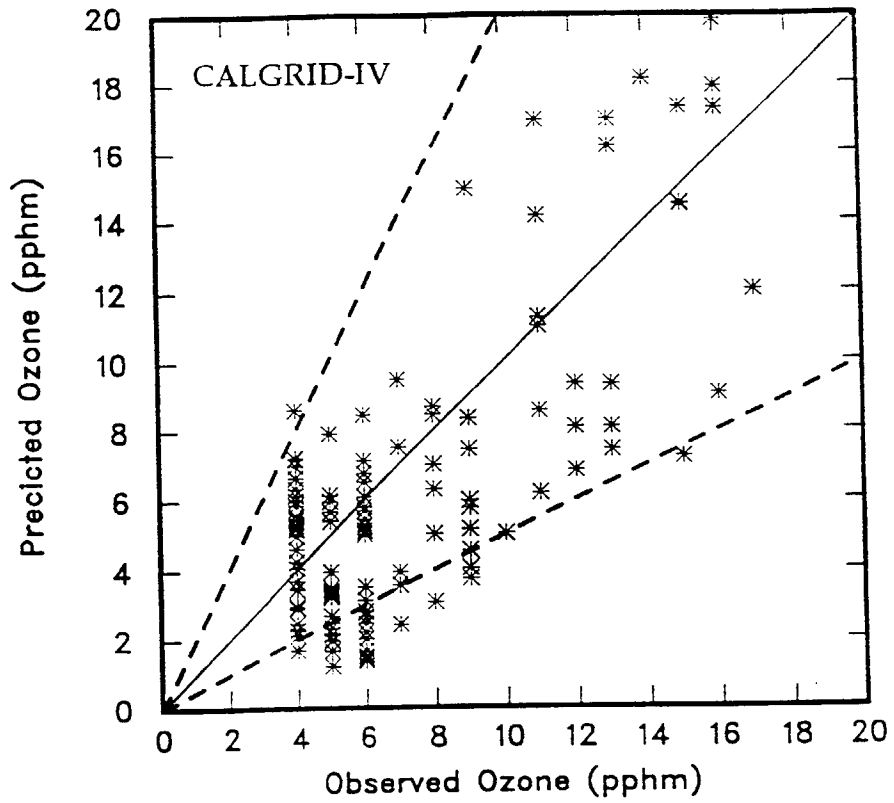


Figure 6-5b. Scatterplot of Hourly Ozone Concentration Residuals for the 5-7 September, 1984 Episode -- 6 September, 1984.

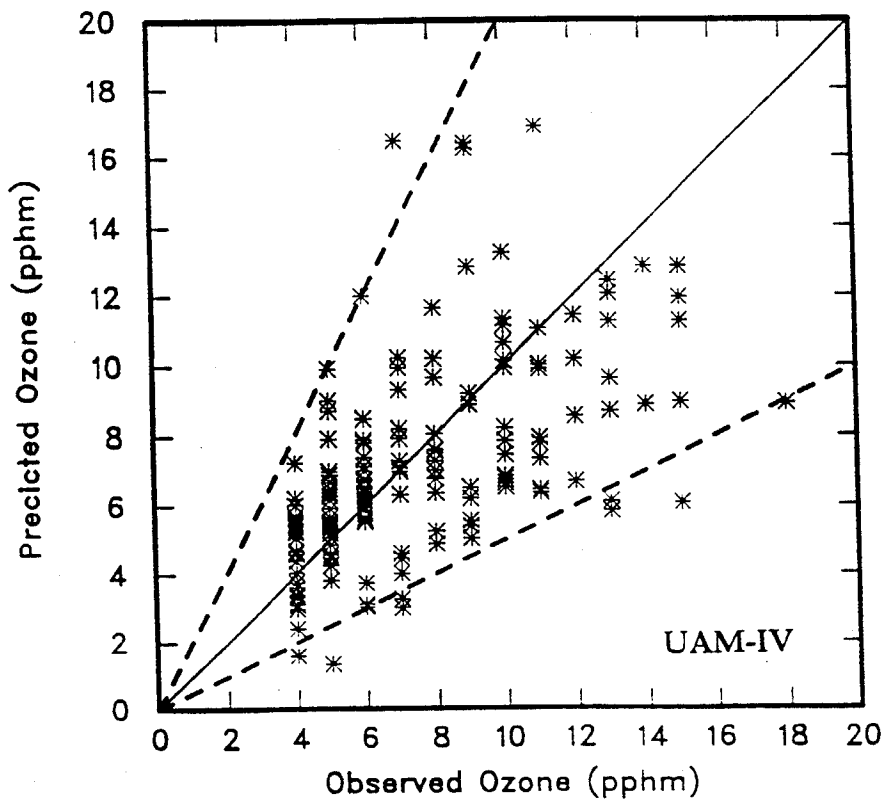
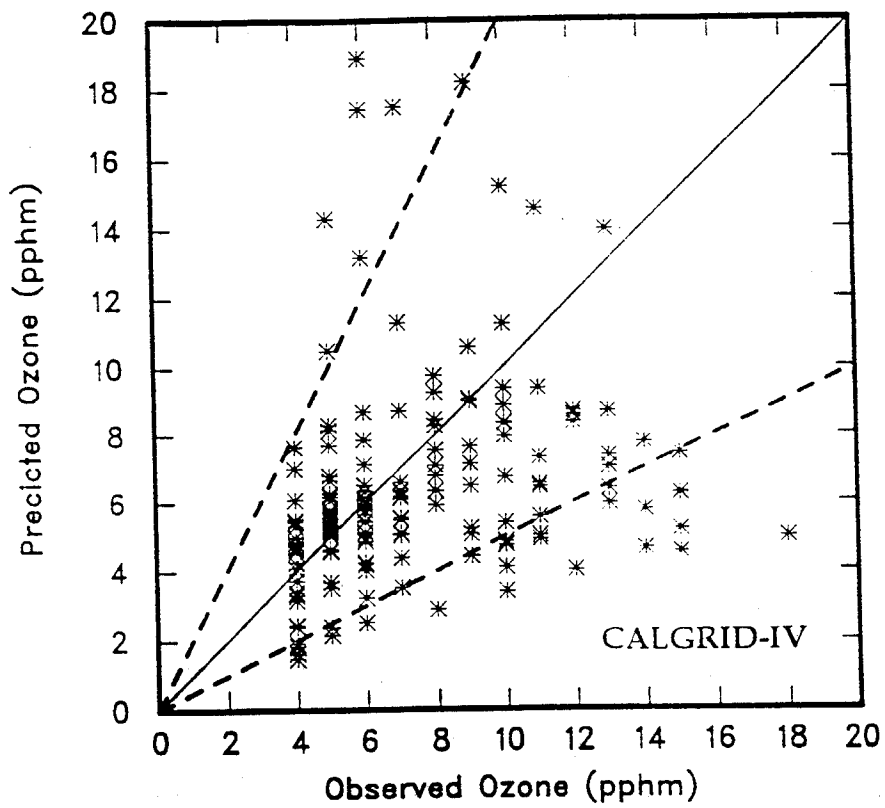


Figure 6-5c.

Scatterplot of Hourly Ozone Concentration Residuals for the 5-7 September, 1984 Episode -- 7 September, 1984.

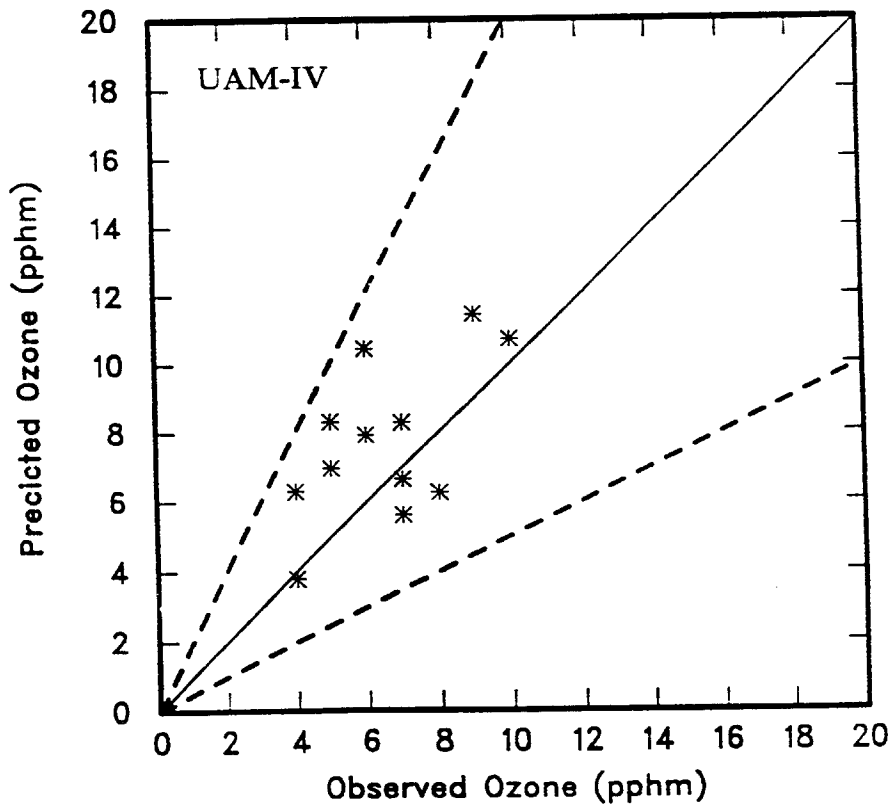
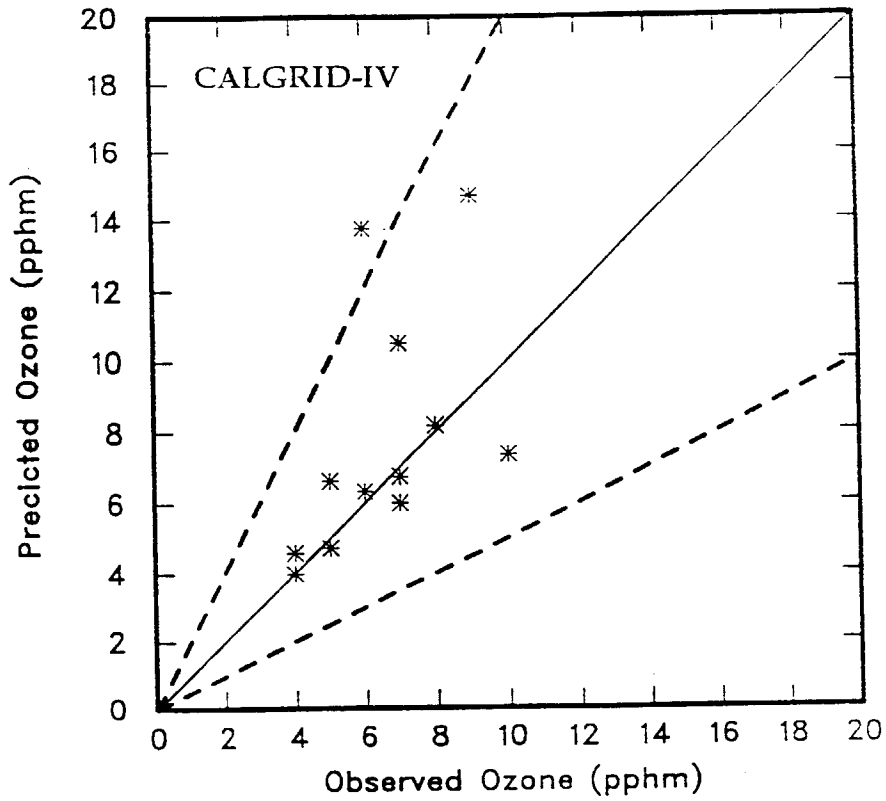


Figure 6-6a. Scatterplot of Daily Maximum Ozone Concentration Residuals for the 5-7 September, 1984 Episode -- 5 September, 1984.

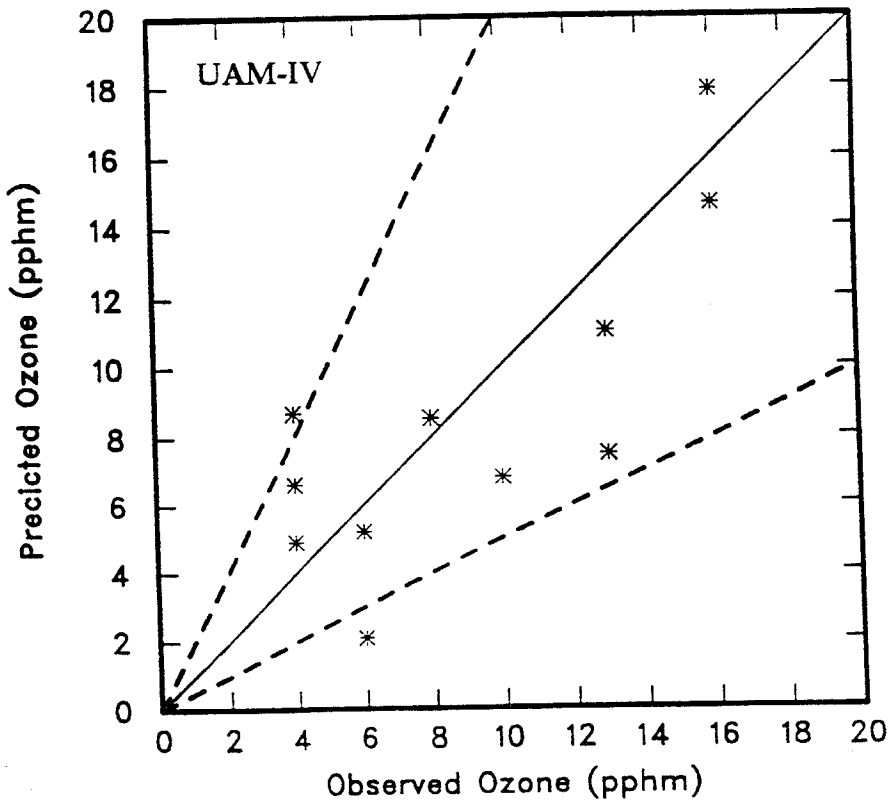
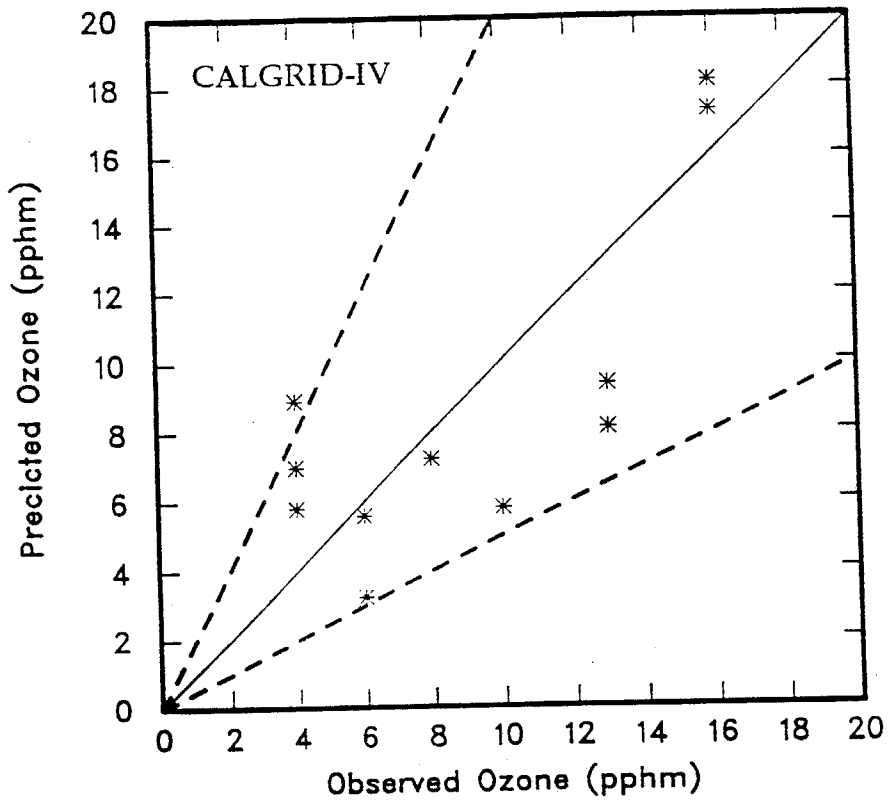


Figure 6-6b. Scatterplot of Daily Maximum Ozone Concentration Residuals for the 5-7 September, 1984 Episode – 6 September, 1984.

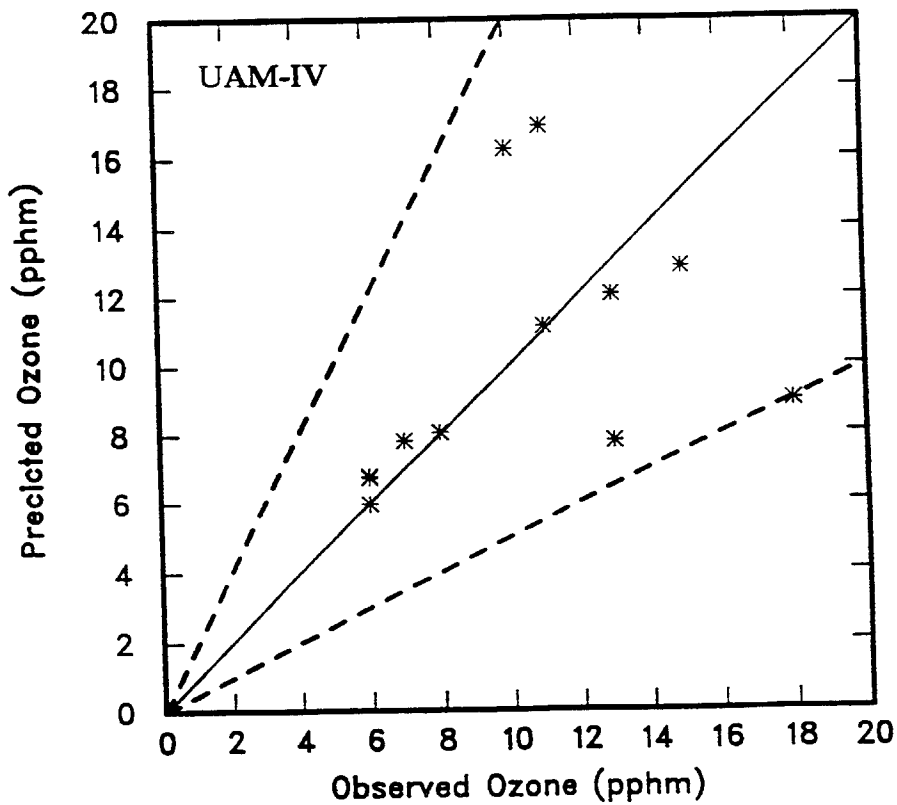
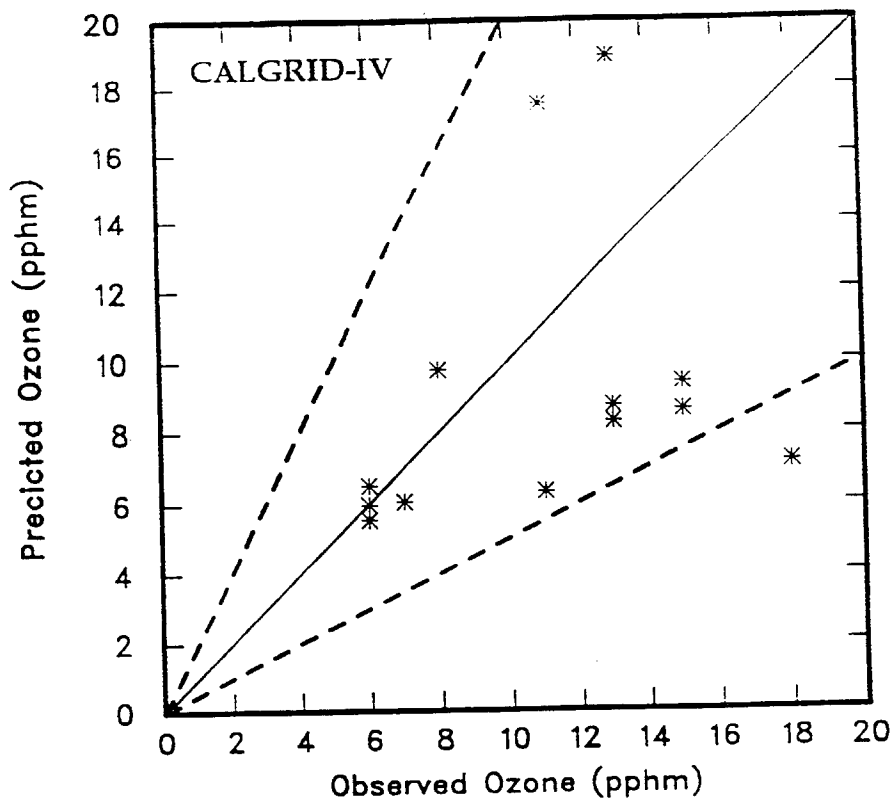


Figure 6-6c. Scatterplot of Daily Maximum Ozone Concentration Residuals for the 5-7 September, 1984 Episode -- 7 September, 1984.

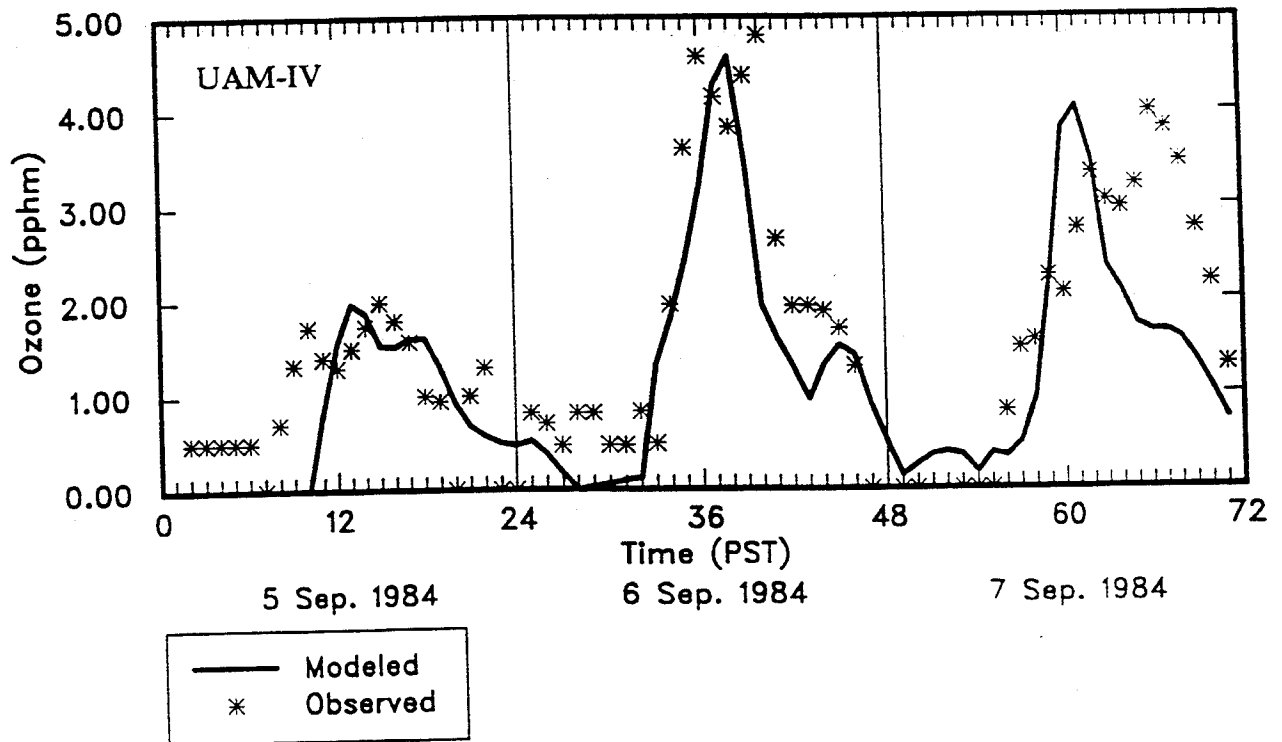
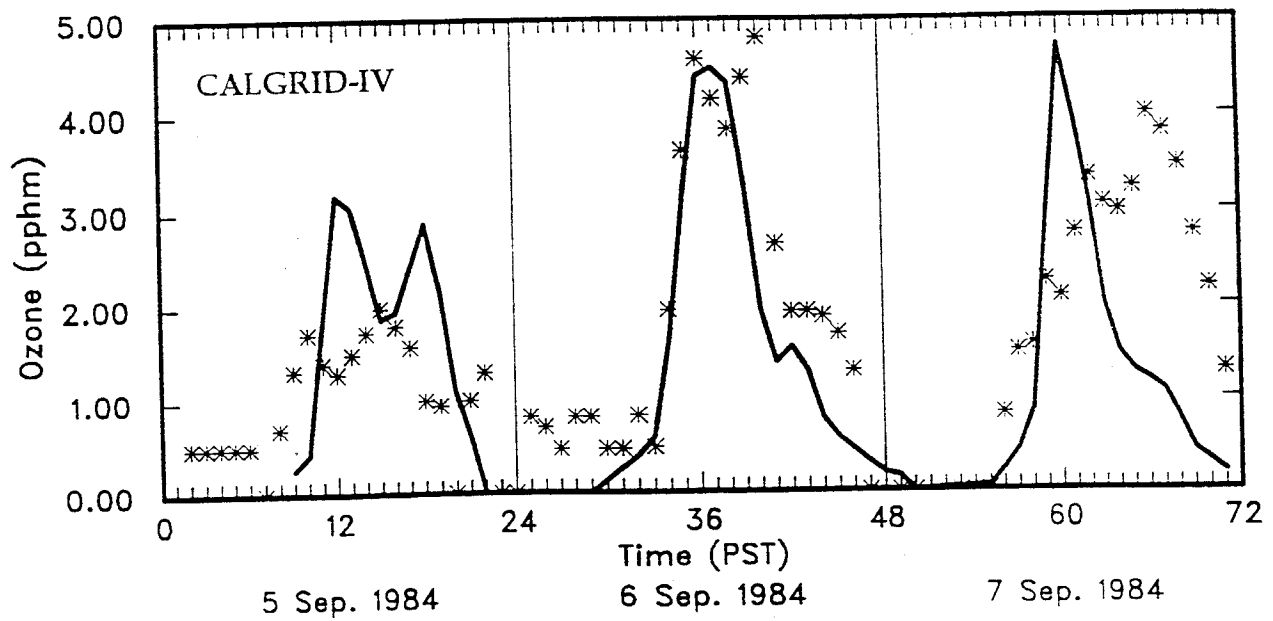


Figure 6-7. Standard Deviation of Ozone Estimates and Observations as a Function of Time Throughout the 5-7 September, 1984 Episode.

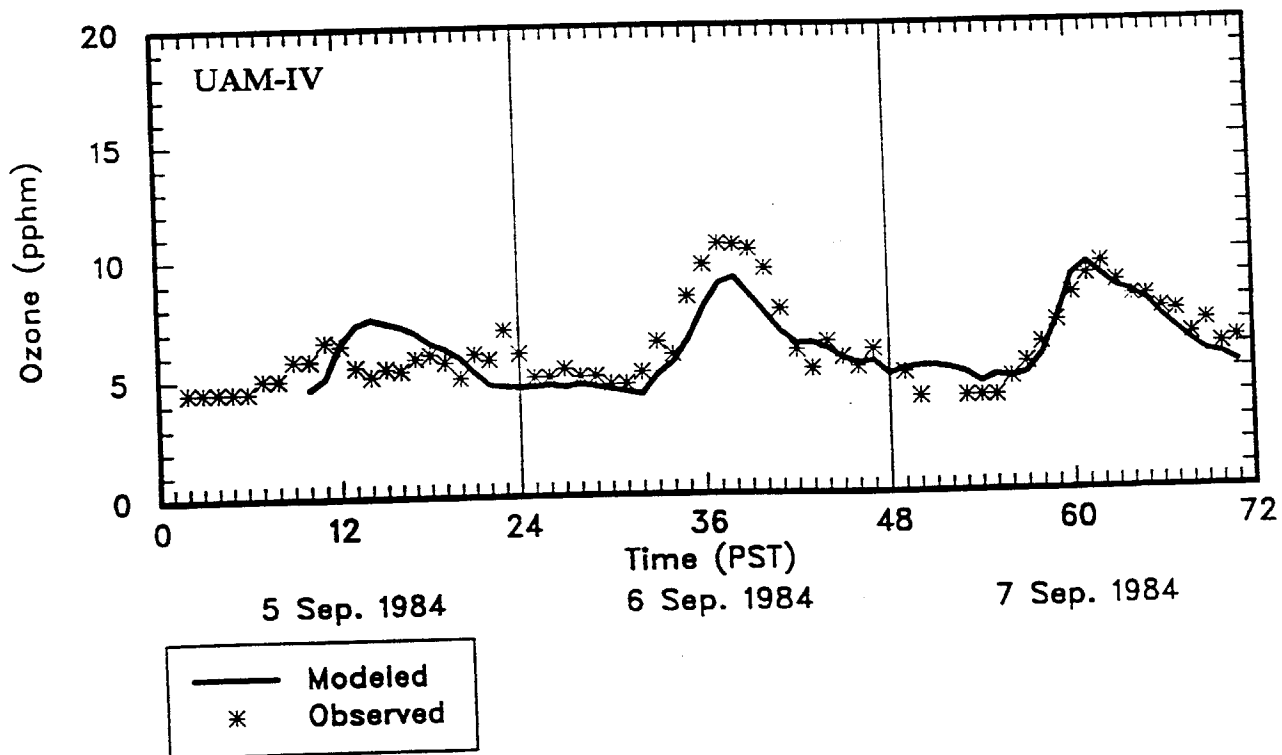
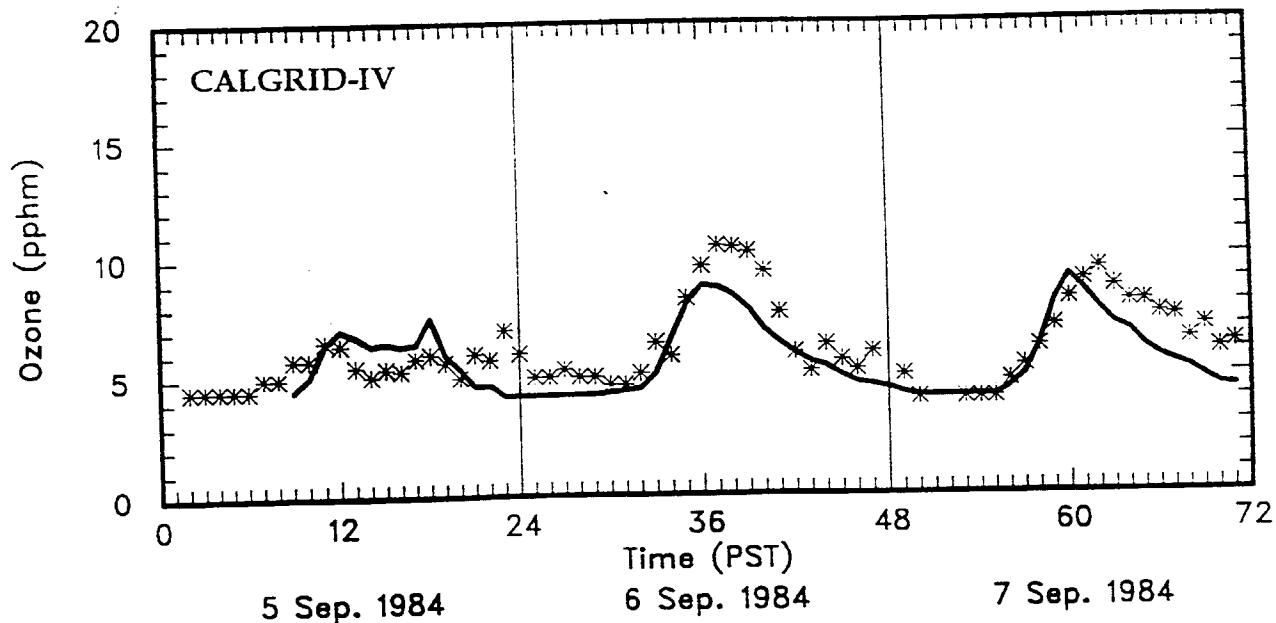


Figure 6-8. Mean Value of Ozone Estimates and Observations as a Function of Time Throughout the 5-7 September, 1984 Episode.

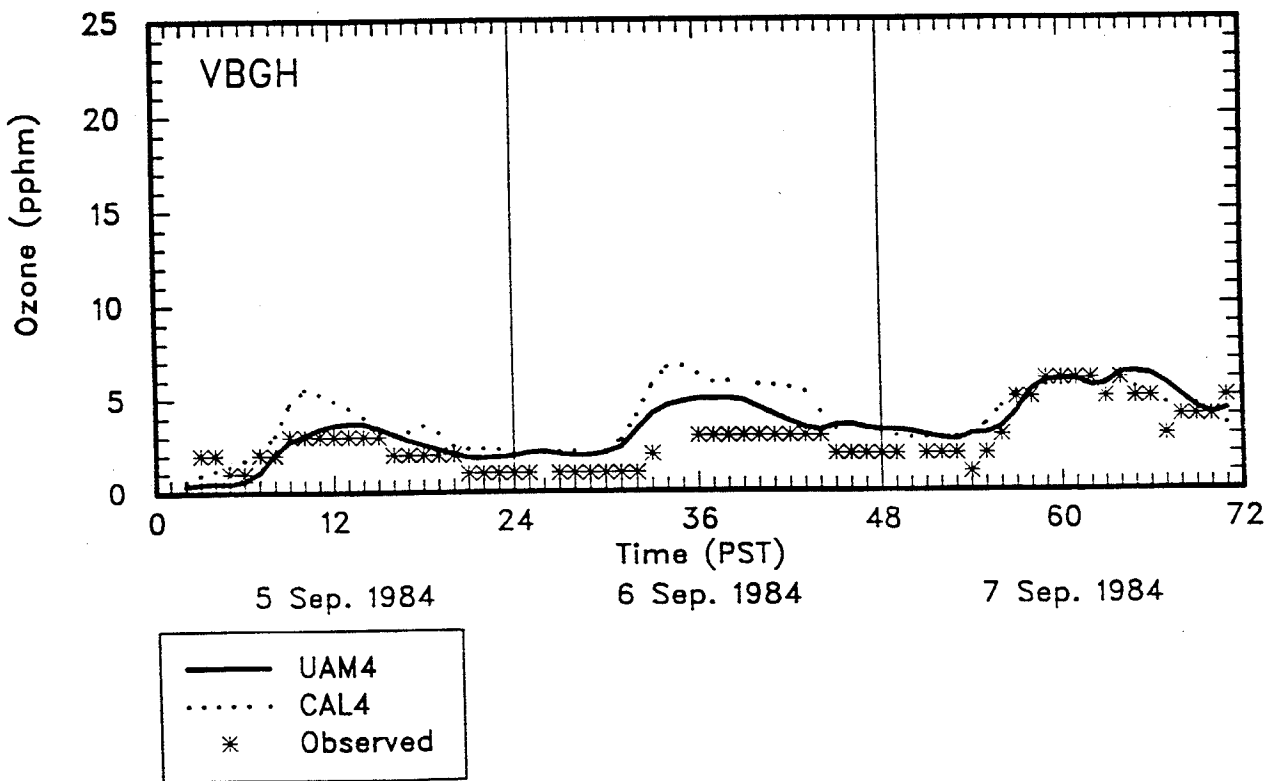
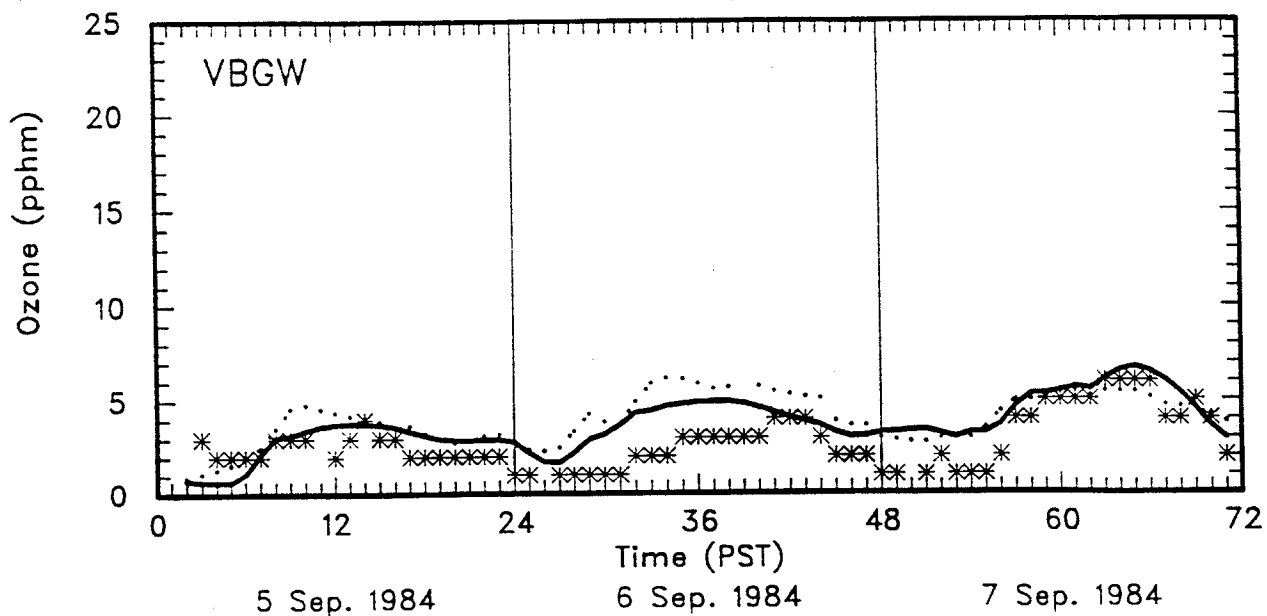


Figure 6-9. Time Series of Hourly Estimated and Observed Ozone Concentrations for the 5-7 September, 1984 Episode.

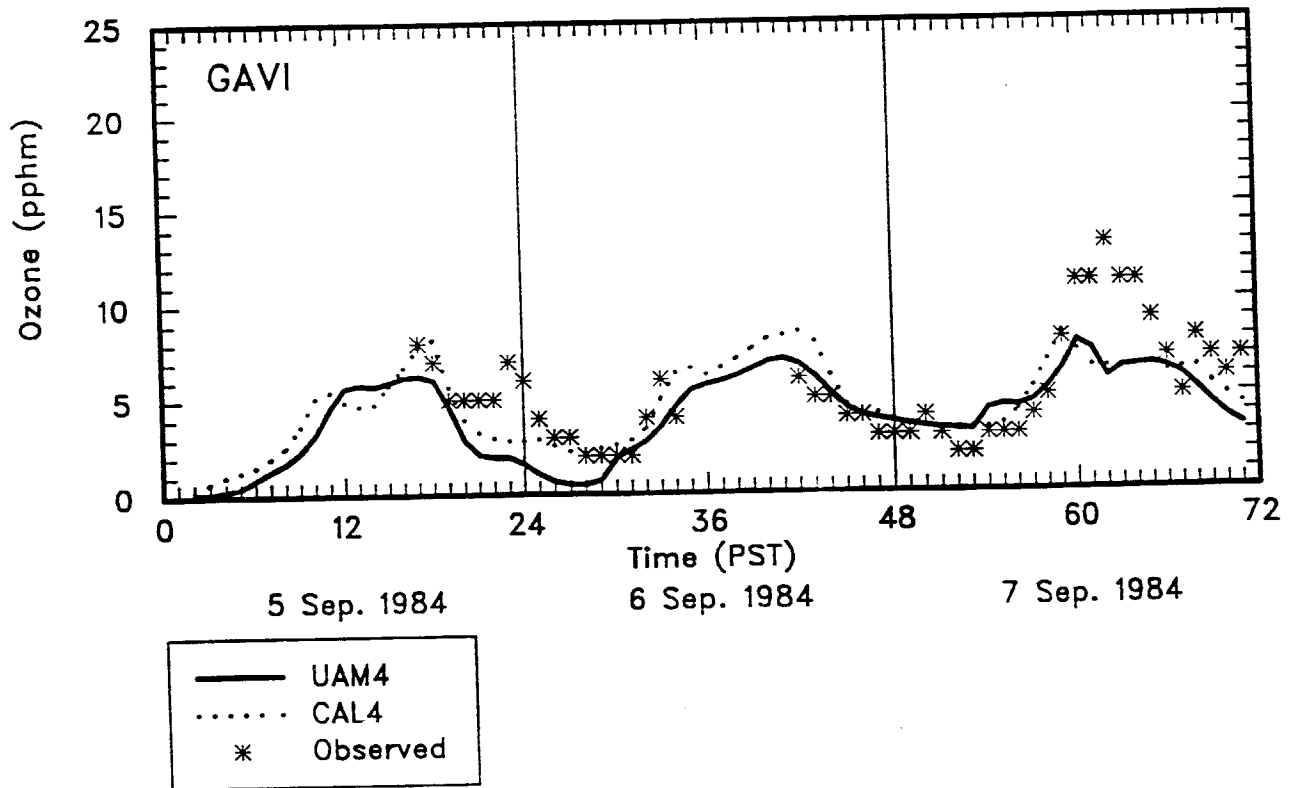
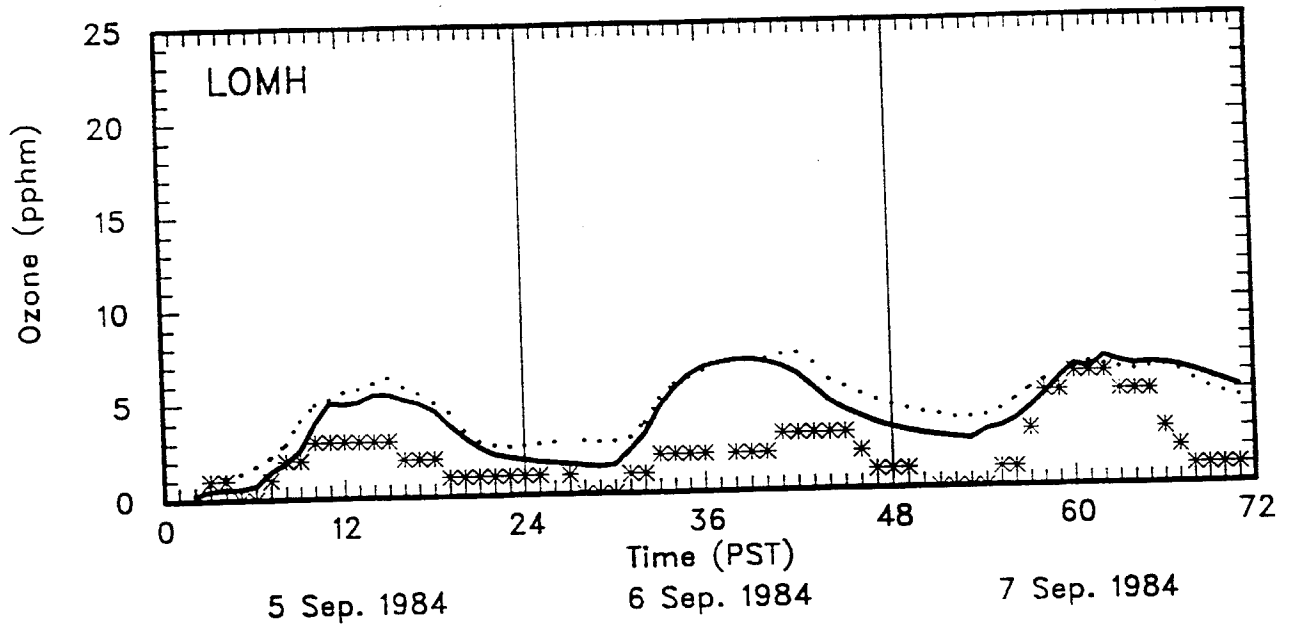


Figure 6-9. Continued.

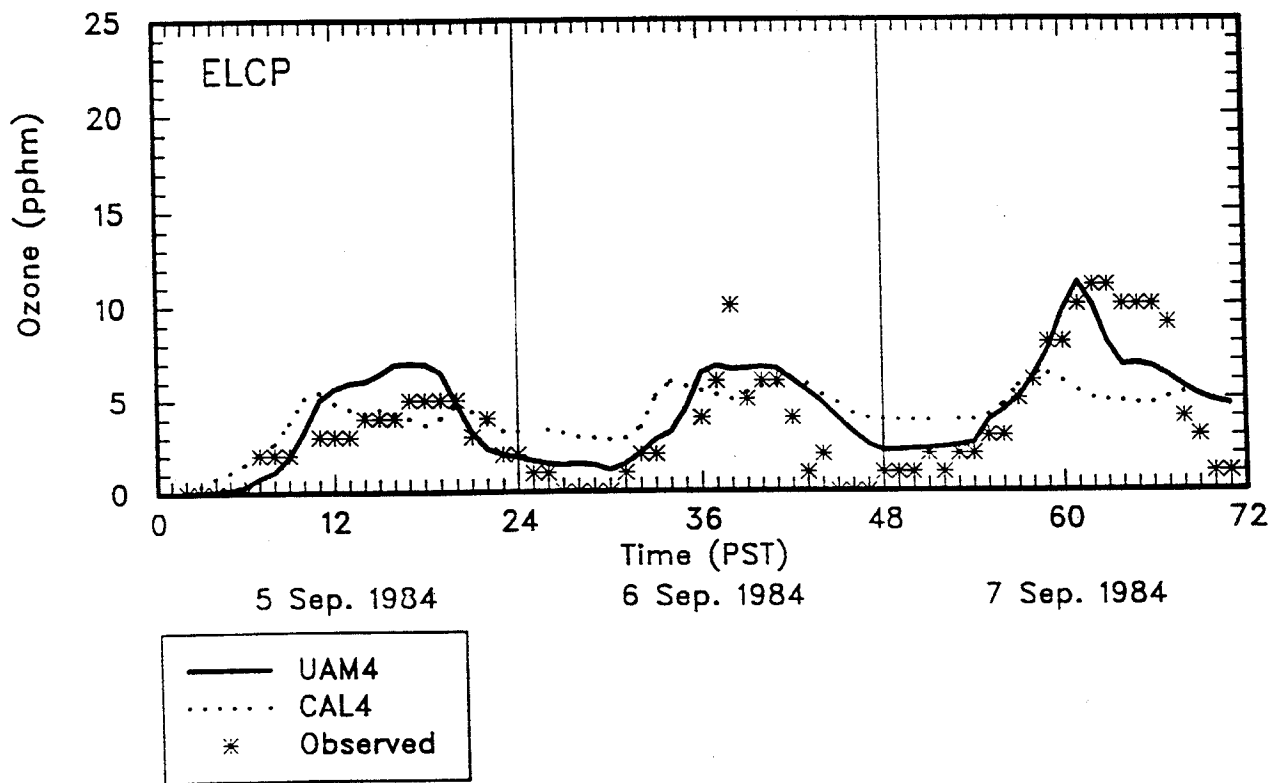
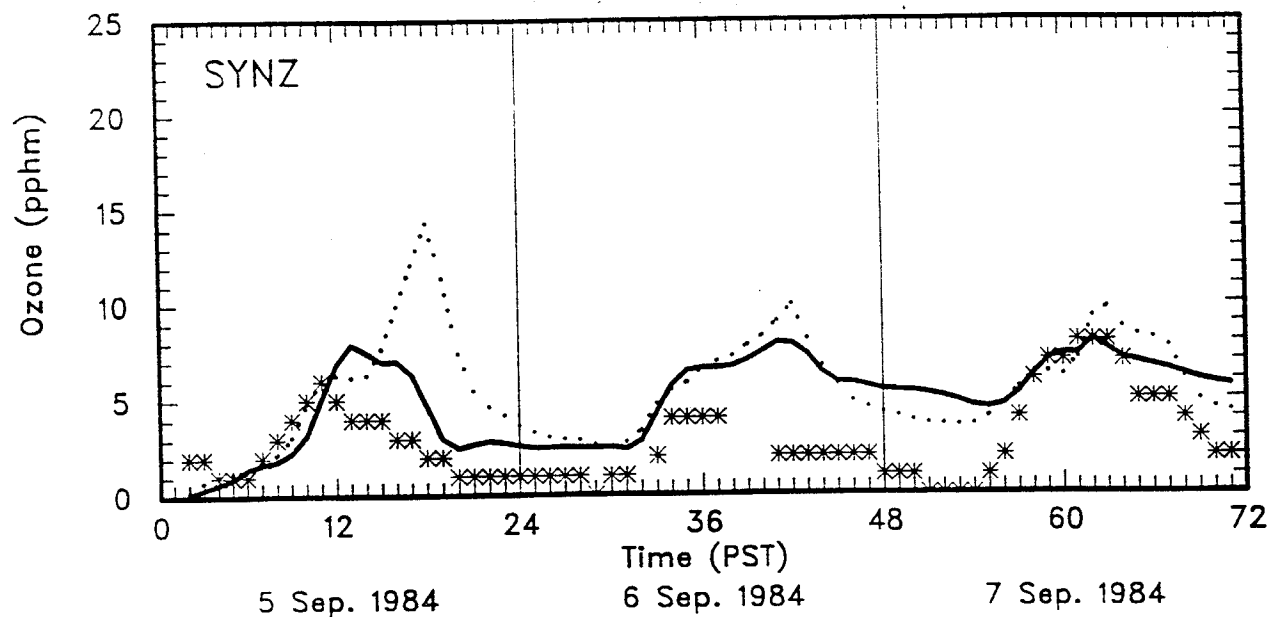


Figure 6-9. Continued.

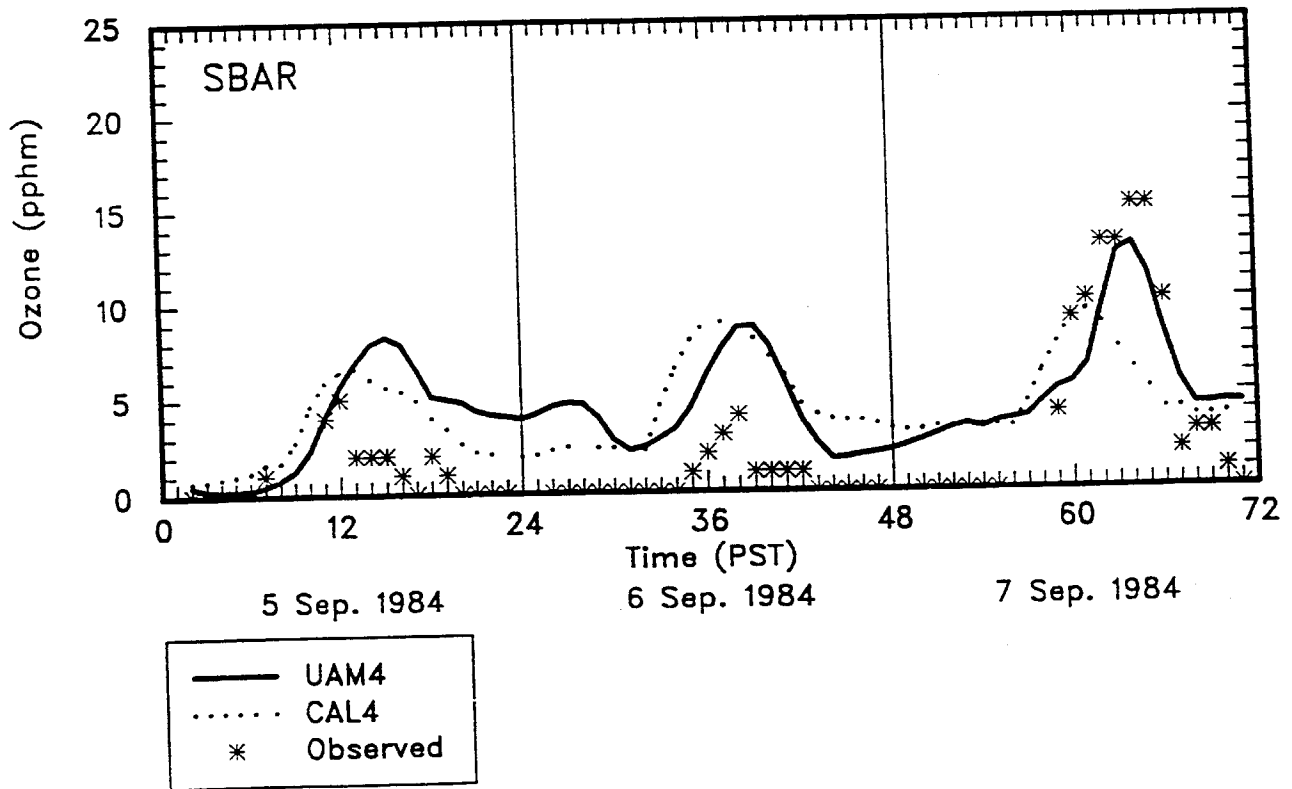
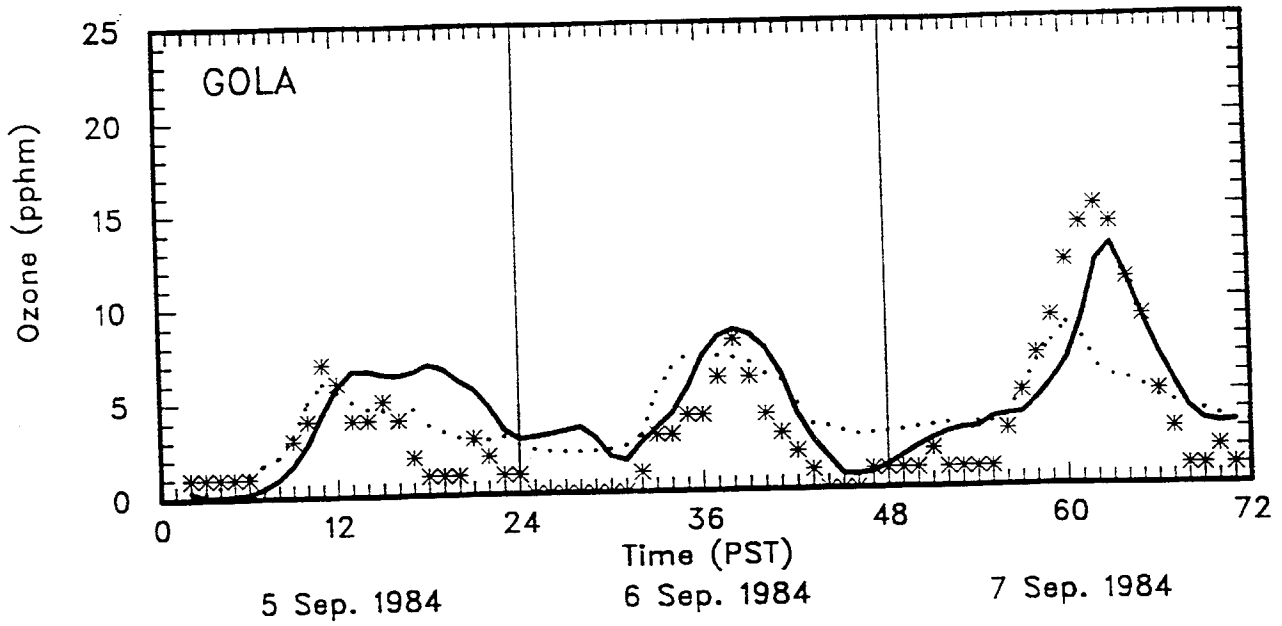


Figure 6-9. Continued.

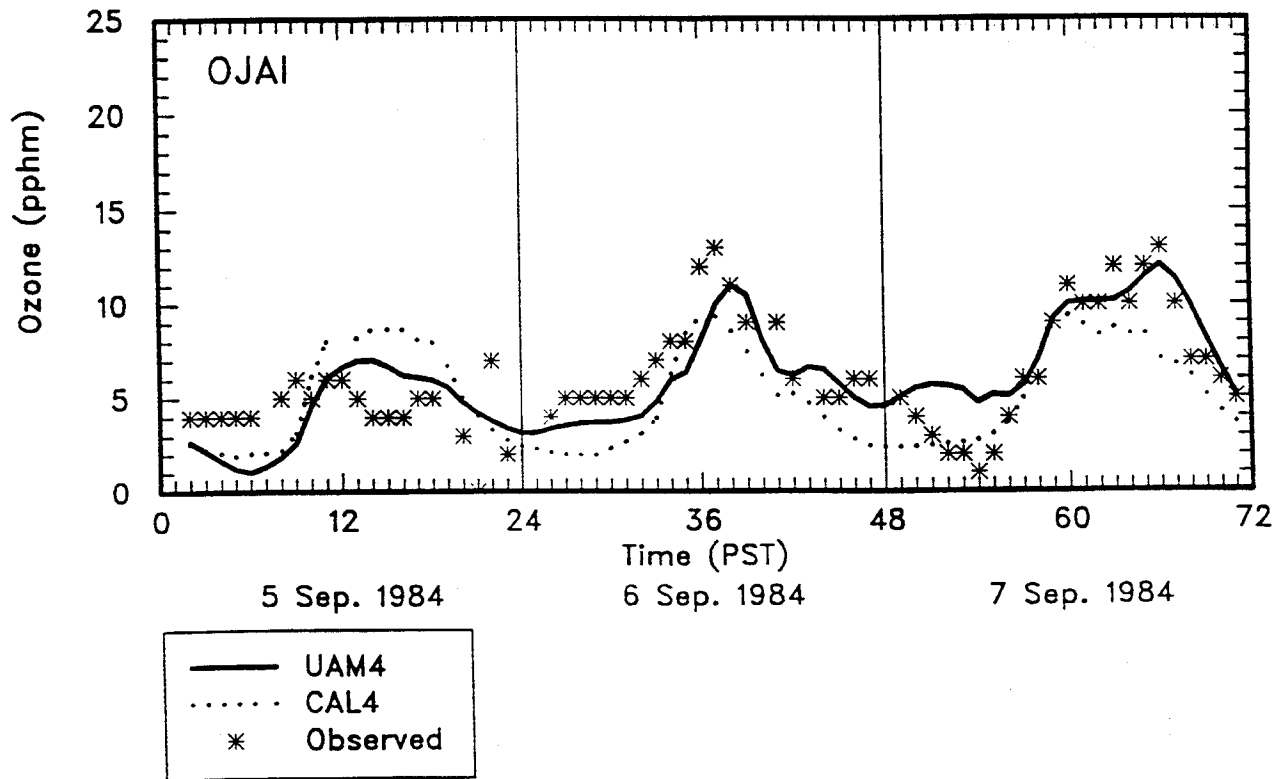
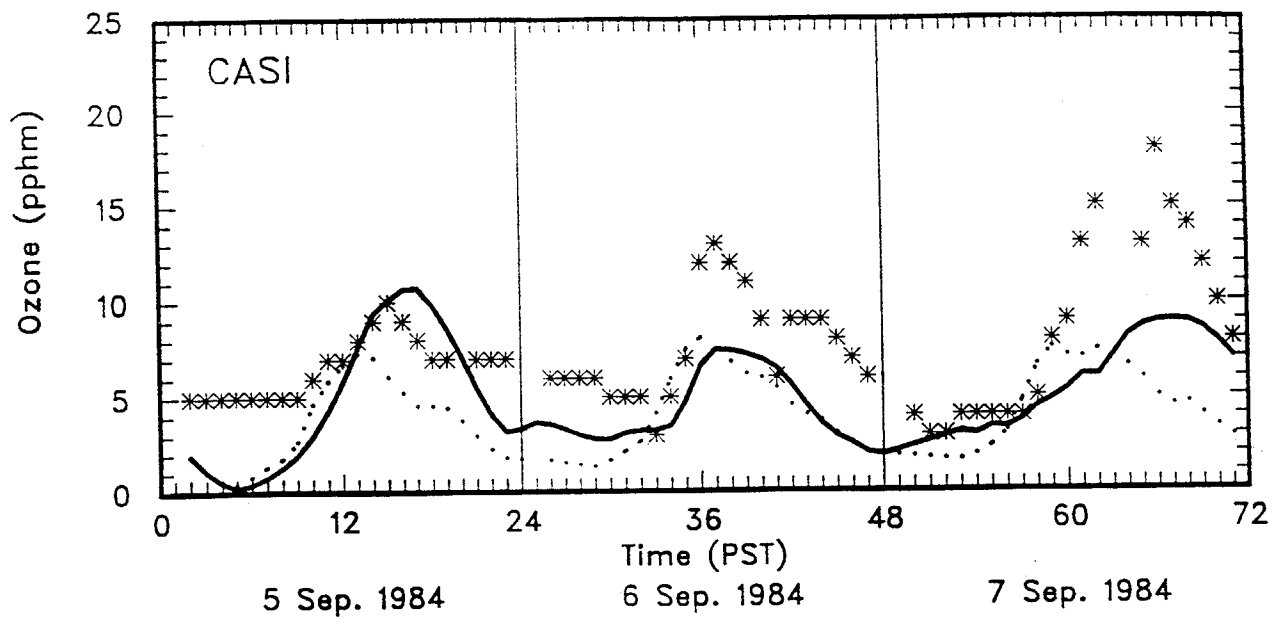


Figure 6-9. Continued.

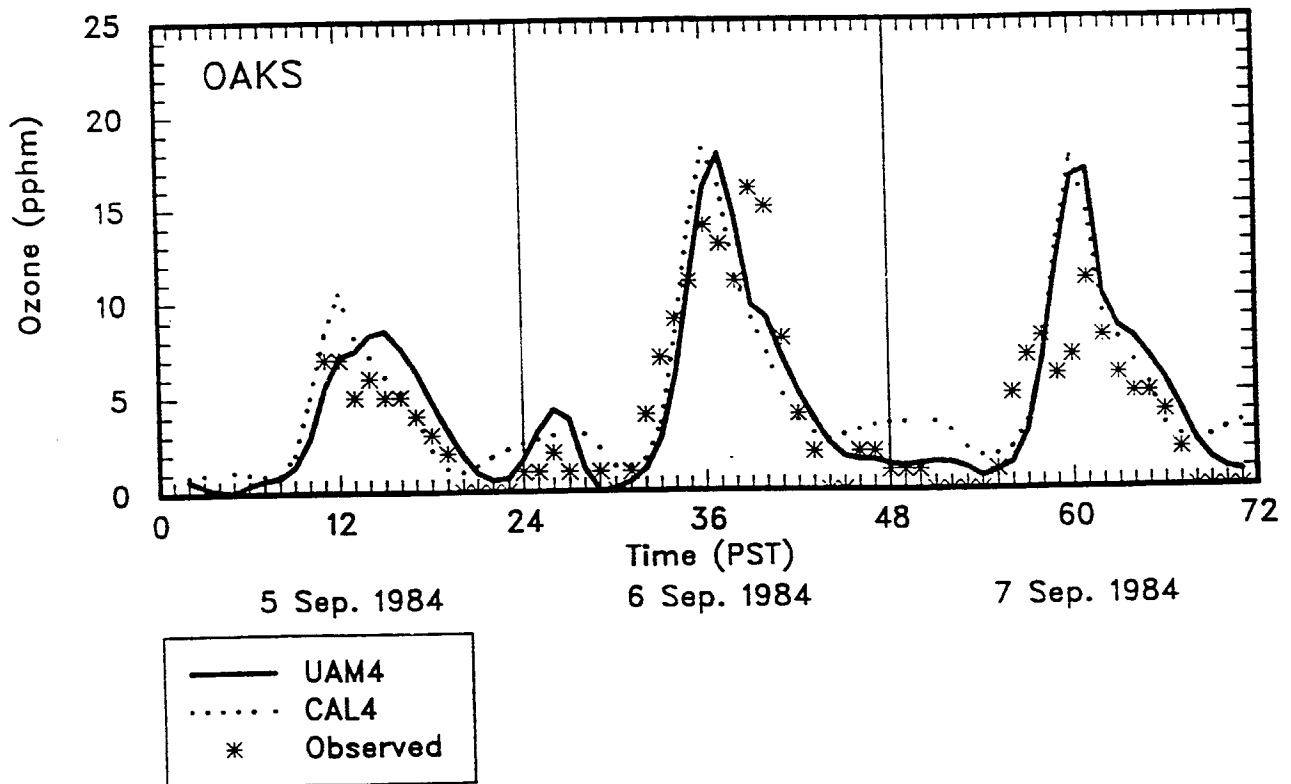
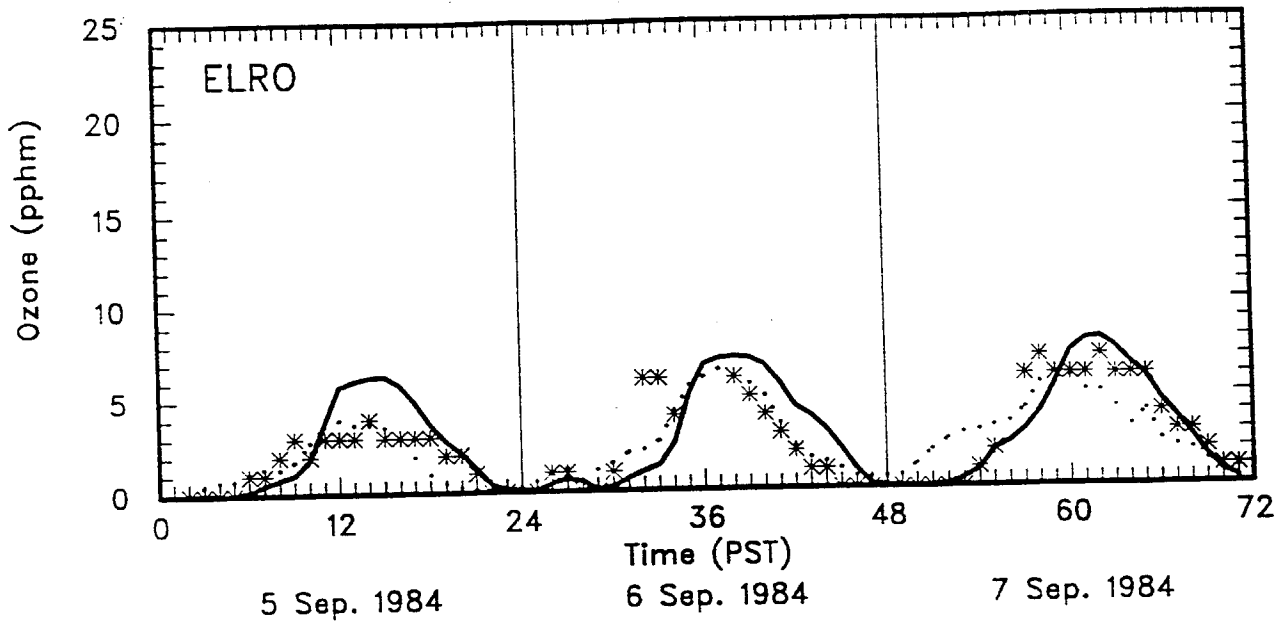


Figure 6-9. Continued.

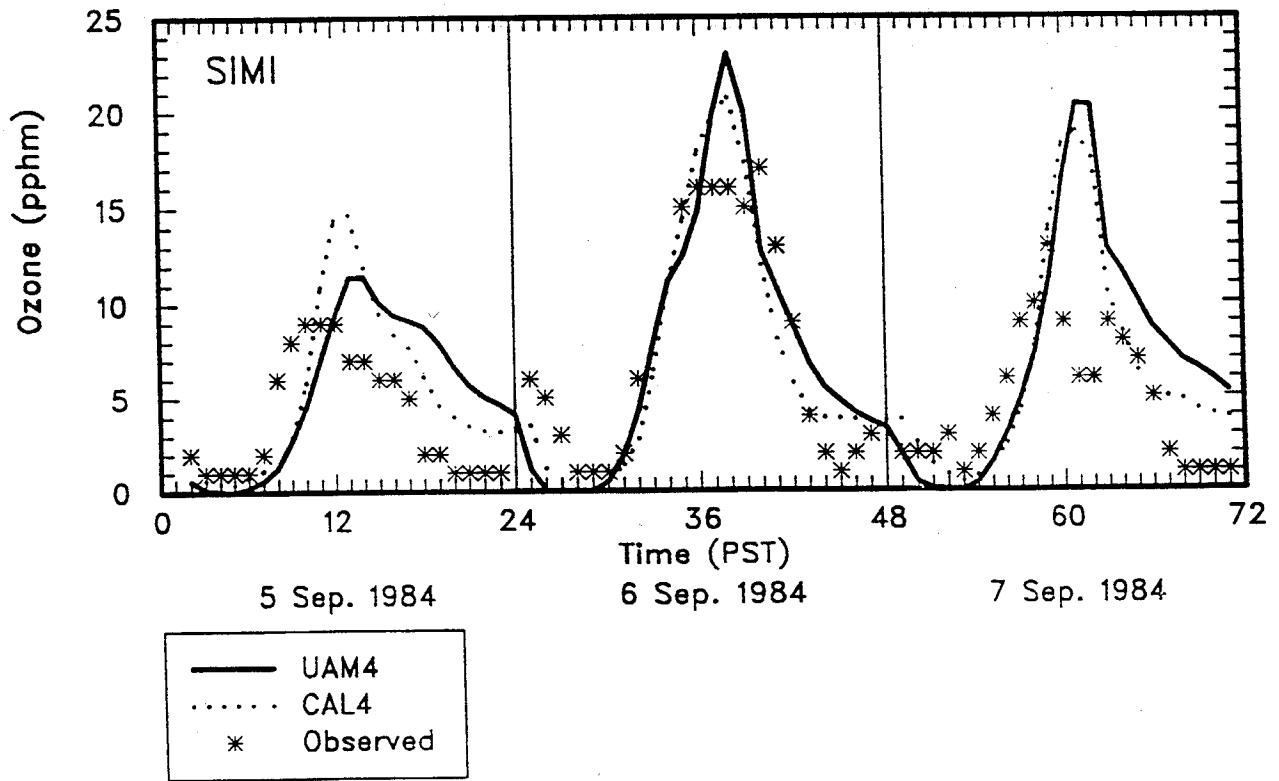
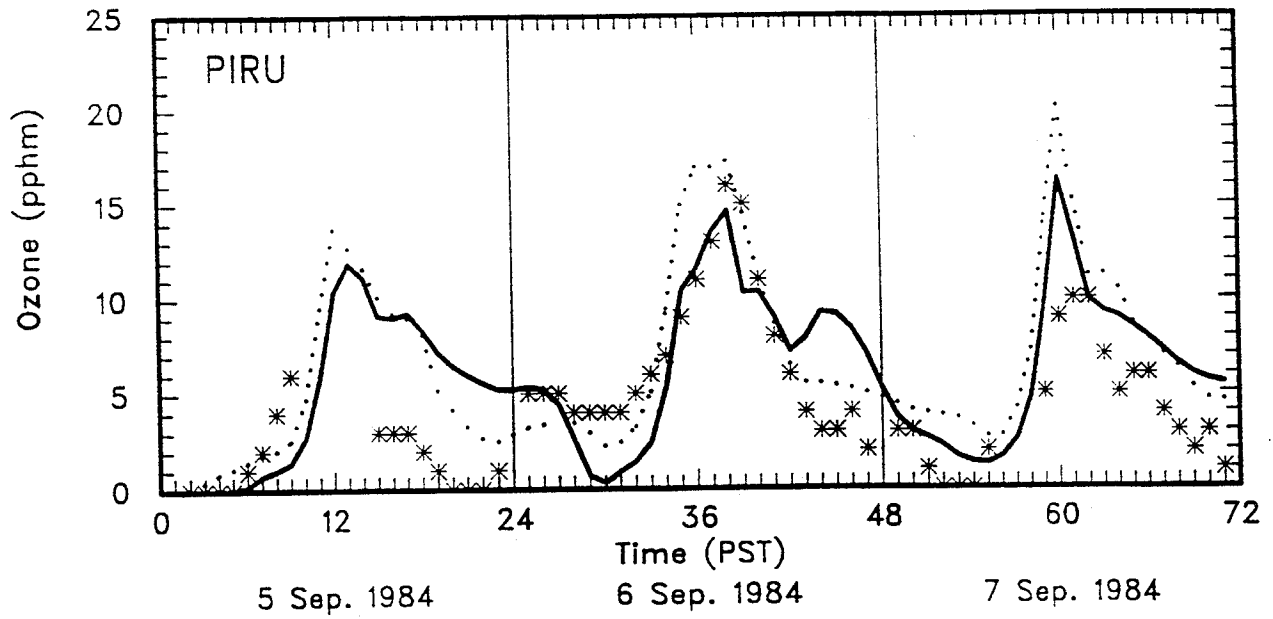


Figure 6-9. Concluded.

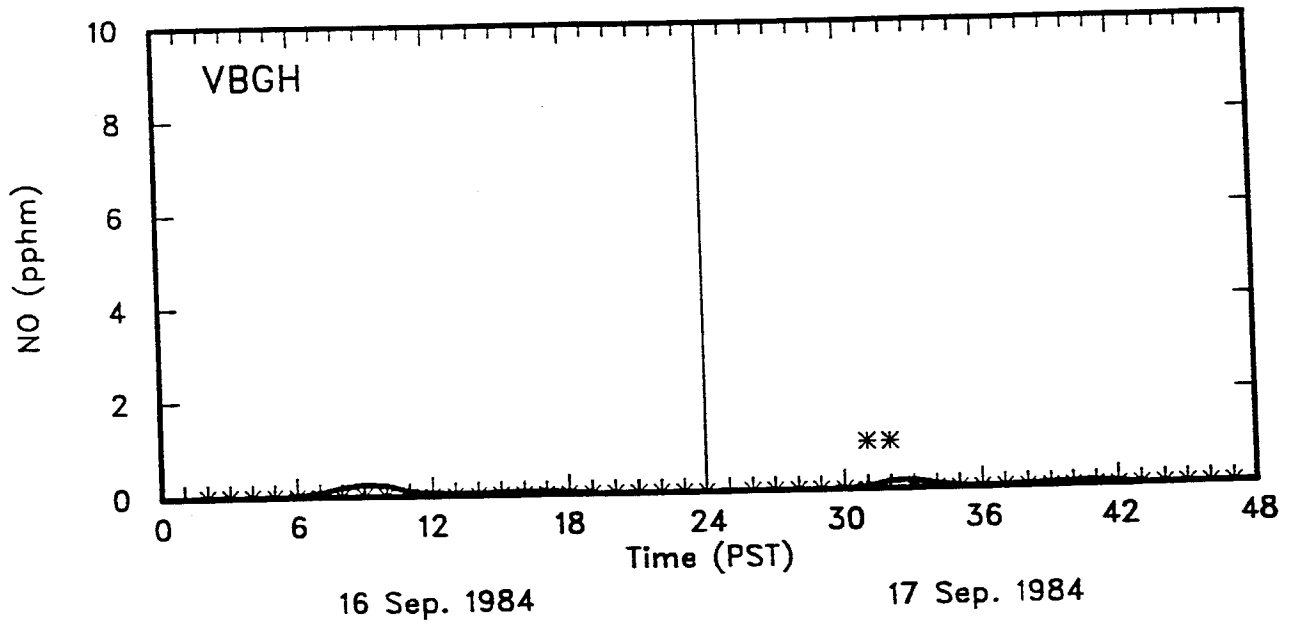
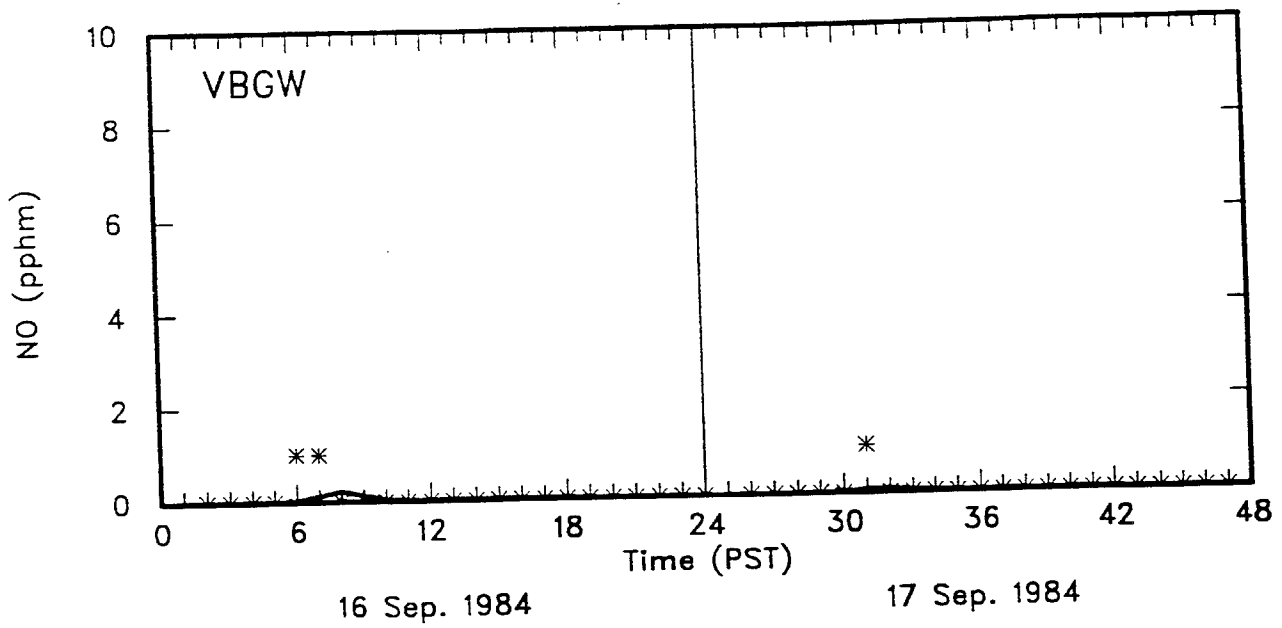


Figure 6-9. Time Series of Hourly Estimated and Observed NO Concentrations for the 5-7 September, 1984 Episode.

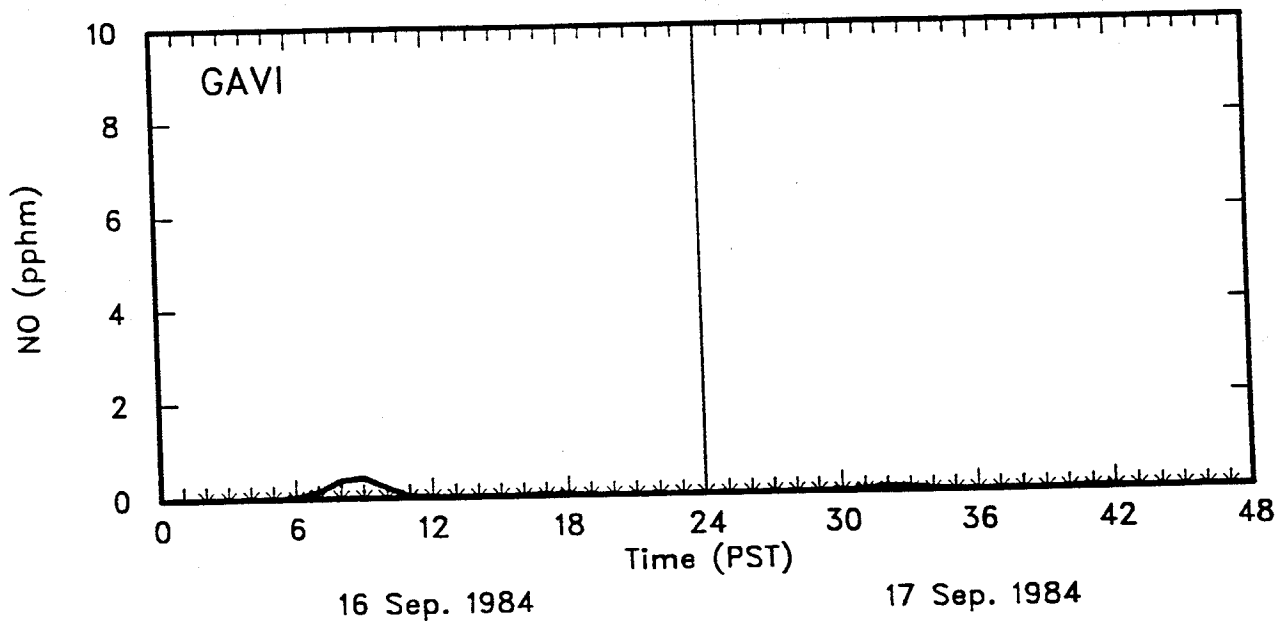
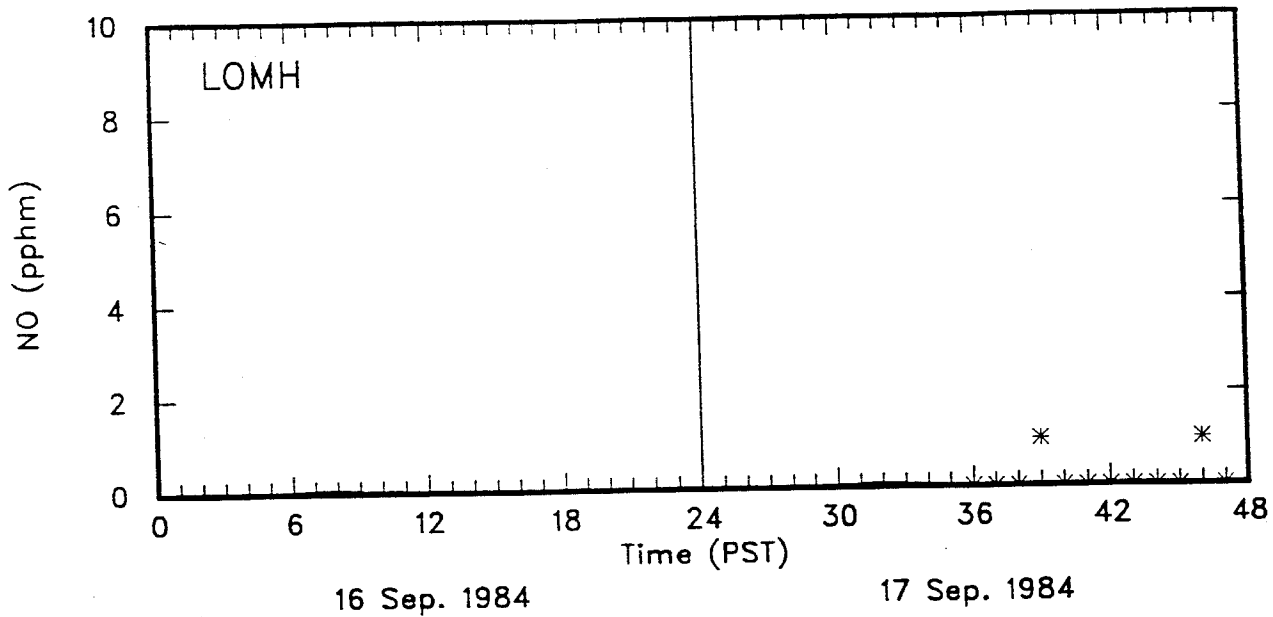


Figure 6-9. Continued.

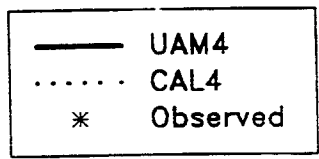
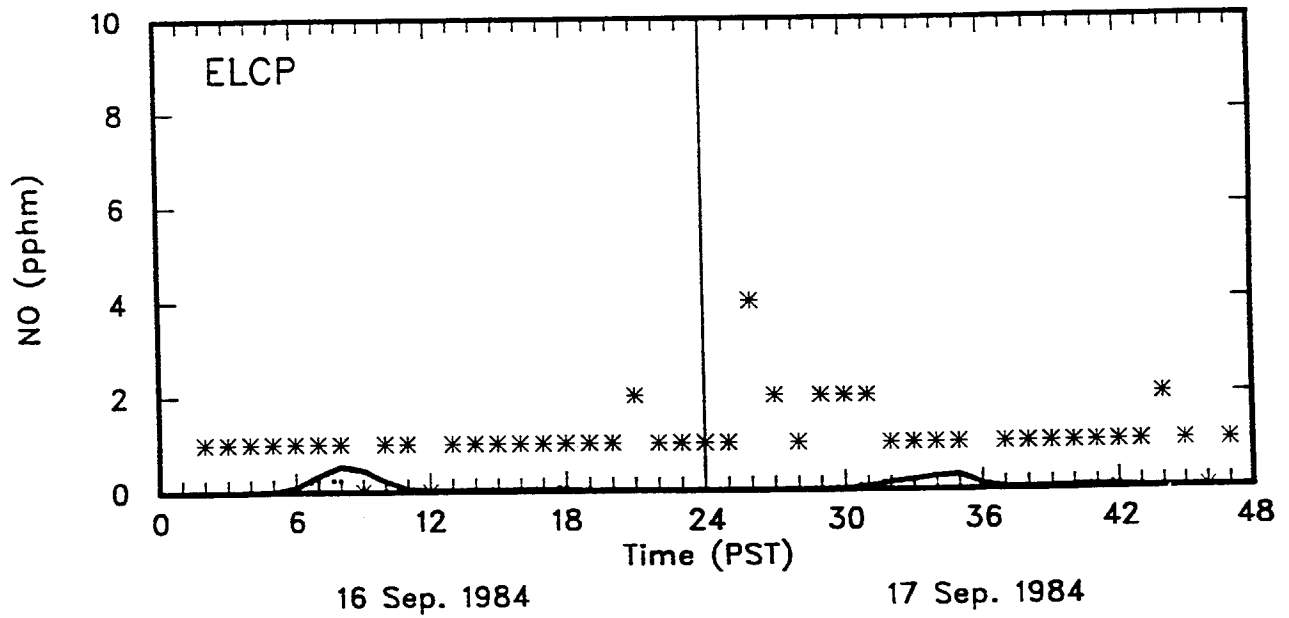
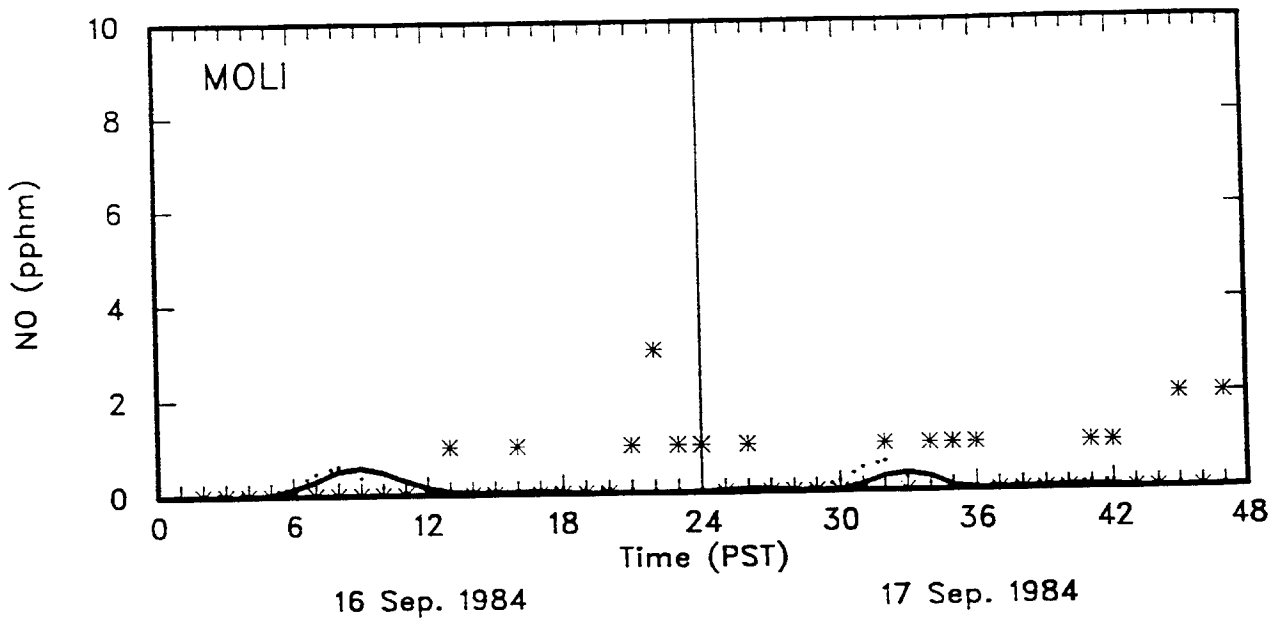


Figure 6-9. Continued.

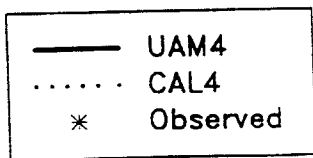
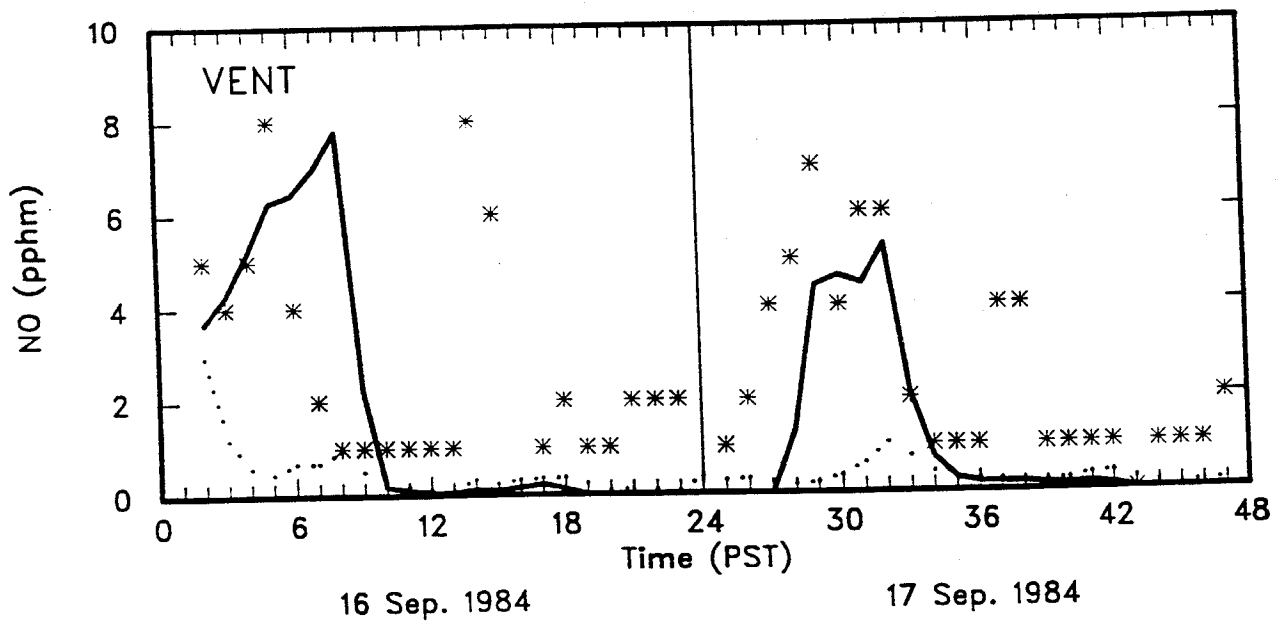
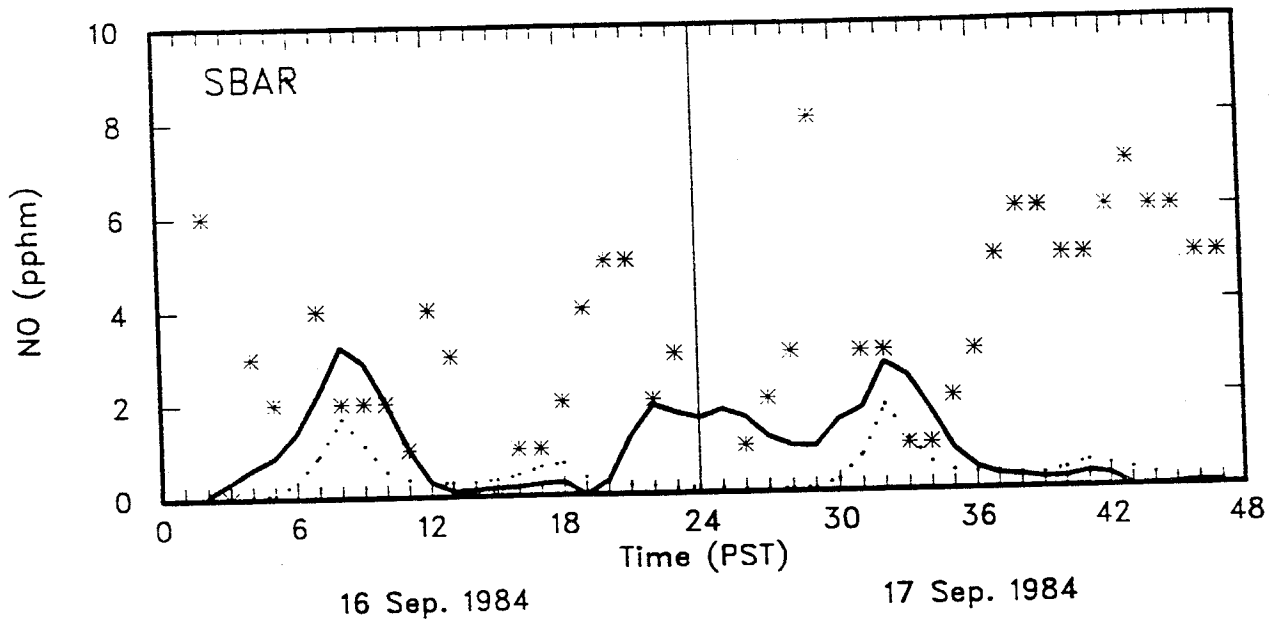


Figure 6-9. Continued.

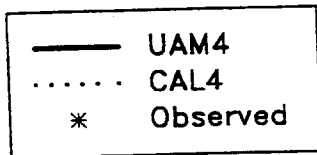
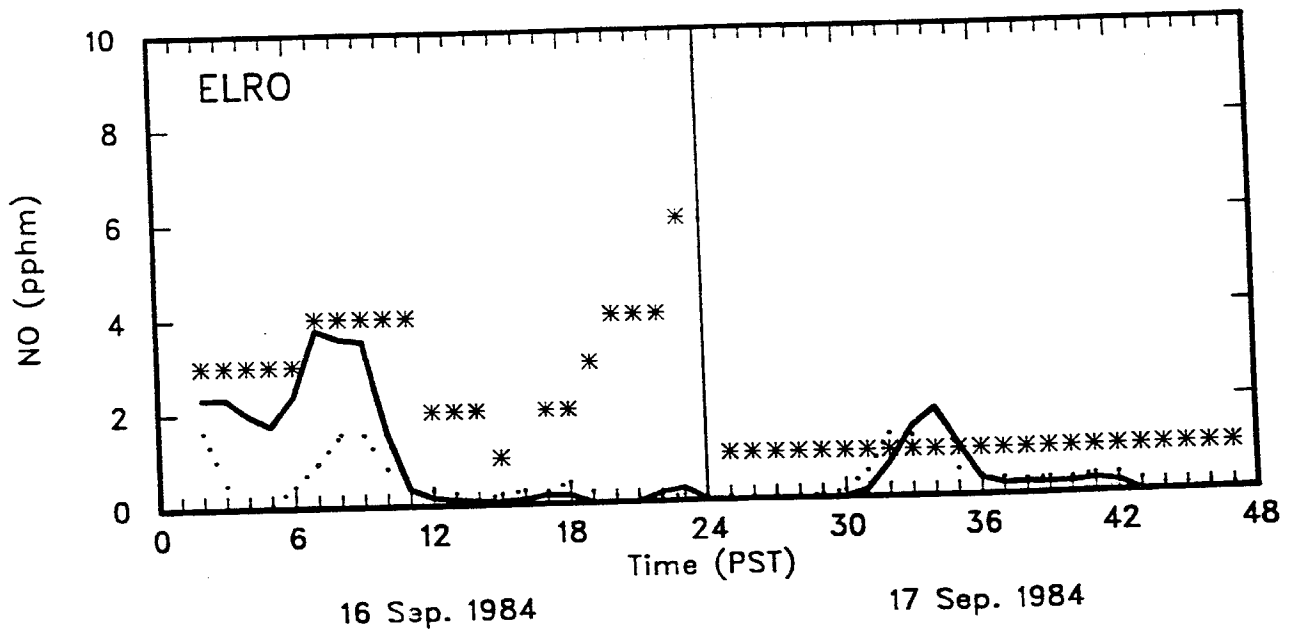
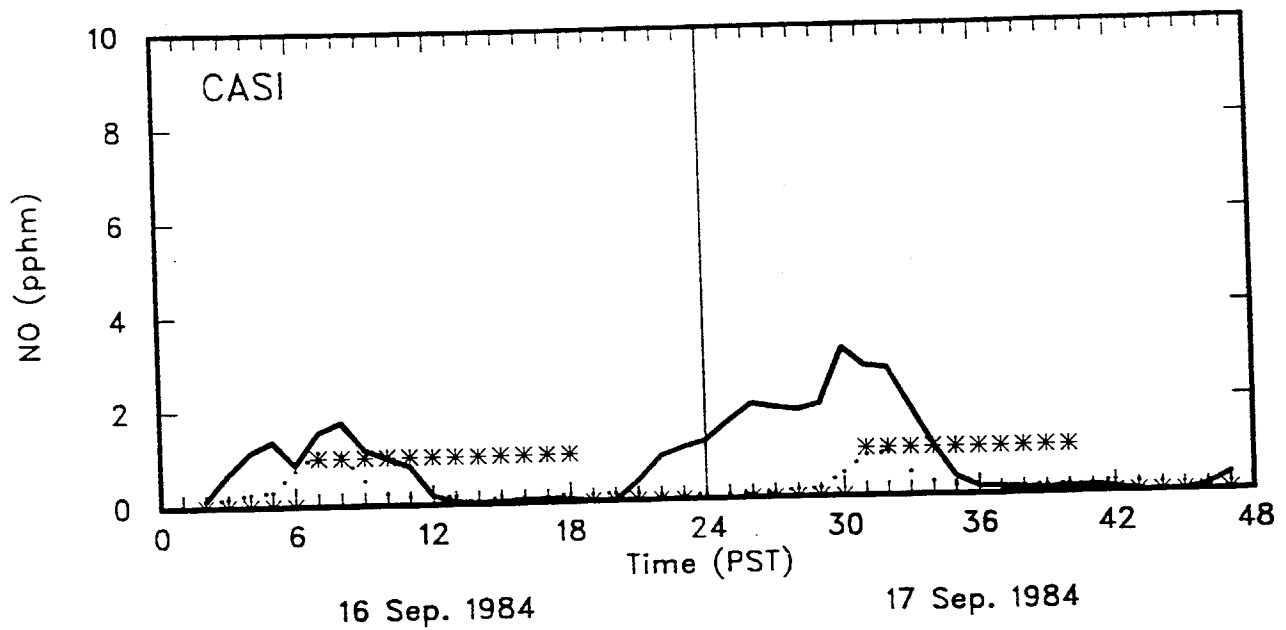


Figure 6-9. Continued.

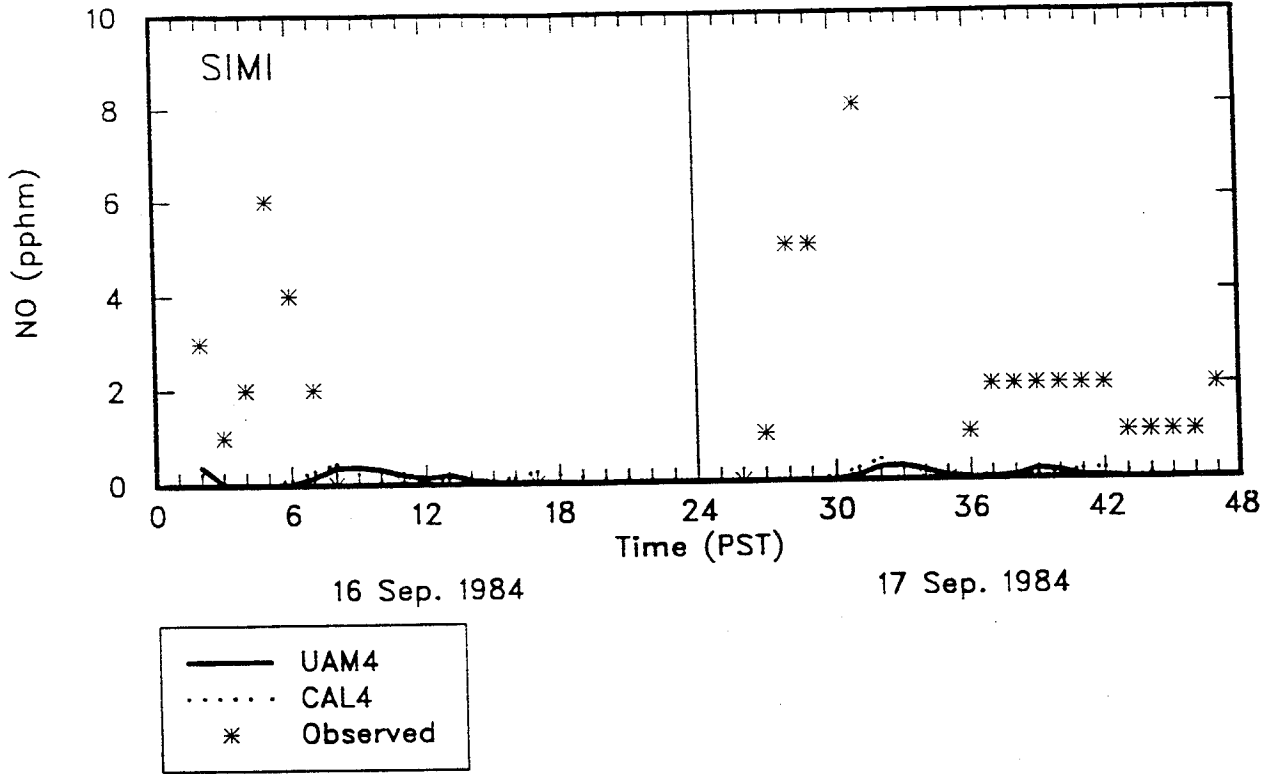


Figure 6-9. Concluded.

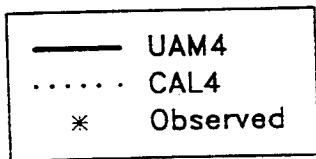
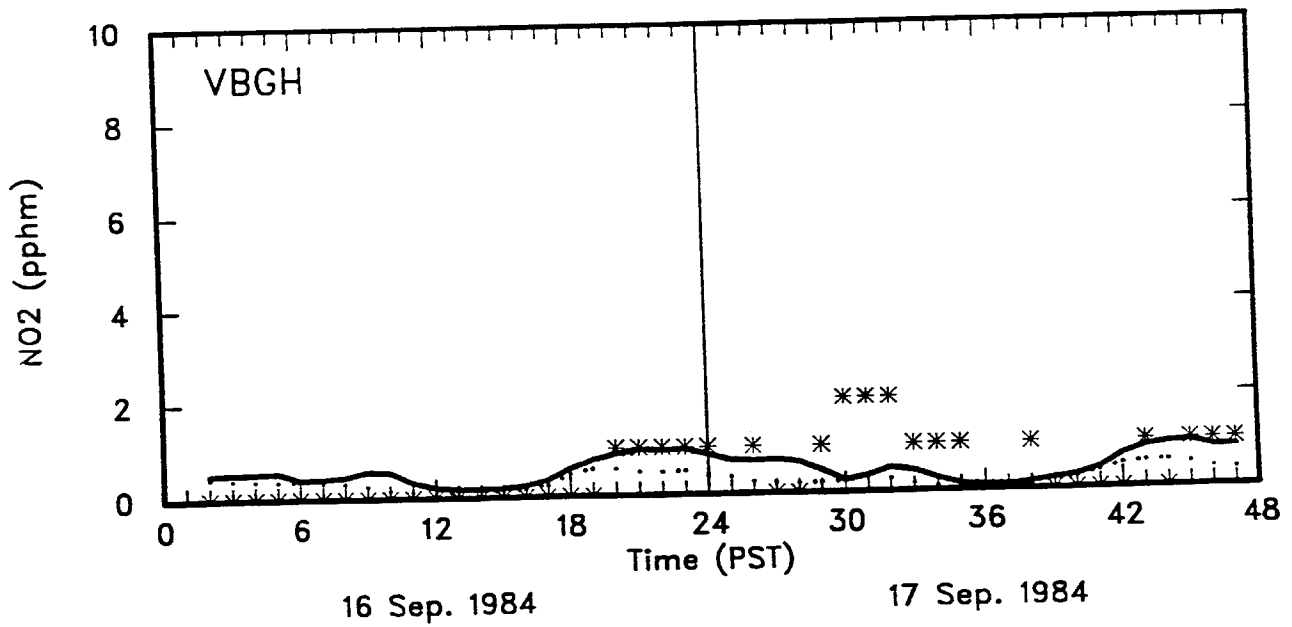
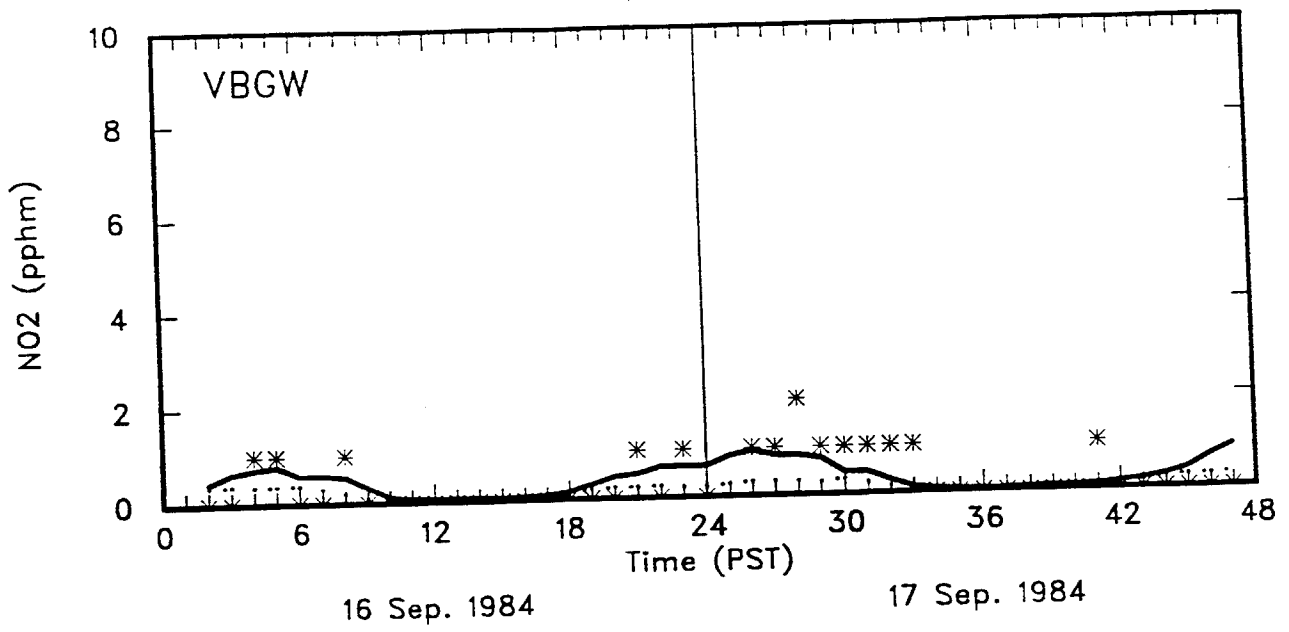


Figure 6-9. Time Series of Hourly Estimated and Observed NO<sub>2</sub> Concentrations for the 5-7 September, 1984 Episode.

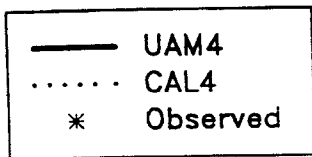
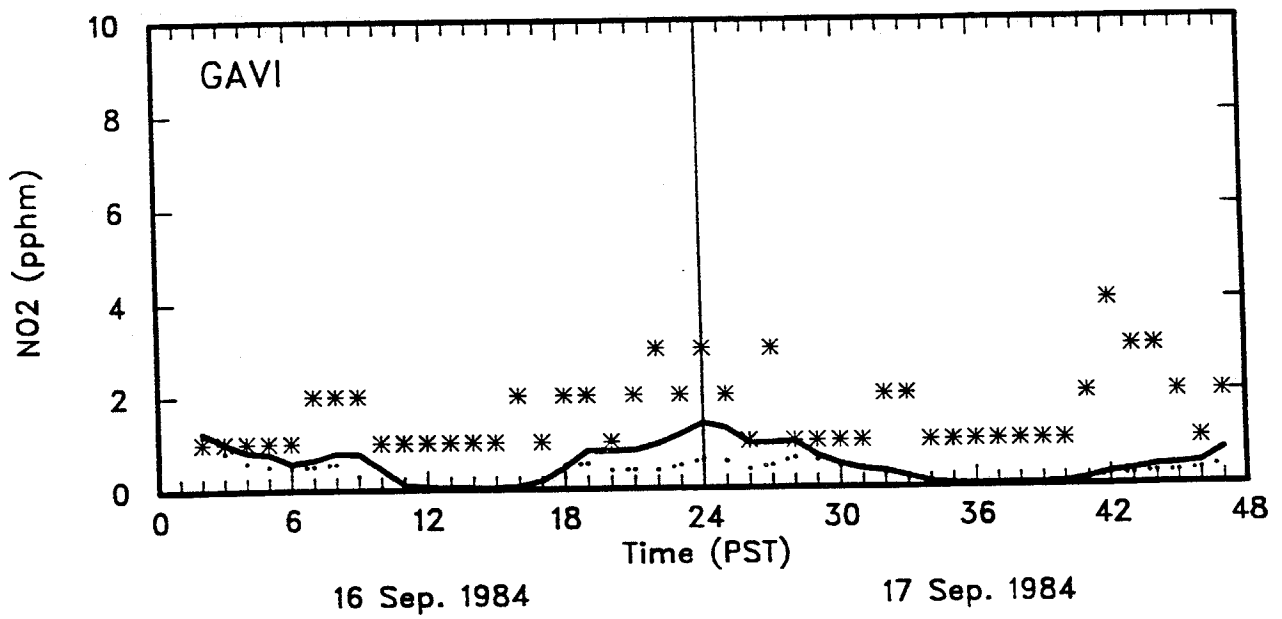
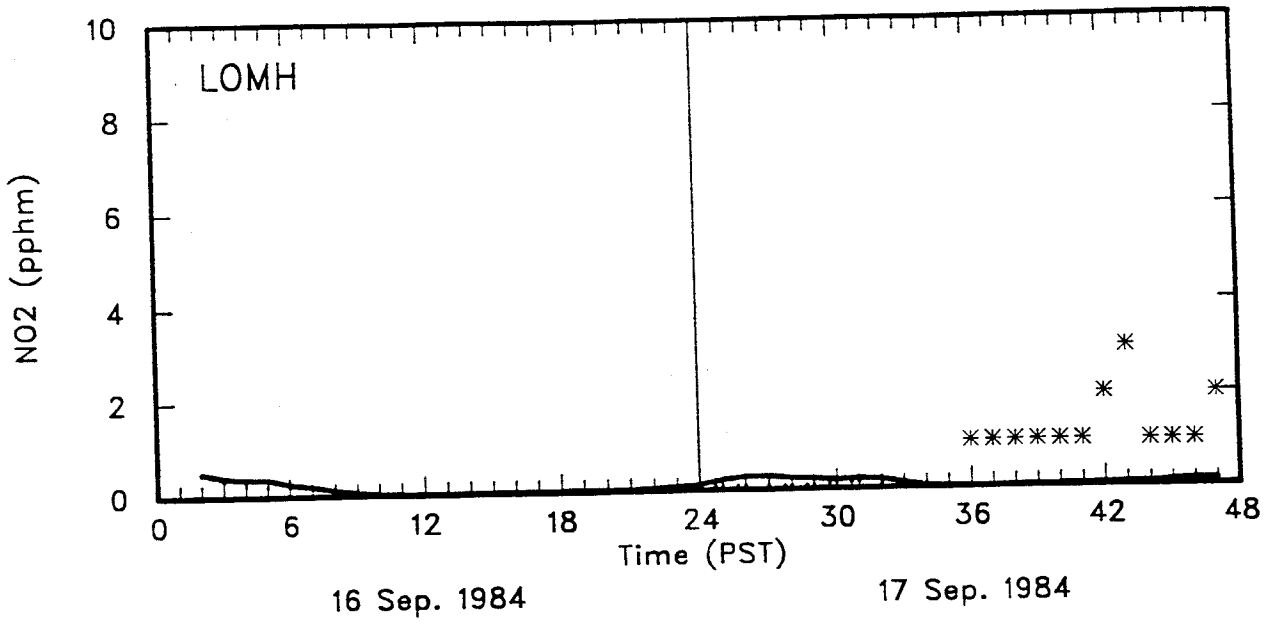


Figure 6-9. Continued.

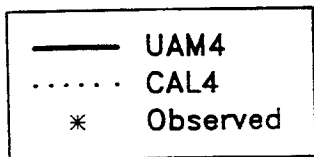
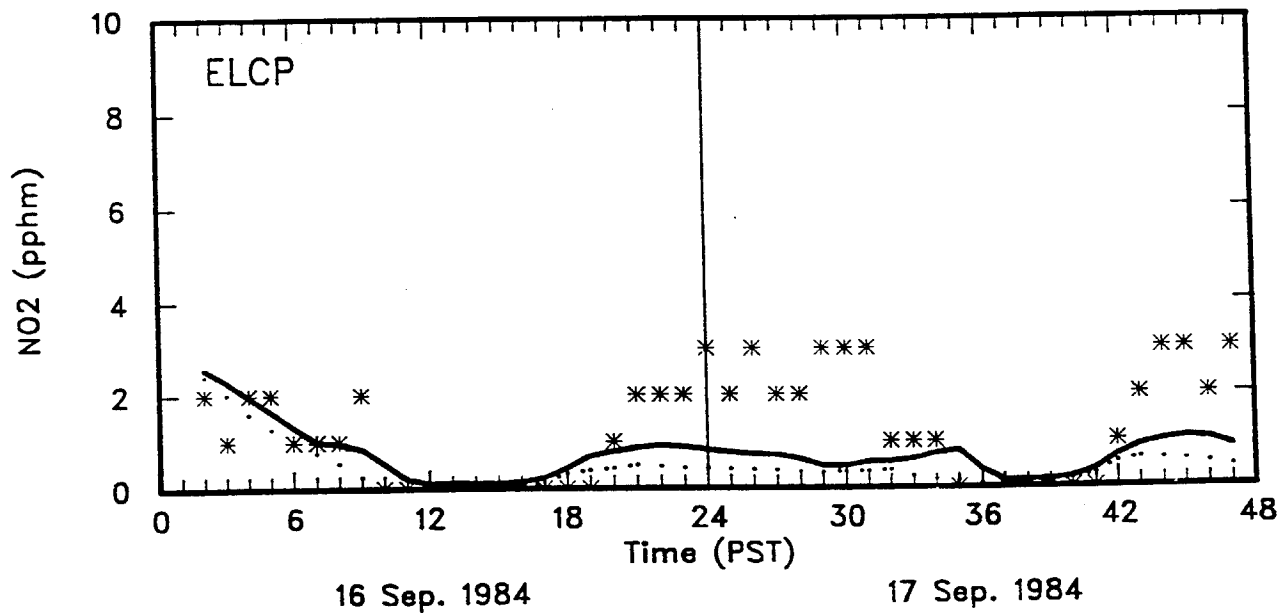
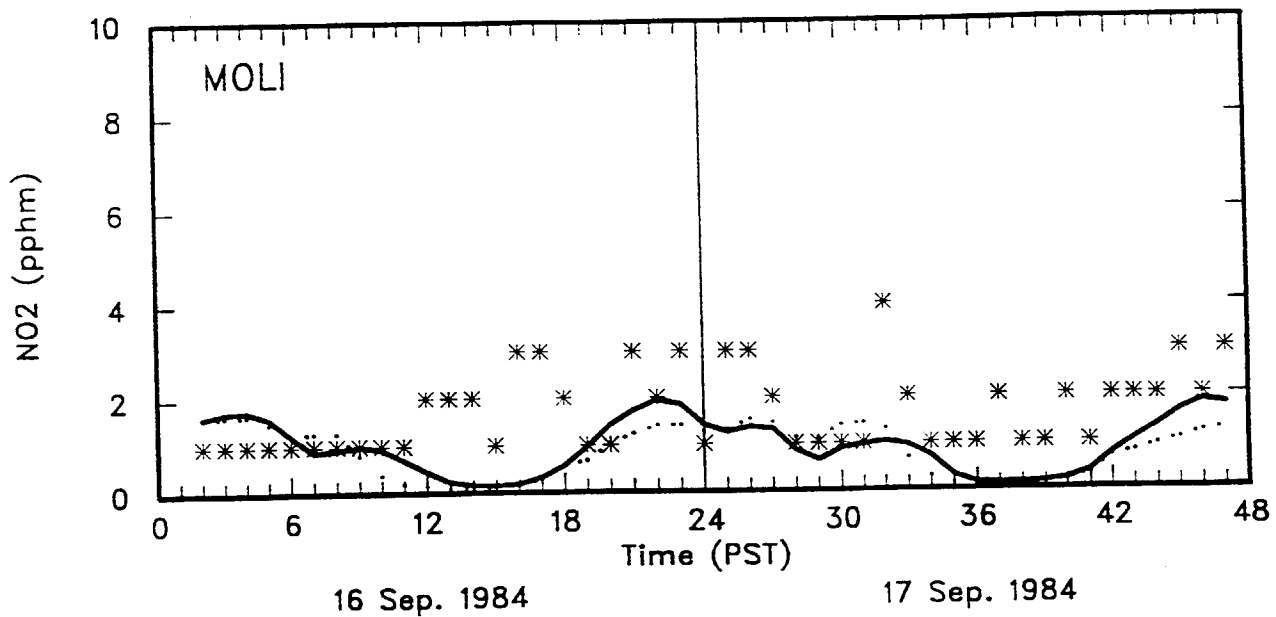


Figure 6-9. Continued.

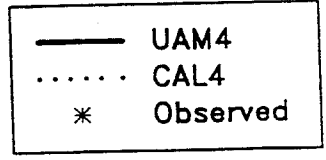
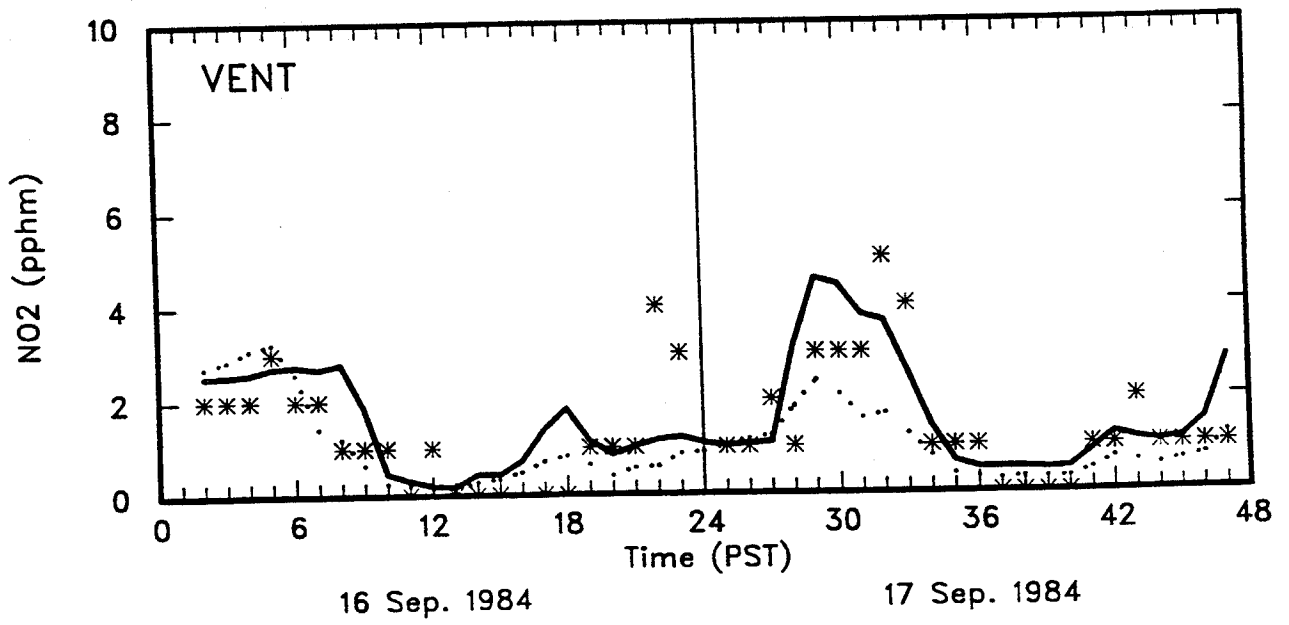
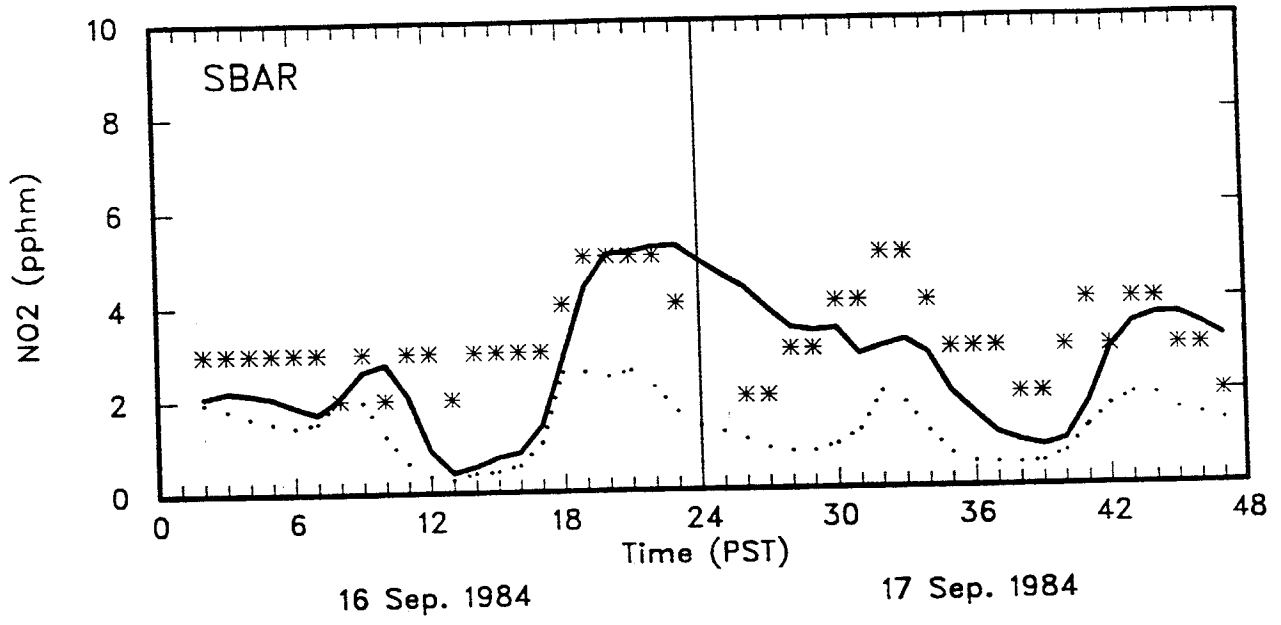


Figure 6-9. Continued.

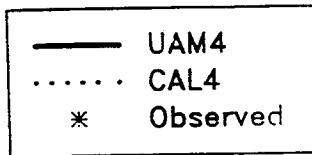
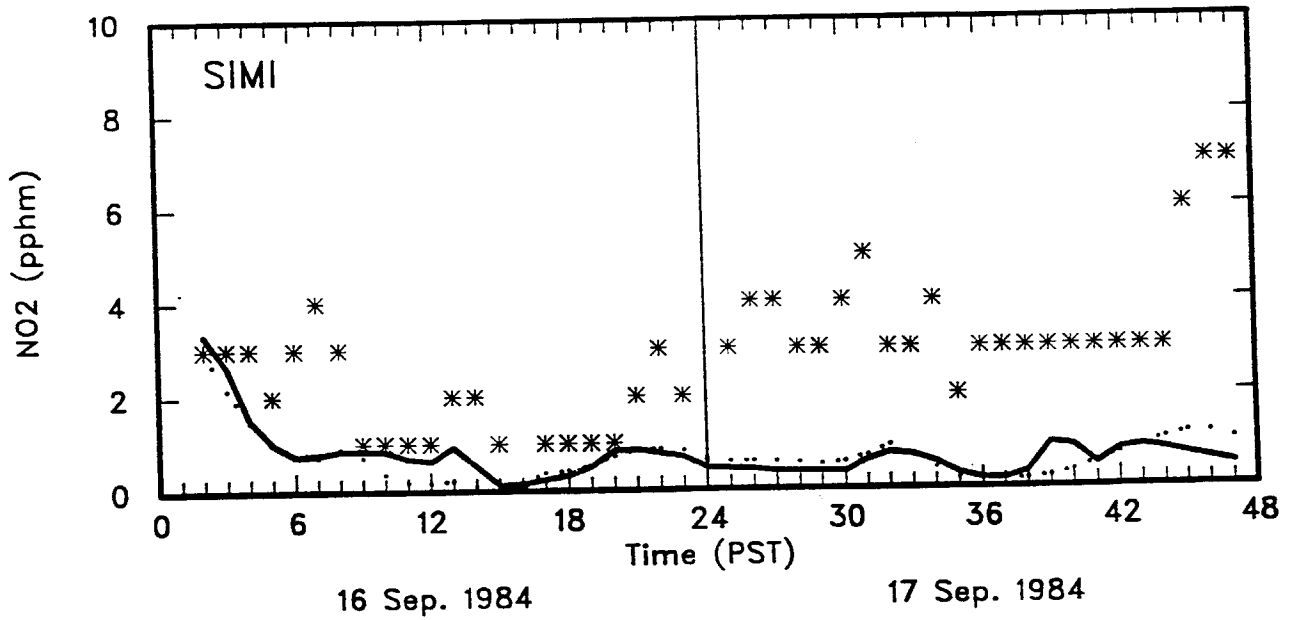
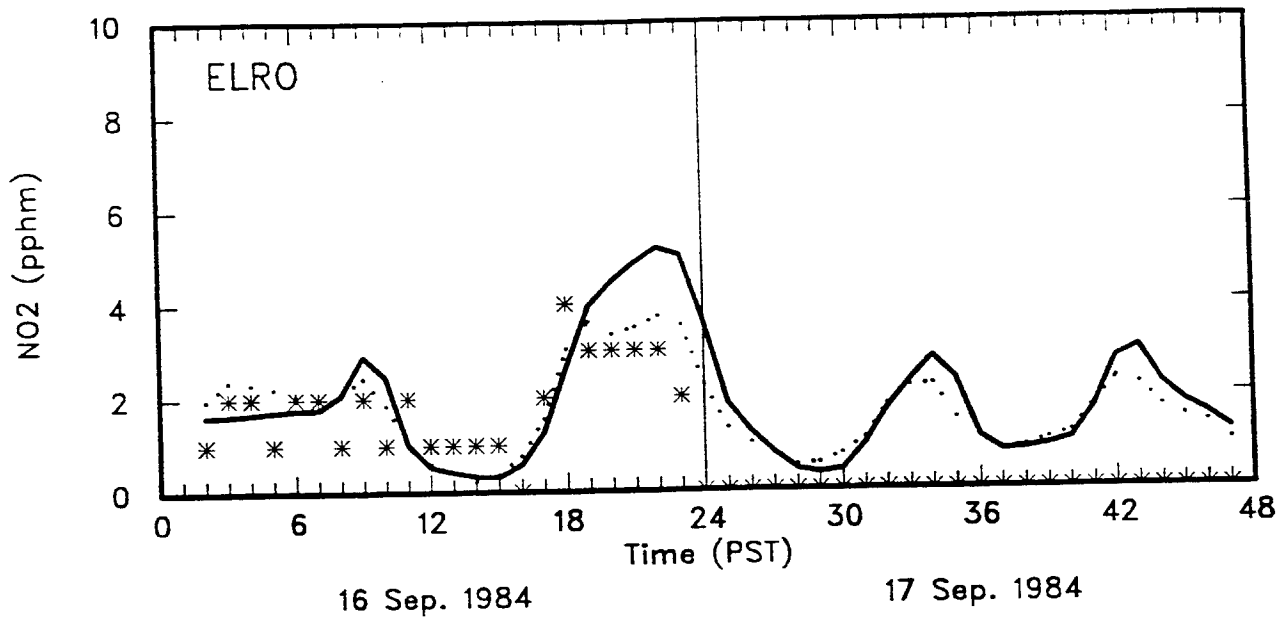
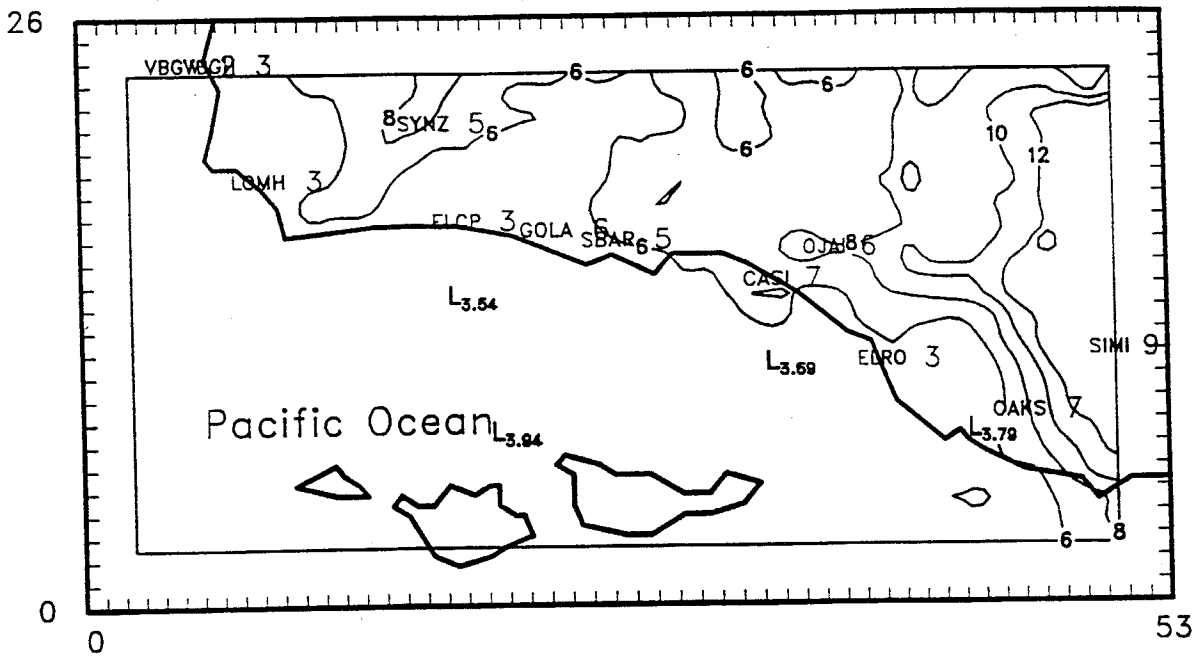


Figure 6-9. Concluded.

CALGRID-IV



UAM-IV

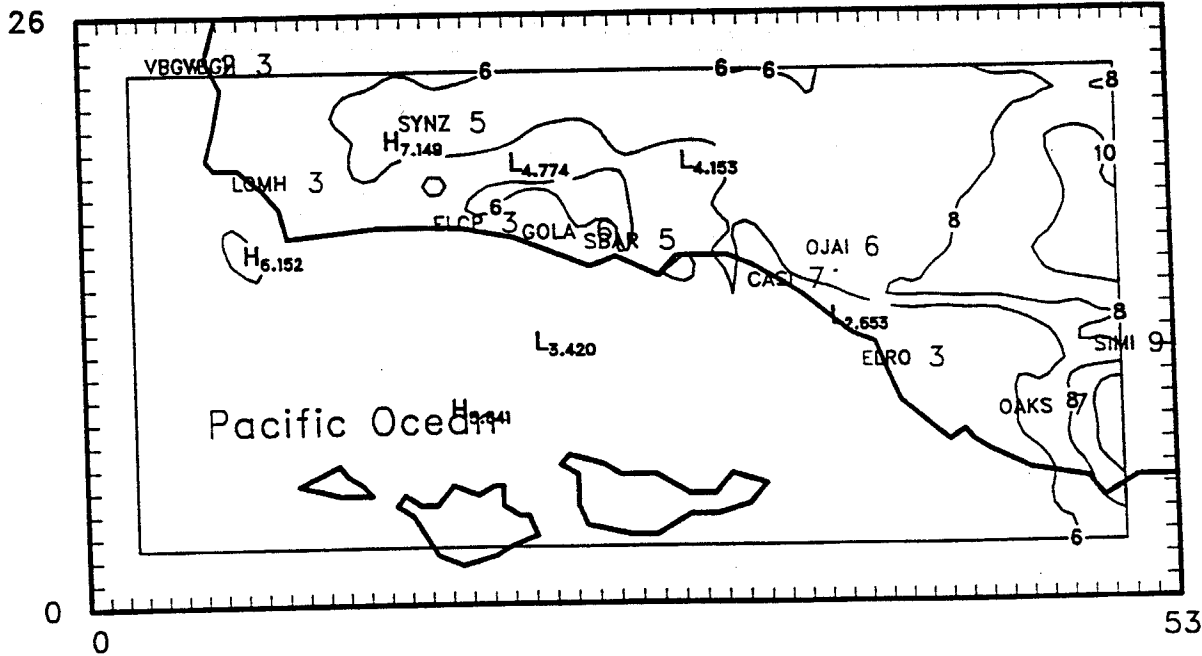


Figure 6-10a. Ground Level Ozone Isopleths of Hourly Ozone Concentrations for the 5-7 September, 1984 Episode -- 5 September, 1200 PST.

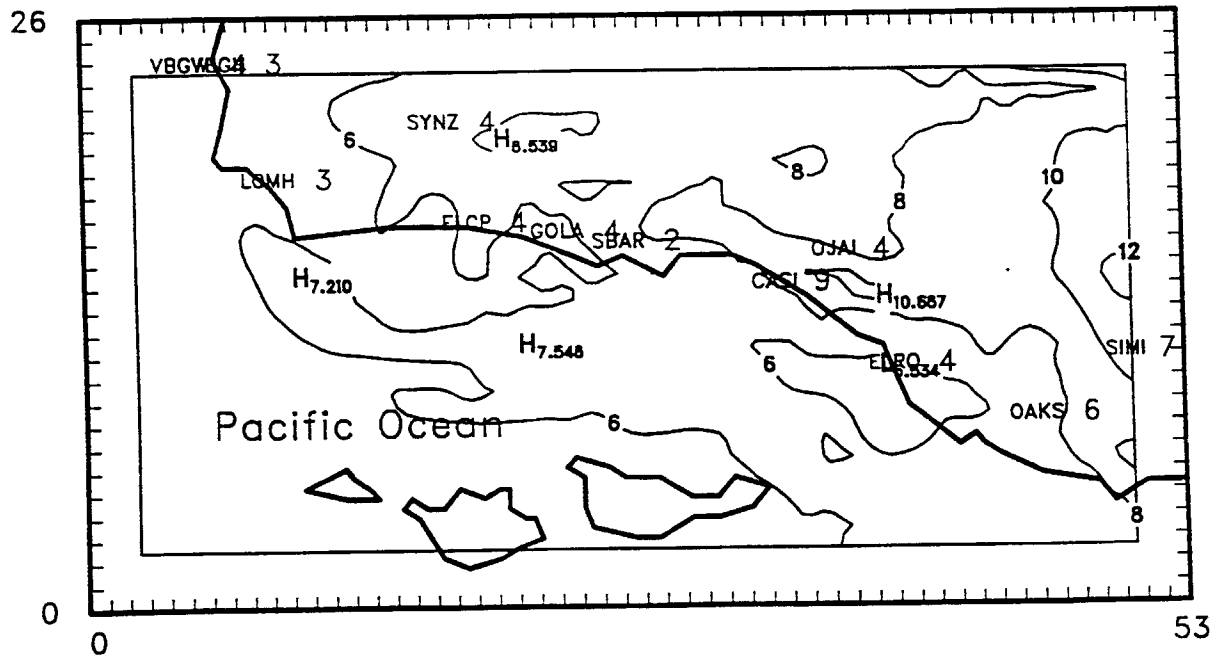
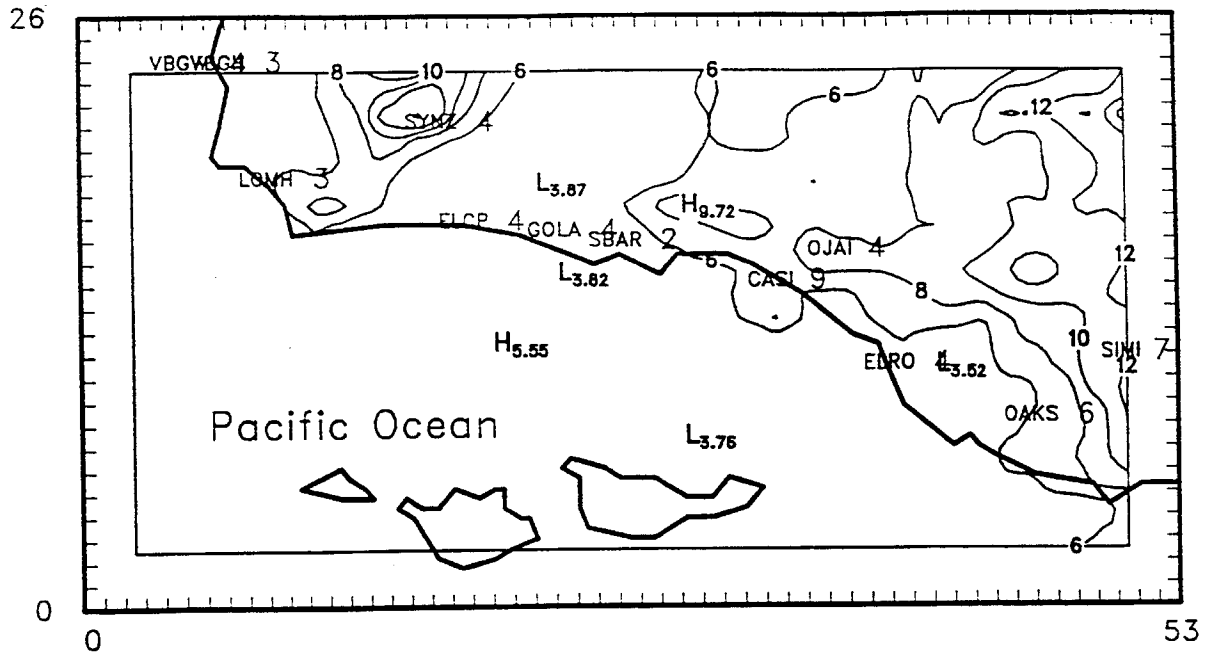
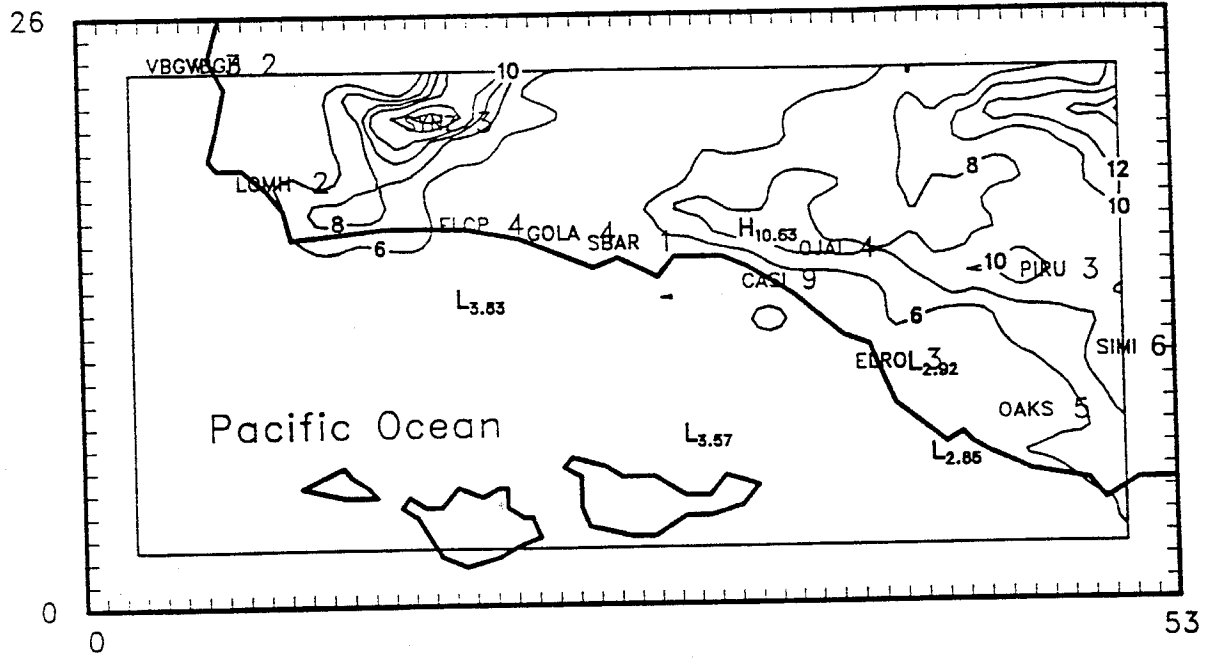


Figure 6-10b. Ground Level Ozone Isopleths of Hourly Ozone Concentrations for the 5-7 September, 1984 Episode – 5 September, 1400 PST.

CALGRID-IV



UAM-IV

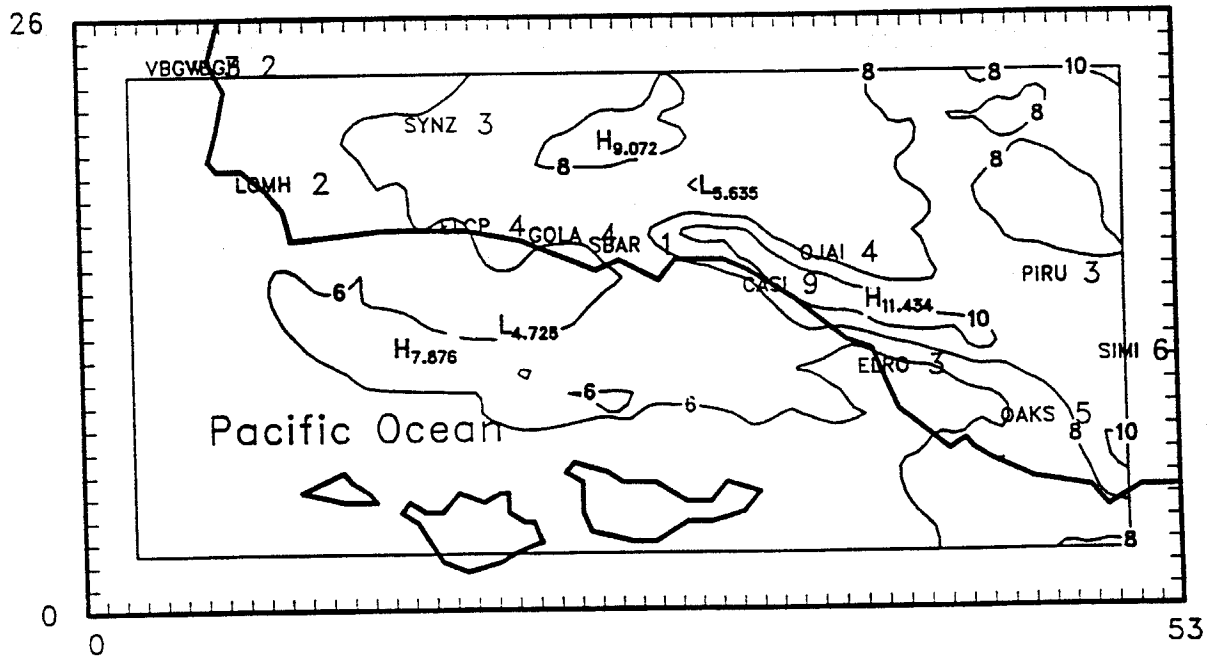


Figure 6-10c. Ground Level Ozone Isopleths of Hourly Ozone Concentrations for the 5-7 September, 1984 Episode - 5 September, 1600 PST.

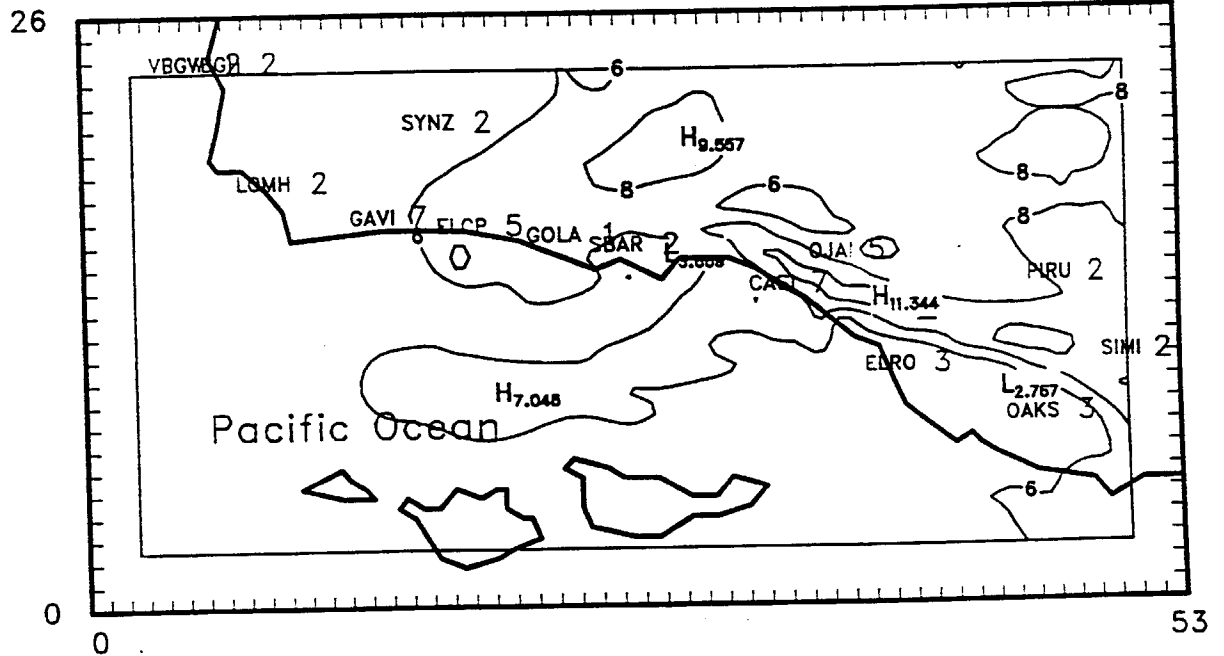
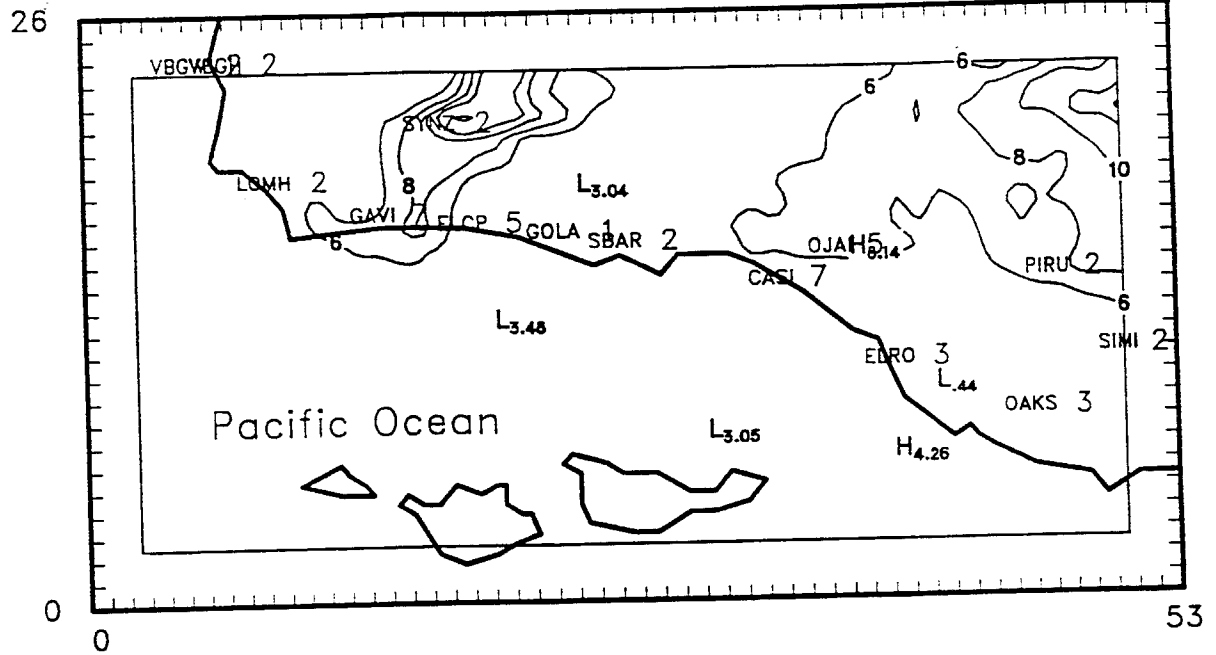


Figure 6-10d. Ground Level Ozone Isopleths of Hourly Ozone Concentrations for the 5-7 September, 1984 Episode – 5 September, 1800 PST.

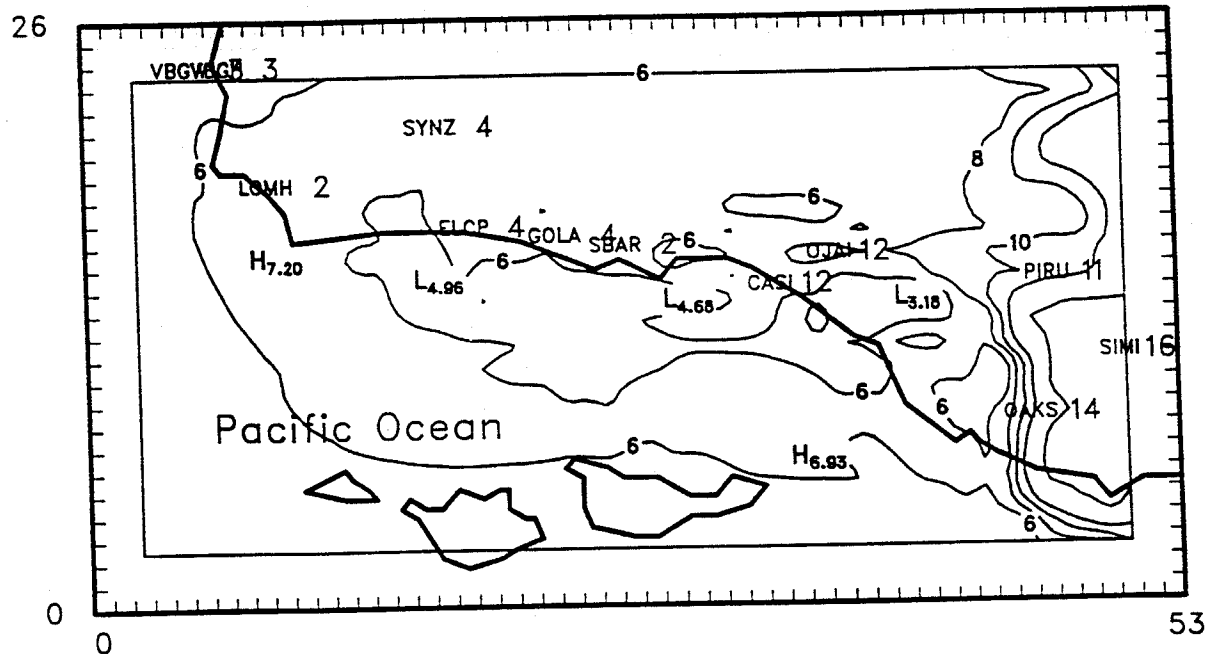
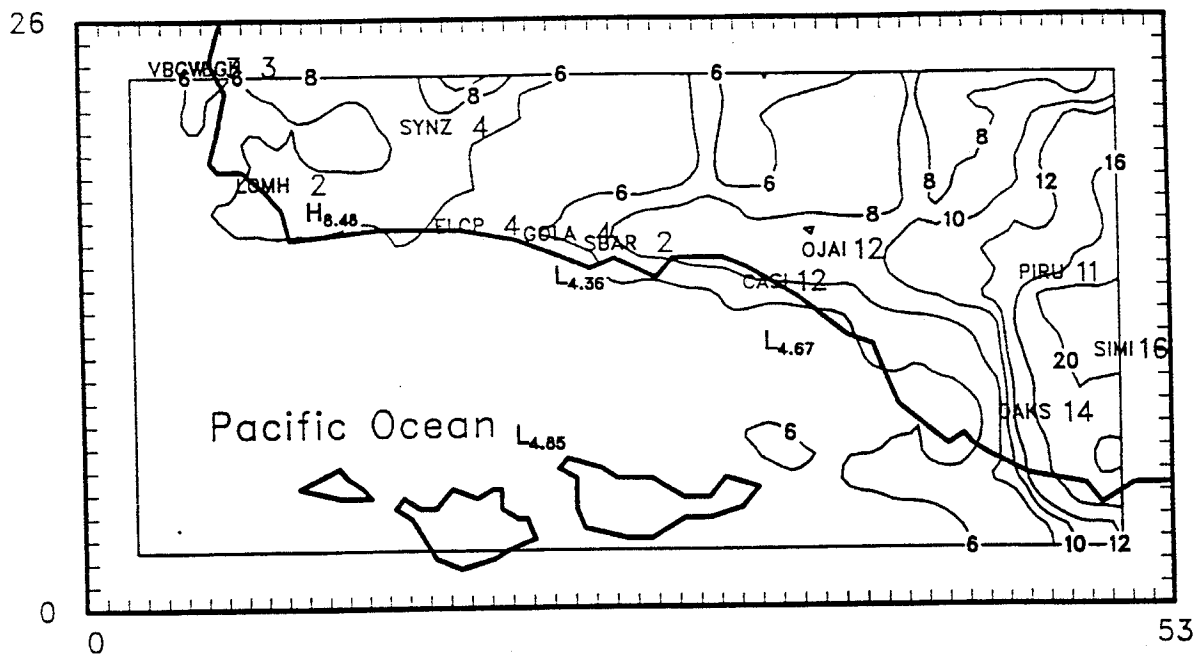


Figure 6-10e. Ground Level Ozone Isopleths of Hourly Ozone Concentrations for the 5-7 September, 1984 Episode - 6 September, 1200 PST.

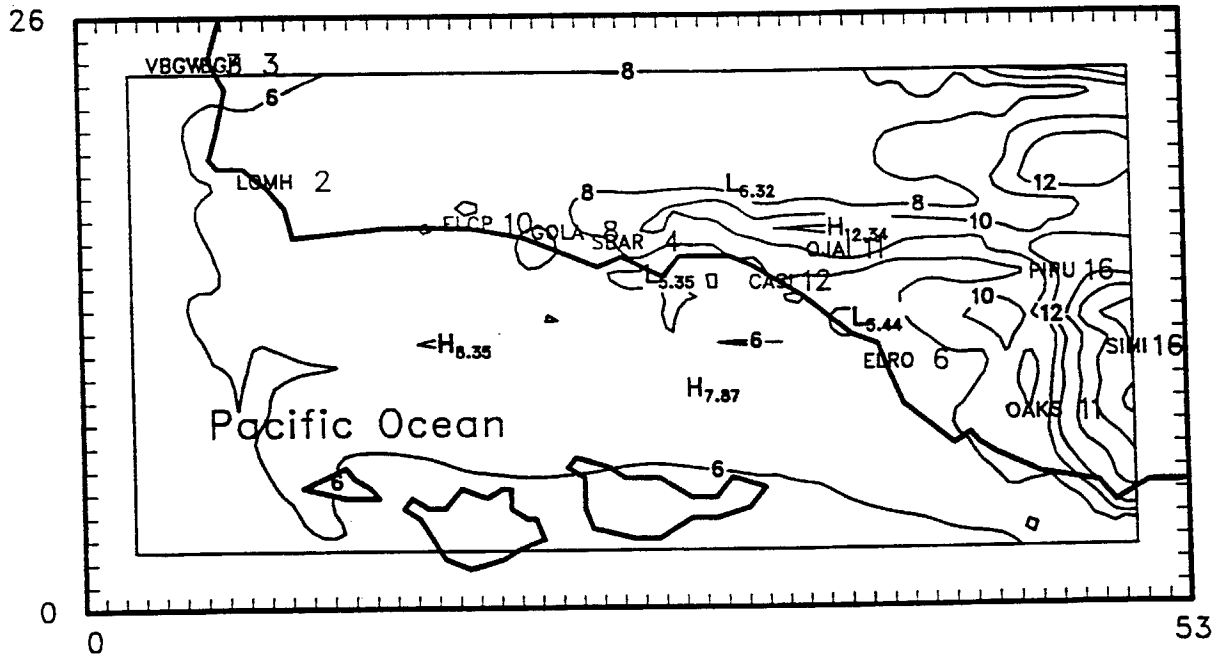
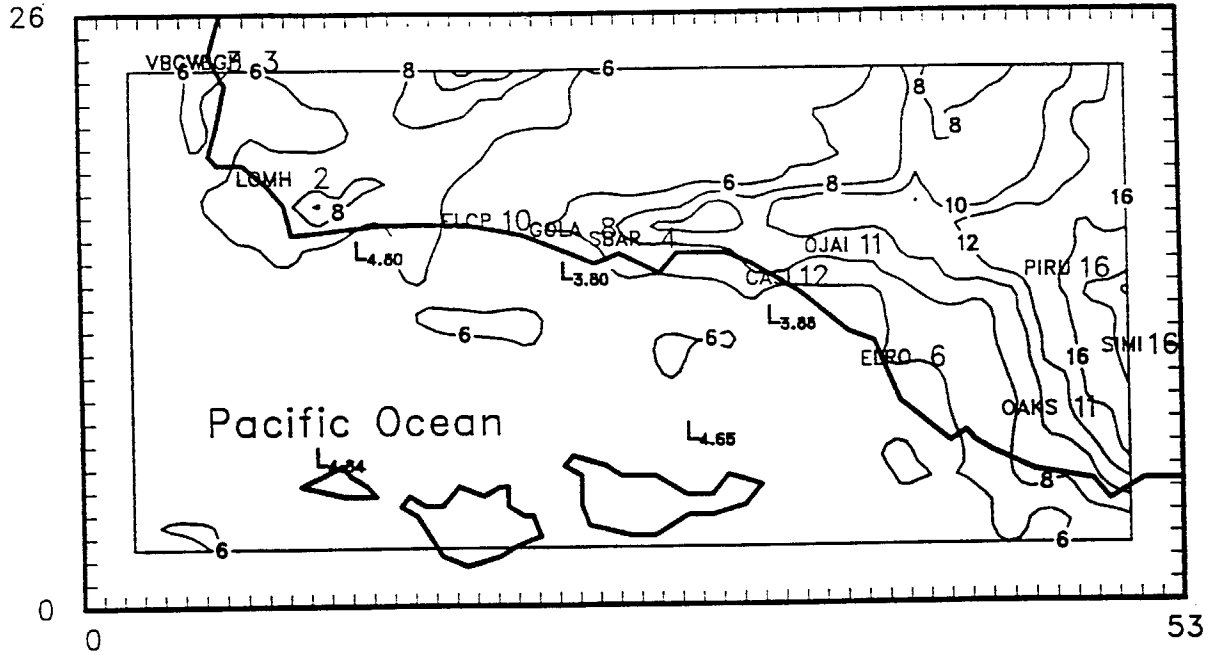
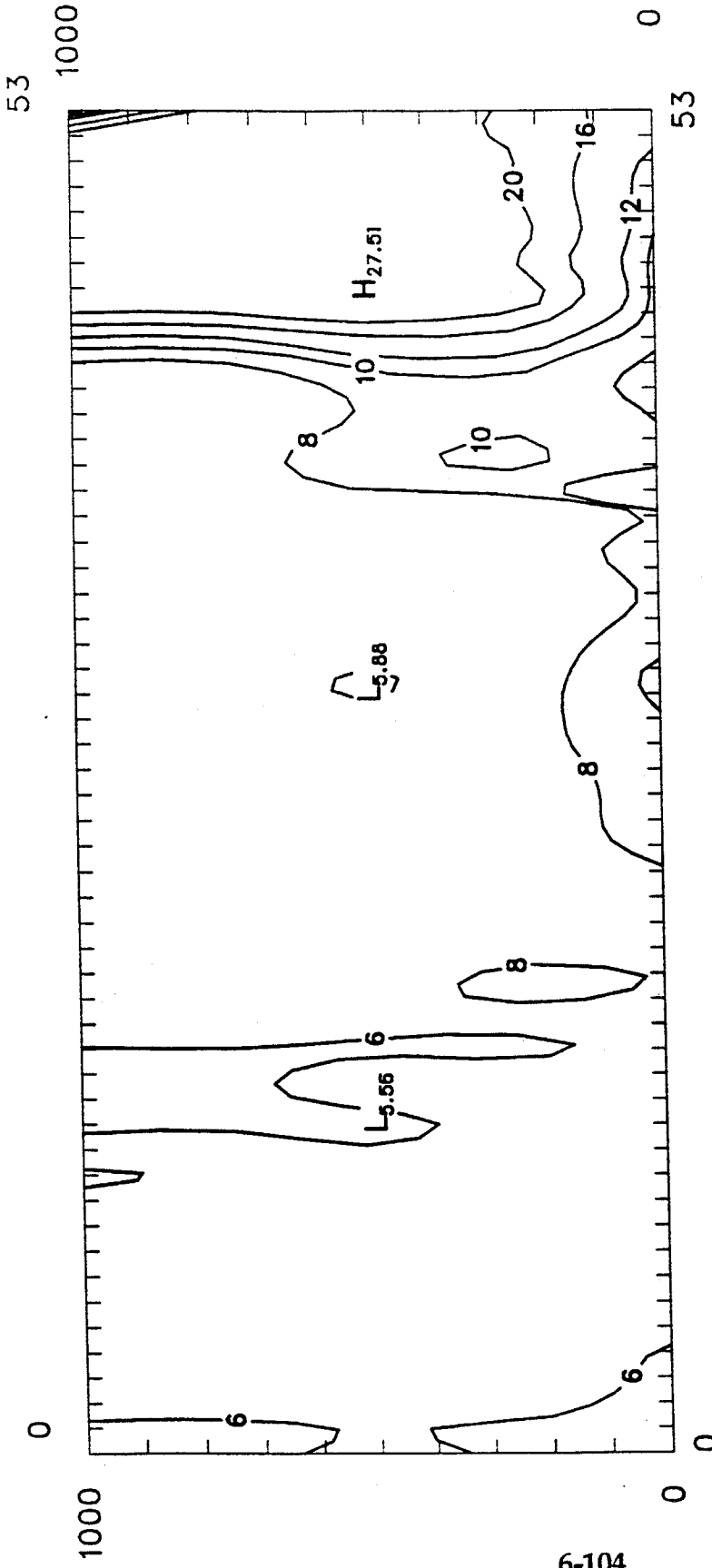


Figure 6-10f. Ground Level Ozone Isopleths of Hourly Ozone Concentrations for the 5-7 September, 1984 Episode – 6 September, 1400 PST.



92 610  
2050  
dem

E-W Slice J = 18 Hour 14 (pst)

Date 9/ 6/84

03 140084250AIR001  
CCHT140084250AIR001

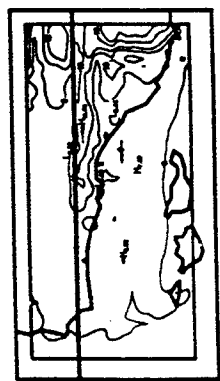
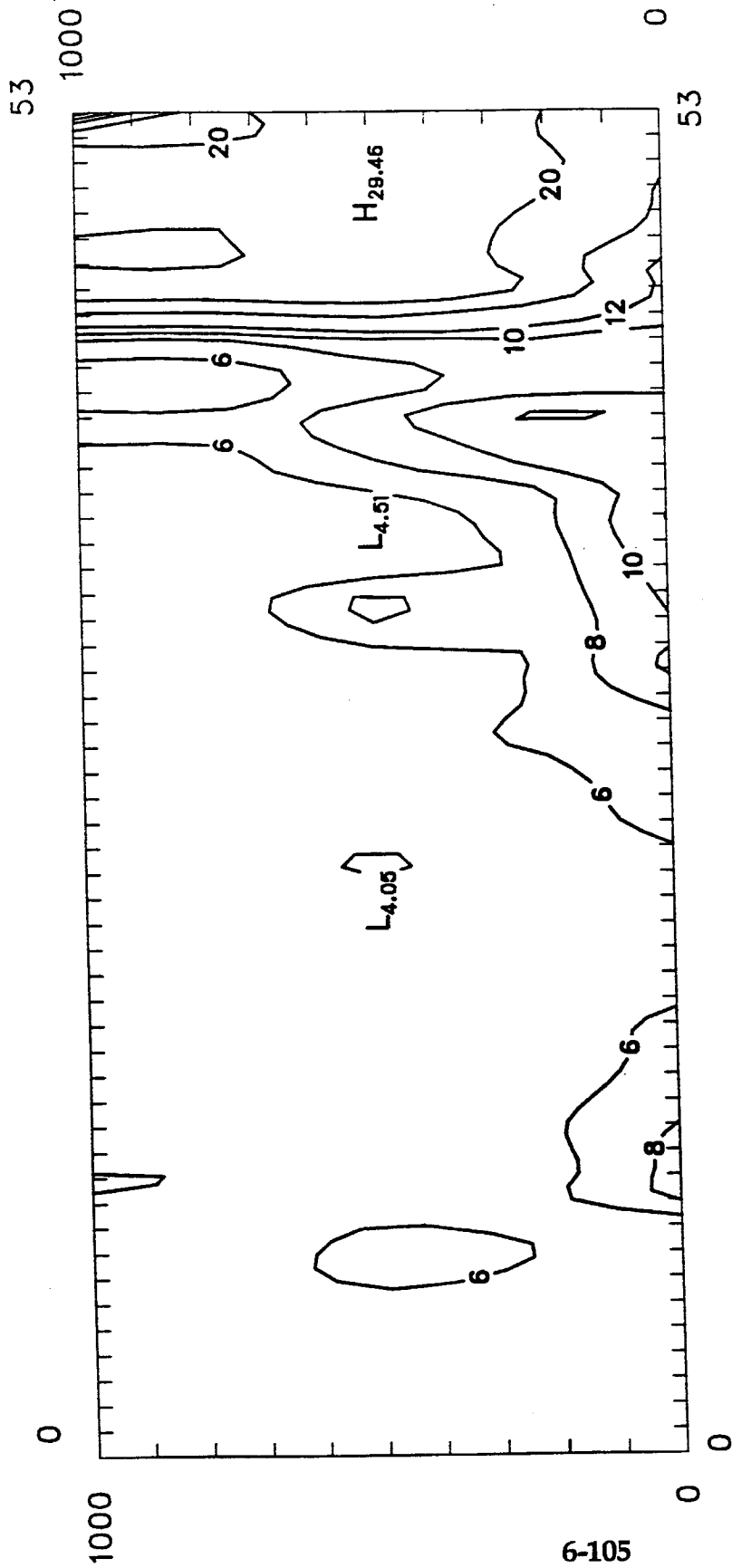


Figure 6-10f-s1. UAM-IV Vertical Ozone Isopleths Along East-West Transect for the 5-7 September, 1984 Episode -- 6 September, 1400 PST.



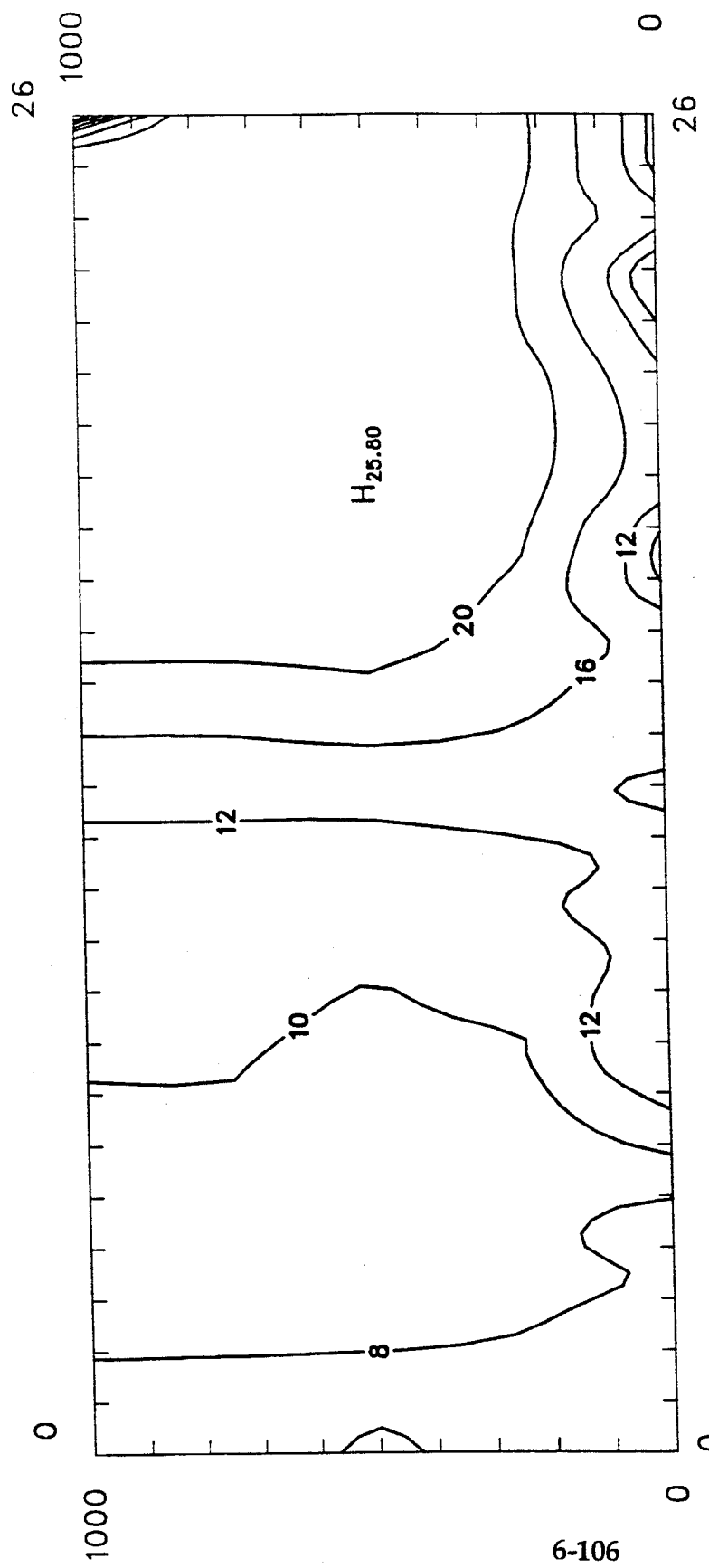
E-W Slice J = 18 Hour 14 (pst)

Date 9/ 6/84

03 1400B4250C64502  
CCHT1400B4250C64001

92 610  
1725  
dem

Figure 6-10f-s2. CALGRID-IV Vertical Ozone Isoleths Along East-West Transect for the 5-7 September, 1984 Episode -- 6 September, 1400 PST.



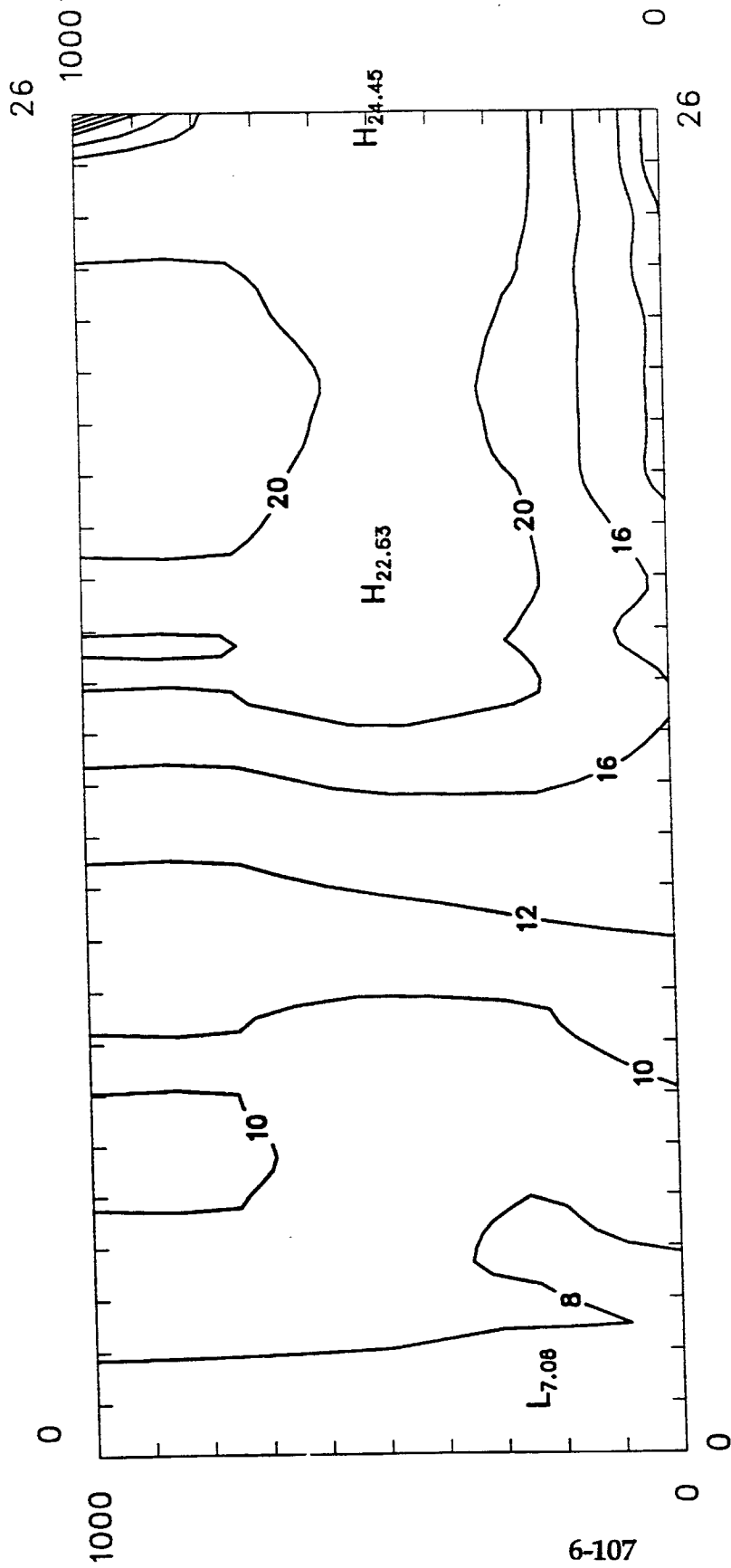
92 610  
2037  
dem

N-S Slice I = 48 Hour 14 (pst)  
Date 9/ 6/84

O3 140084250AIR001  
CCHT140084250AIR001



Figure 6-10f-s3. UAM-IV Vertical Ozone Isopleths Along North-South Transect for the 5-7 September, 1984 Episode -- 6 September, 1400 PST.



92 610  
1712  
dem

N-S Slice I = 48 Hour 14 (pst)

Date 9/ 6/84

03 140084250CG4502  
CCITT140084250CG4001



Figure 6-10f-s4. CALGRID-IV Vertical Ozone Isopleths Along North-South Transect for the 5-7 September, 1984 Episode -- 6 September, 1400 PST.

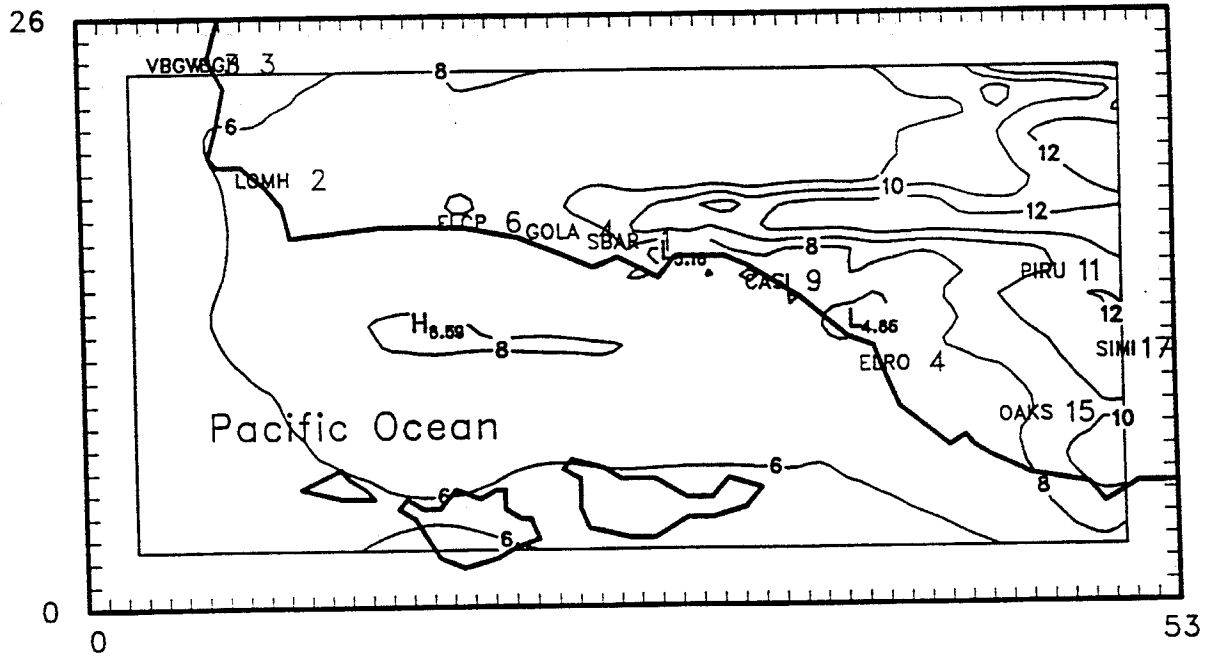
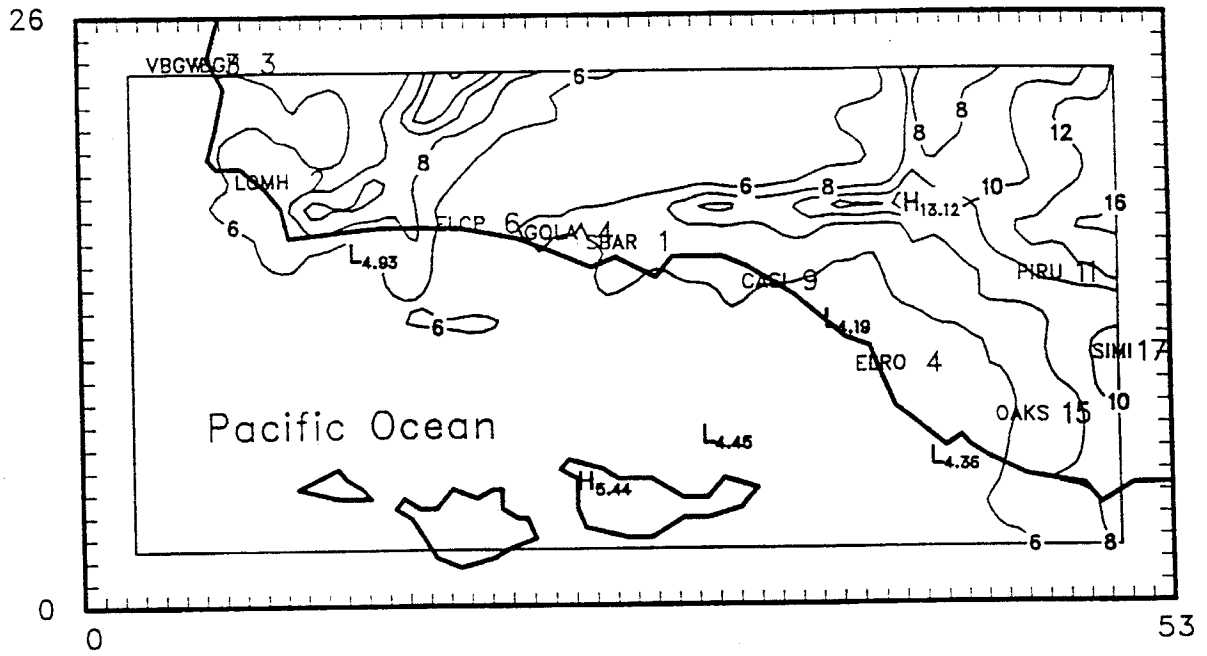
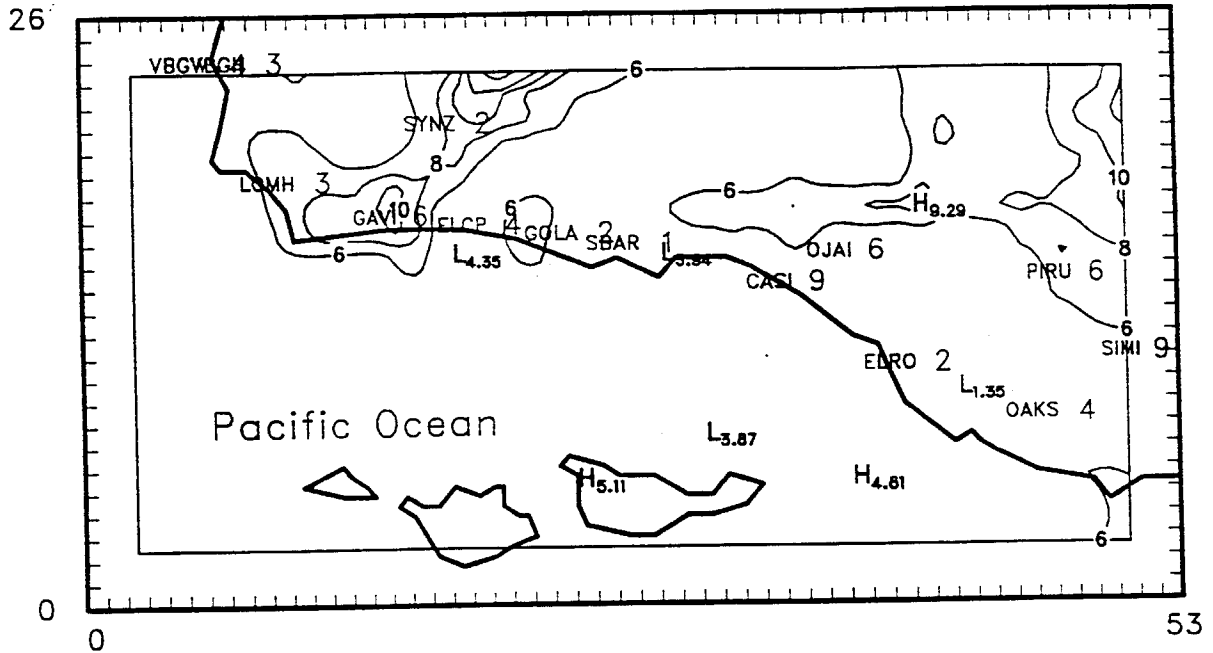


Figure 6-10g. Ground Level Ozone Isopleths of Hourly Ozone Concentrations for the 5-7 September, 1984 Episode -- 6 September, 1600 PST.

CALGRID-IV



UAM-IV

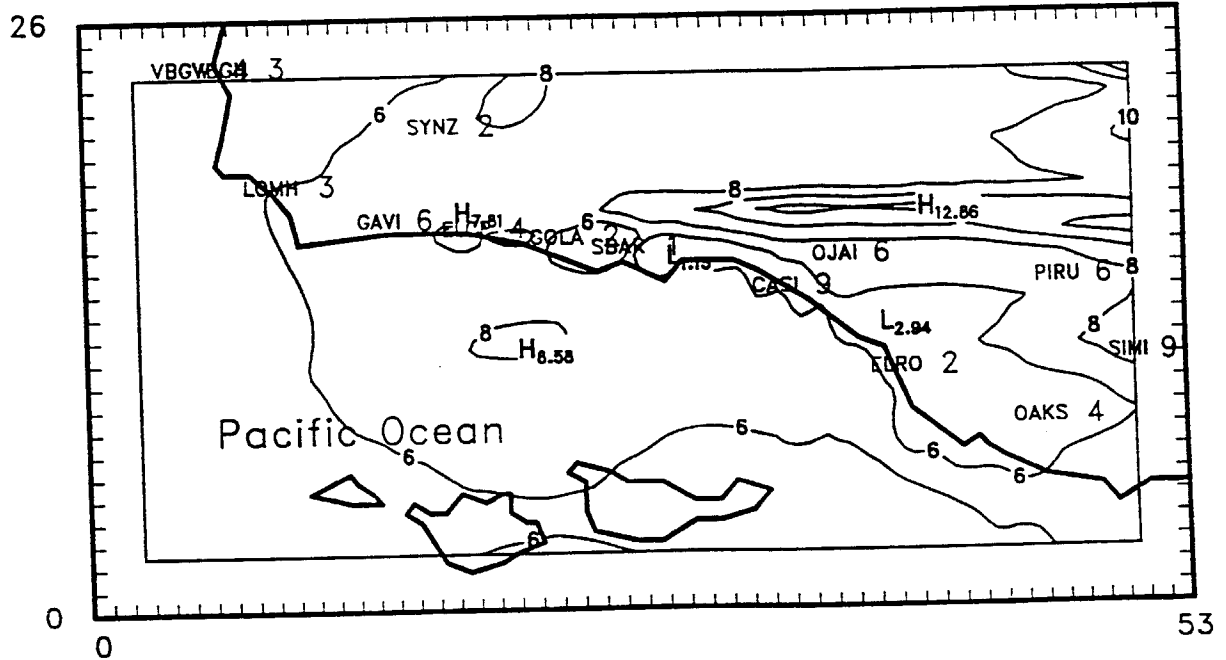
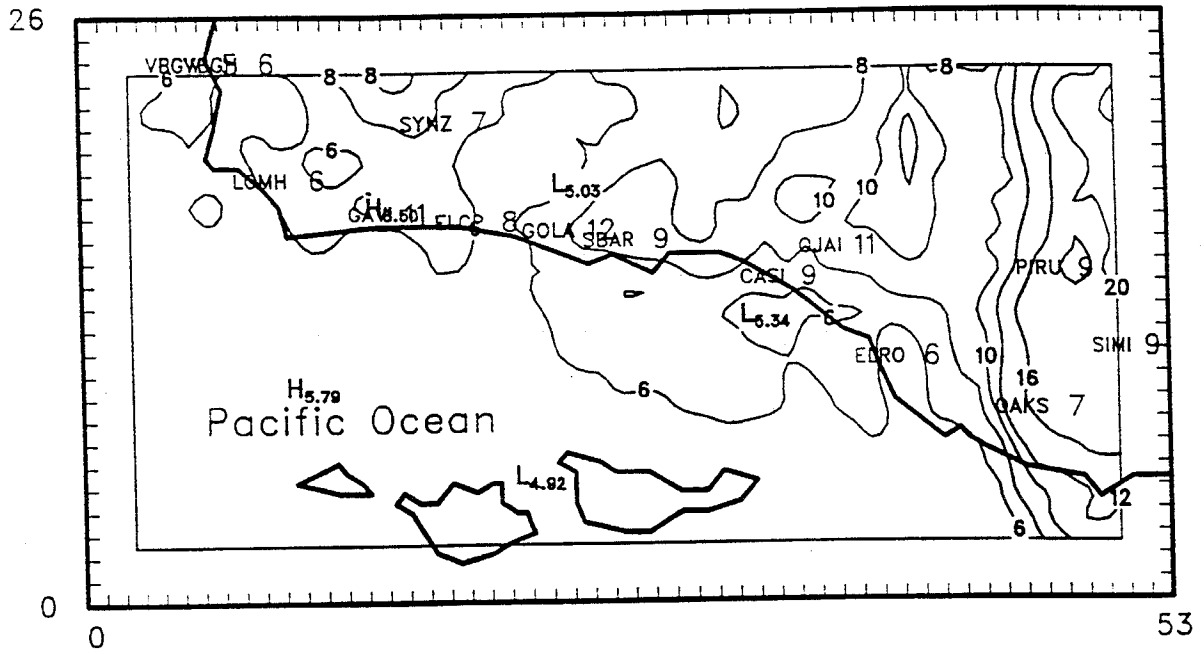


Figure 6-10h. Ground Level Ozone Isopleths of Hourly Ozone Concentrations for the 5-7 September, 1984 Episode – 6 September, 1800 PST.

CALGRID-IV



UAM-IV

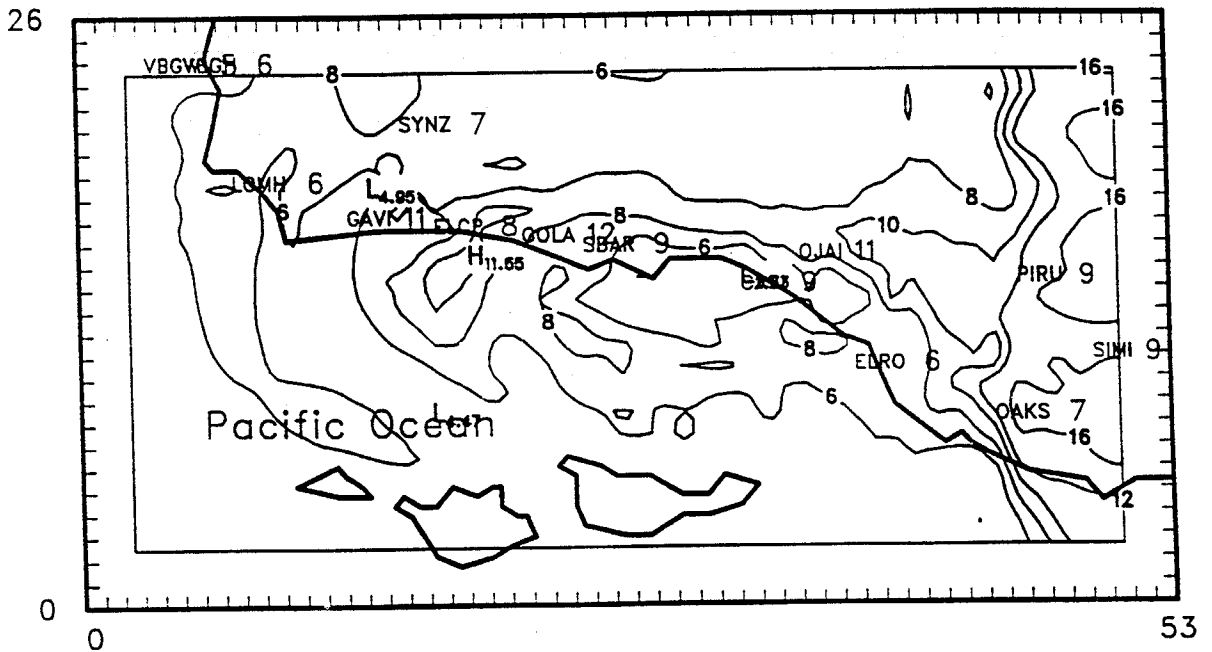


Figure 6-10i Ground Level Ozone Isopleths of Hourly Ozone Concentrations for the 5-7 September, 1984 Episode - 7 September, 1200 PST.

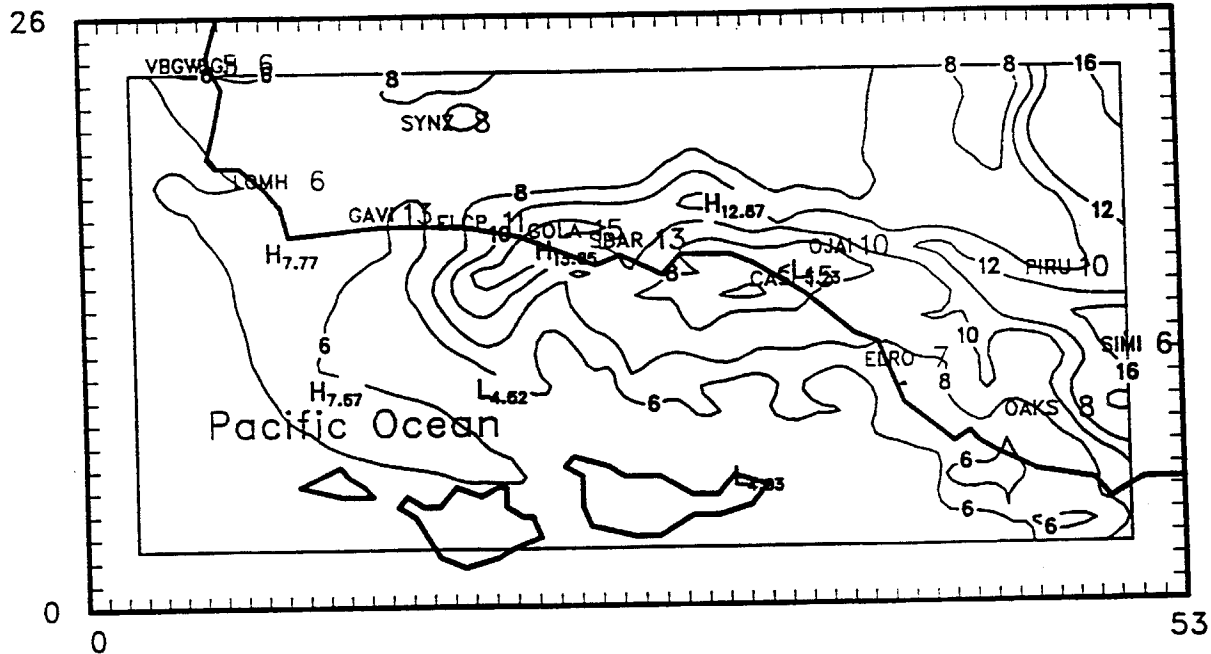
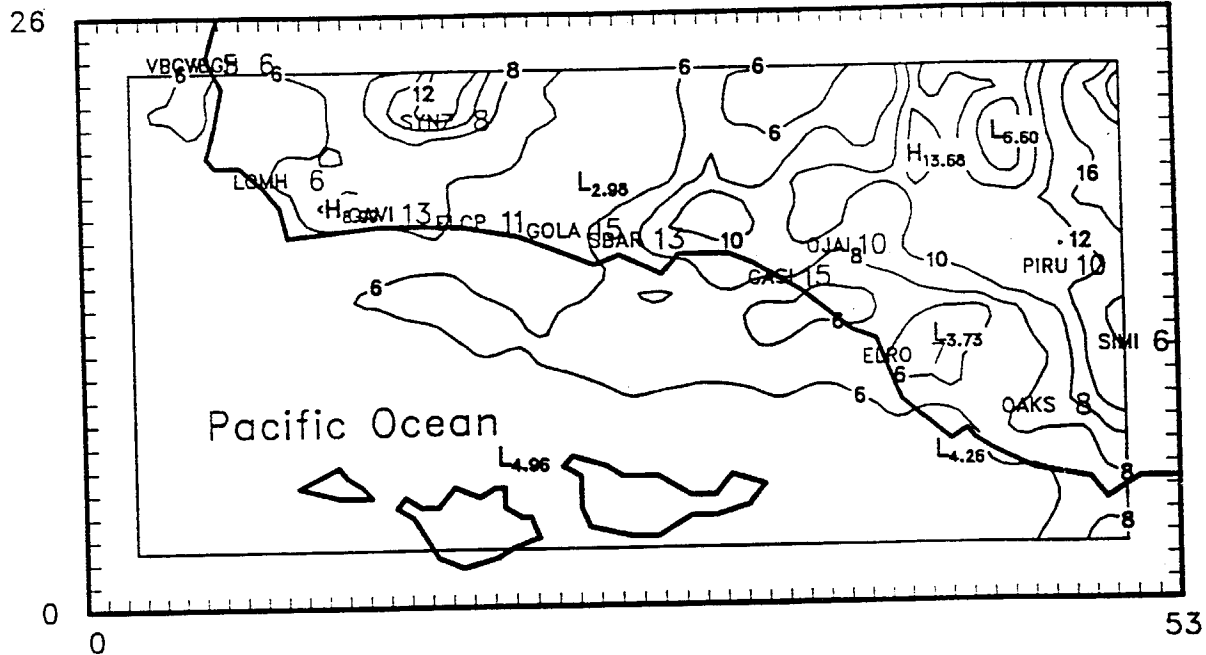
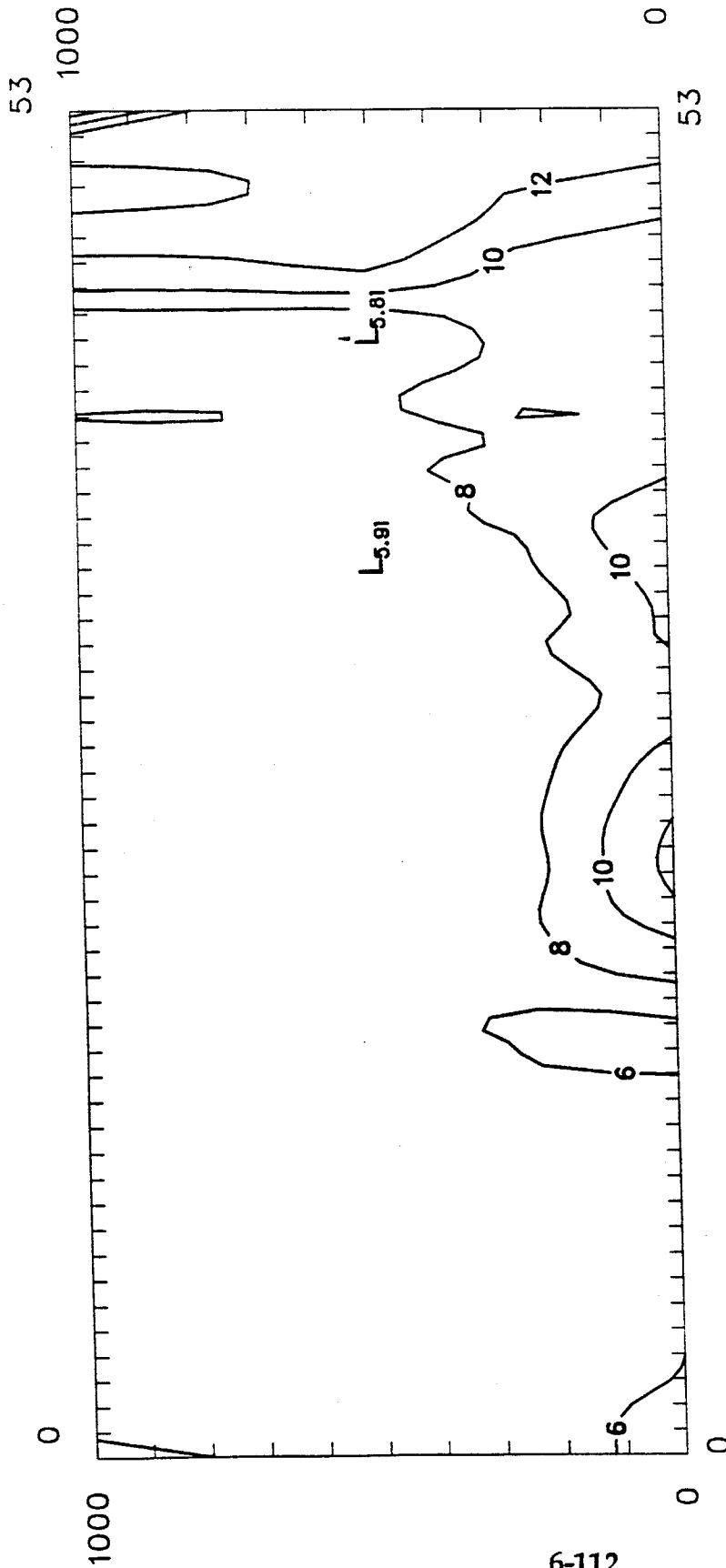


Figure 6-10j. Ground Level Ozone Isopleths of Hourly Ozone Concentrations for the 5-7 September, 1984 Episode – 7 September, 1400 PST.



E-W Slice J = 17 Hour 14 (pst)

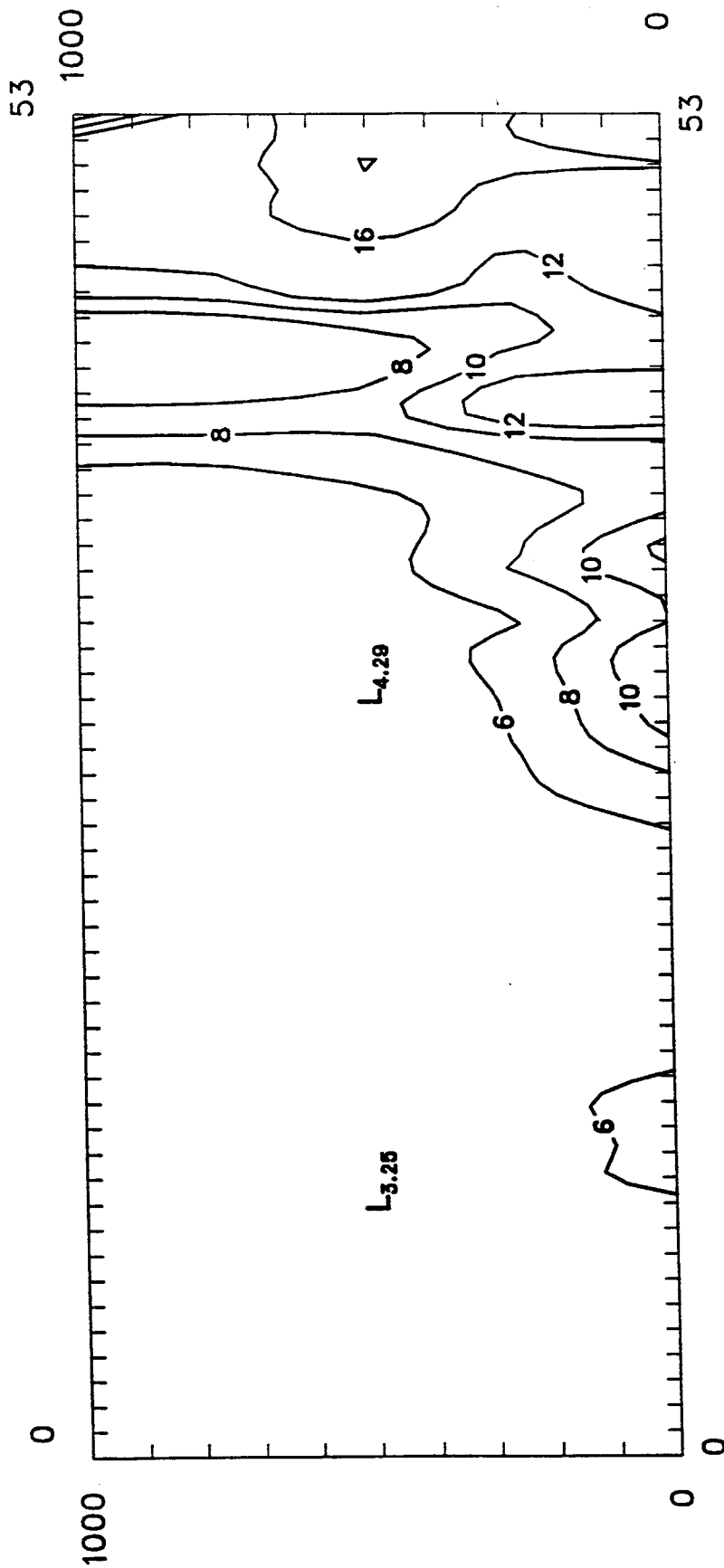
Date 9/7/84

O3 140084251AIR001  
CCHT140084251AIR001

92 610  
2127  
dem



Figure 6-10j-s1. UAM-IV Vertical Ozone Isopleths Along East-West Transect for the 5-7 September, 1984 Episode -- 7 September, 1400 PST.



92 610  
18 2  
dem

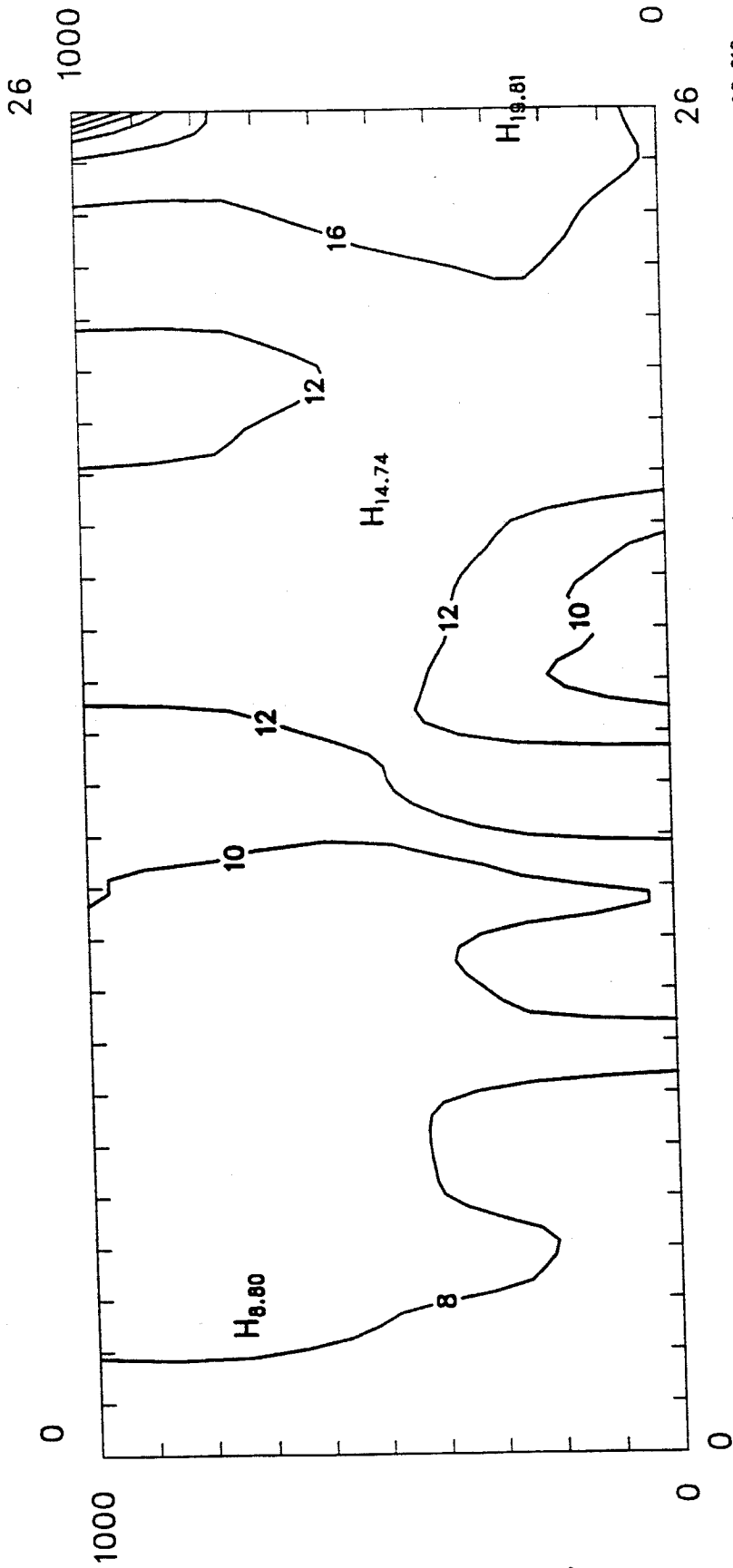
E-W Slice J = 17 Hour 14 (pst)

Date 9/ 7/84

03 14008425ICG4502  
CCHT14008425ICG4001



Figure 6-10j-s2. CALGRID-IV Vertical Ozone Isopleths Along East-West Transect for the 5-7 September, 1984 Episode -- 7 September, 1400 PST.



92 610  
21 6  
dem

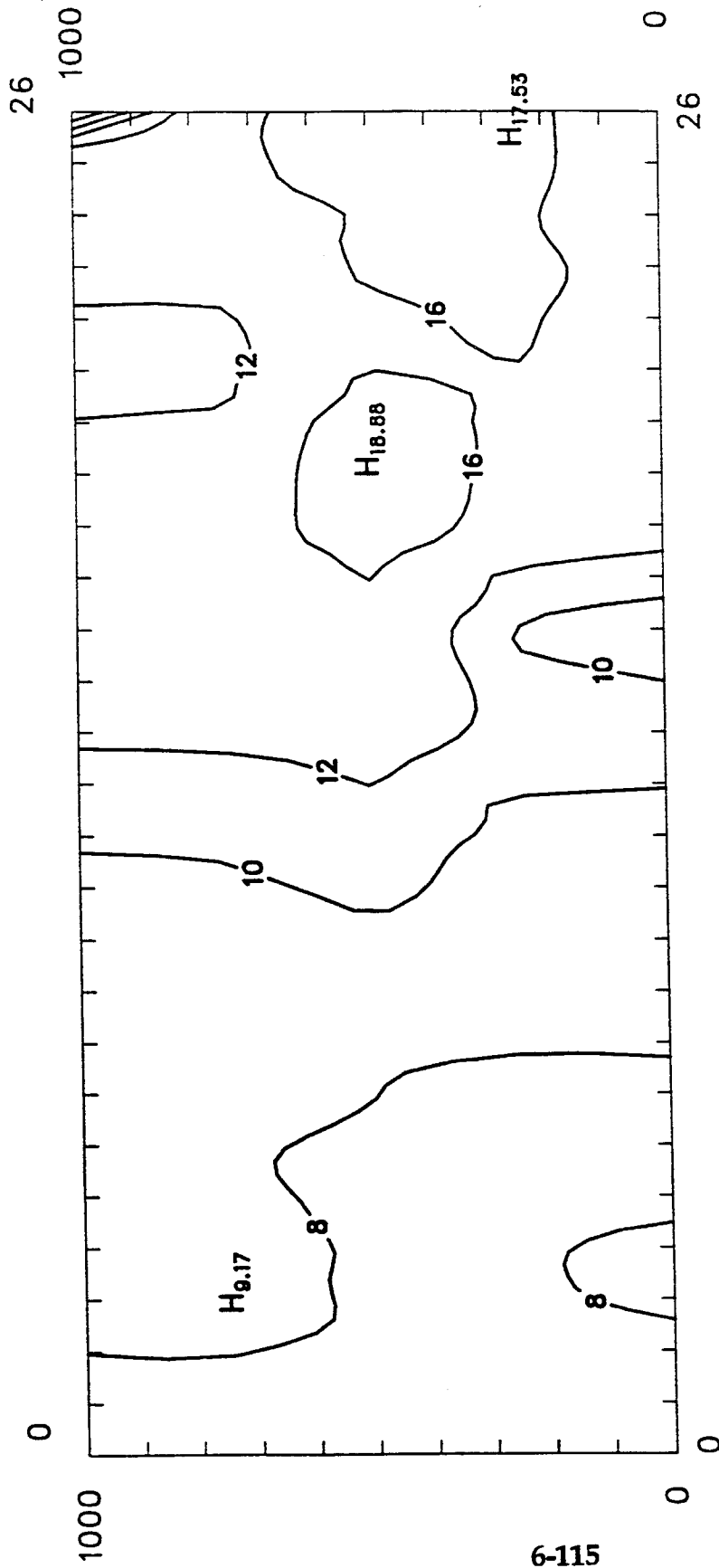
N-S Slice I = 48 Hour 14 (pst)

Date 9/7/84

03 140084251AIR001  
CCHT140084251AIR001



Figure 6-10j-s3. UAM-IV Vertical Ozone Isopleths Along North-South Transect for the 5-7 September, 1984 Episode -- 7 September, 1400 PST.



N-S Slice 1 = 48 Hour 14 (pst)

Date 9/7/84

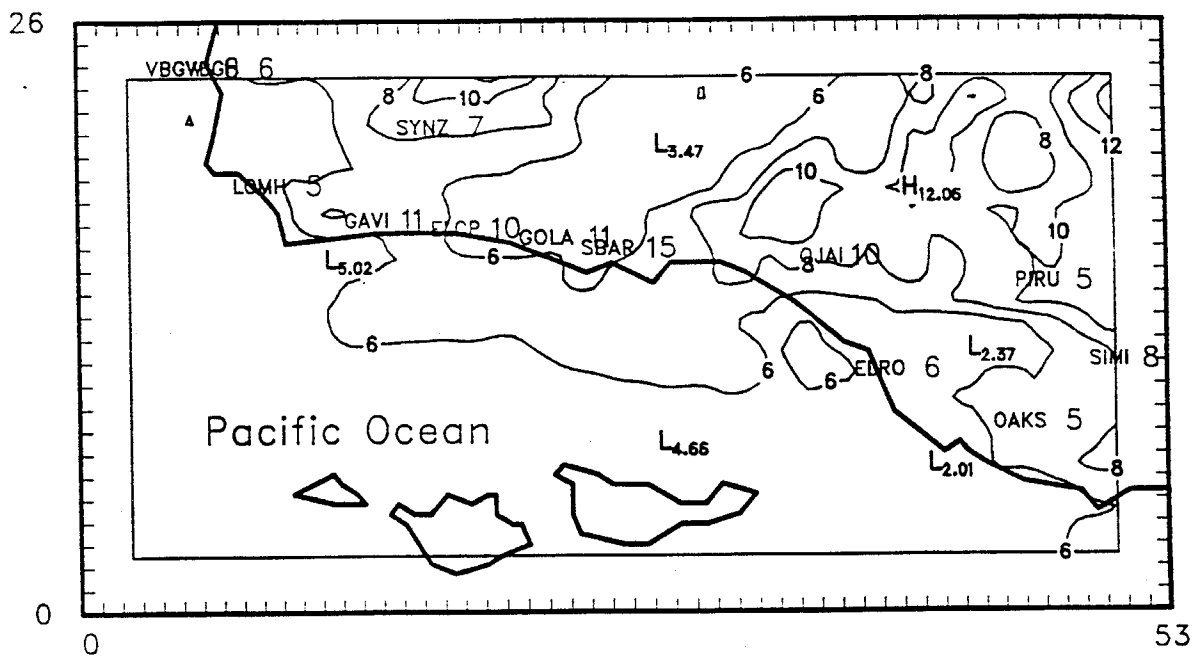
03 140084251CG4502  
 CCHT140084251CG4001

92 610  
 1741  
 dem



Figure 6-10j-s4. CALGRID-IV Vertical Ozone Isopleths Along North-South Transect for the 5-7 September, 1984 Episode -- 7 September, 1400 PST.

CALGRID-IV



UAM-IV

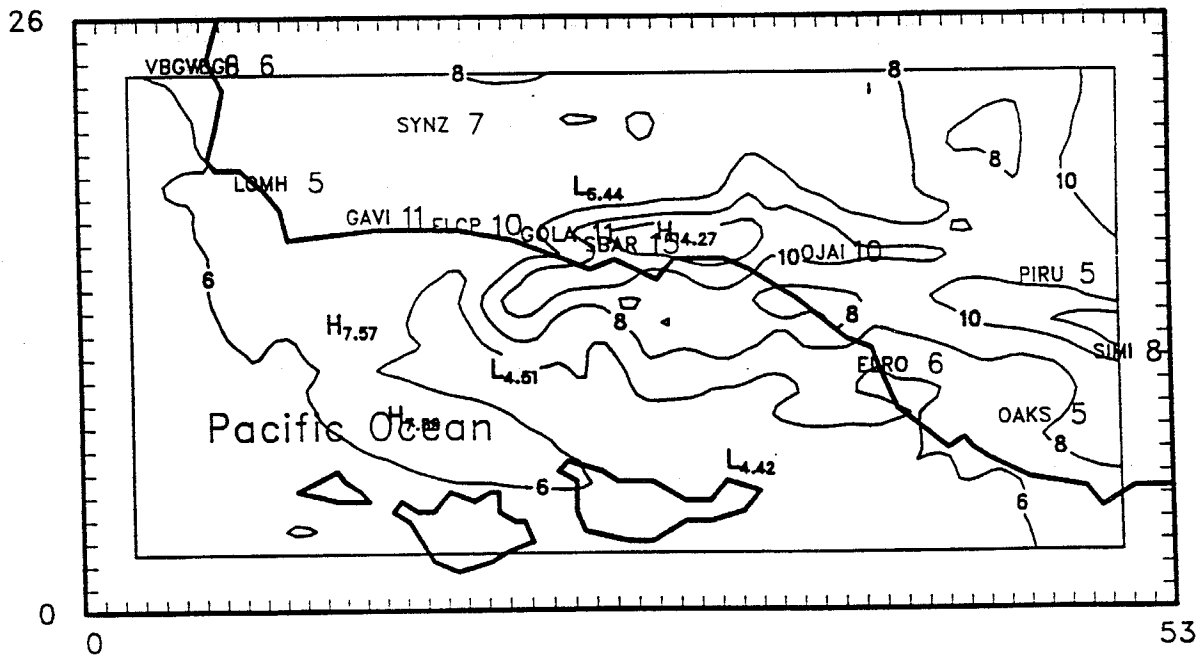
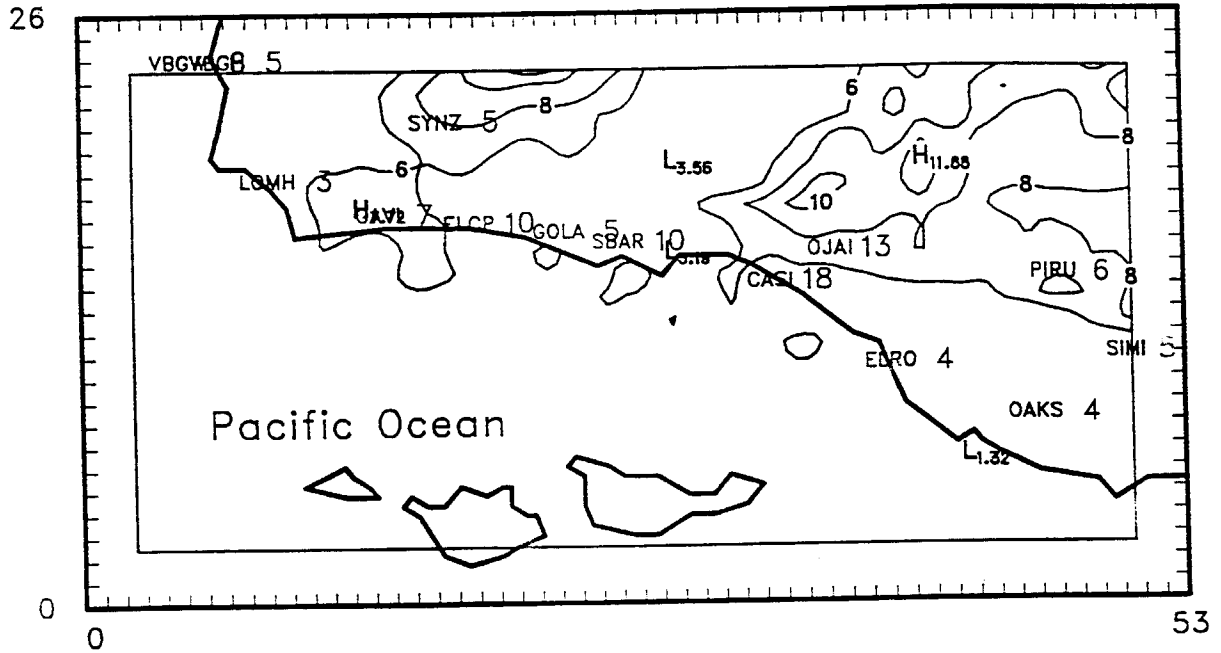


Figure 6-10k. Ground Level Ozone Isopleths of Hourly Ozone Concentrations for the 5-7 September, 1984 Episode -- 7 September, 1600 PST.

CALGRID-IV



UAM-IV

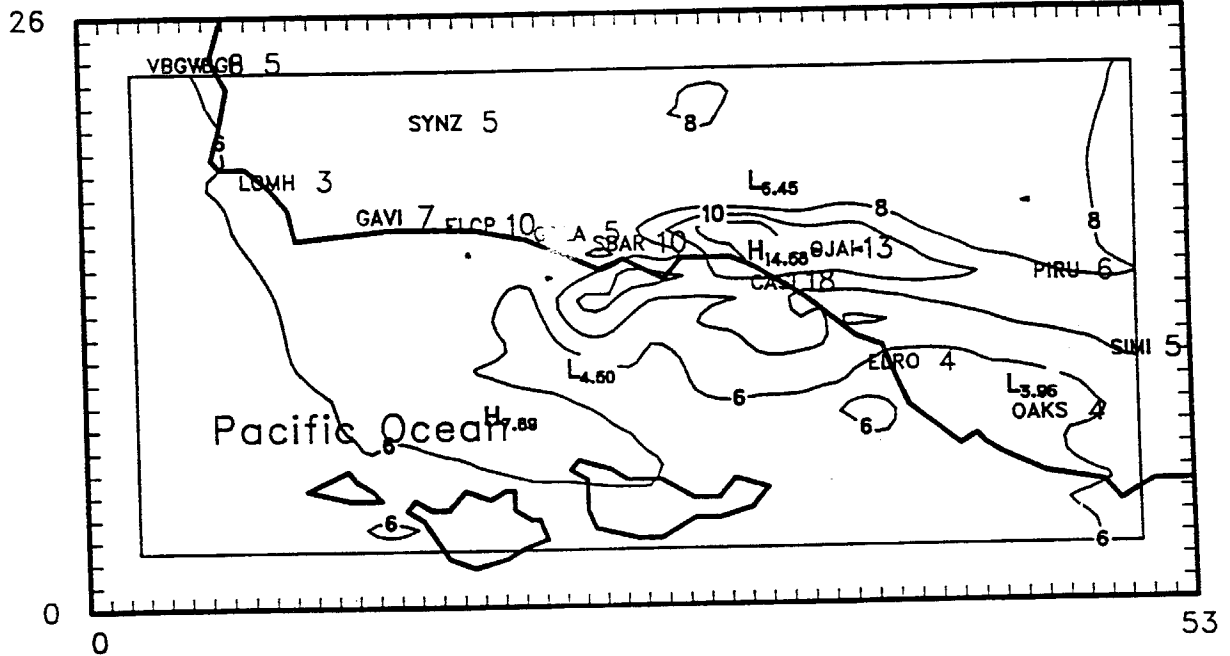
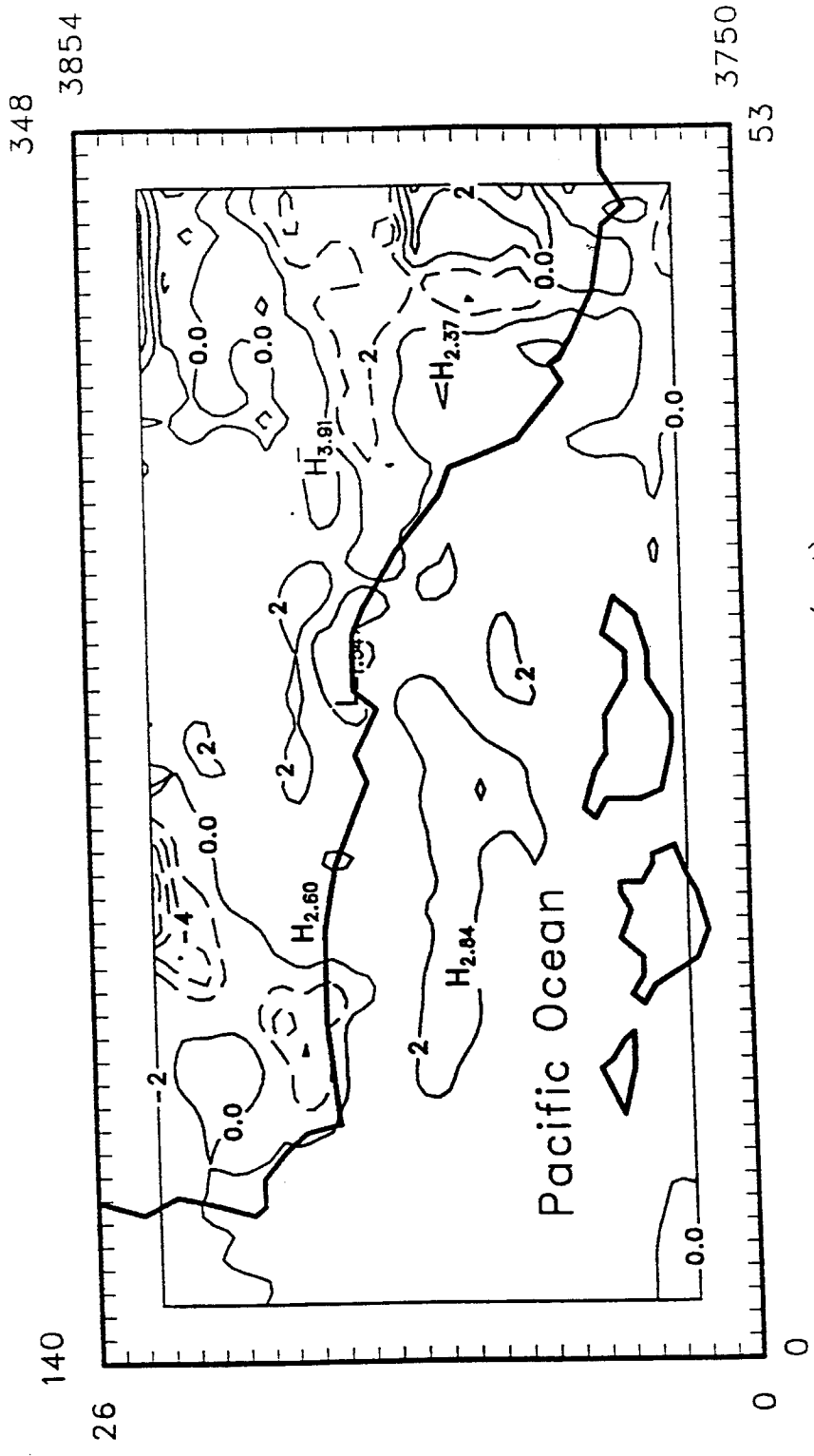


Figure 6-101. Ground Level Ozone Isopleths of Hourly Ozone Concentrations for the 5-7 September, 1984 Episode – 7 September, 1800 PST.

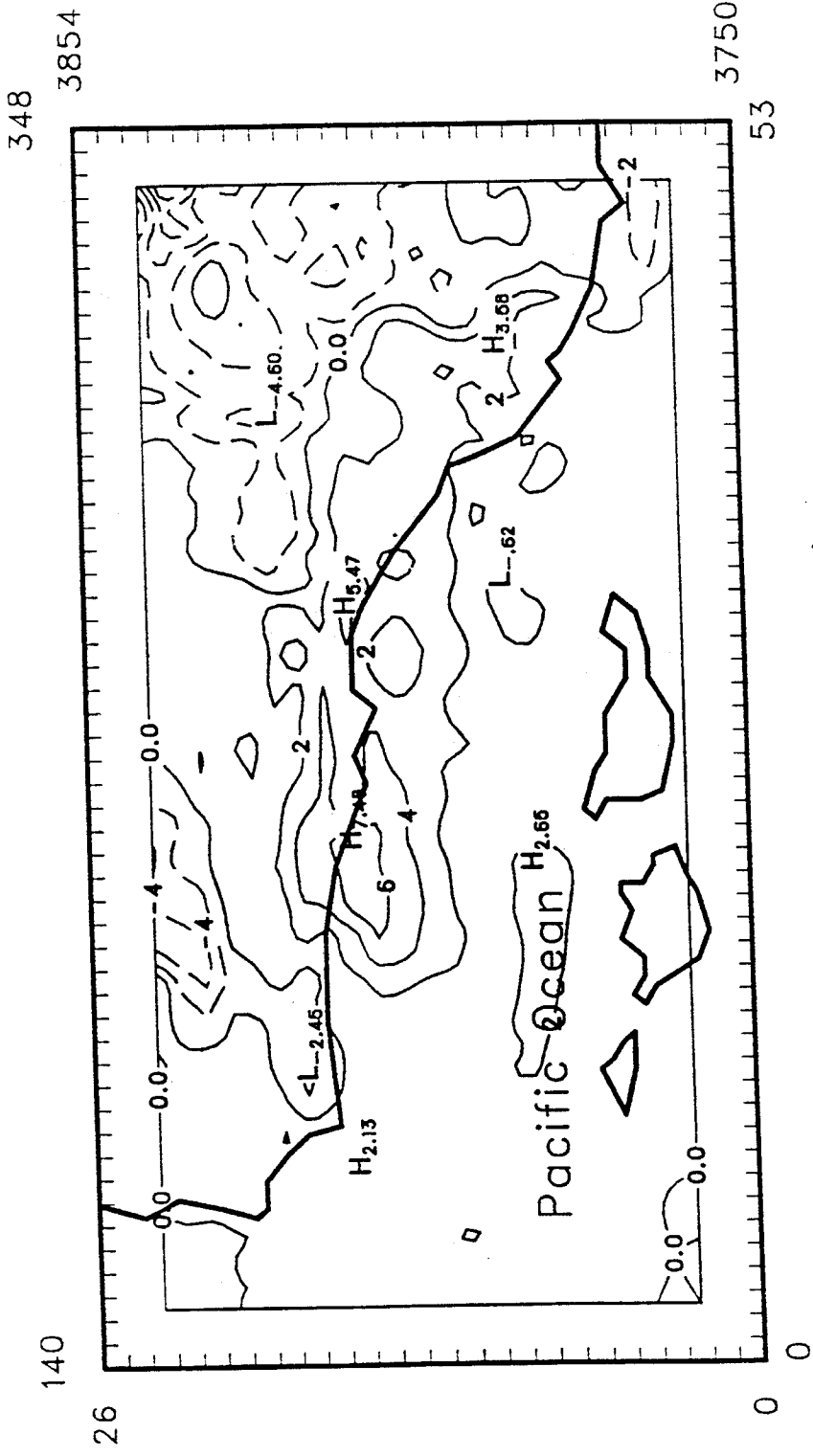




Level 1 Hour 99 (pst)

Date 9/ 6/84

Figure 6.11b. Maximum Daily Ozone Residual Plot (UAM-IV Minus CALGRID-IV) for the 5-7 September, 1984 Episode -- 6 September, 1984.



Level 1 Hour 99 (pst)

Date 9/7/84

Figure 6-11c. Maximum Daily Ozone Residual Plot (UAM-IV Minus CALGRID-IV) for the 5-7 September, 1984 Episode -- 7 September, 1984.

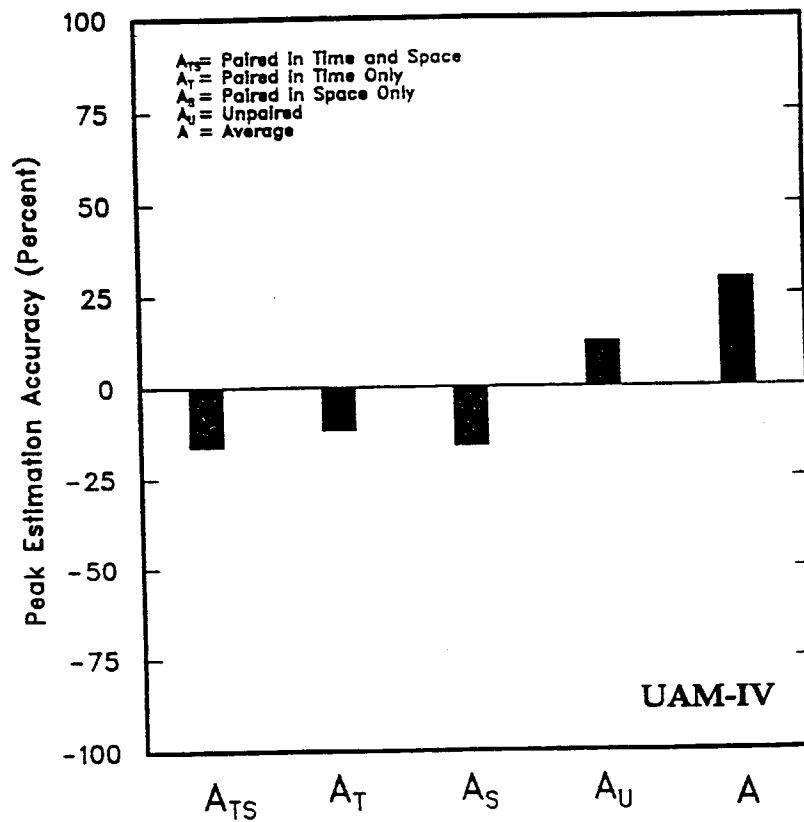
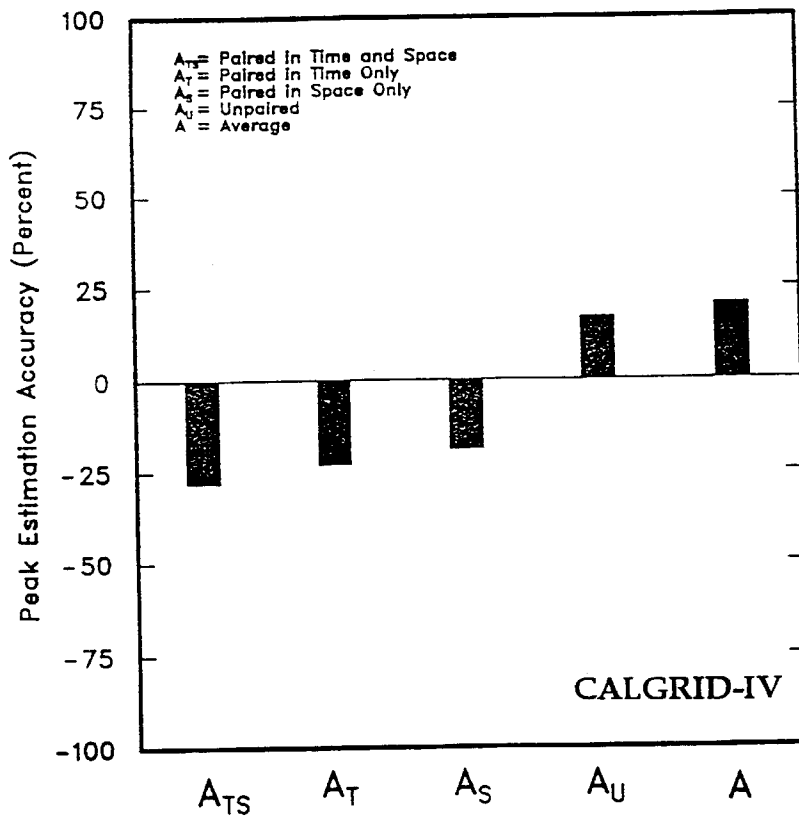


Figure 6-12a. Measures of Peak Ozone Estimation Accuracy for the 16-17 September, 1984 Episode – 16 September, 1984.

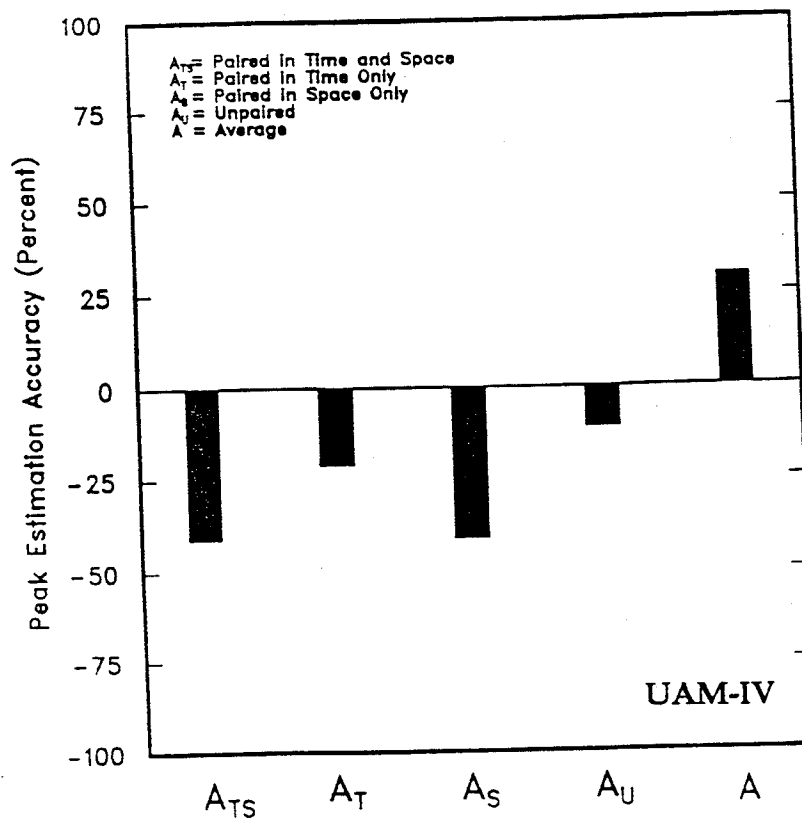
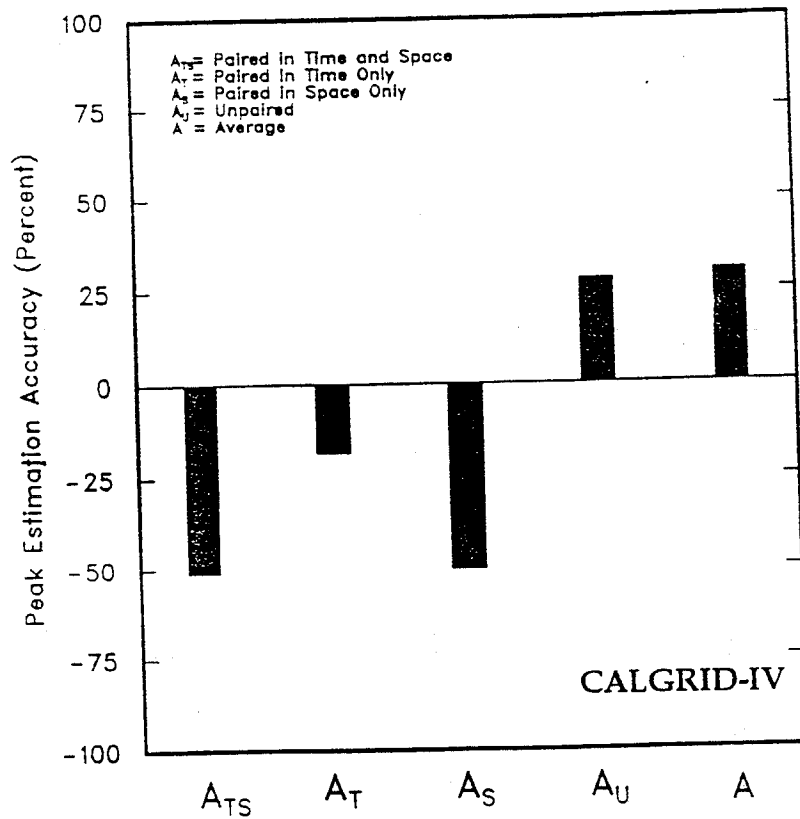


Figure 6-12b. Measures of Peak Ozone Estimation Accuracy for the 16-17 September, 1984 Episode -- 17 September, 1984.

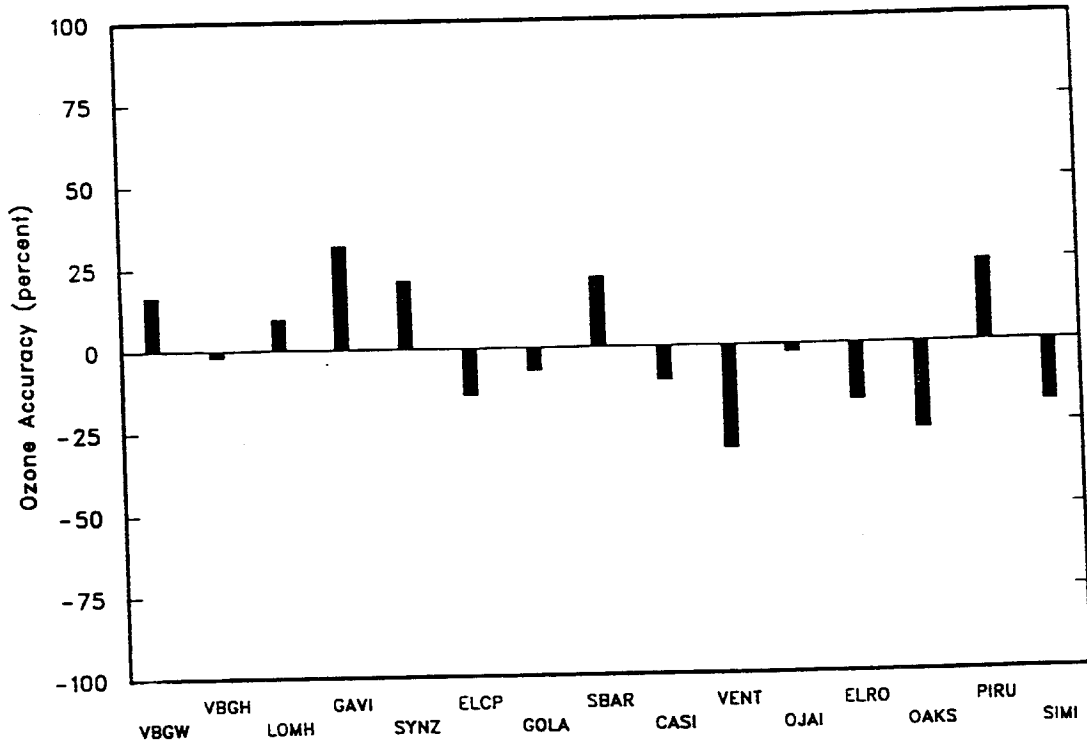
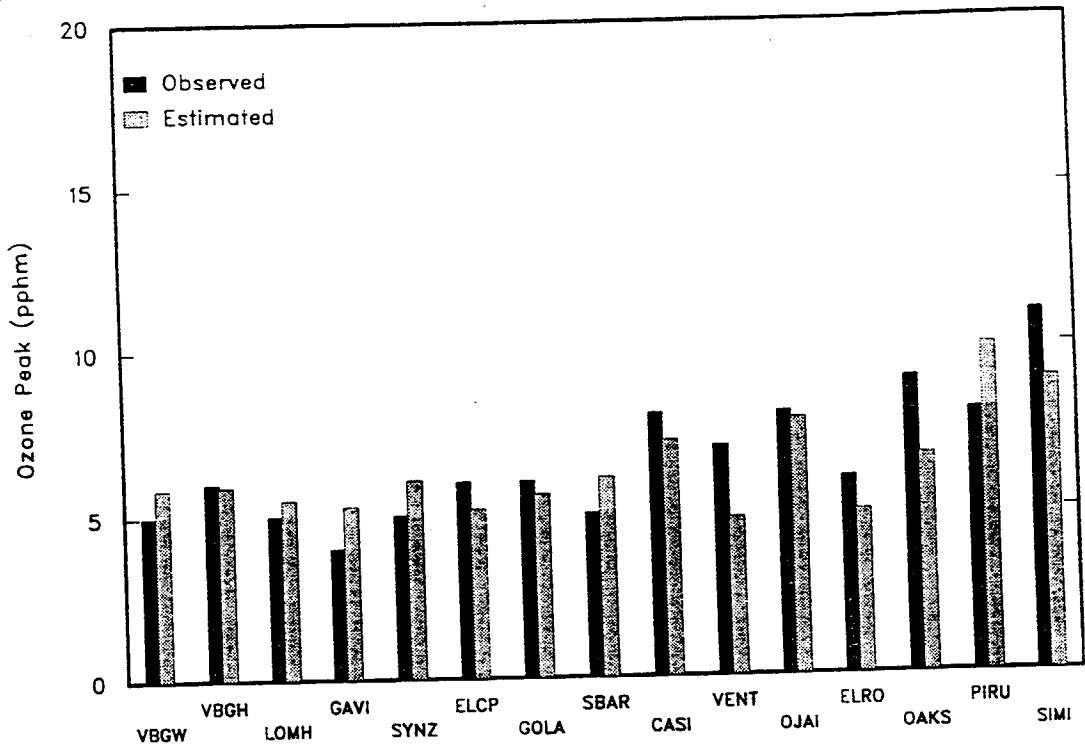


Figure 6-12c. Maximum Estimated and Observed Ozone Concentrations and Statio. Accuracy Estimates for the 16-17 September, 1984 CALGRID-IV Simulation -- 16 September, 1984.

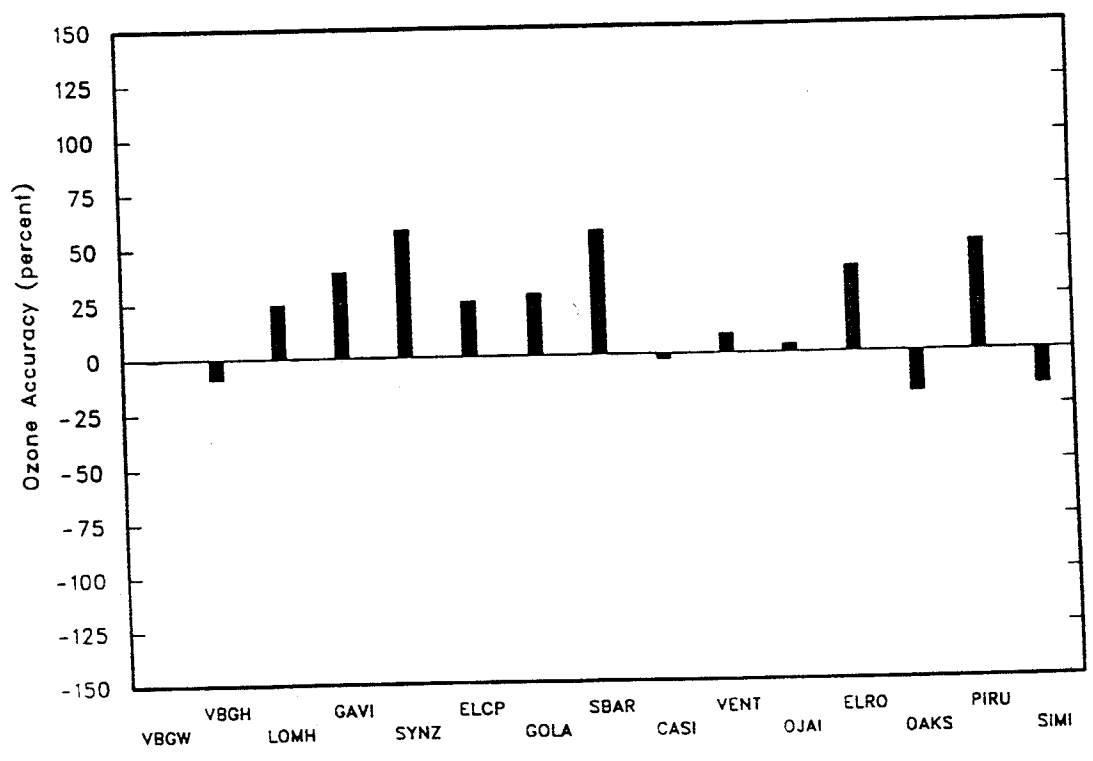
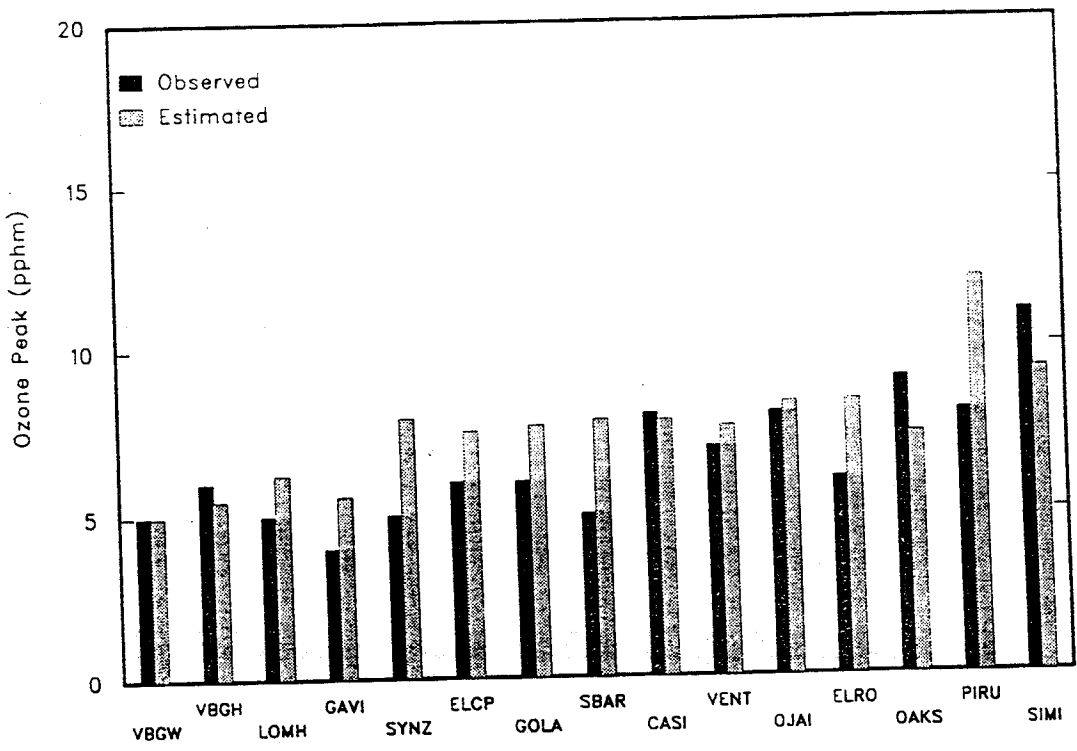


Figure 6-12d. Maximum Estimated and Observed Ozone Concentrations and Station Accuracy Estimates for the 16-17 September, 1984 UAM-IV Simulation - 16 September, 1984.

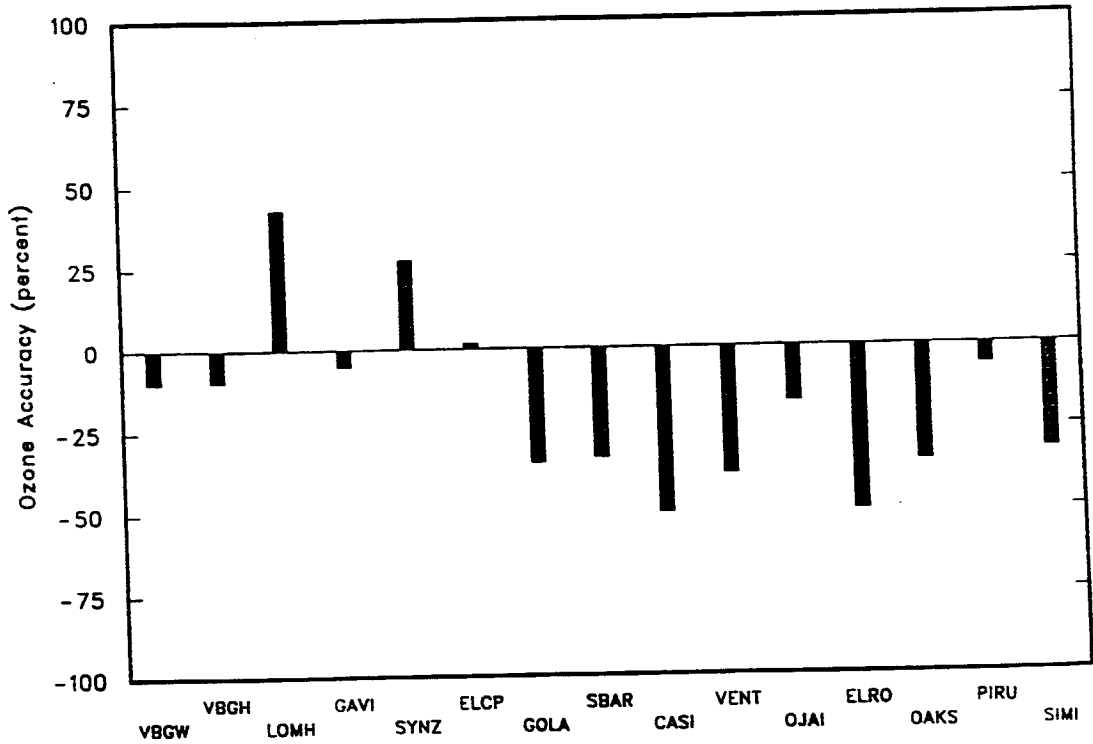
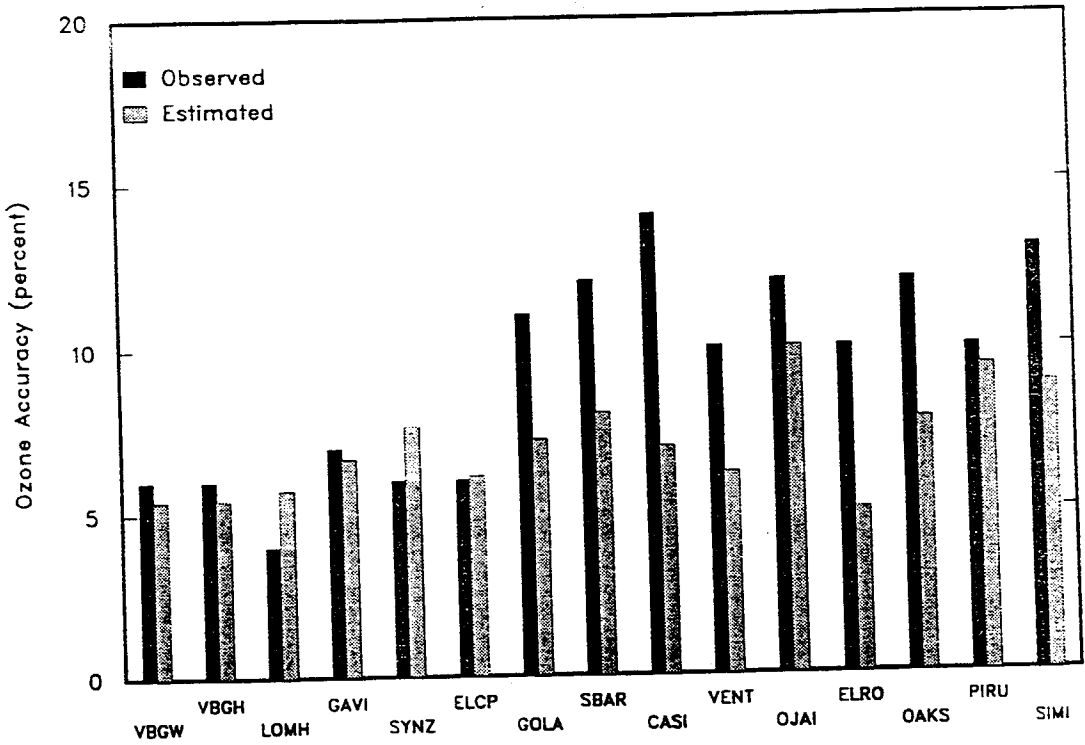


Figure 6-12e. Maximum Estimated and Observed Ozone Concentrations and Station Accuracy Estimates for the 16-17 September, 1984 CALGRID-IV Simulation -- 17 September, 1984.

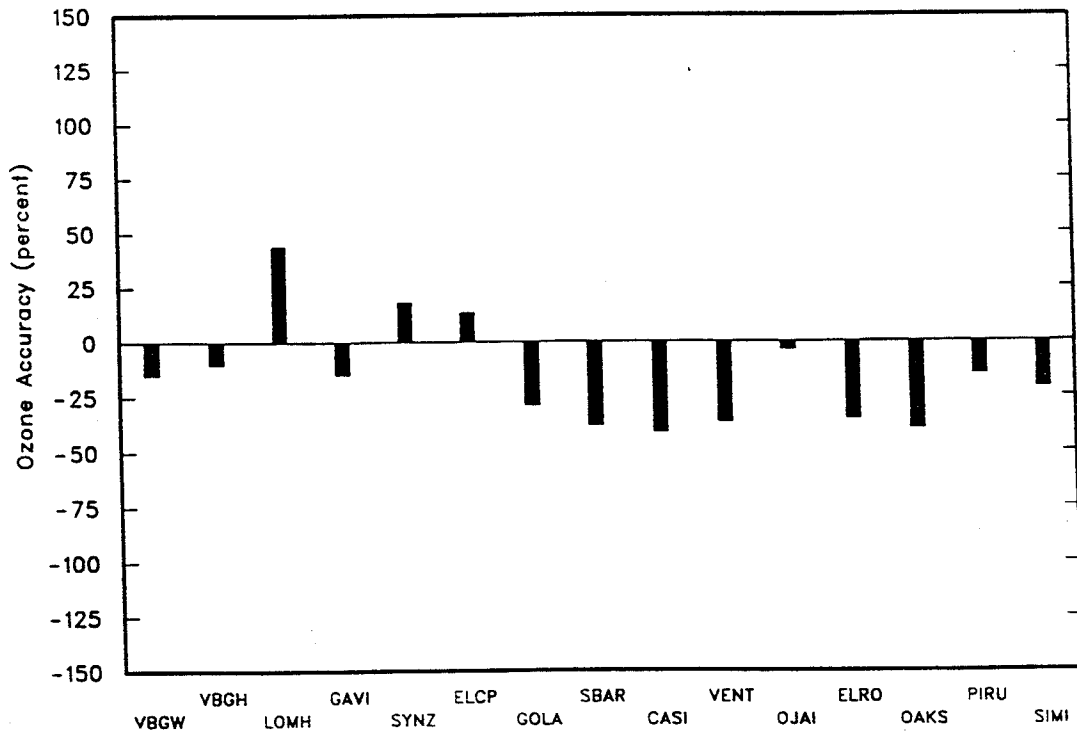
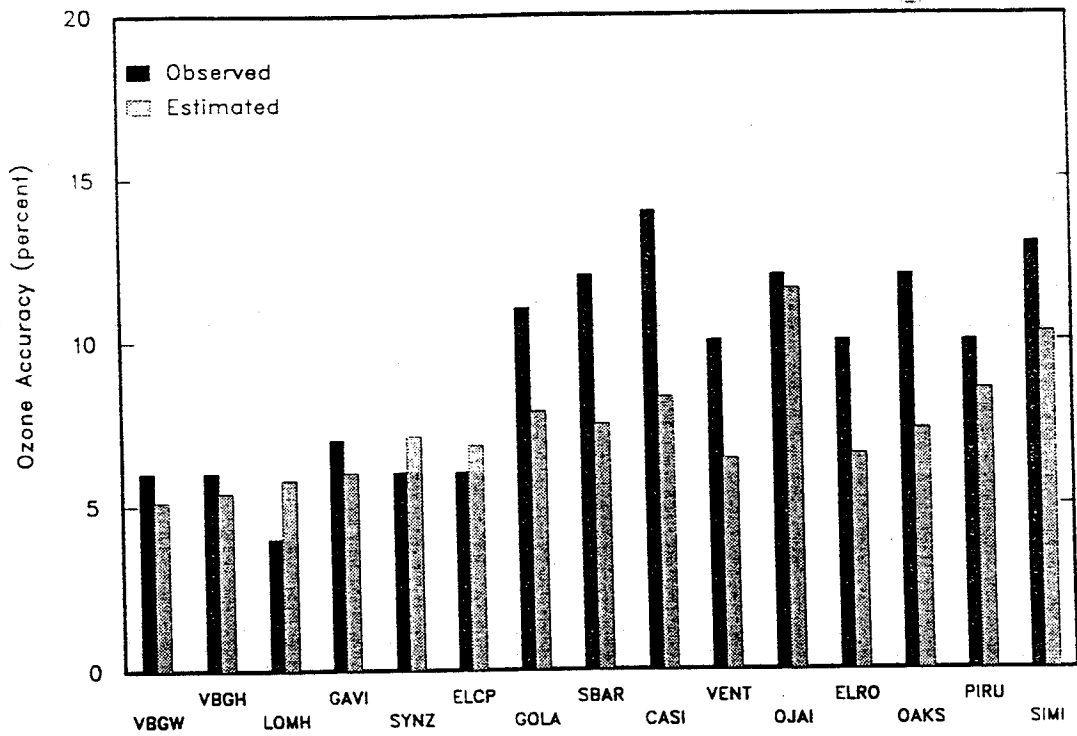


Figure 6-12f. Maximum Estimated and Observed Ozone Concentrations and Station Accuracy Estimates for the 16-17 September, 1984 UAM-IV Simulation - 17 September, 1984.

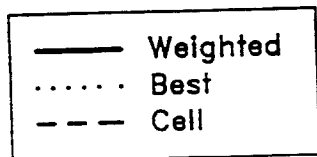
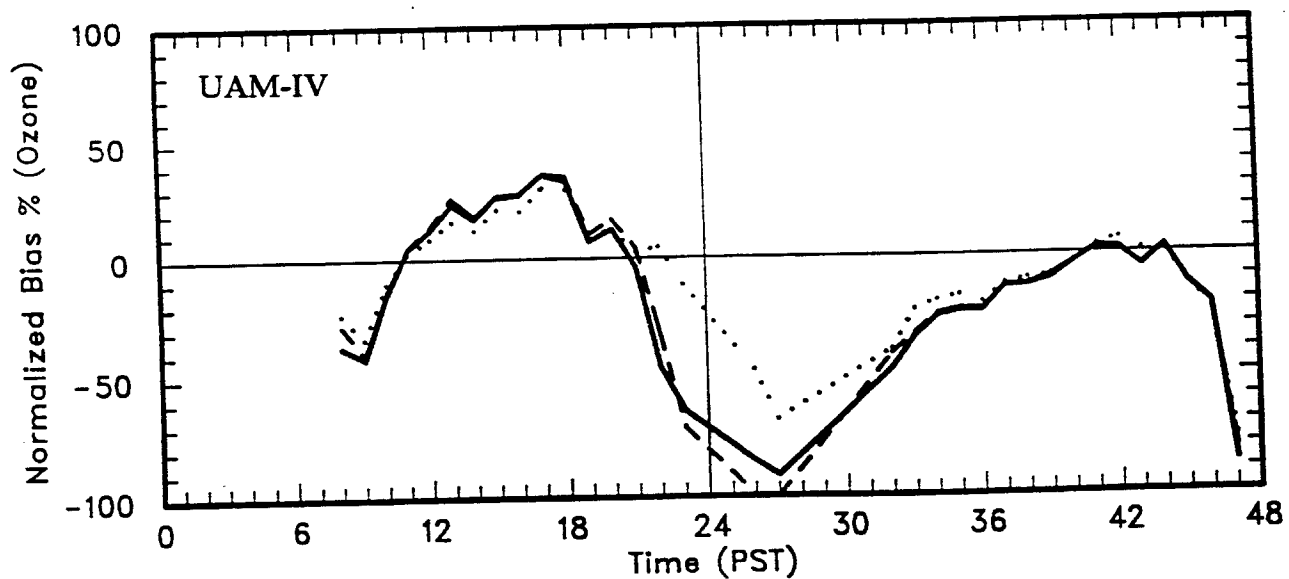
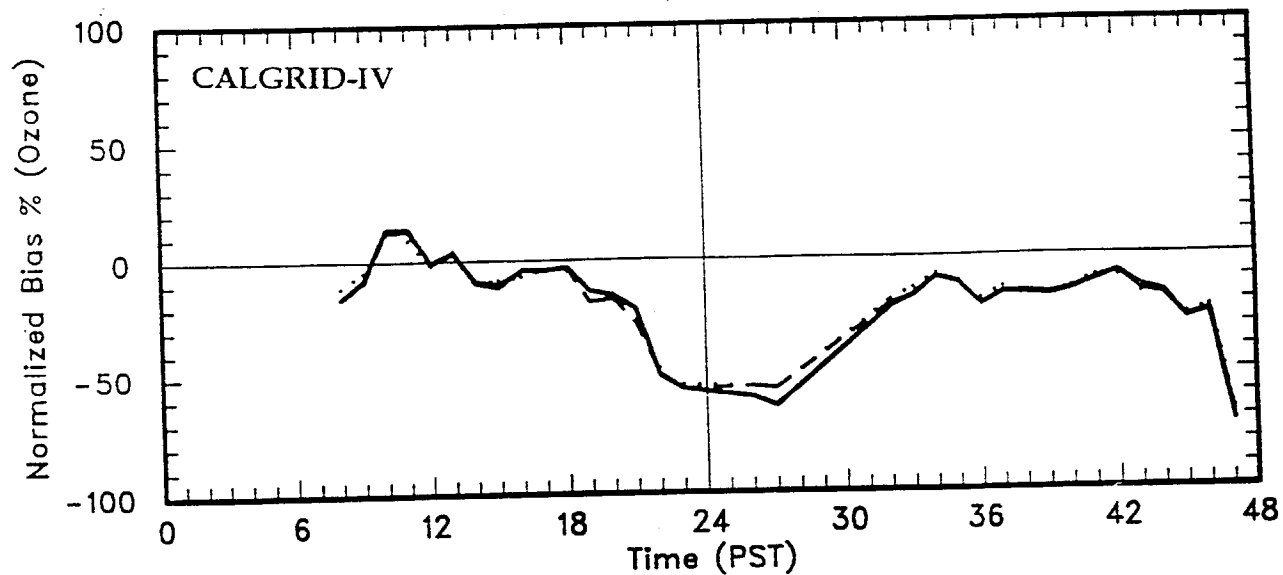


Figure 6-13. Normalized Bias in Ozone Estimation as a Function of Time Throughout the 16-17 September, 1984 Episode.

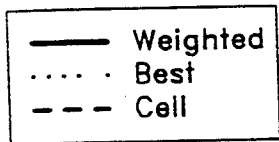
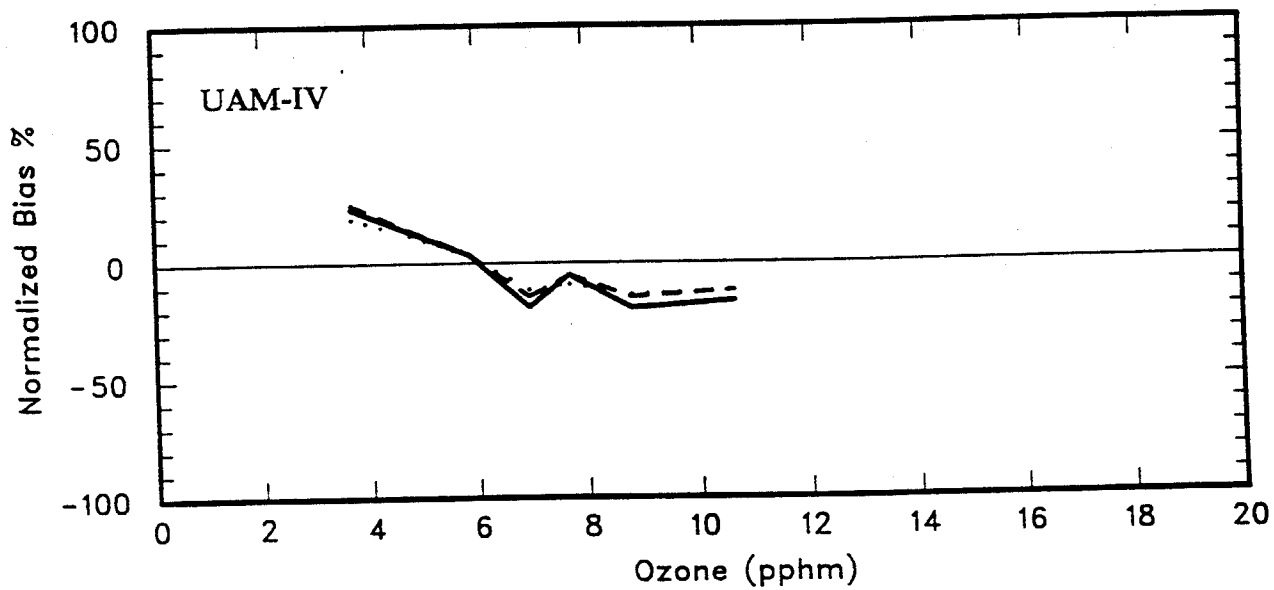
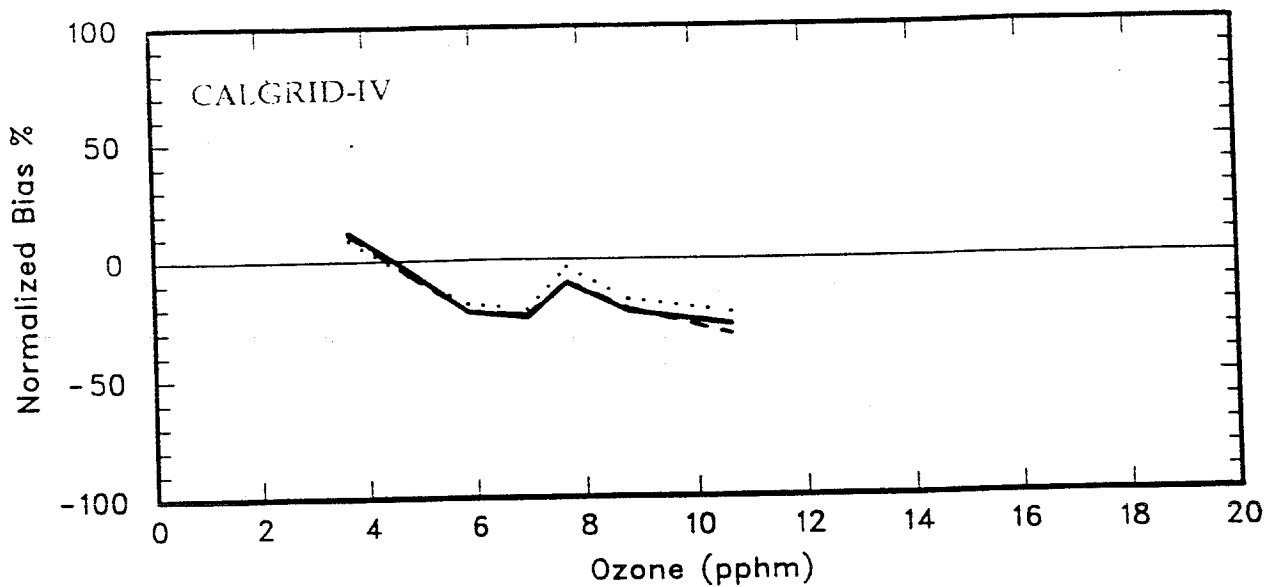


Figure 6-13b. Normalized Bias in Ozone Estimation as a Function of Observed Concentration Level for the 16-17 September, 1984 Episode -- 16 September, 1984.

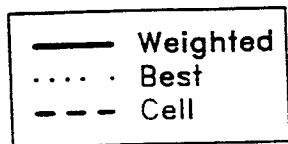
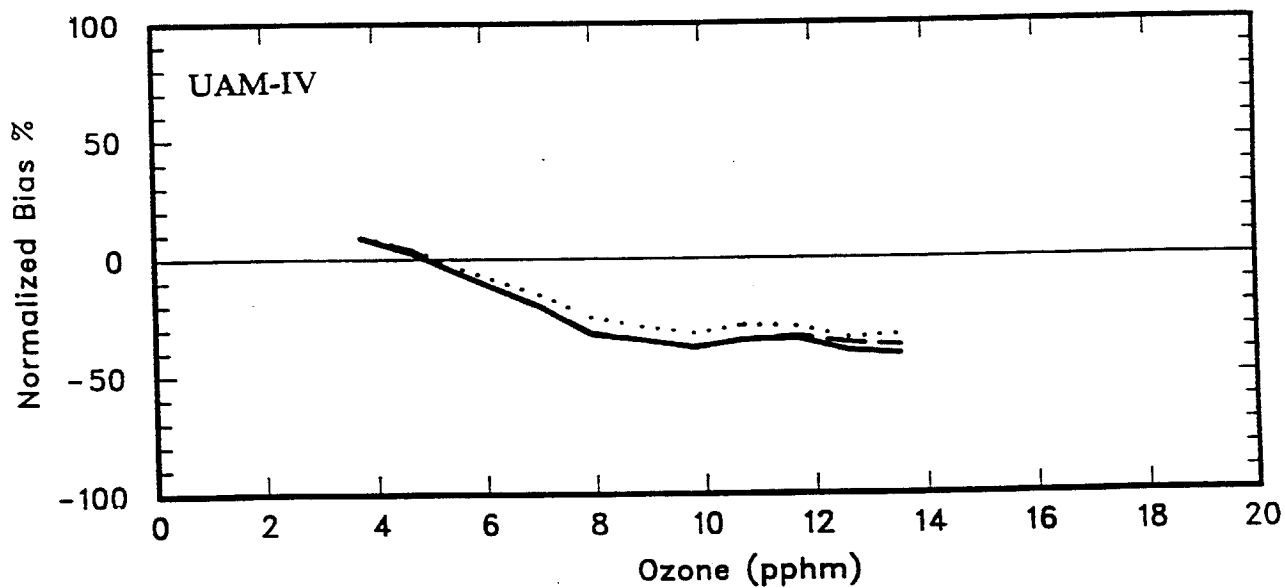
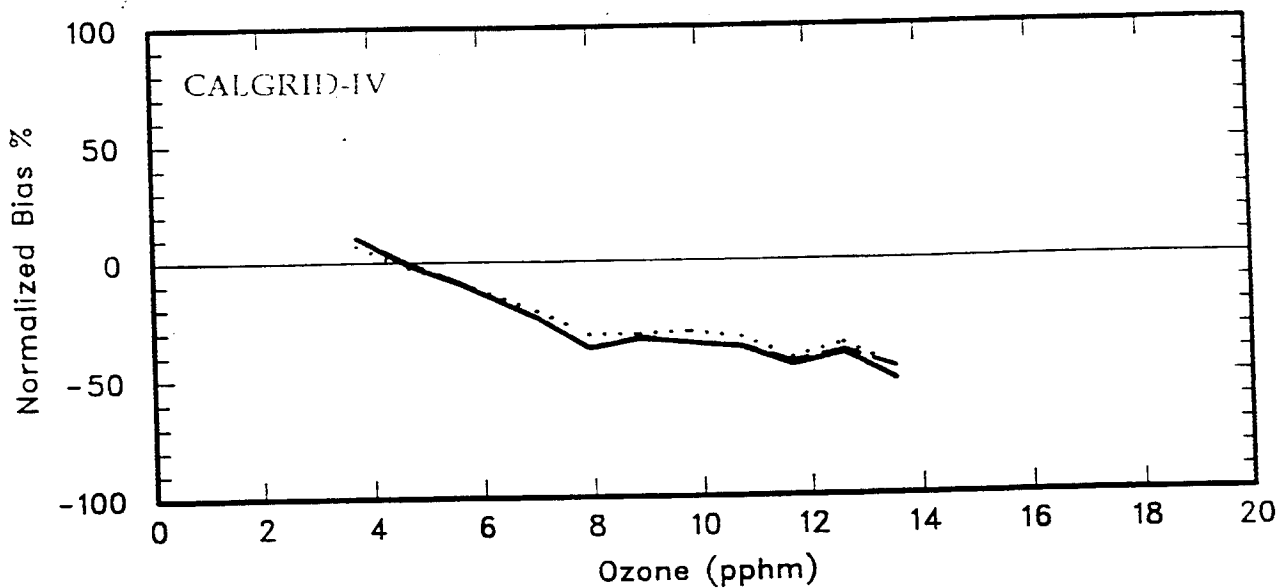


Figure 6-13c. Normalized Bias in Ozone Estimation as a Function of Observed Concentration Level for the 16-17 September, 1984 Episode -- 17 September, 1984.

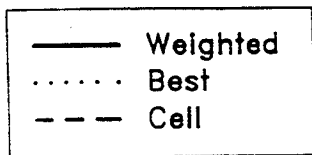
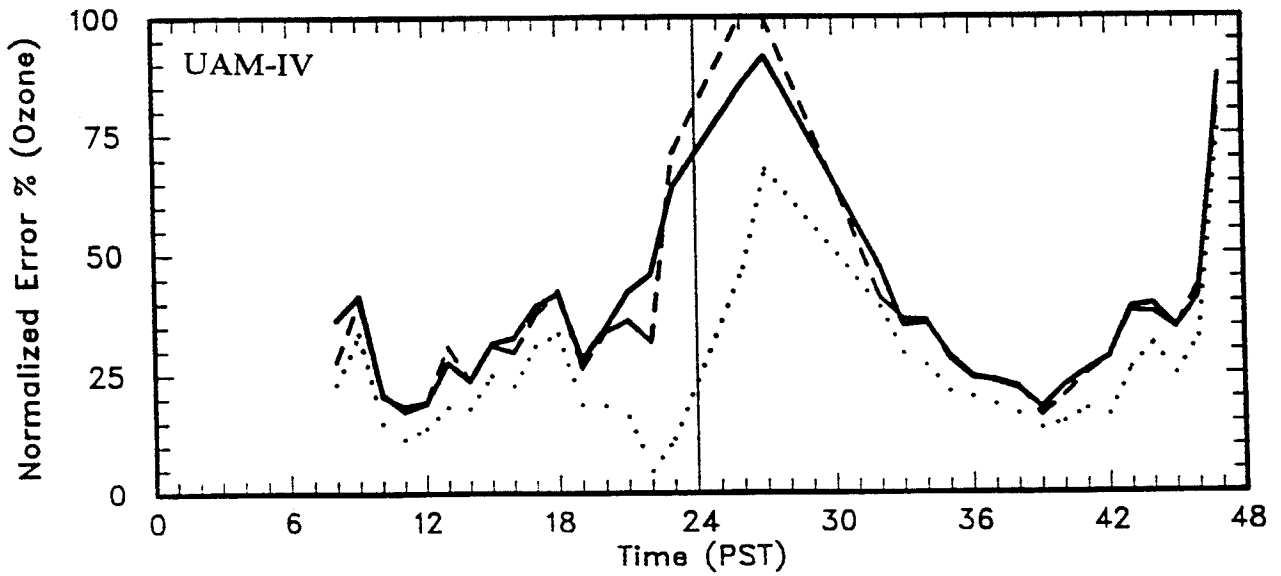
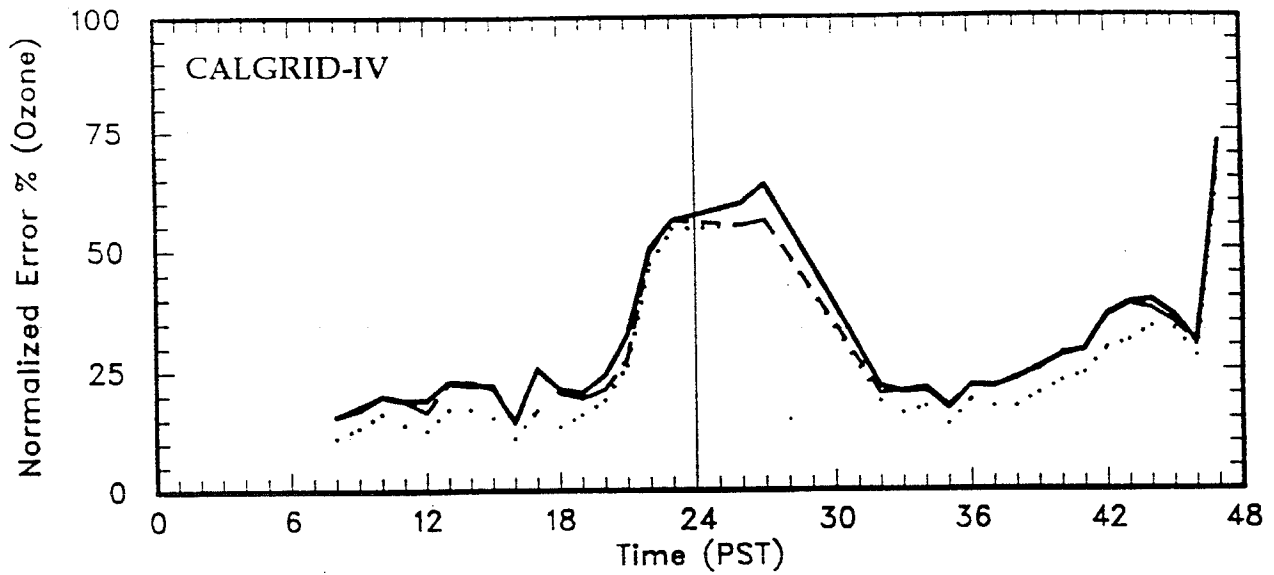


Figure 6-14. Normalized Gross Error in Ozone Estimations as a Function of Time Throughout the 16-17 September, 1984 Episode.

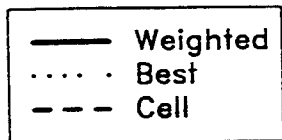
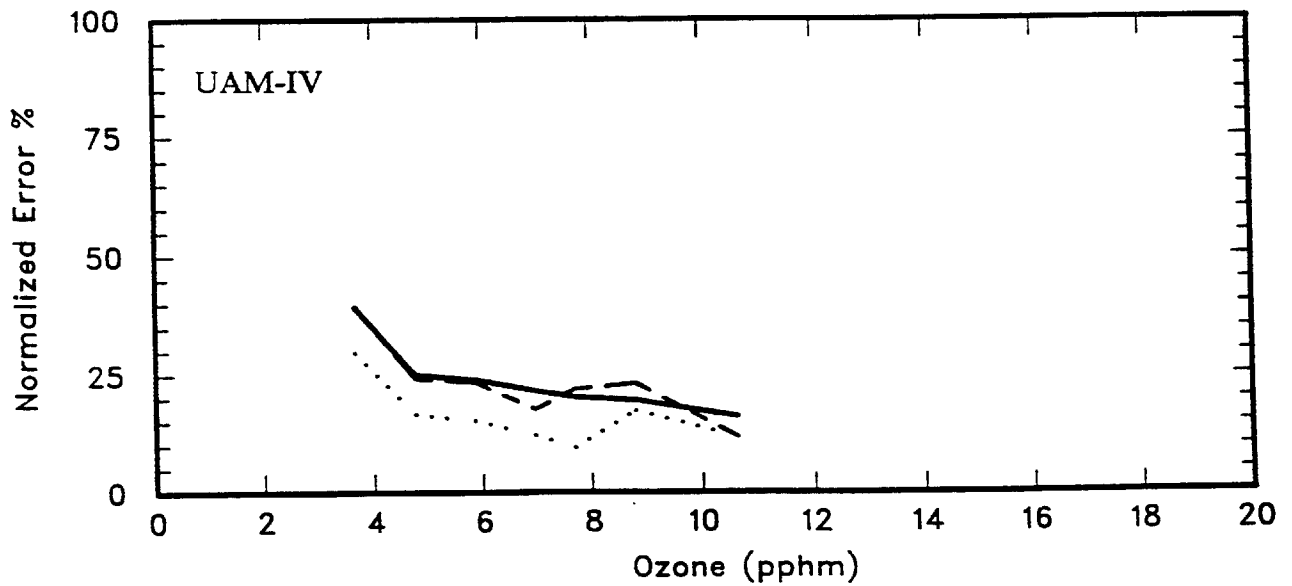
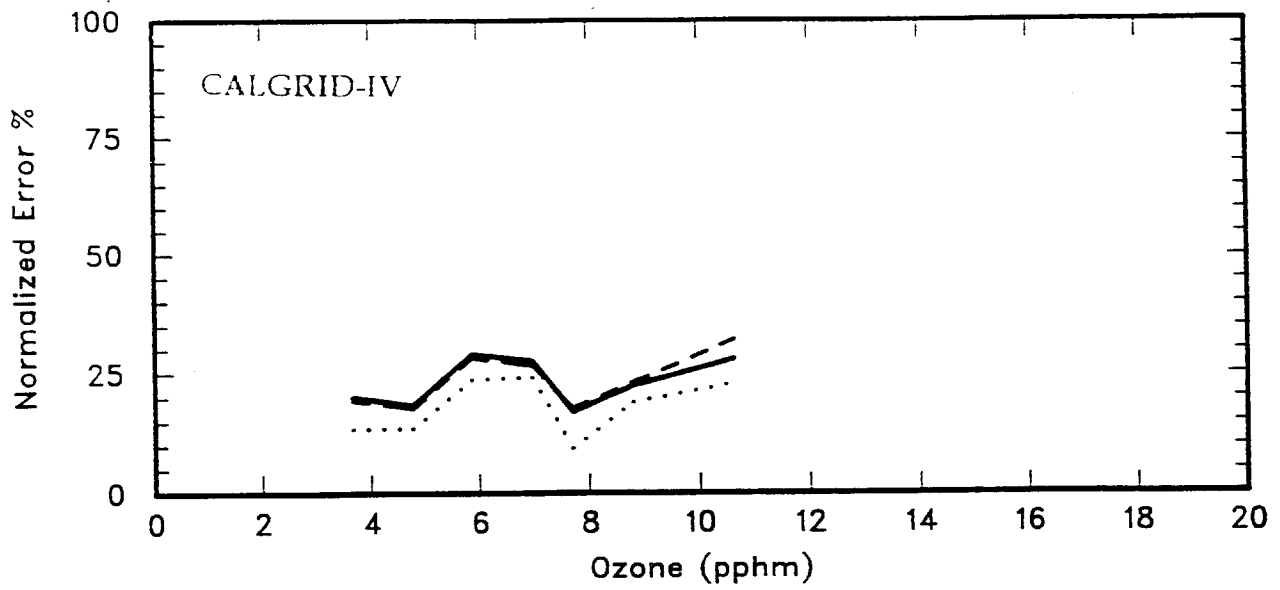


Figure 6-14b. Normalized Gross Error in Ozone Estimation as a Function of Observed Concentration Level for the 16-17 September, 1984 Episode -- 17 September, 1984.

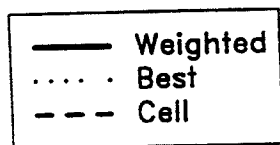
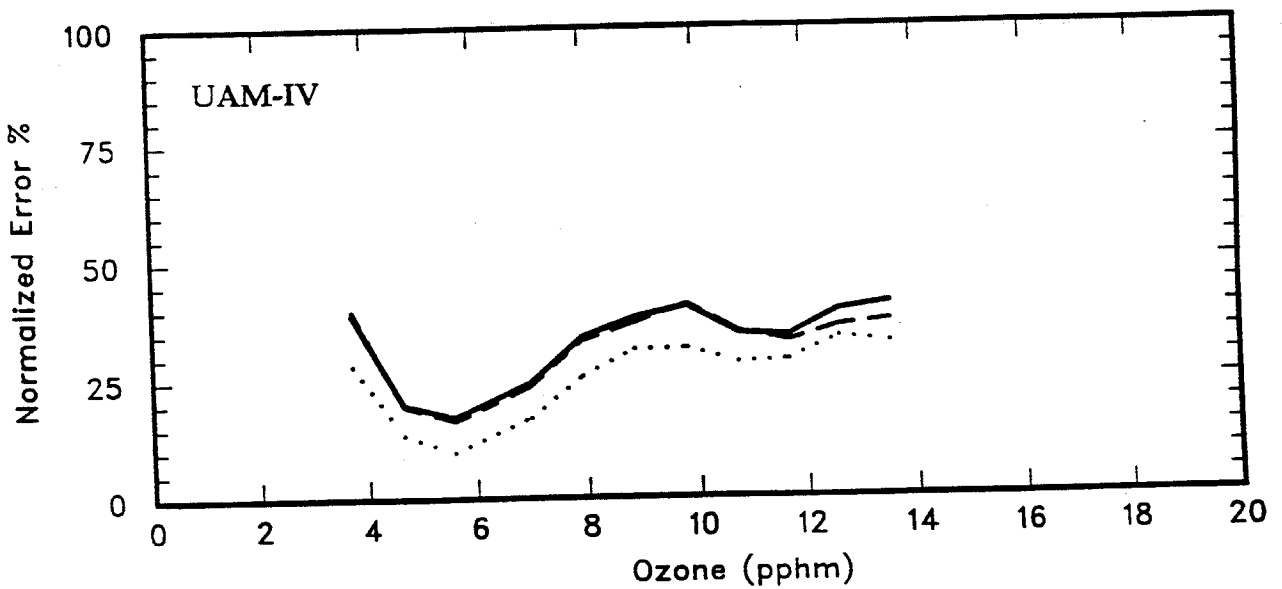
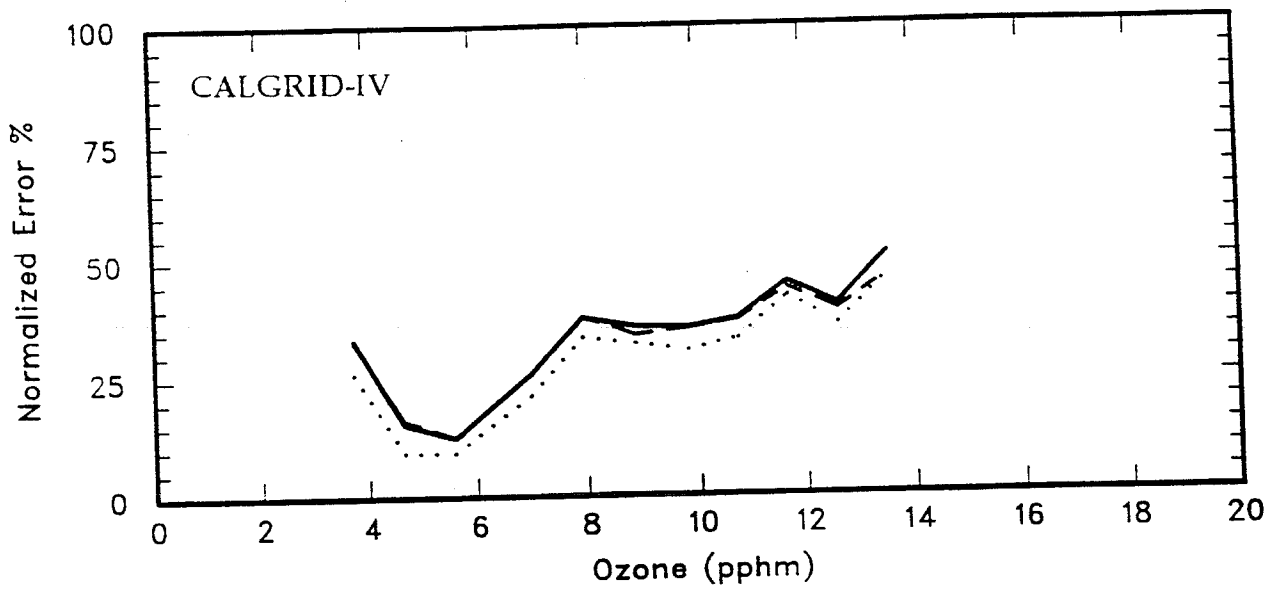
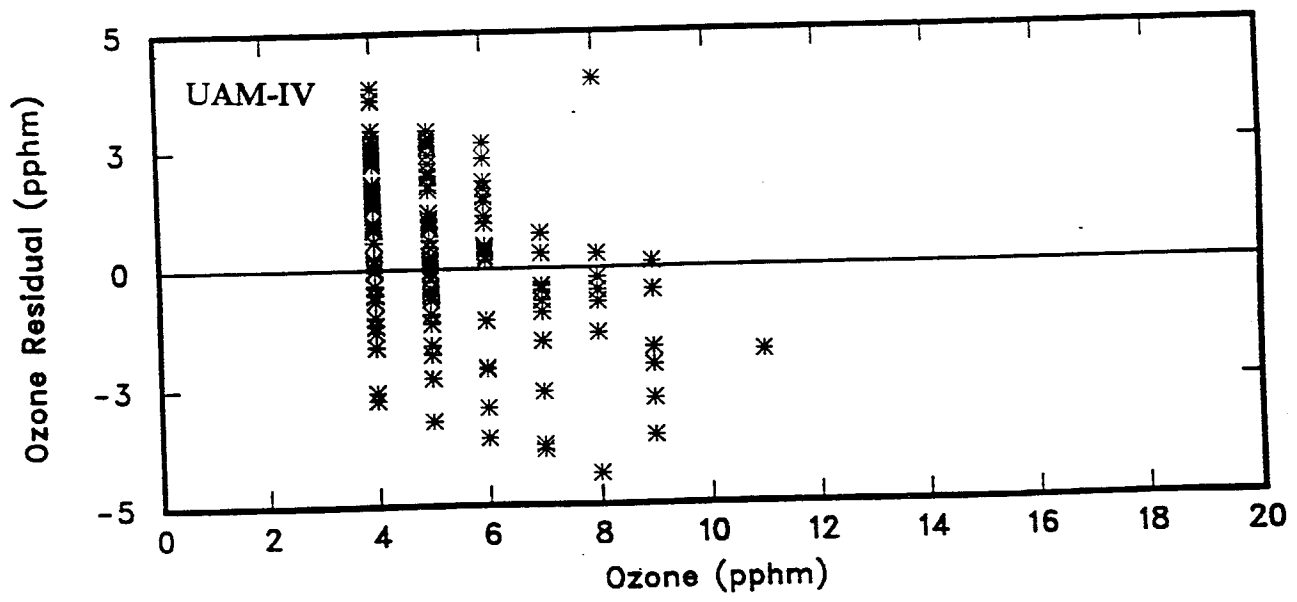
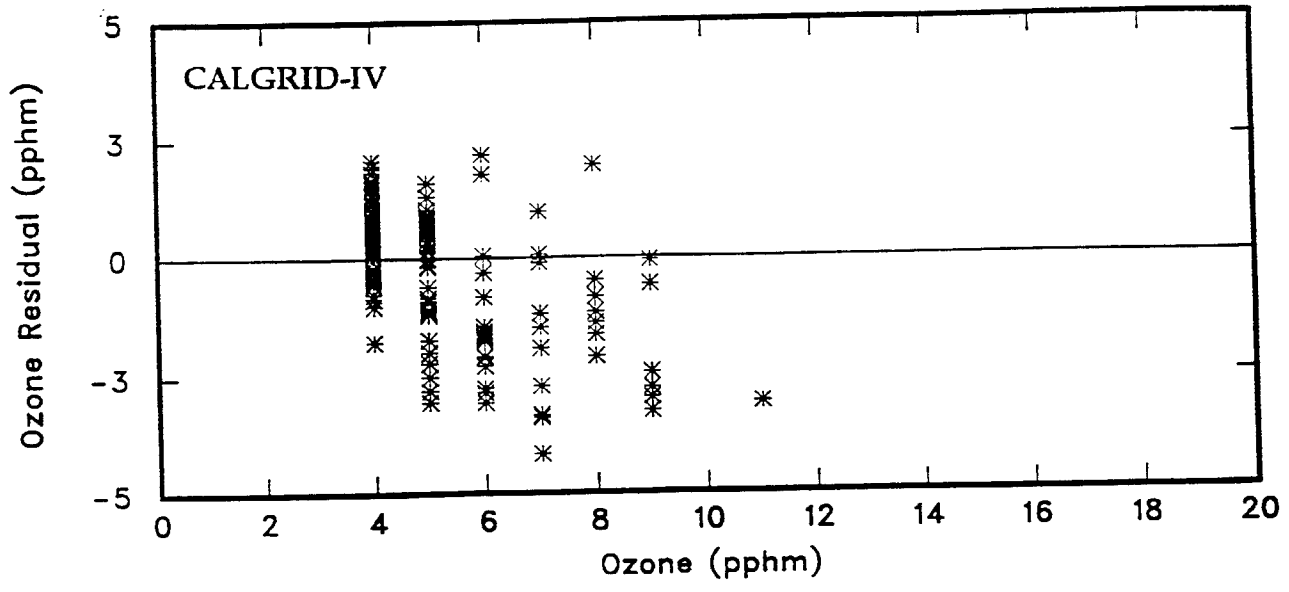
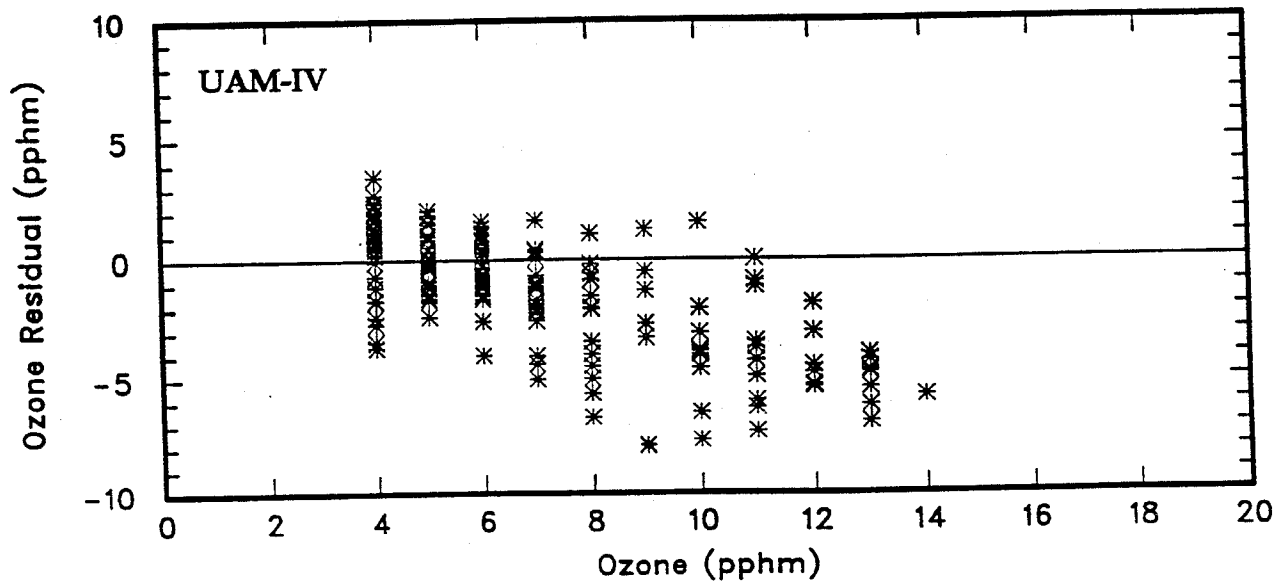
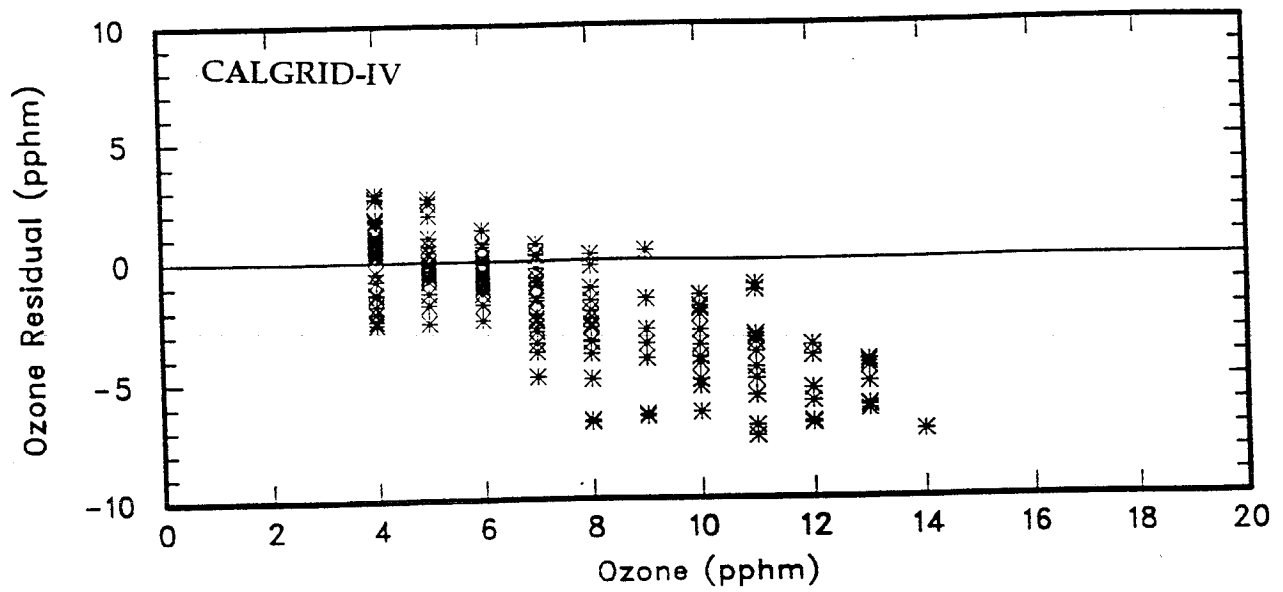


Figure 6-14c. Normalized Gross Error in Ozone Estimation as a Function of Observed Concentration Level for the 16-17 September, 1984 Episode -- 16 September, 1984.



\* Residual = Estimated - Observed

Figure 6-15a. Hourly Ozone Residuals as a Function of Concentration Throughout the 16-17 September, 1984 Episode - 16 September, 1984.



\* Residual = Estimated - Observed

Figure 6-15b. Hourly Ozone Residuals as a Function of Concentration Throughout the 16-17 September, 1984 Episode - 17 September, 1984.

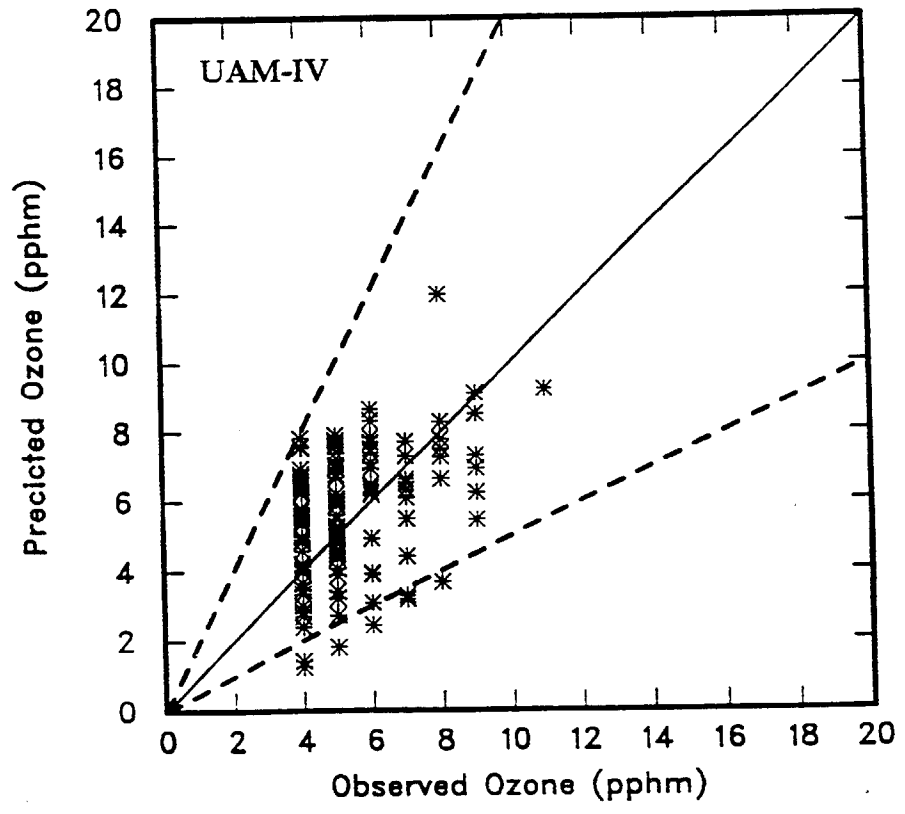
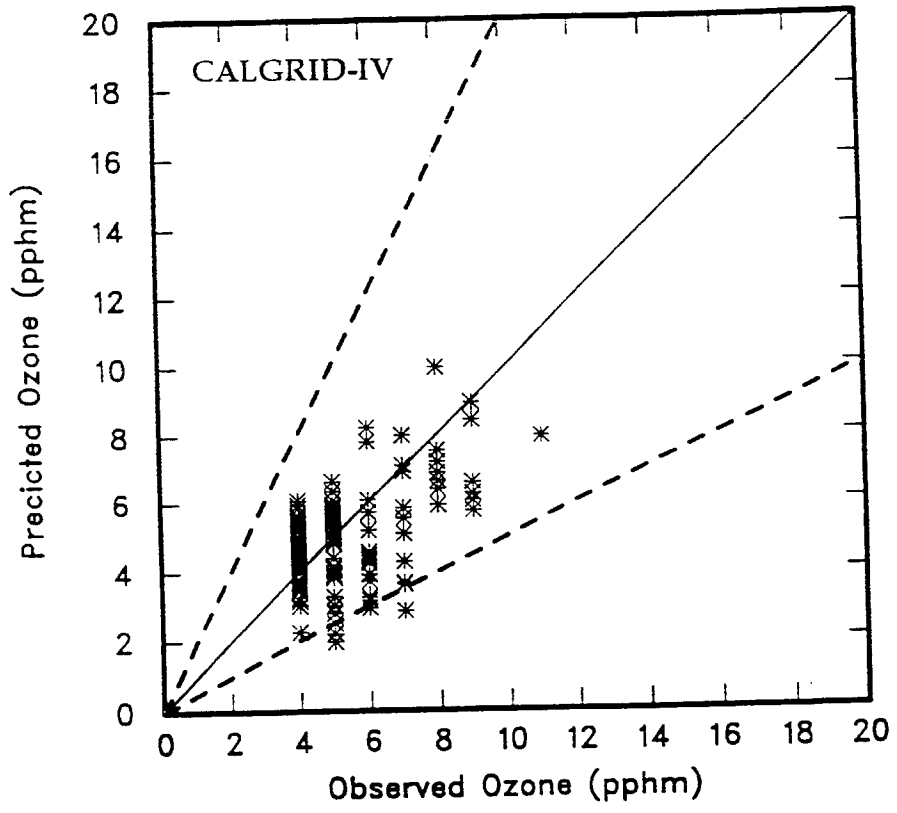


Figure 6-16a. Scatterplot of Hourly Ozone Concentration Residuals for the 16-17 September, 1984 Episode -- 16 September, 1984.

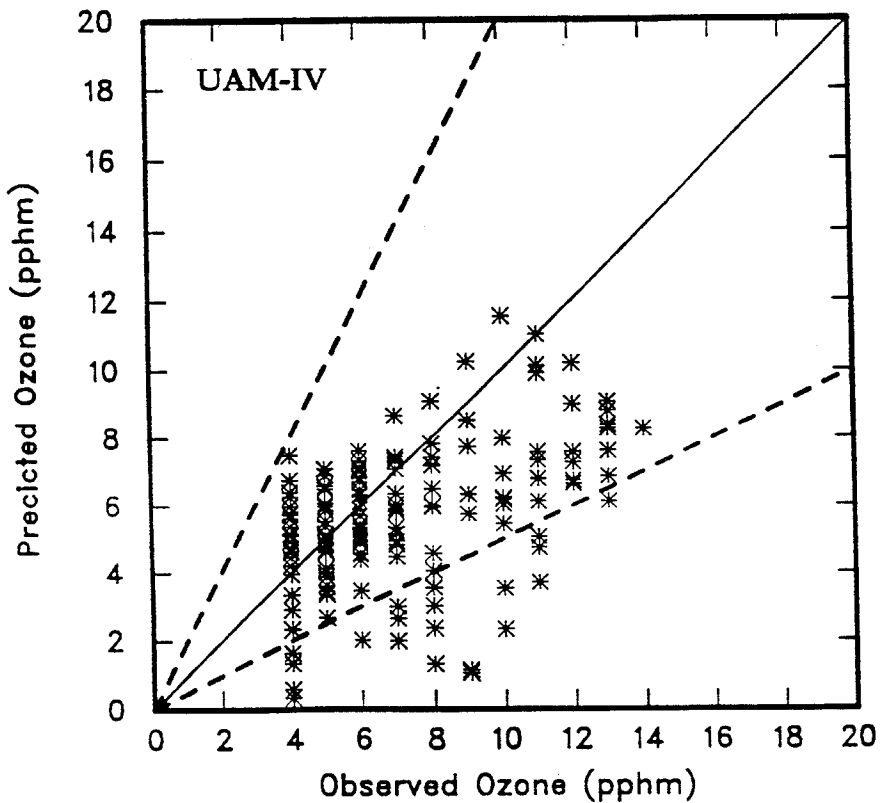
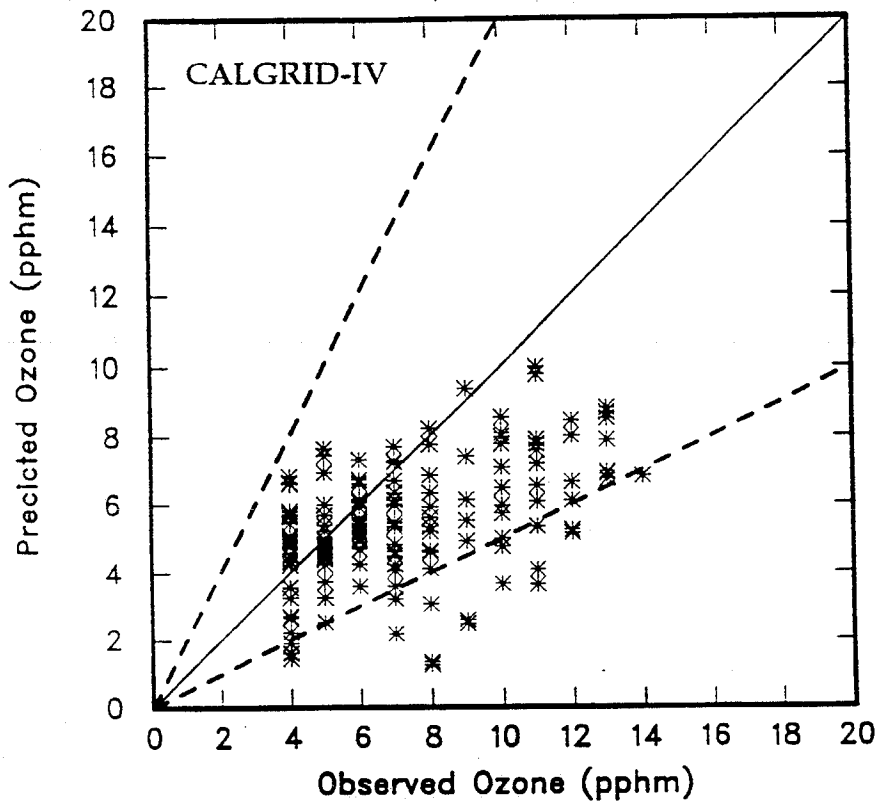


Figure 6-16b. Scatterplot of Hourly Ozone Concentration Residuals for the 16-17 September, 1984 Episode -- 17 September, 1984.

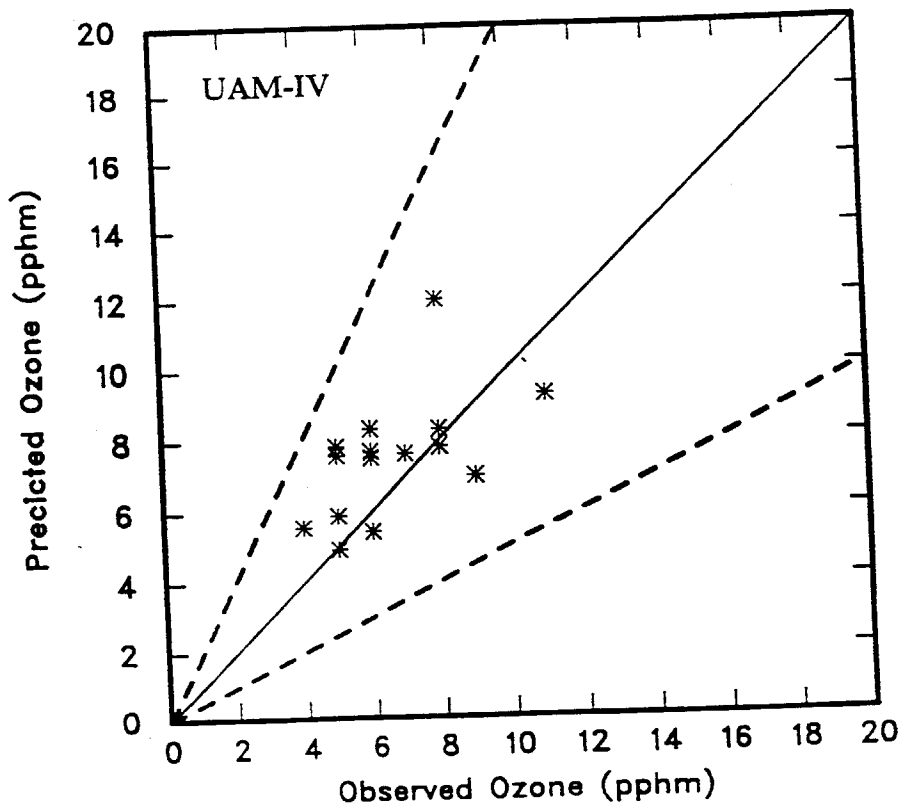
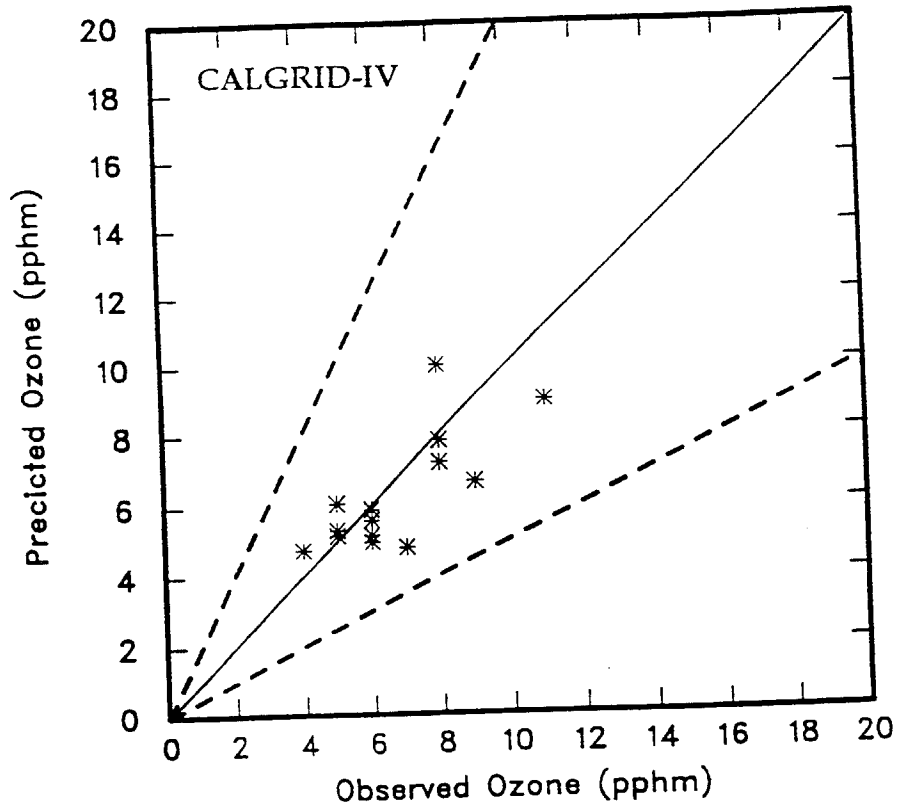


Figure 6-17a. Scatterplot of Daily Maximum Ozone Concentration Residuals for the 16-17 September, 1984 Episode -- 16 September, 1984.

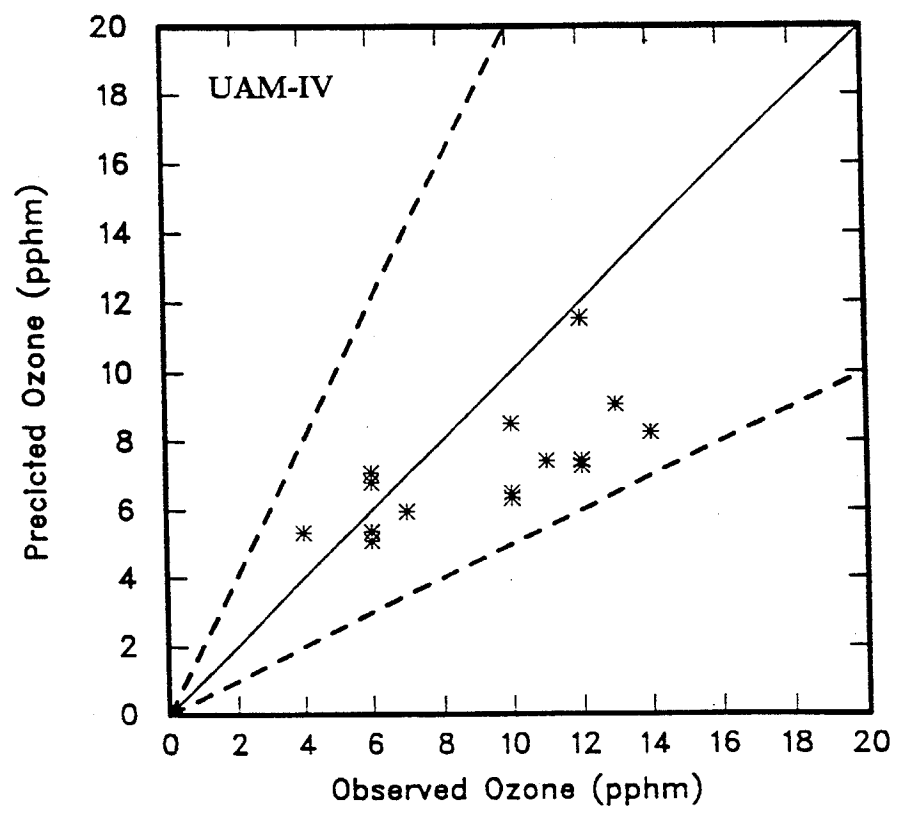
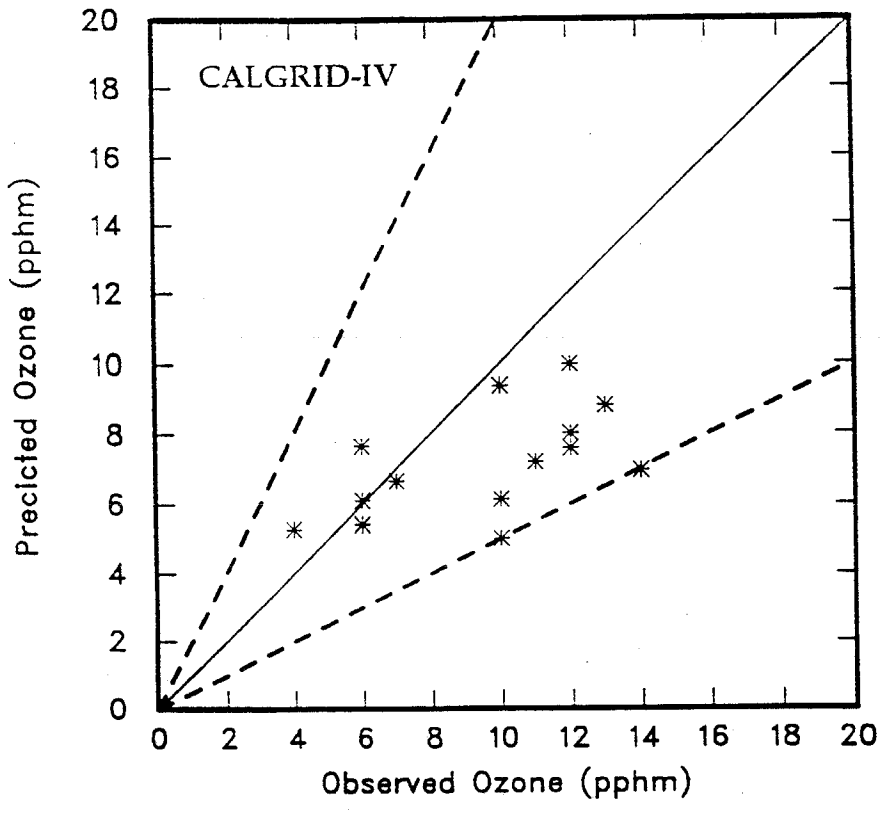


Figure 6-17b. Scatterplot of Daily Maximum Ozone Concentration Residuals for the 16-17 September, 1984 Episode -- 17 September, 1984.

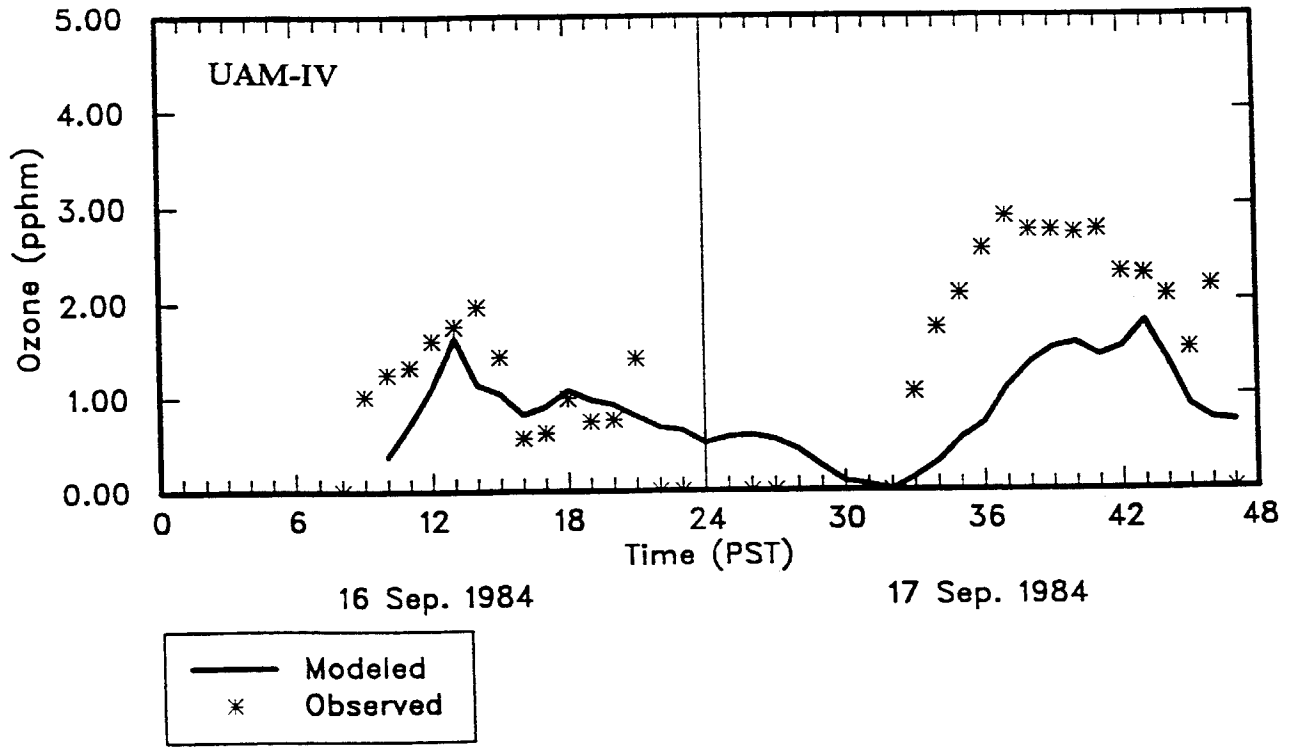
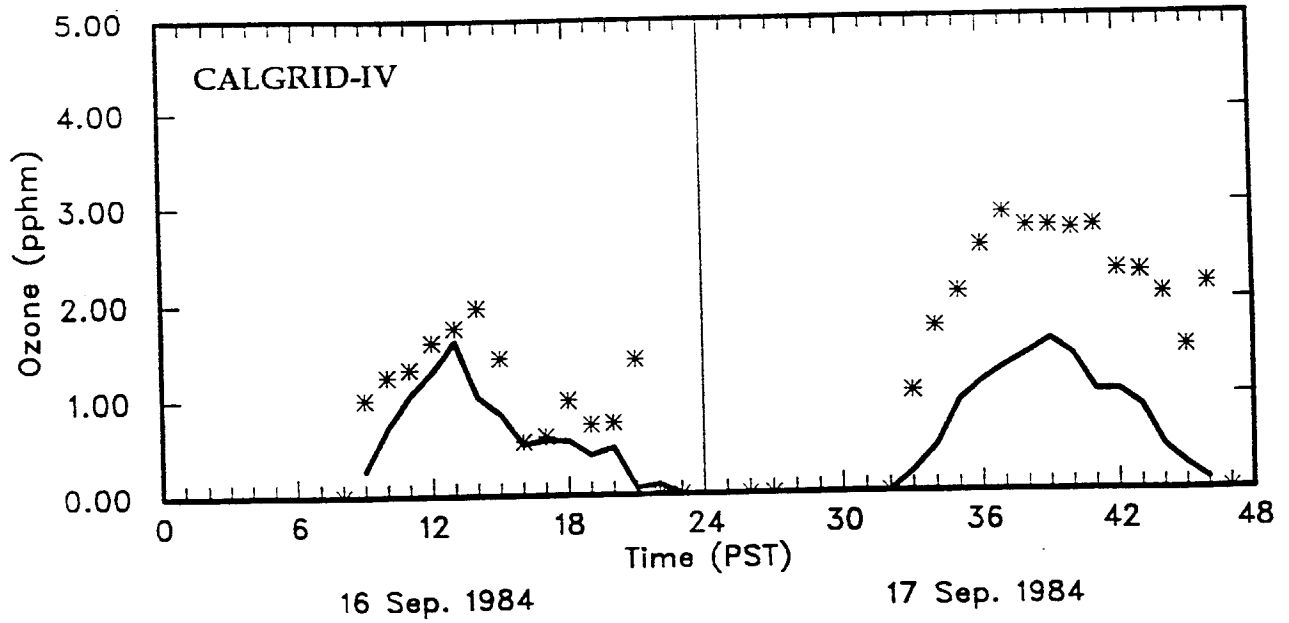


Figure 6-18. Standard Deviation of Ozone Estimates and Observations as a Function of Time Throughout the 16-17 September, 1984 Episode.

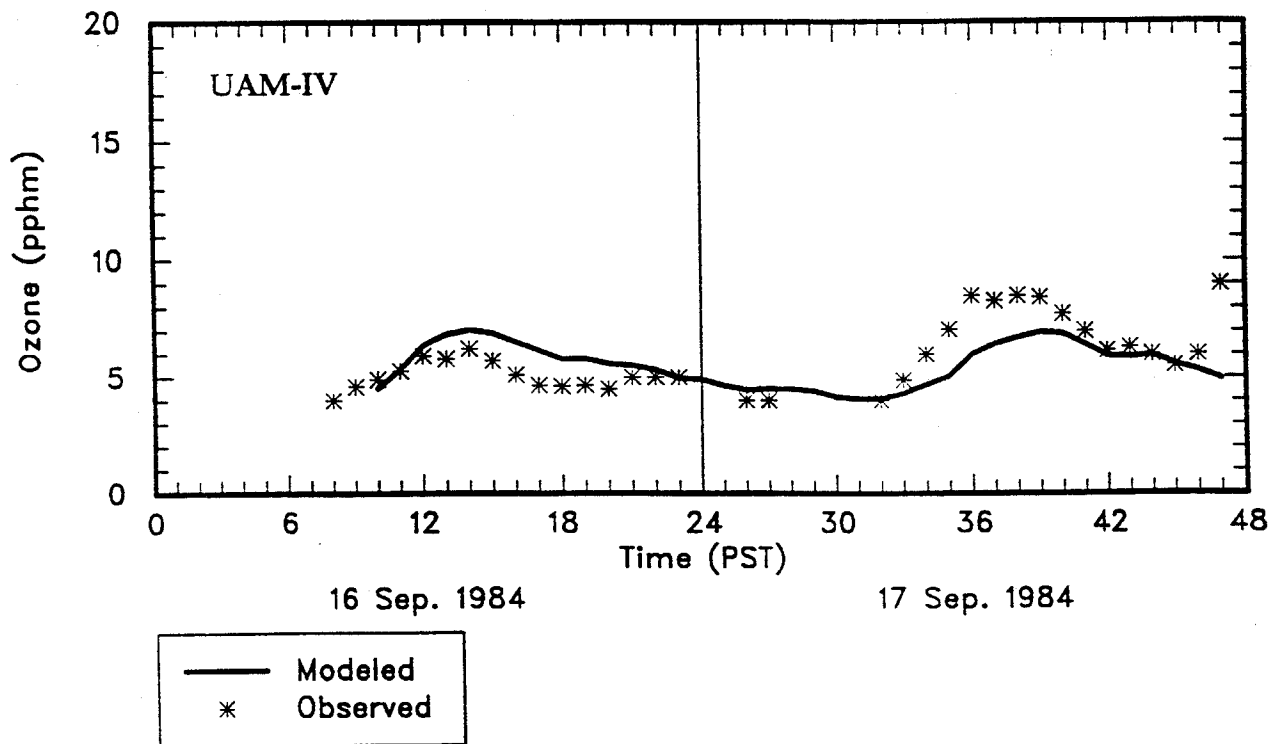
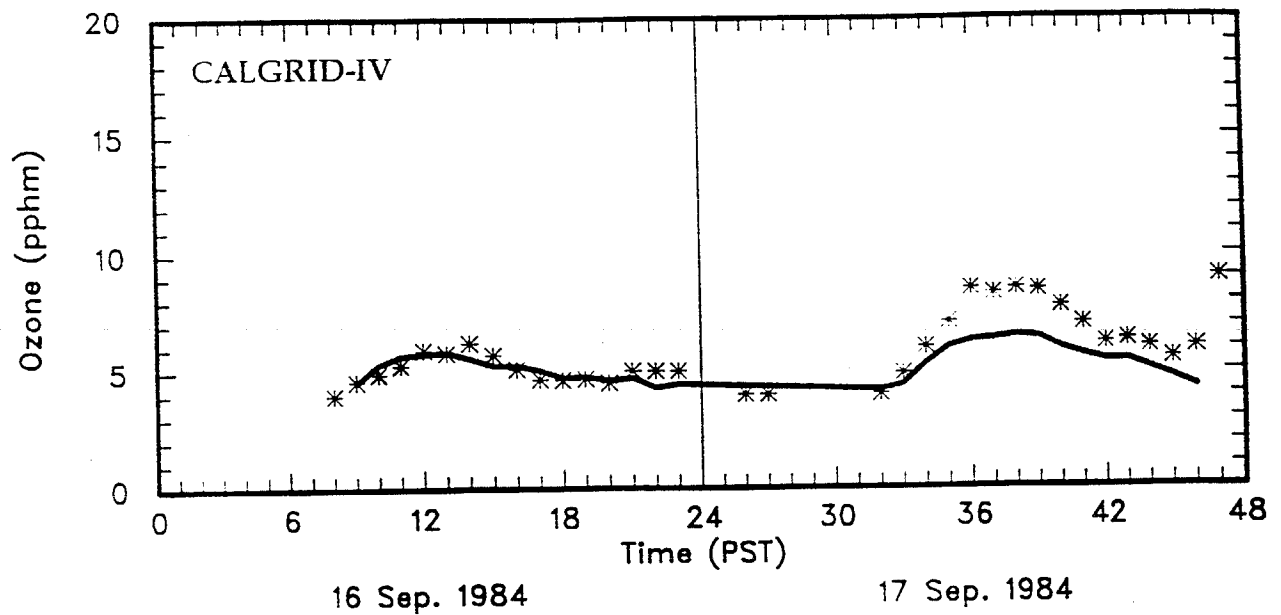


Figure 6-19. Mean Value of Ozone Estimates and Observations as a Function of Time Throughout the 16-17 September, 1984 Episode.

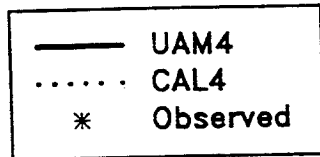
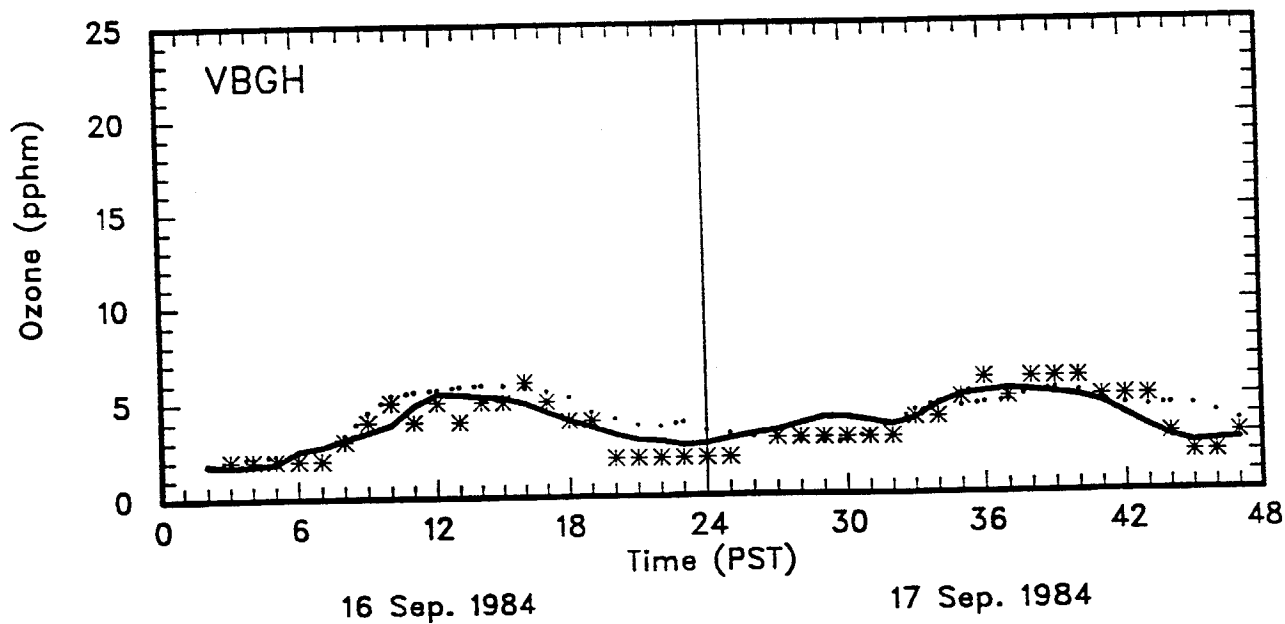
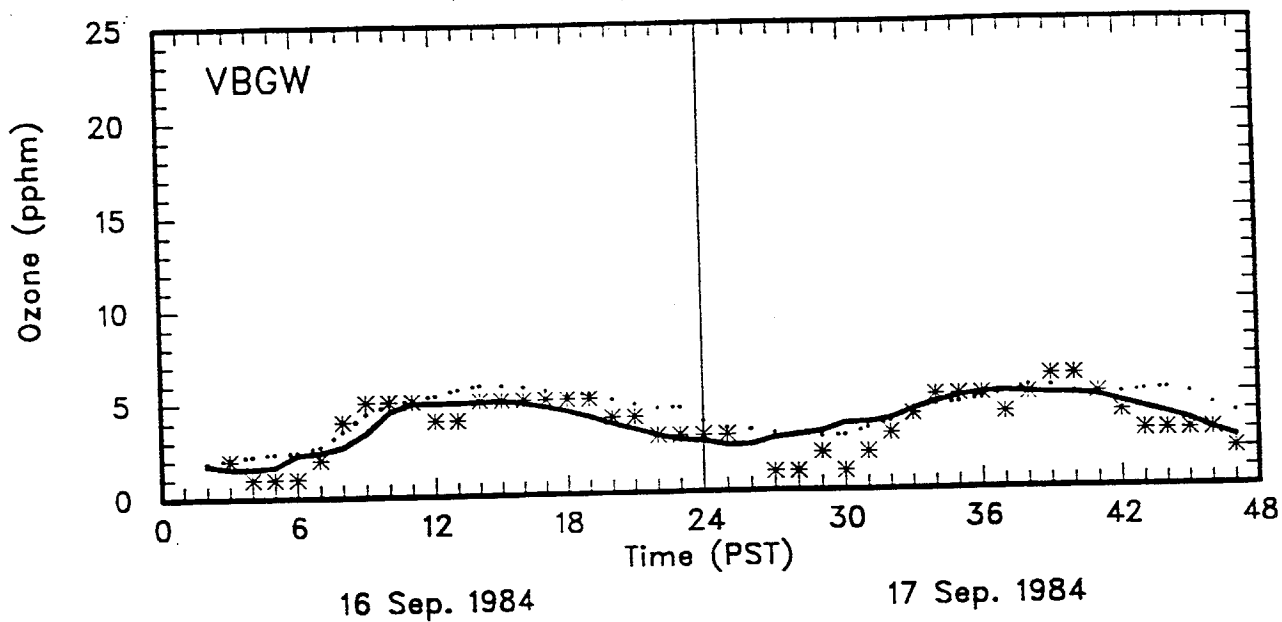


Figure 6-20. Time Series of Hourly Estimated and Observed Ozone Concentrations for the 16-17 September, 1984 Episode.

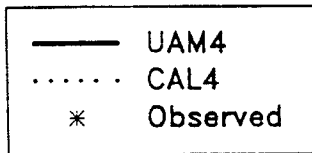
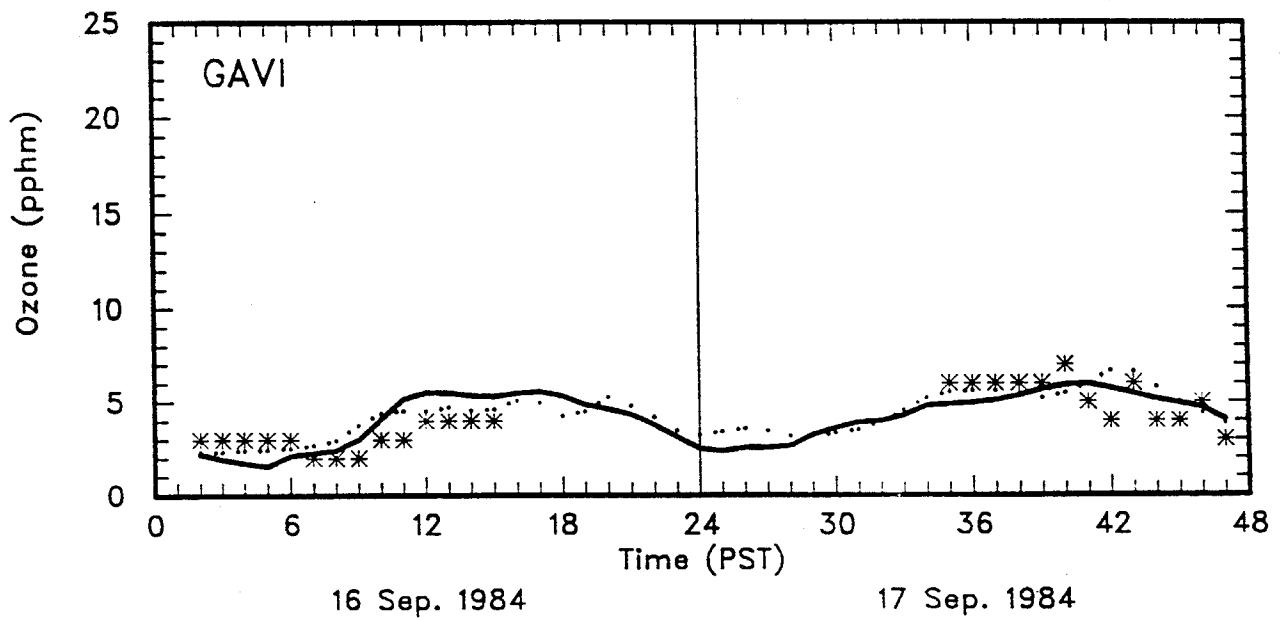
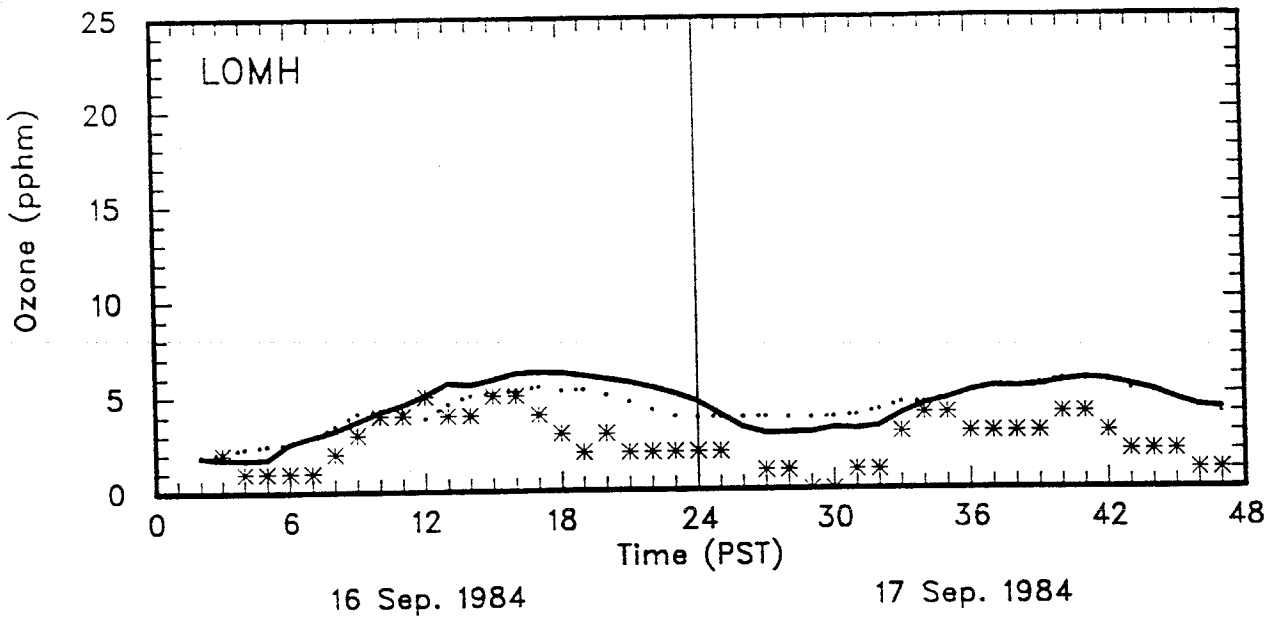


Figure 6-20. Continued.

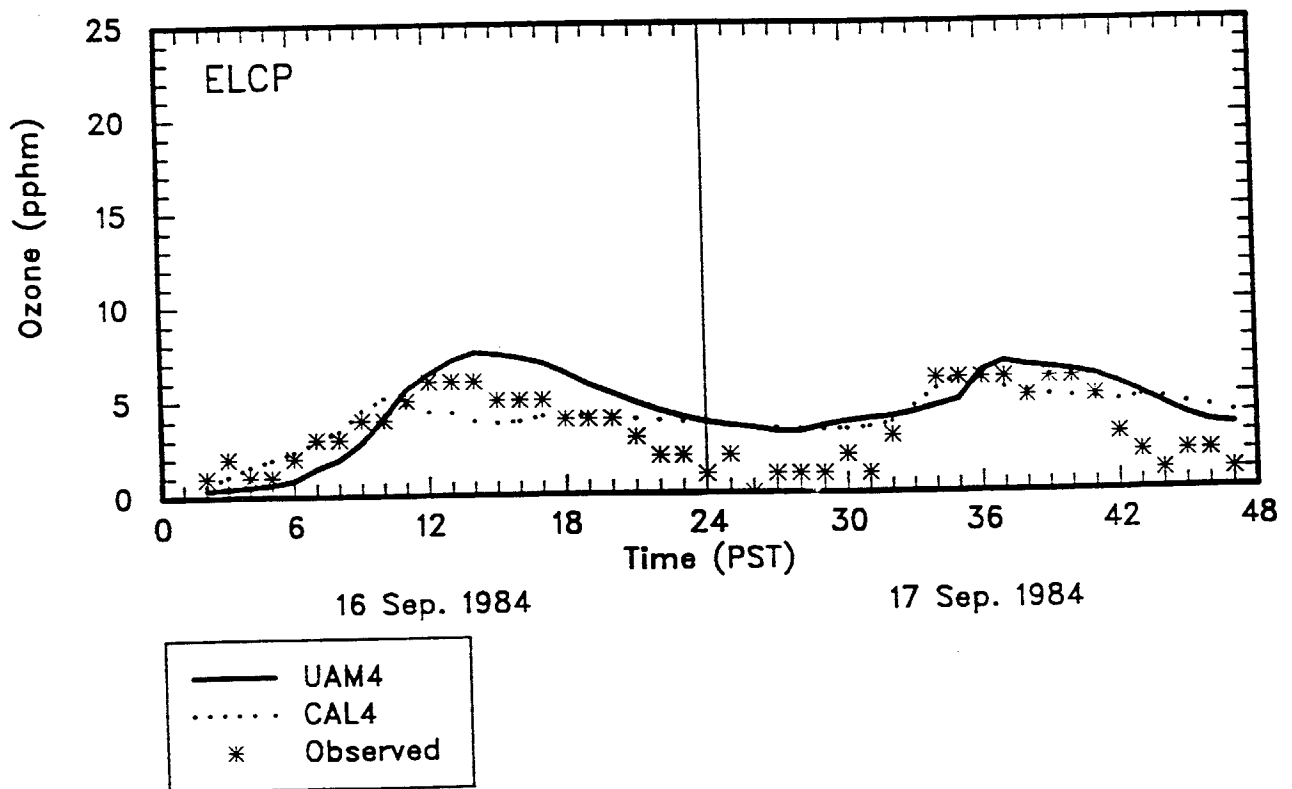
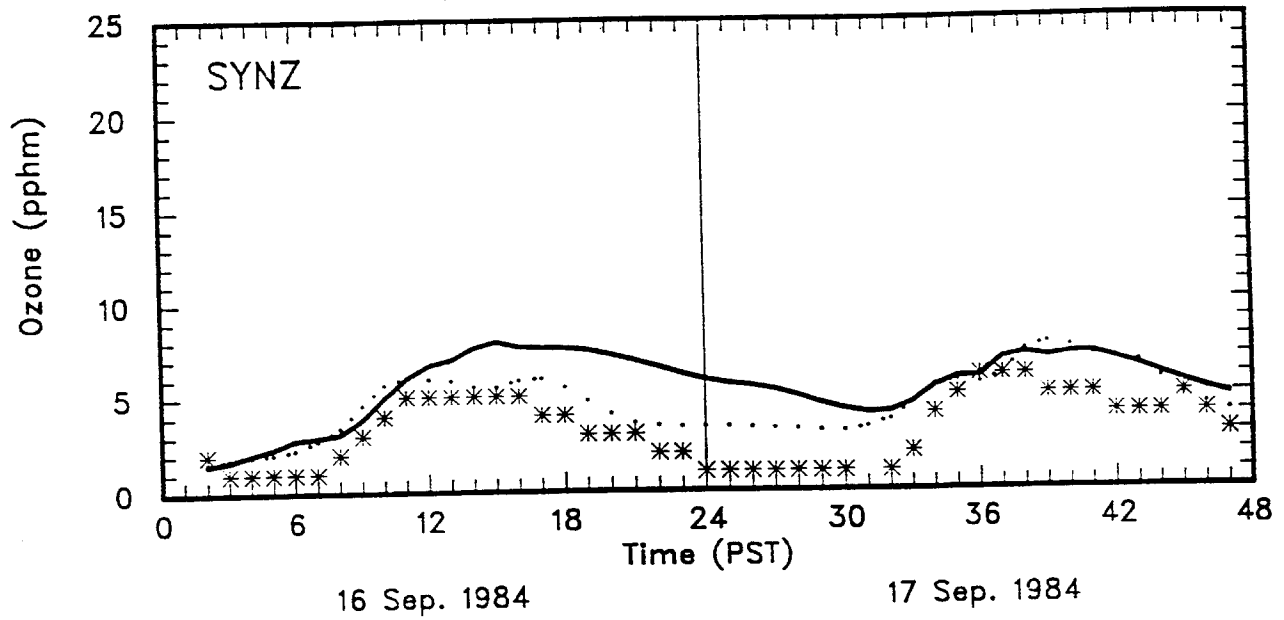


Figure 6-20. Continued.

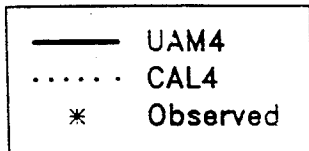
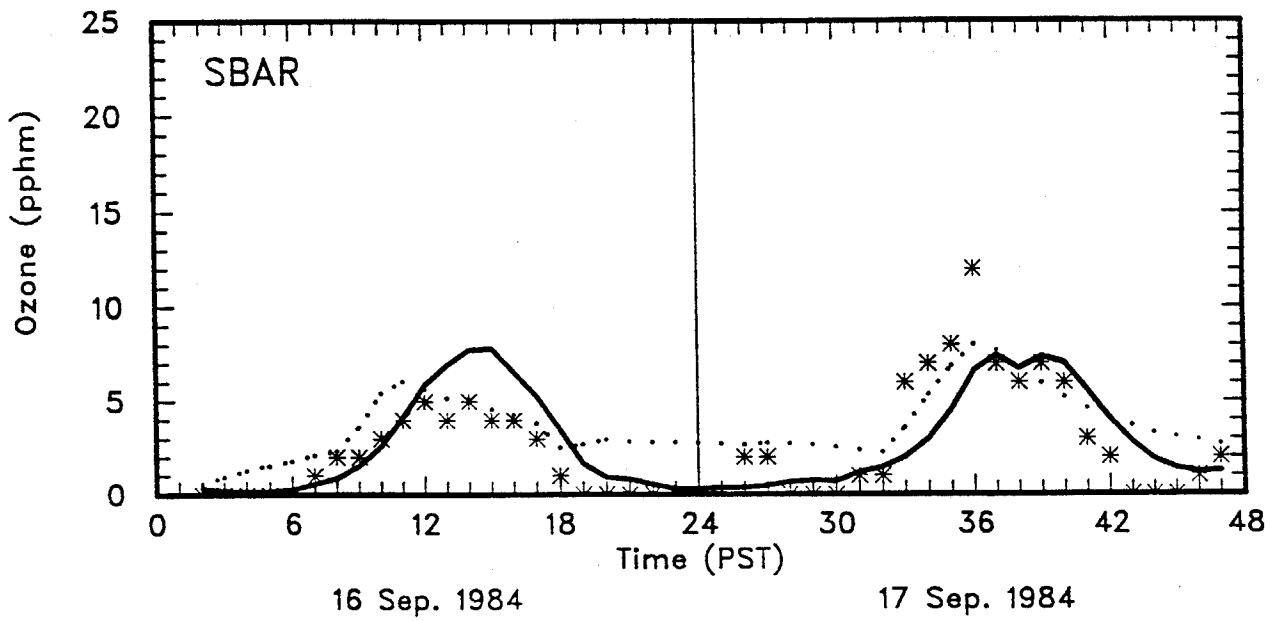
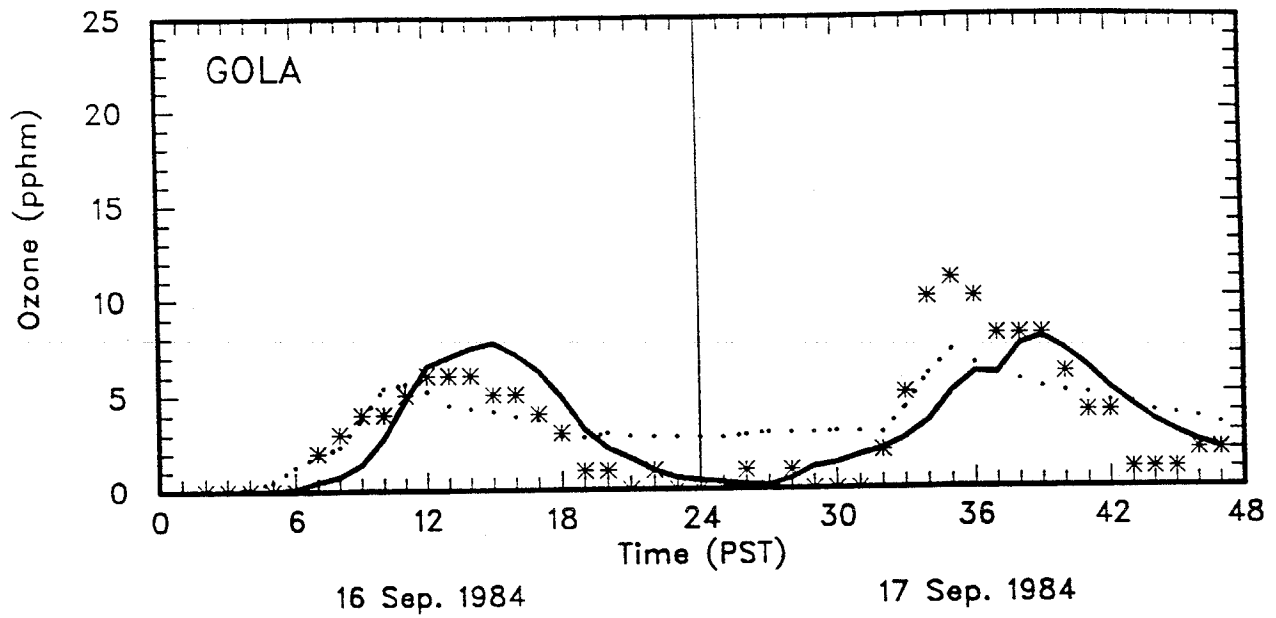


Figure 6-20. Continued.

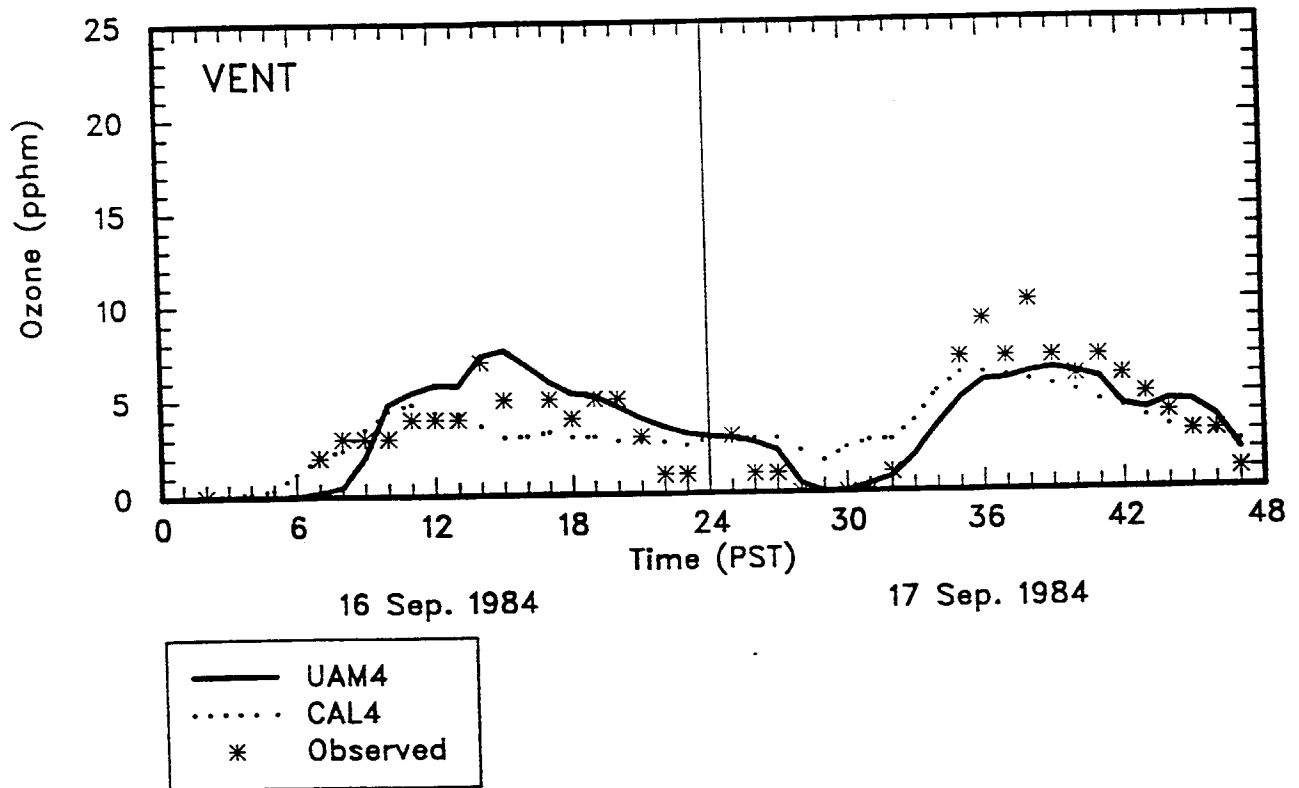
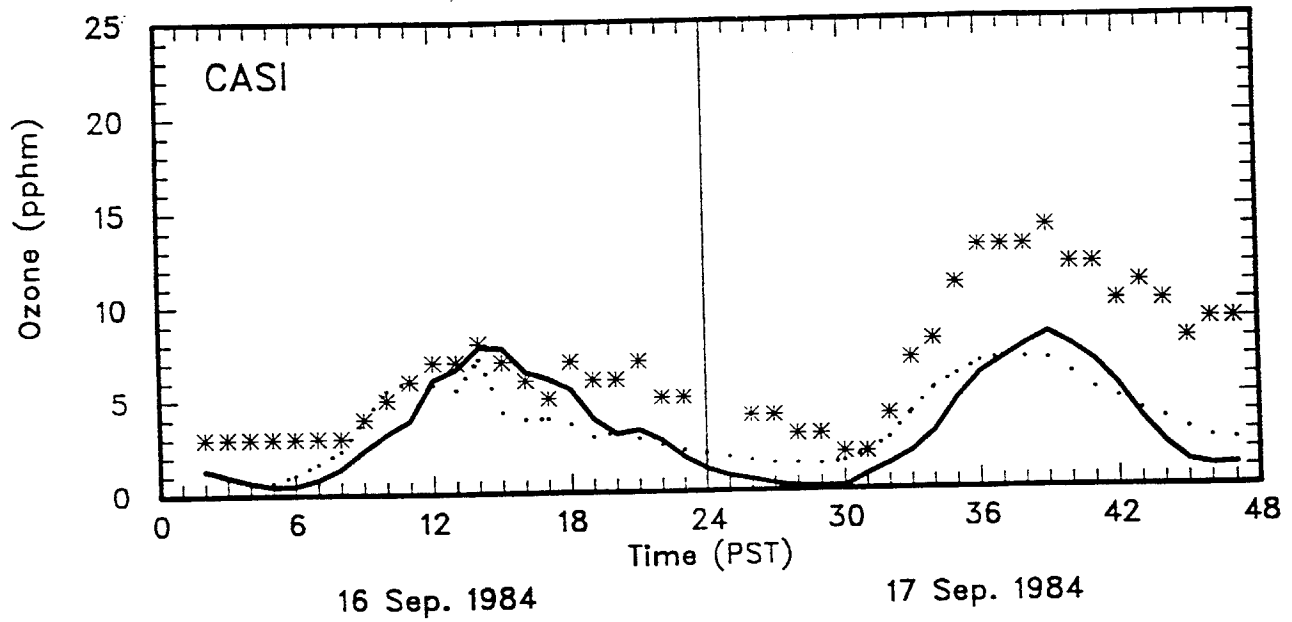


Figure 6-20. Continued.

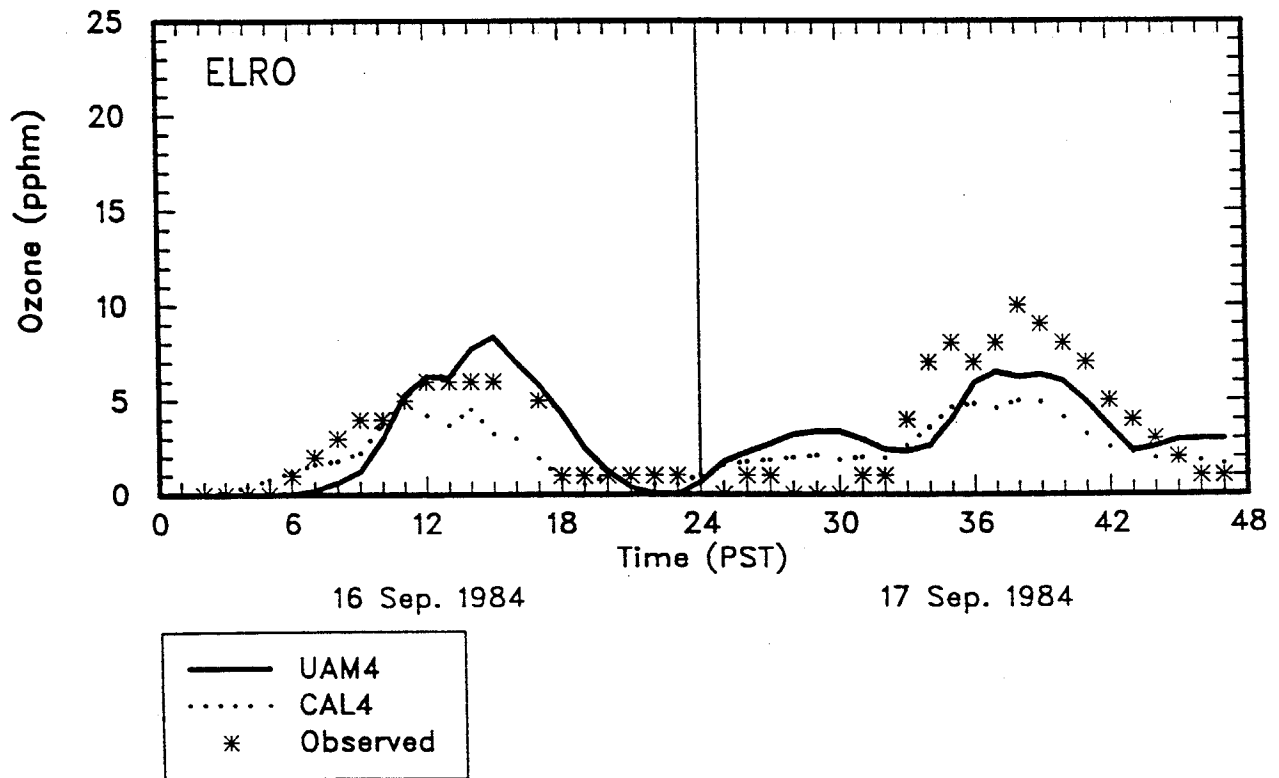
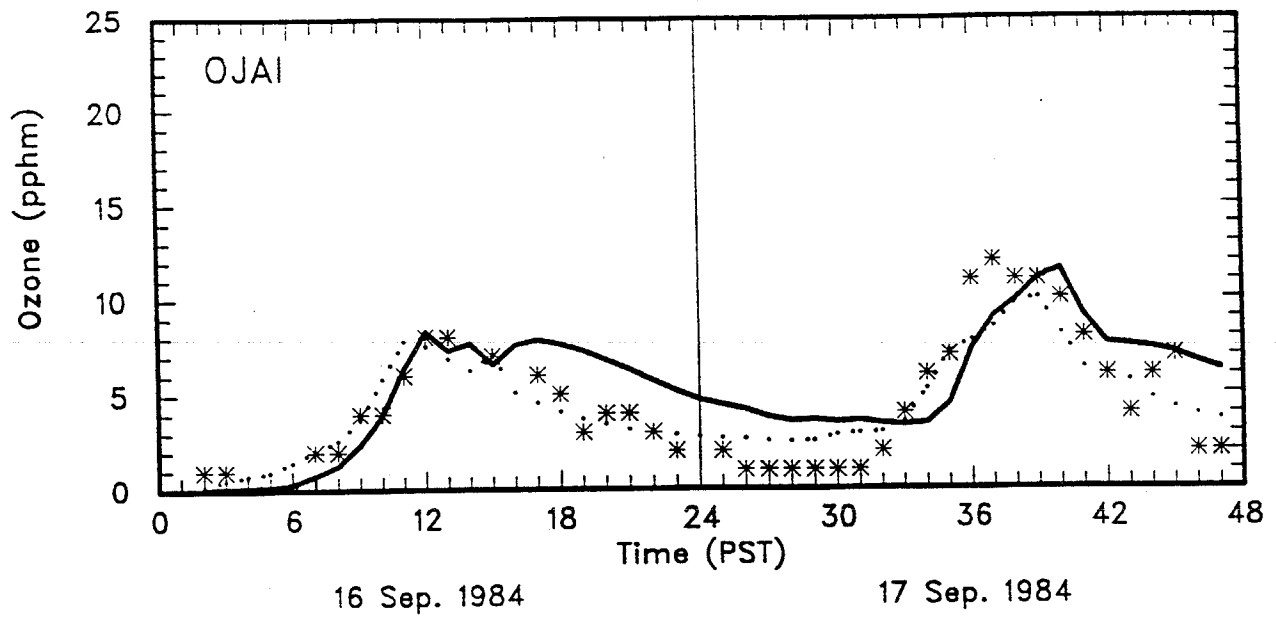


Figure 6-20. Continued.

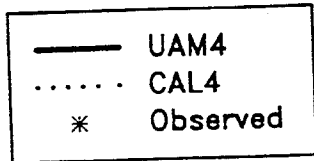
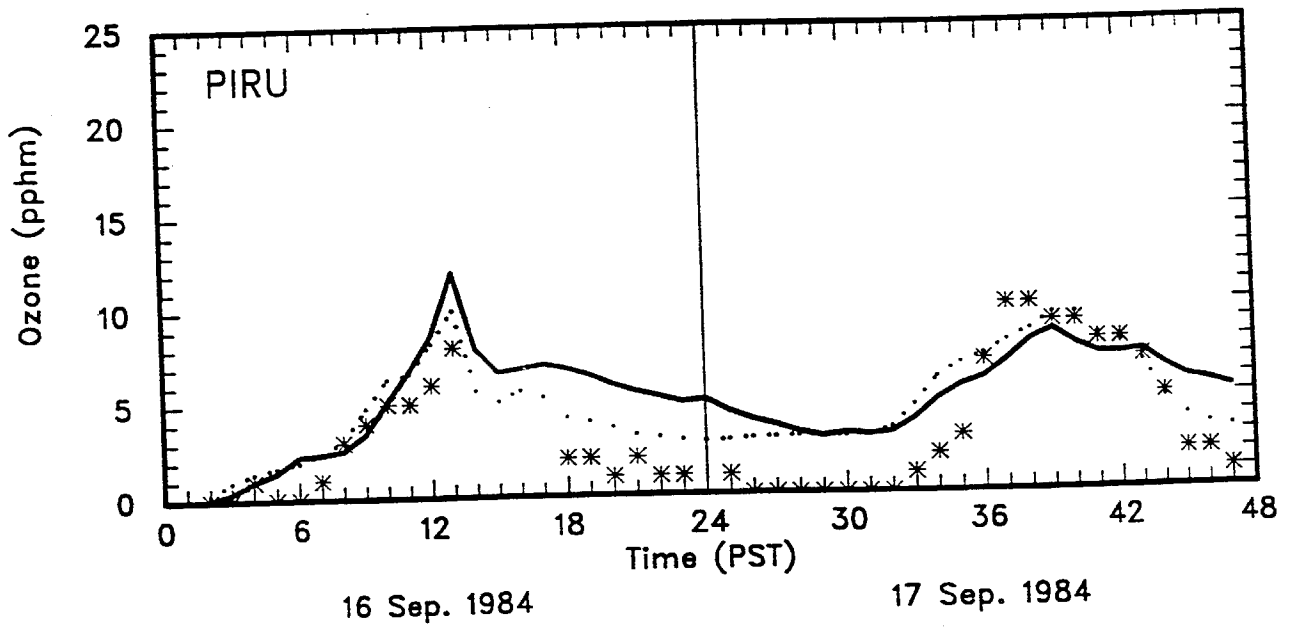
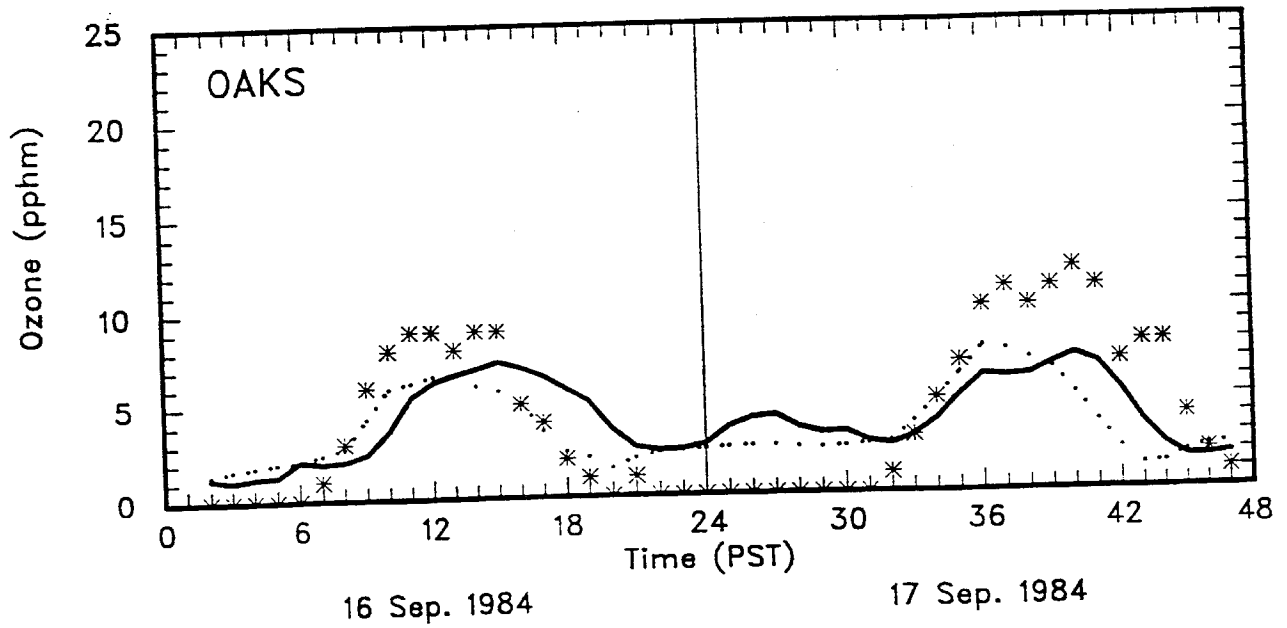


Figure 6-20. Continued.

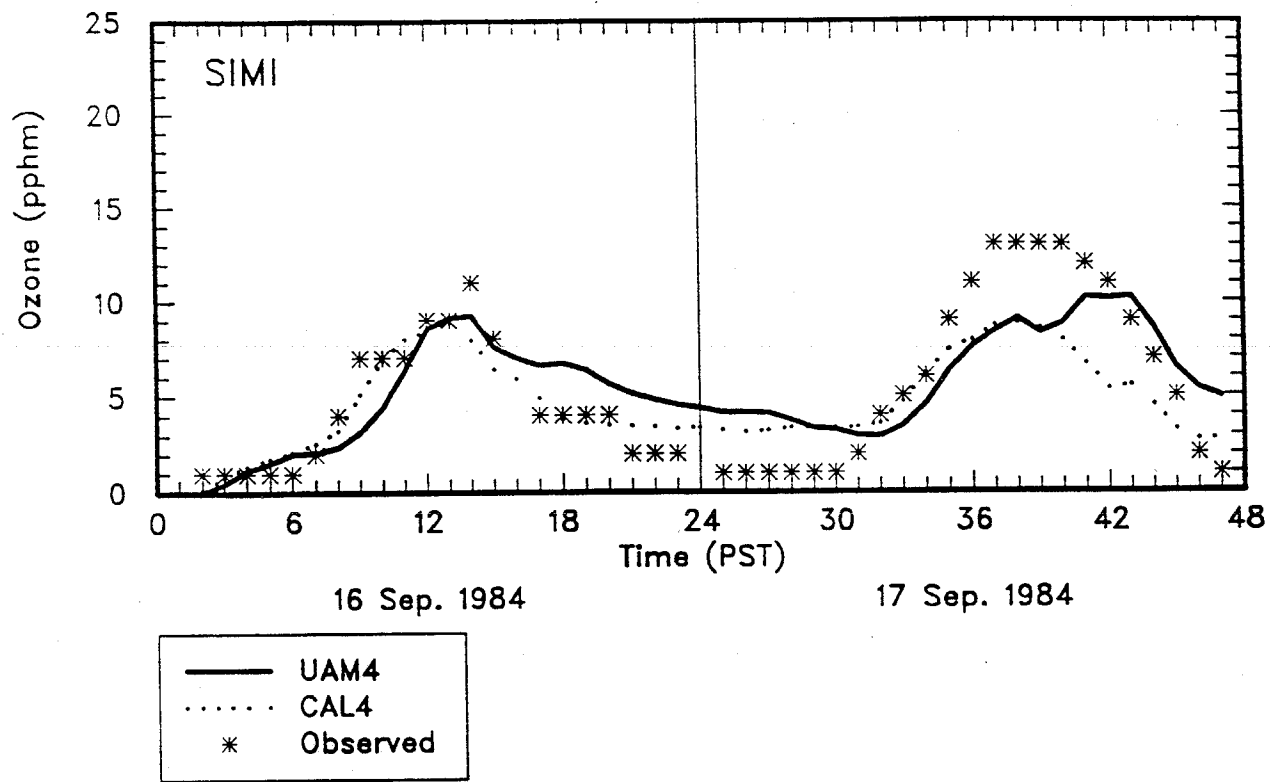


Figure 6-20. Concluded.

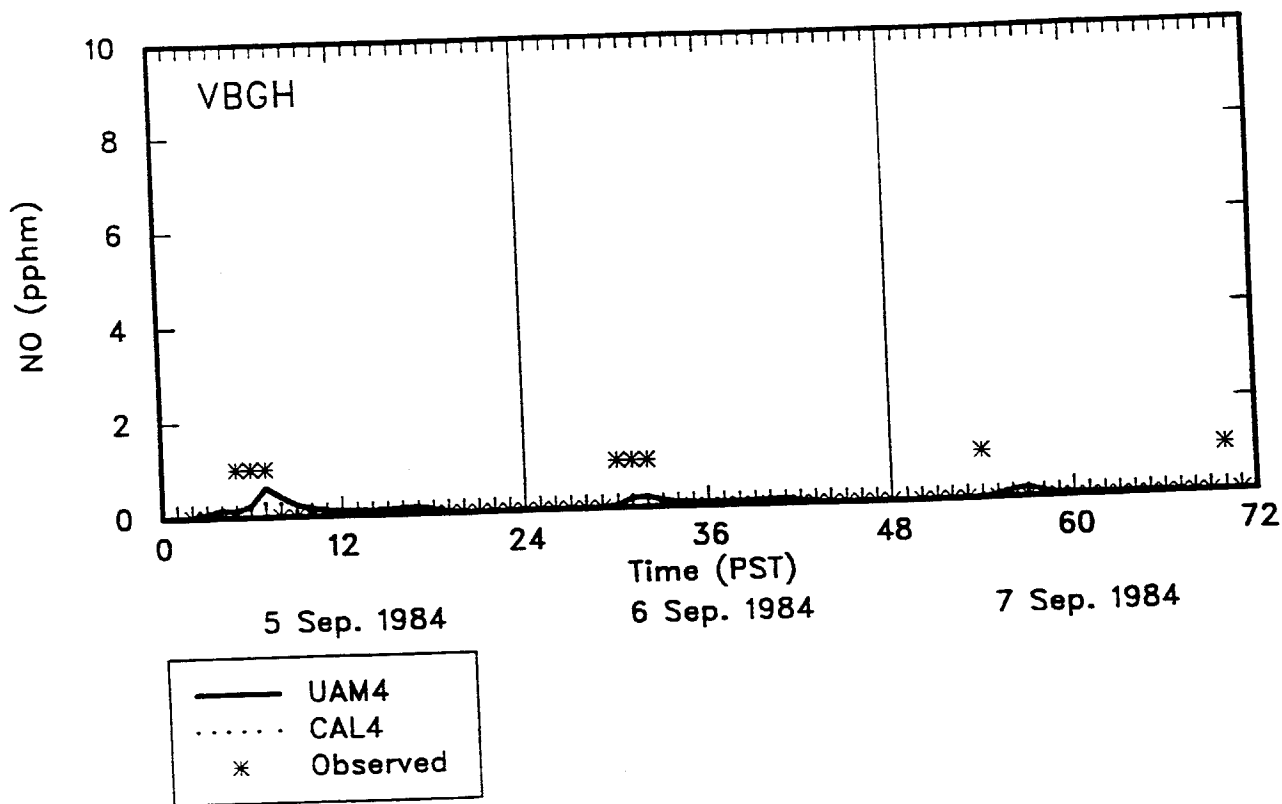
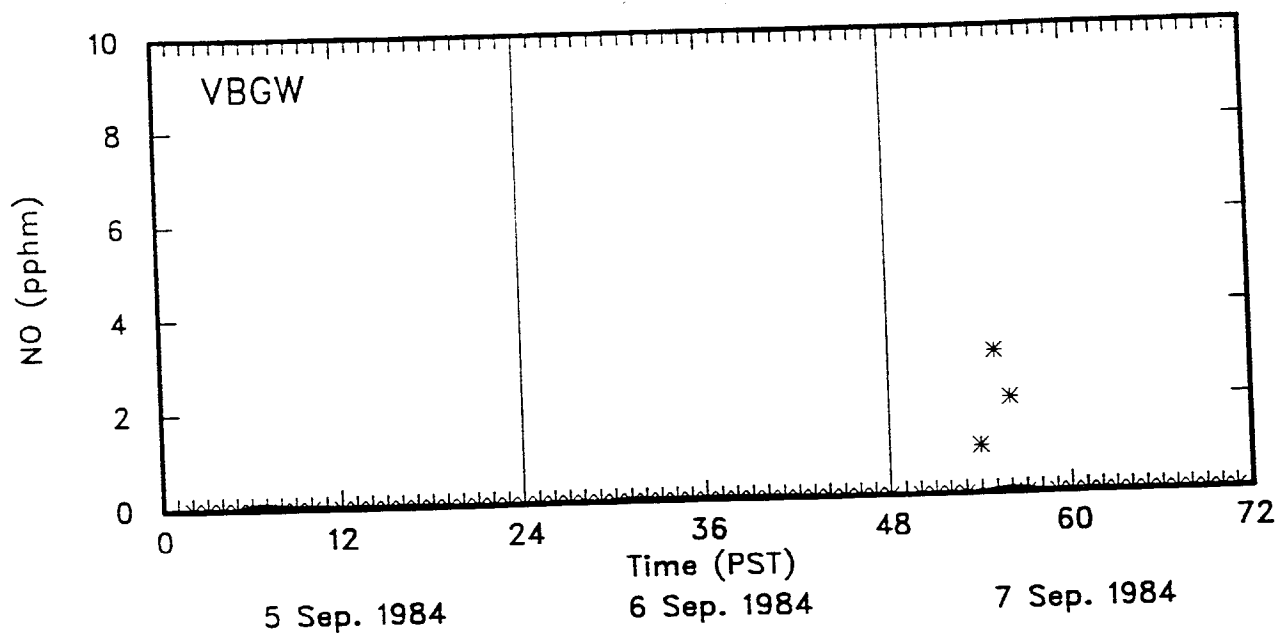


Figure 6-20. Time Series of Hourly Estimated and Observed NO Concentrations for the 16-17 September, 1984 Episode.

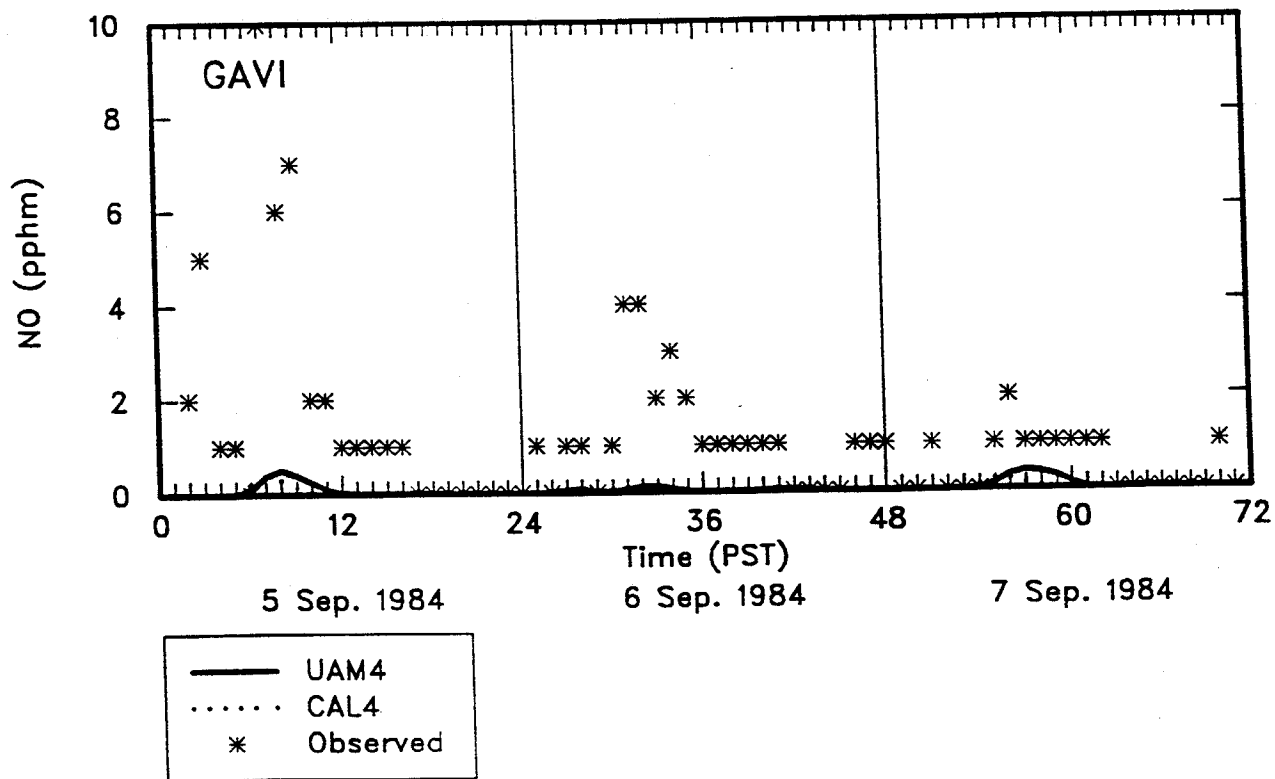
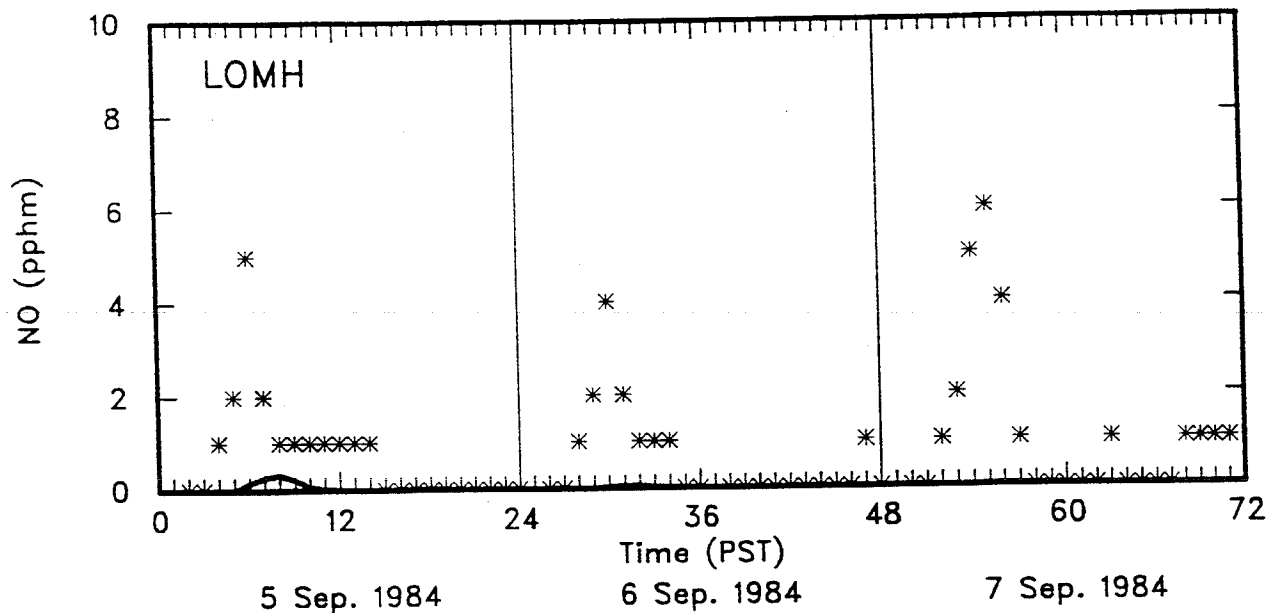


Figure 6-20. Continued.

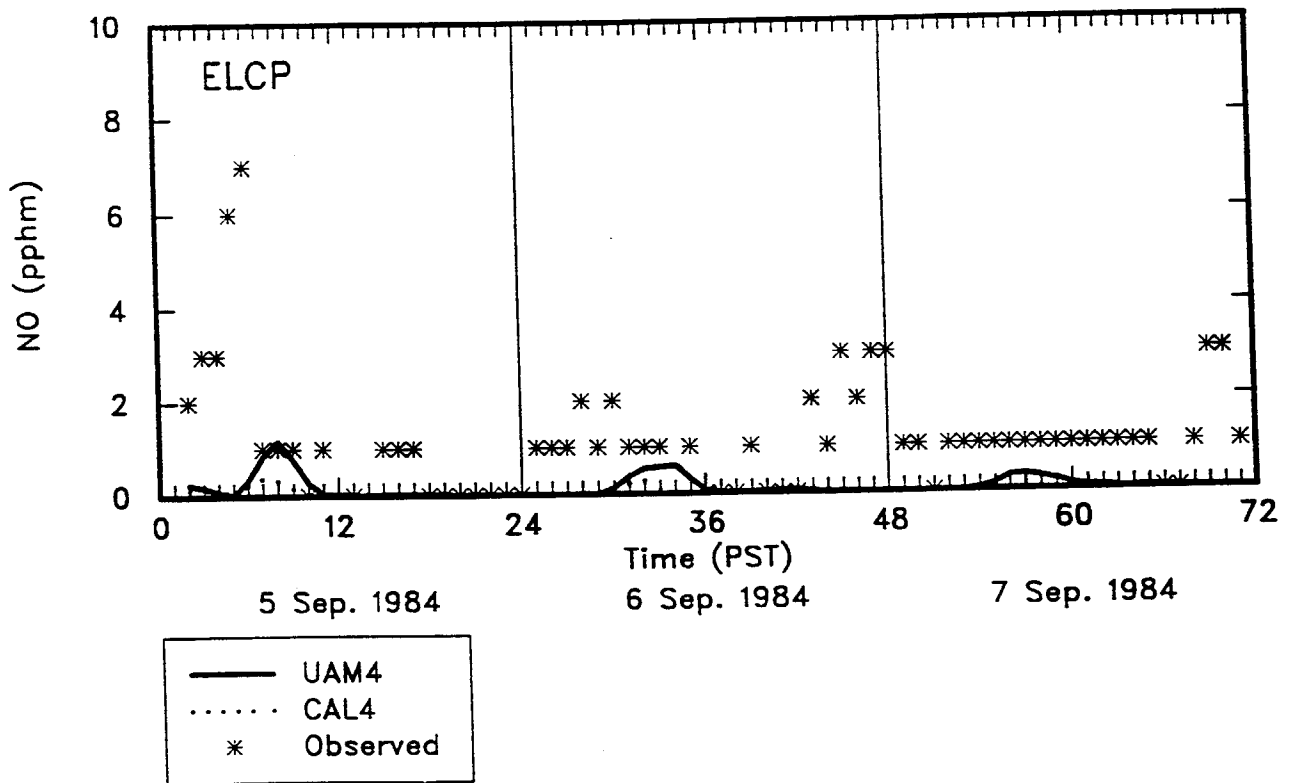
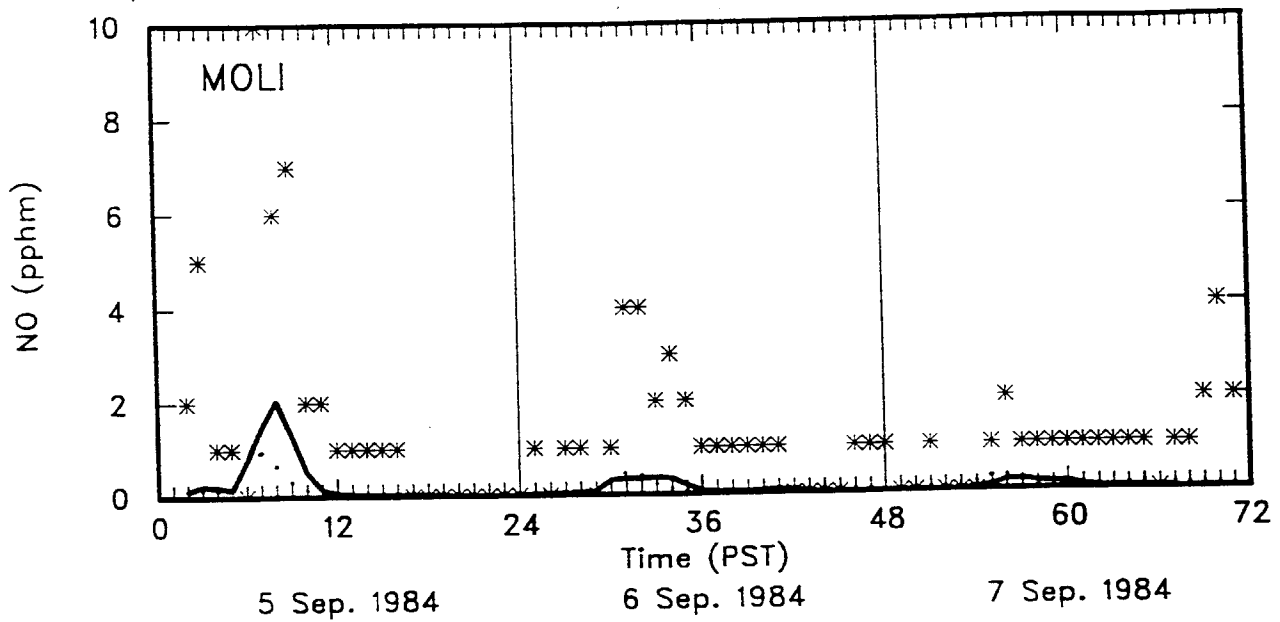


Figure 6-20. Continued.

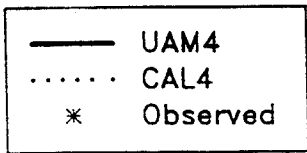
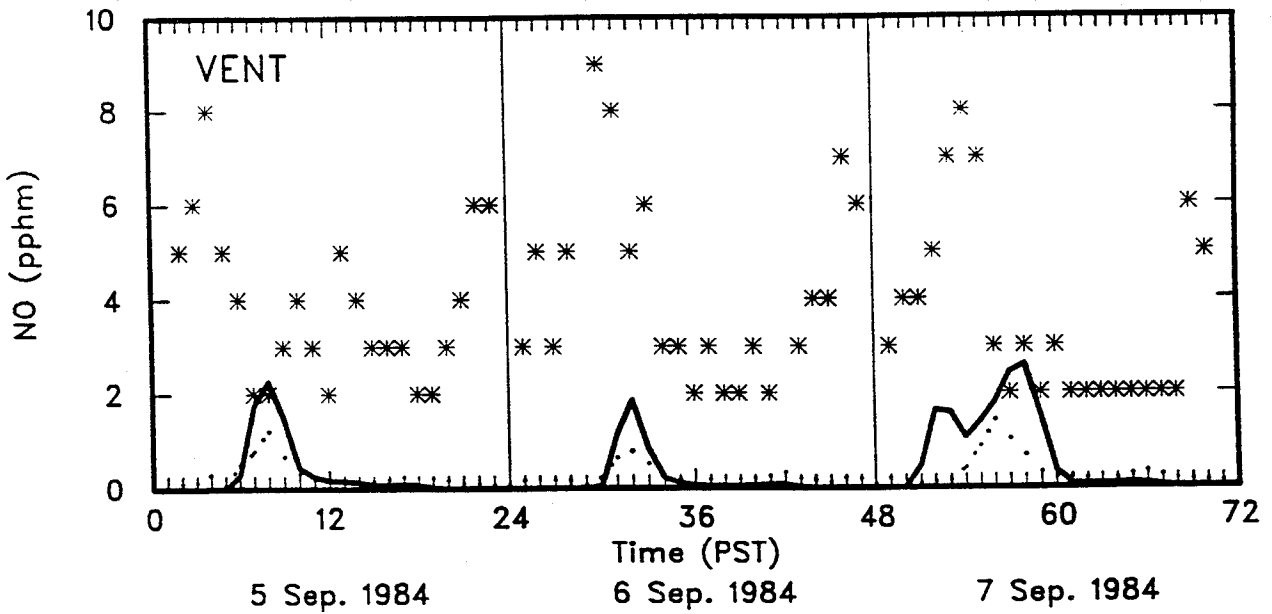
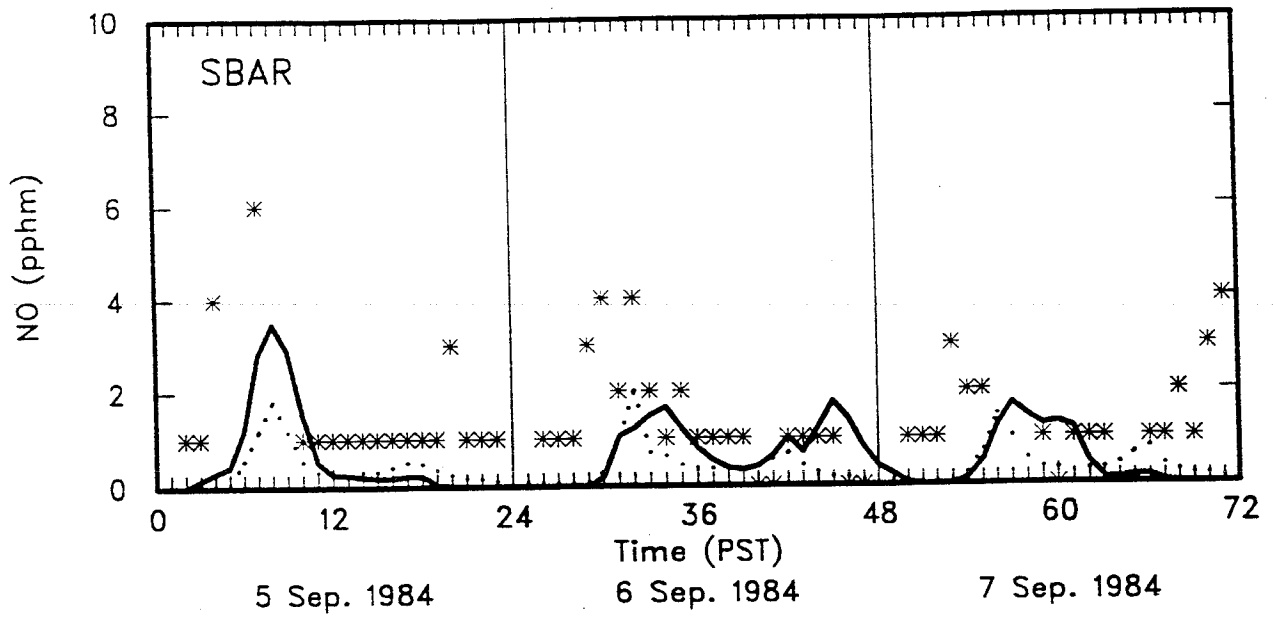


Figure 6-20. Continued.

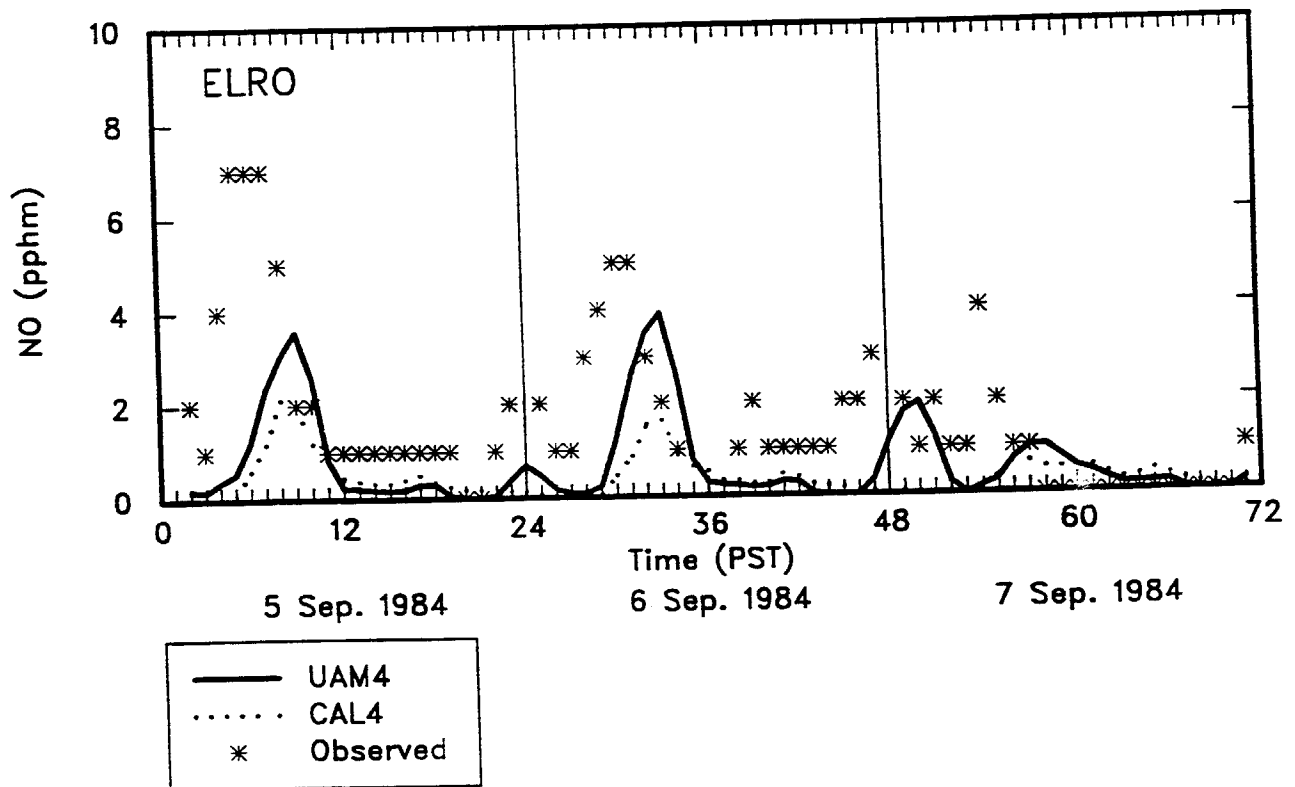
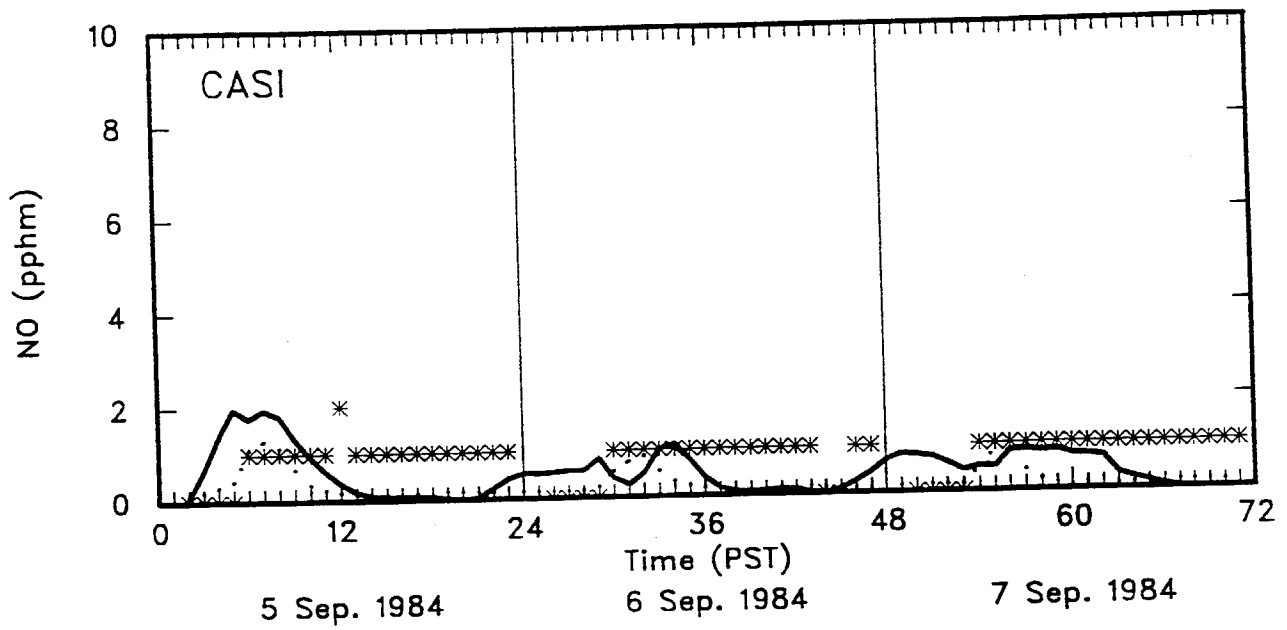


Figure 6-20. Continued.

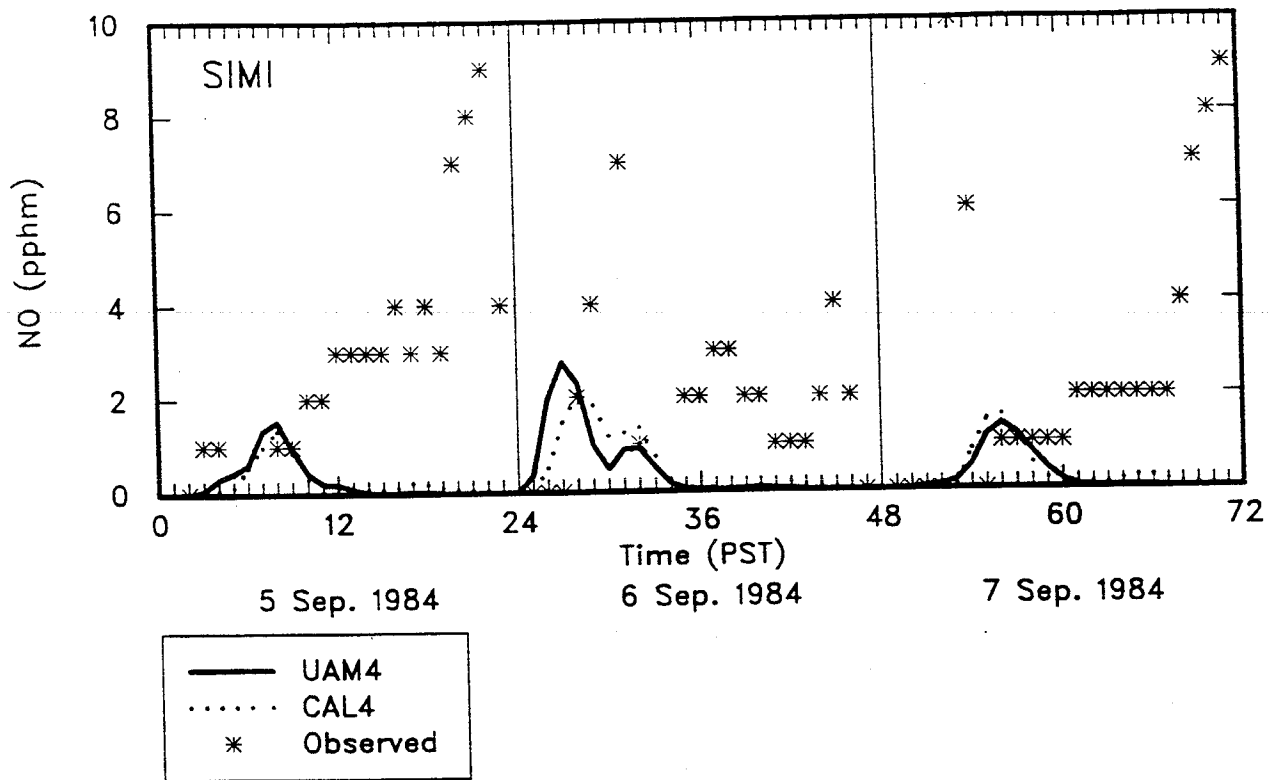
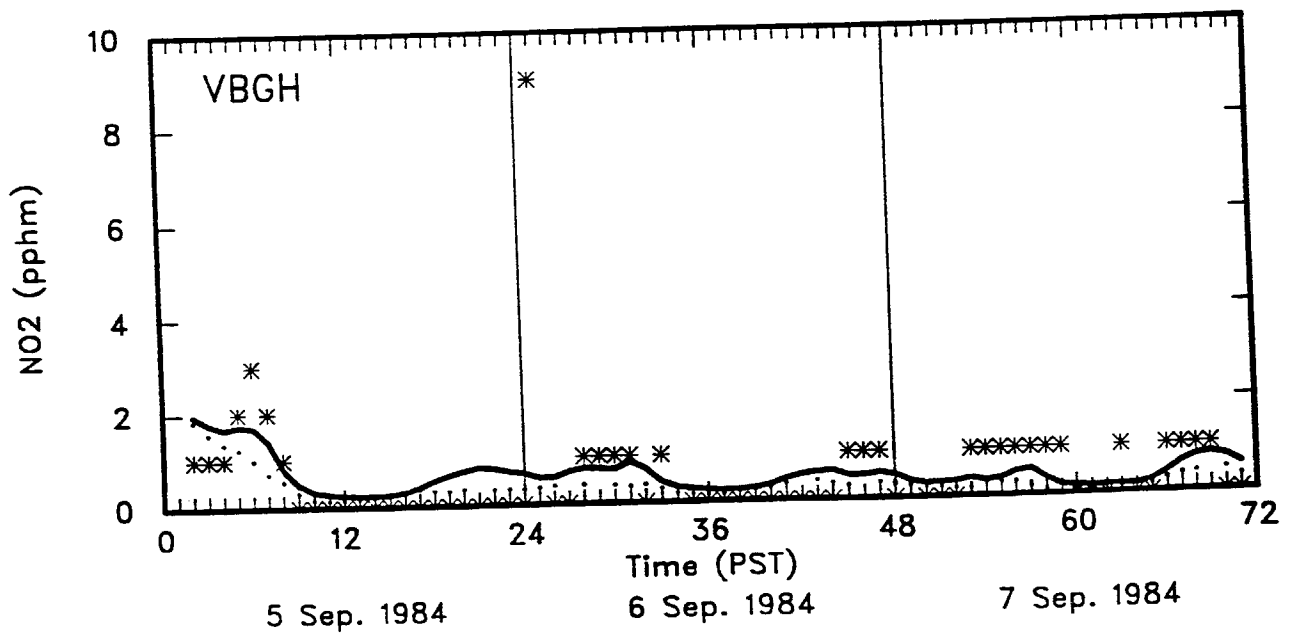
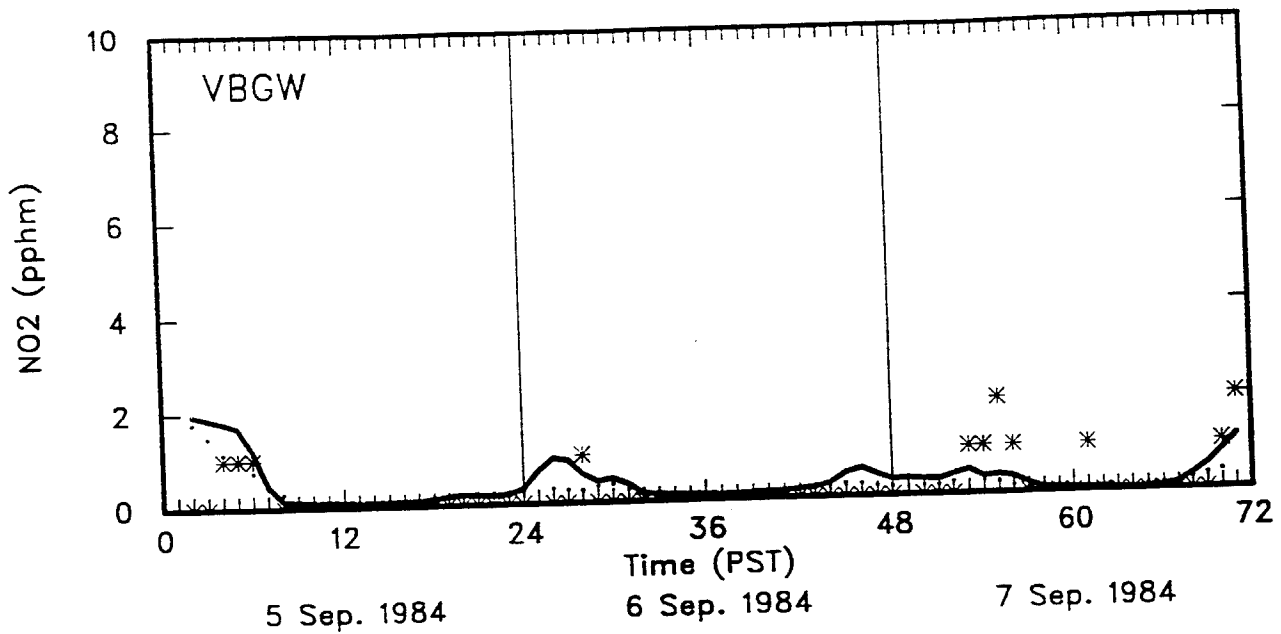


Figure 6-20. Concluded.



—	UAM4
.....	CAL4
*	Observed

Figure 6-20. Time Series of Hourly Estimated and Observed NO<sub>2</sub> Concentrations for the 16-17 September, 1984 Episode.

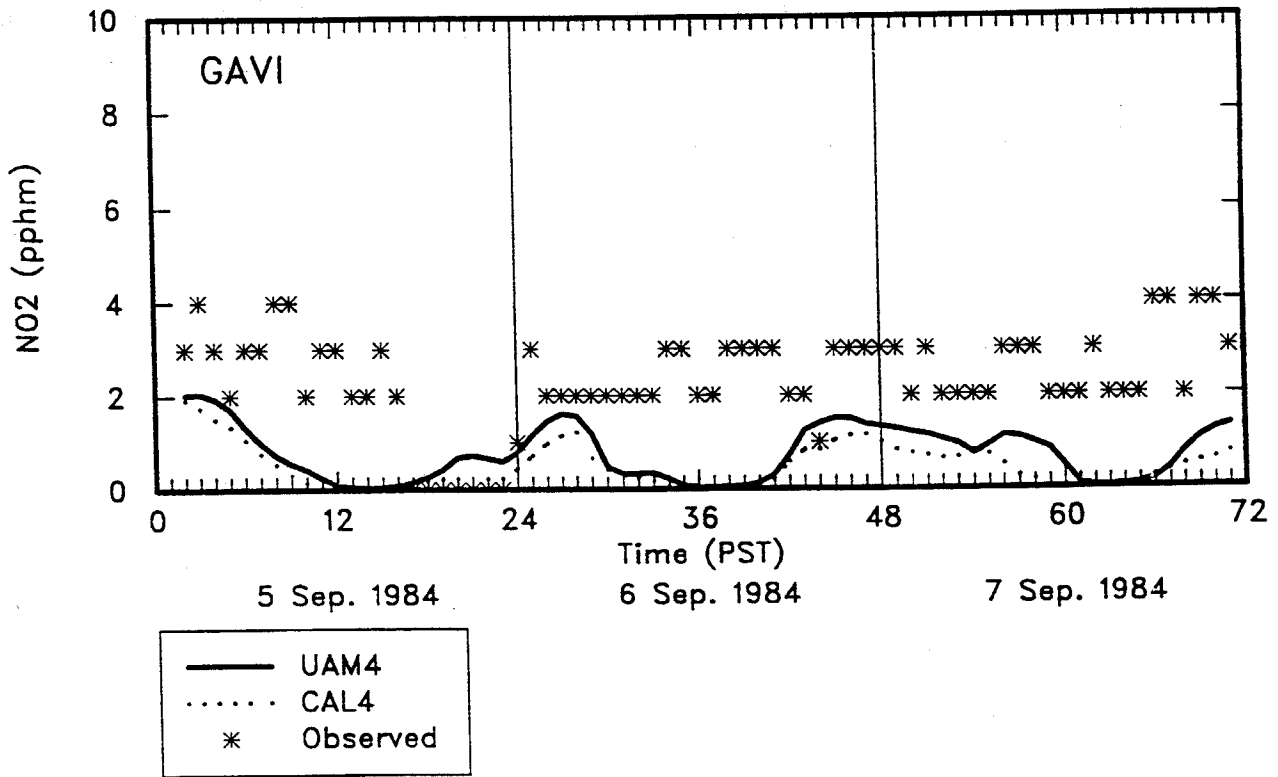
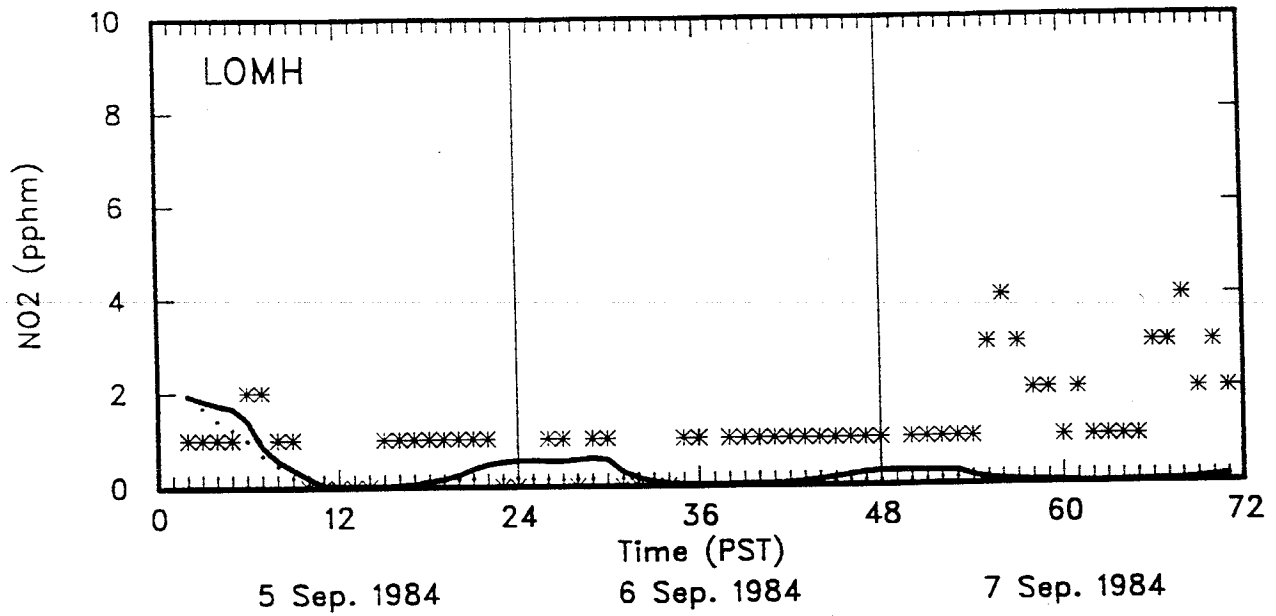


Figure 6-20. Continued.

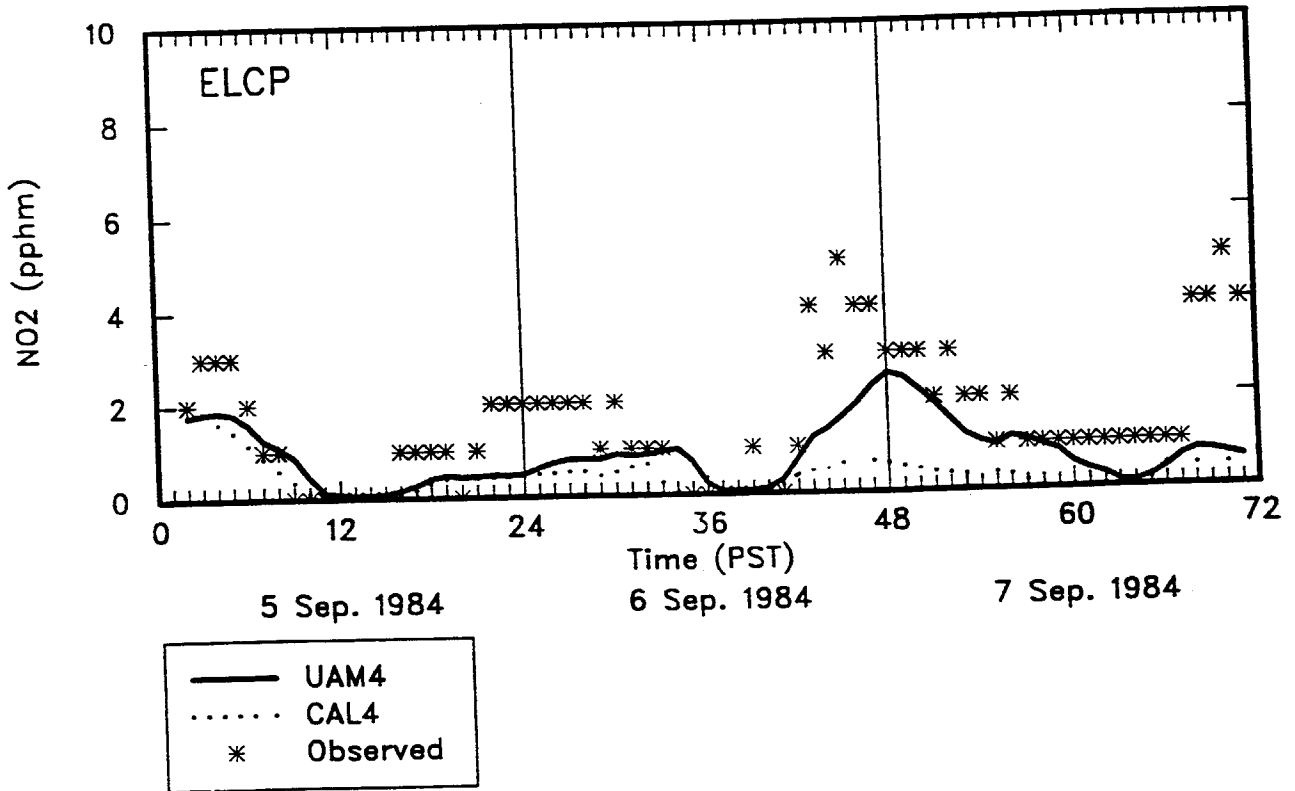
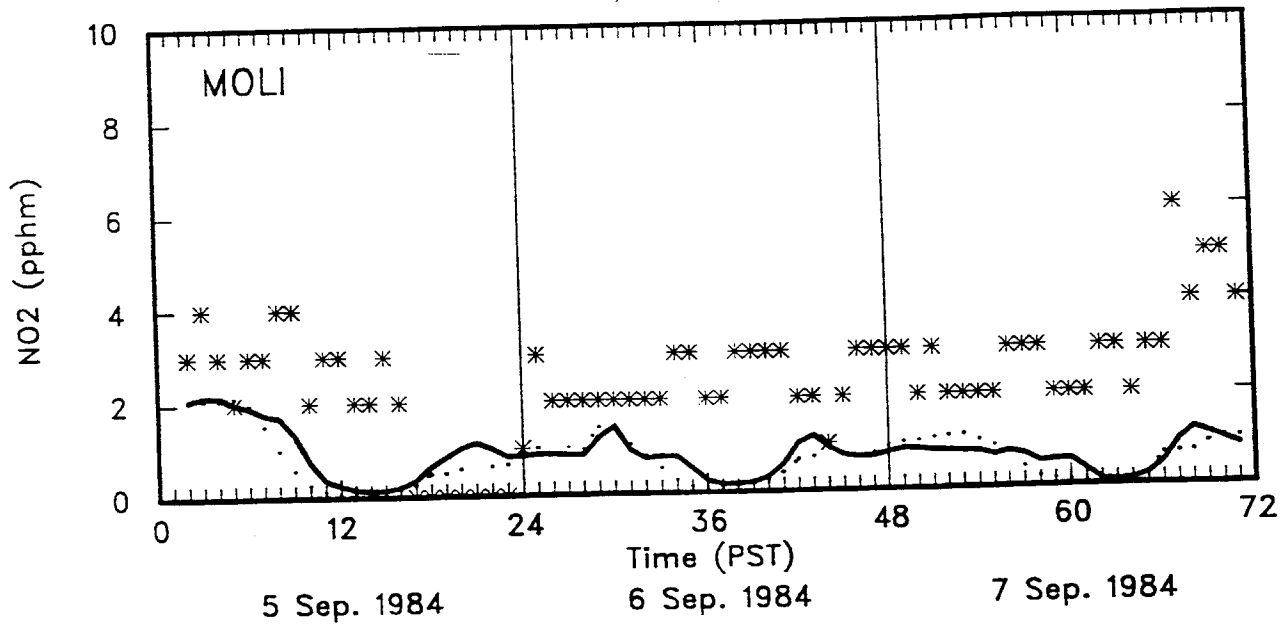


Figure 6-20. Continued.

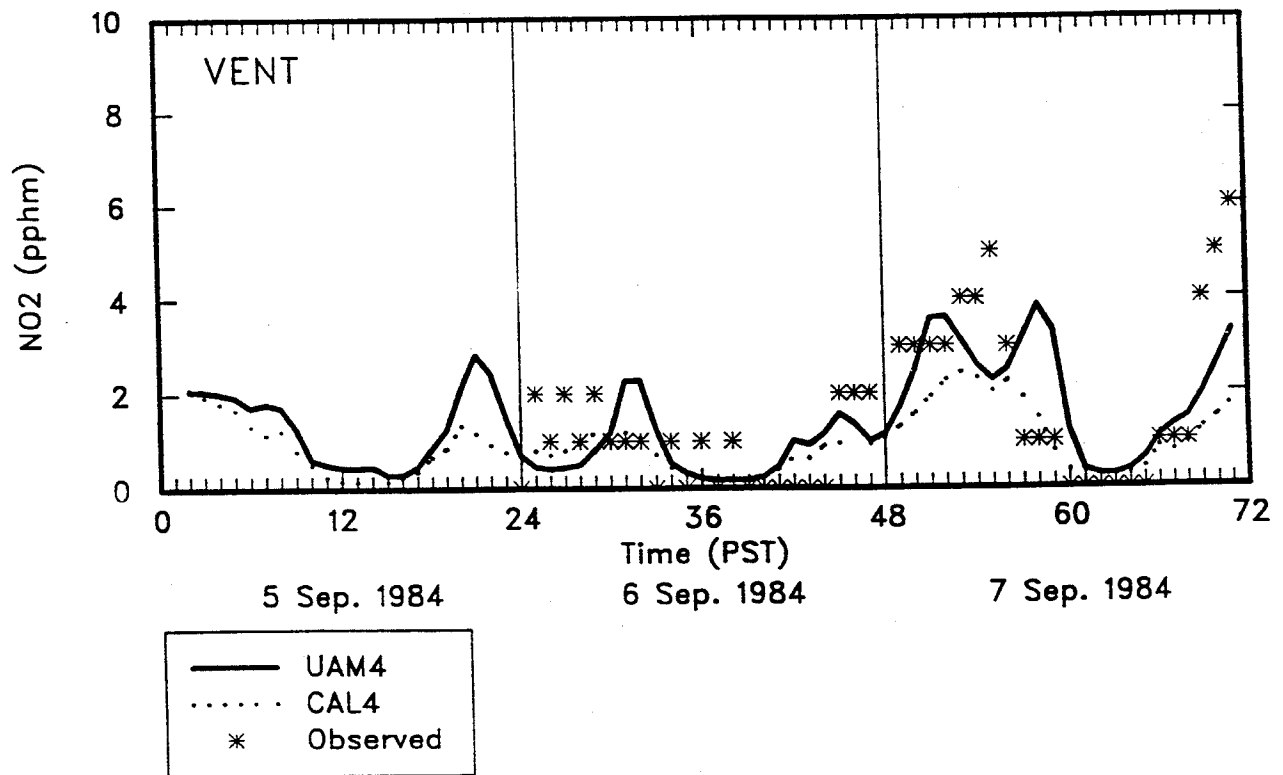
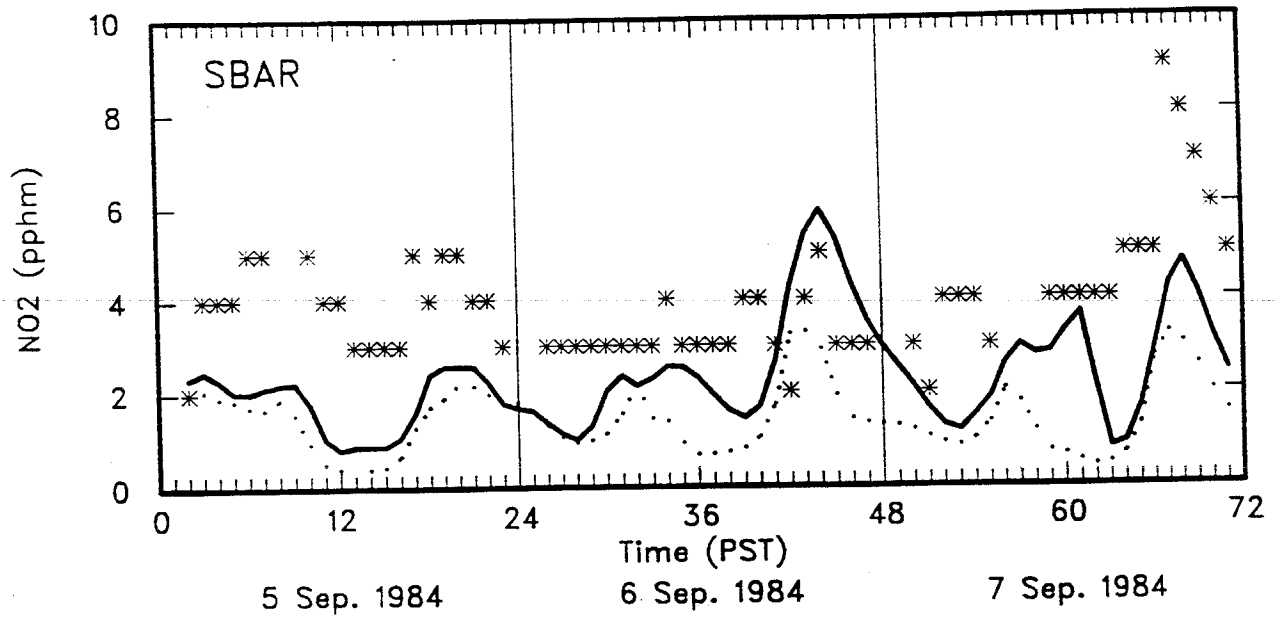


Figure 6-20. Continued.

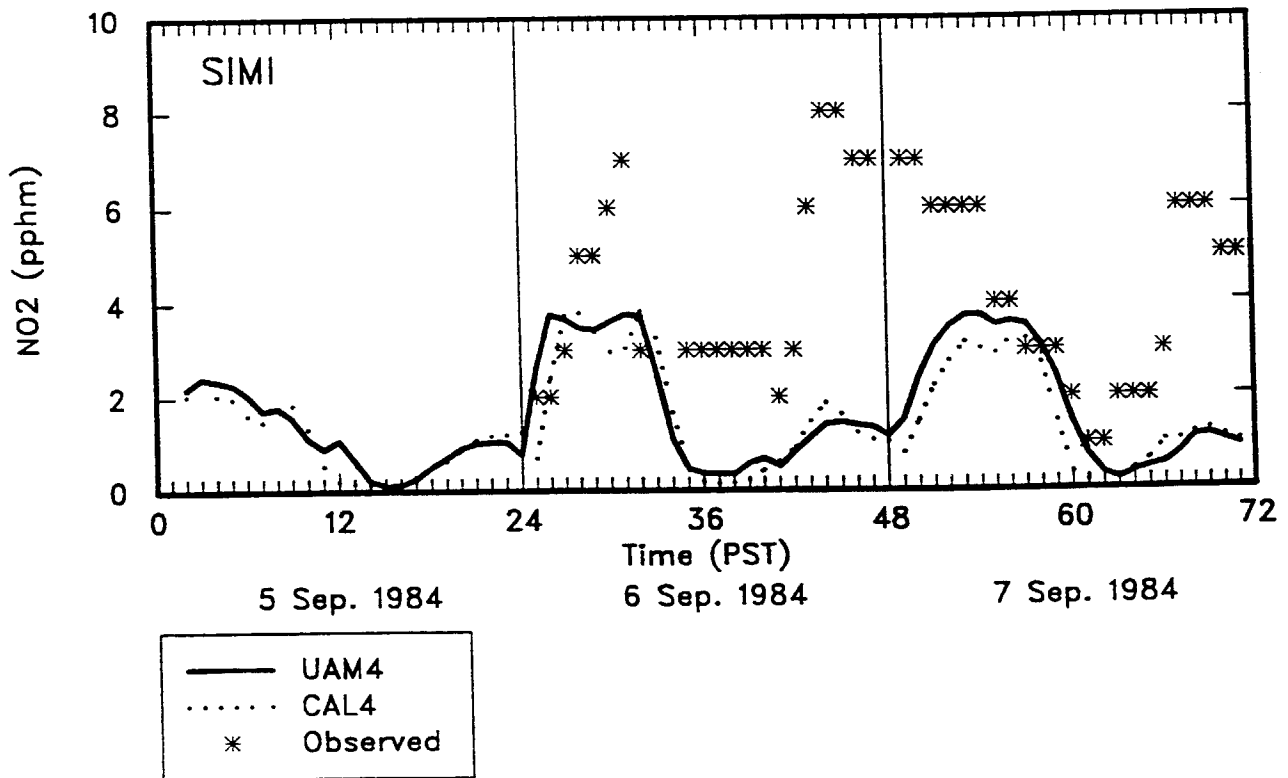
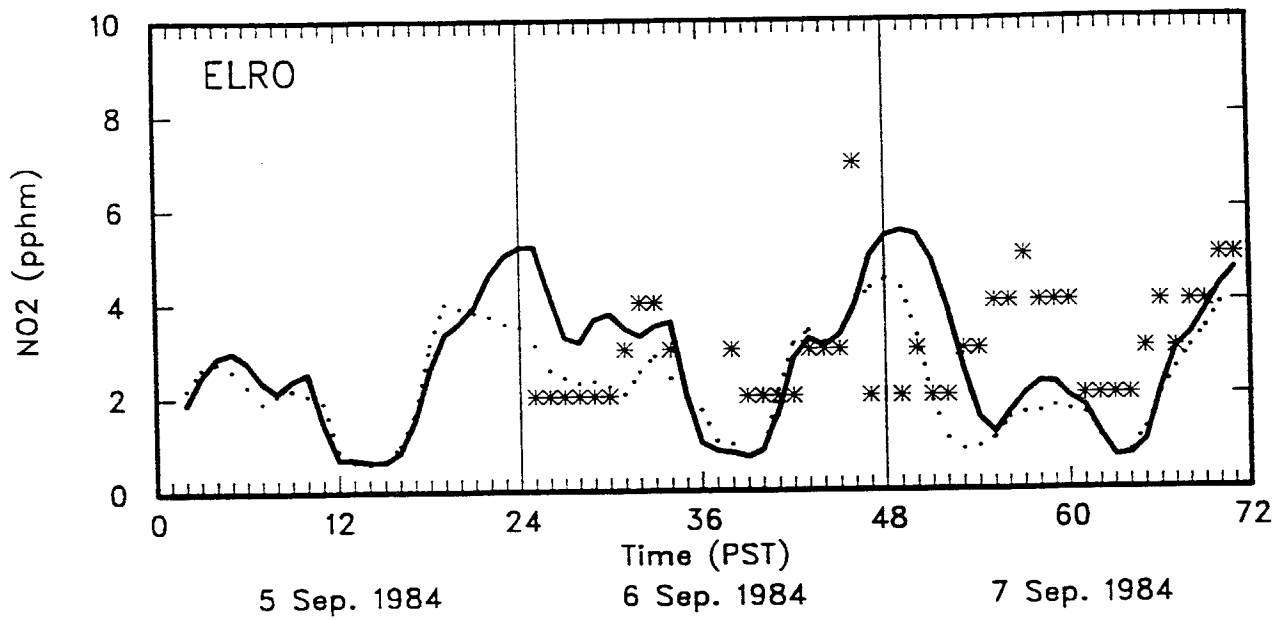
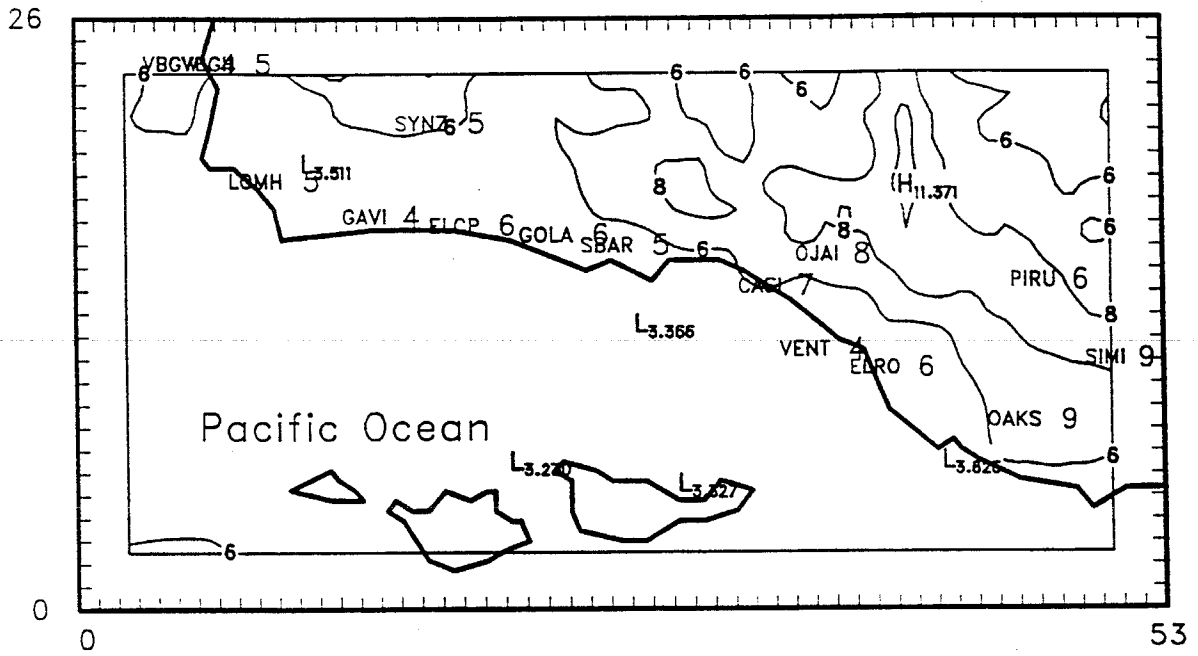


Figure 6-20. Concluded.

CALGRID-IV



UAM-IV

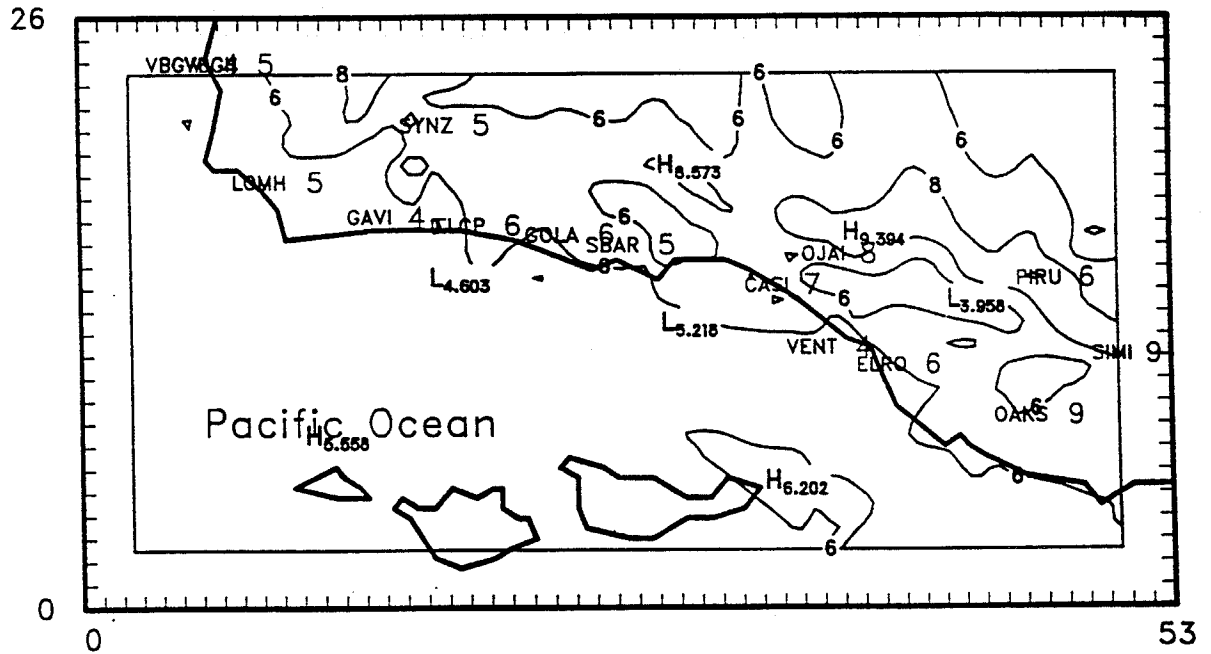
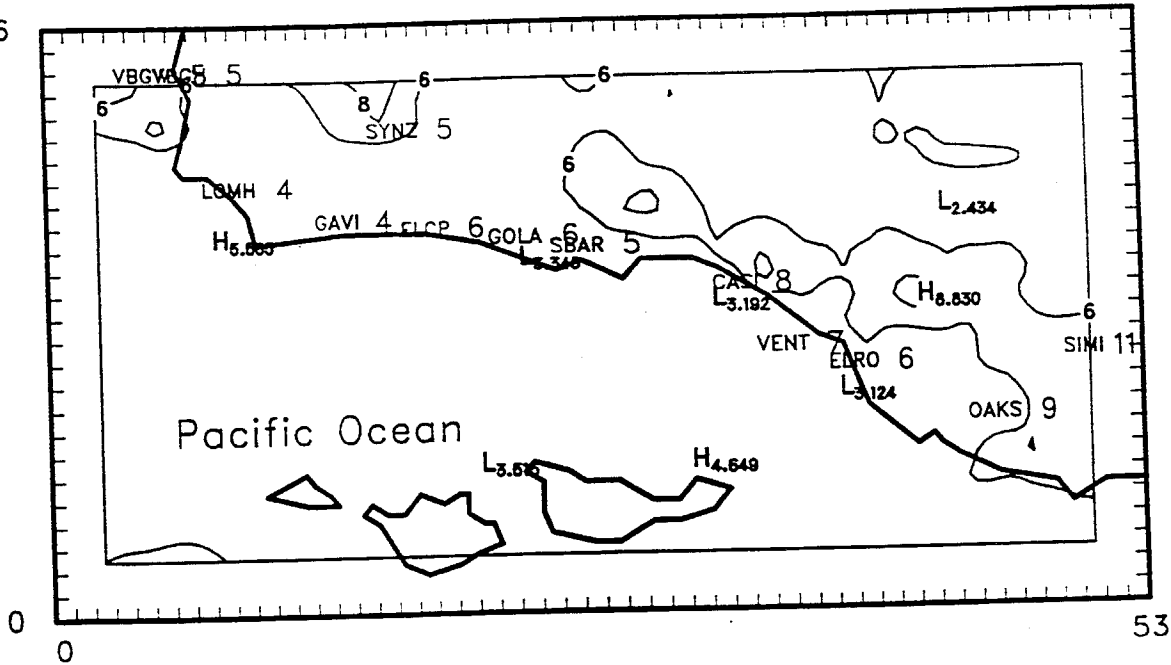


Figure 6-21a. Ground Level Ozone Isopleths of Hourly Ozone Concentrations for the 16-17 September, 1984 Episode -- 16 September, 1200 PST.

26



26

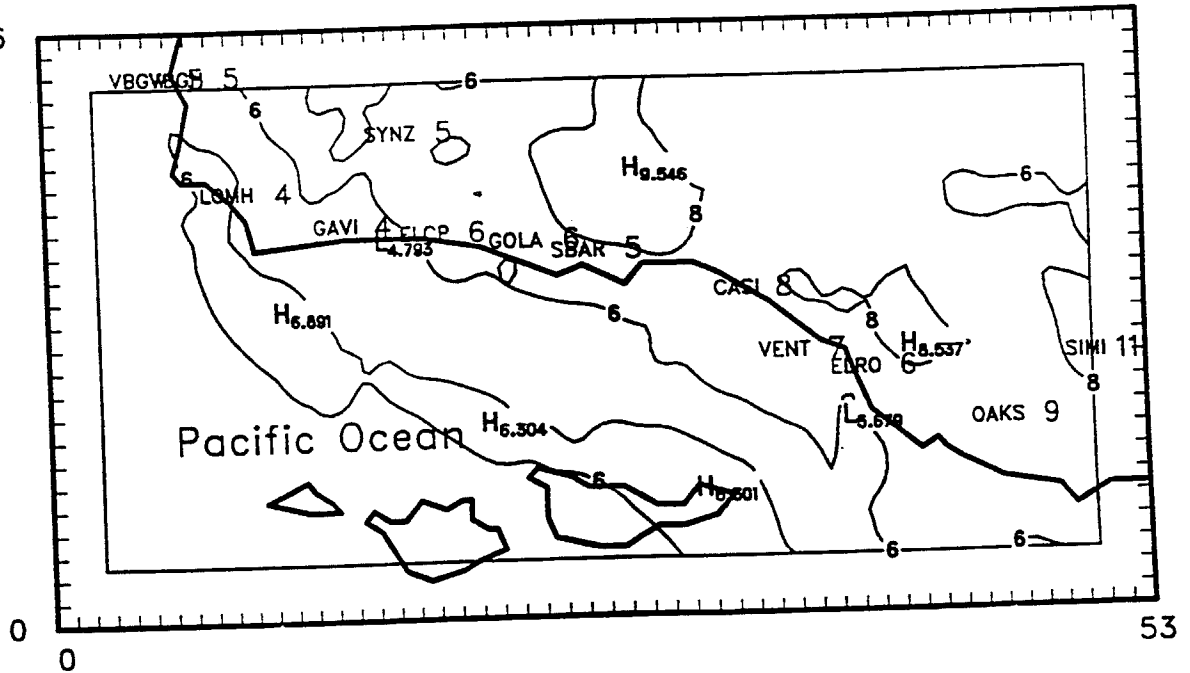
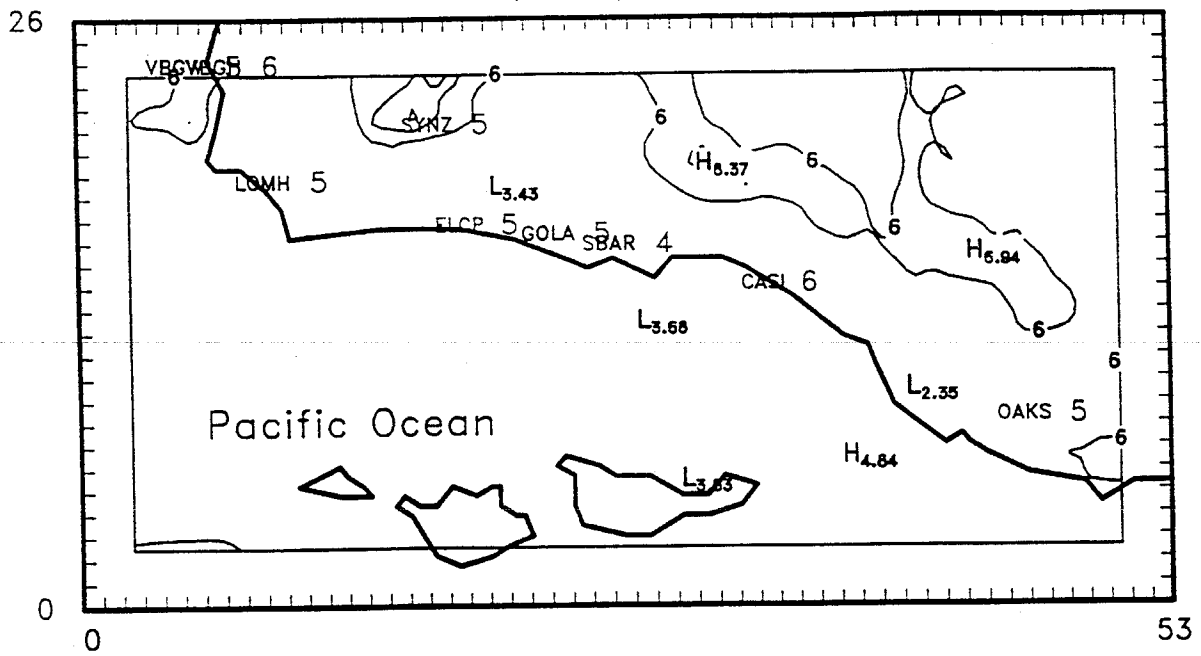


Figure 6-21b. Ground Level Ozone Isopleths of Hourly Ozone Concentrations for the 16-17 September, 1984 Episode – 16 September, 1400 PST.

CALGRID-IV



UAM-IV

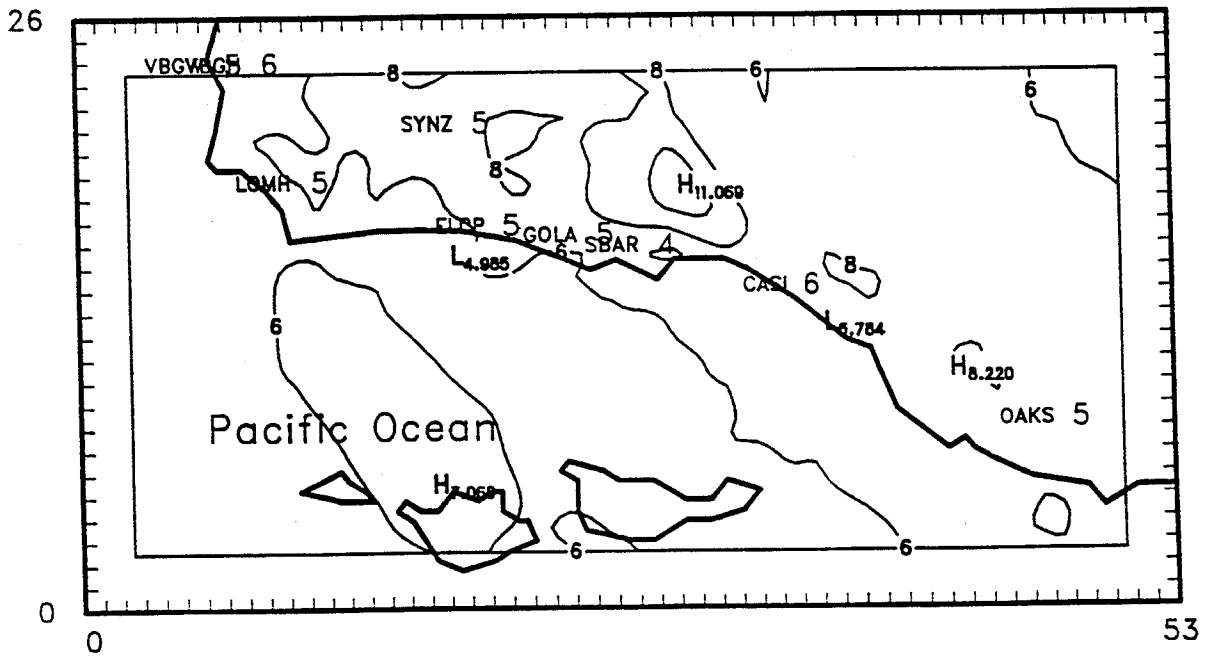
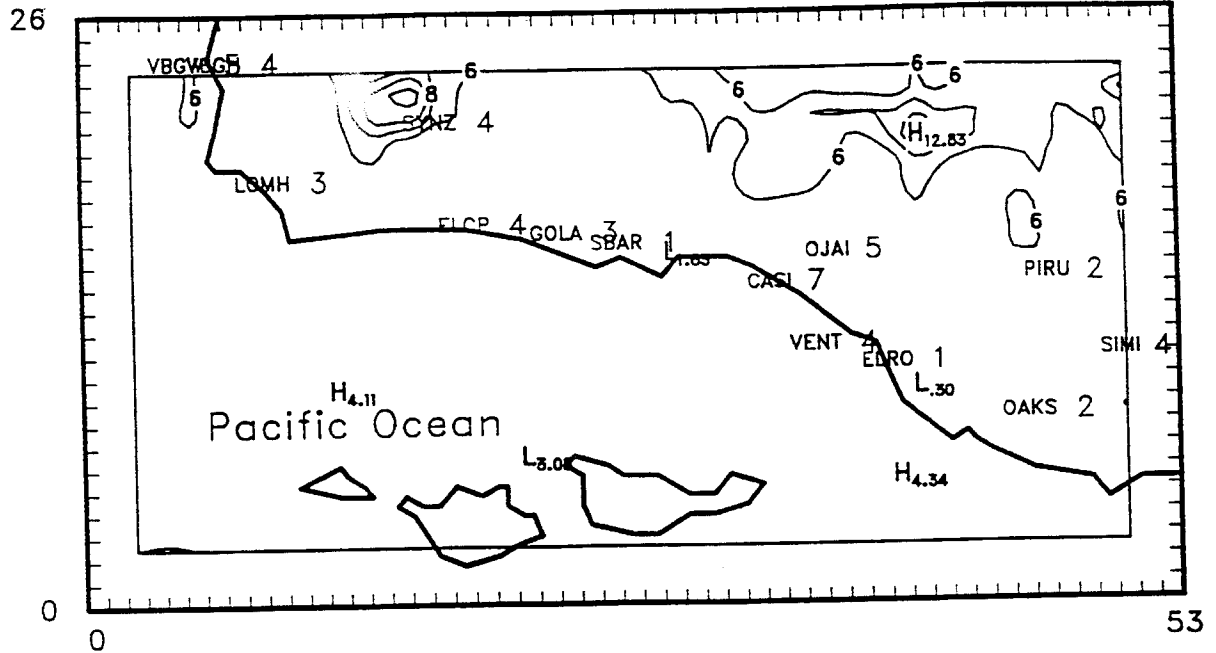


Figure 6-21c. Ground Level Ozone Isopleths of Hourly Ozone Concentrations for the 16-17 September, 1984 Episode – 16 September, 1600 PST.

CALGRID-IV



UAM-IV

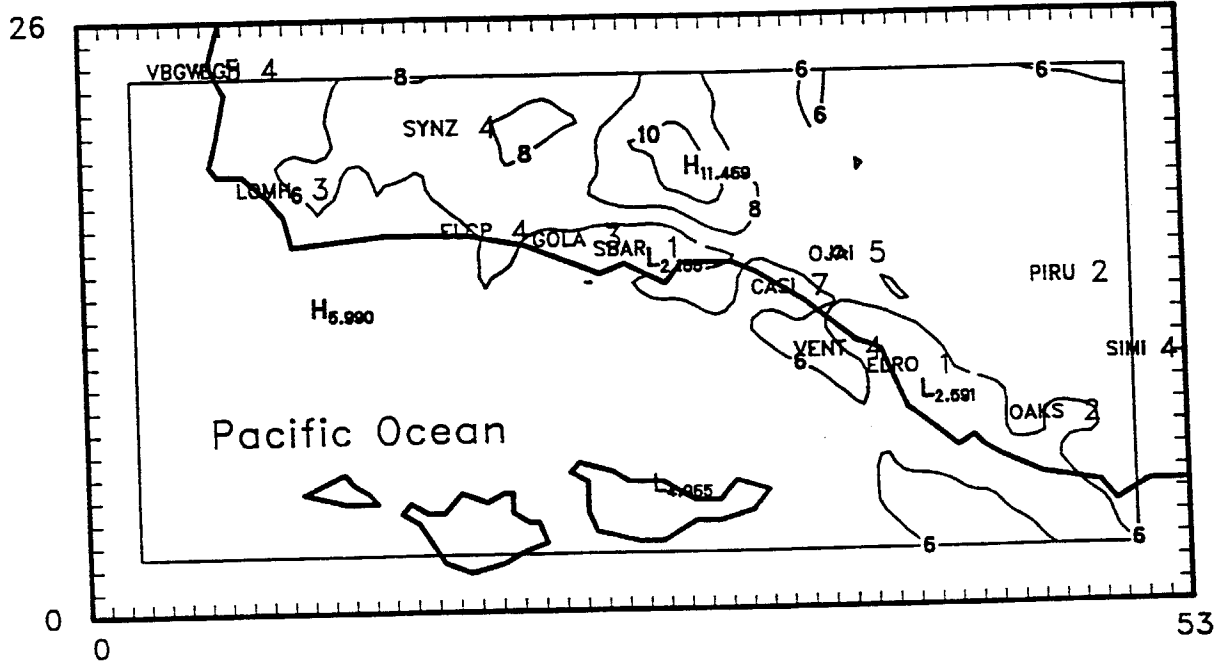
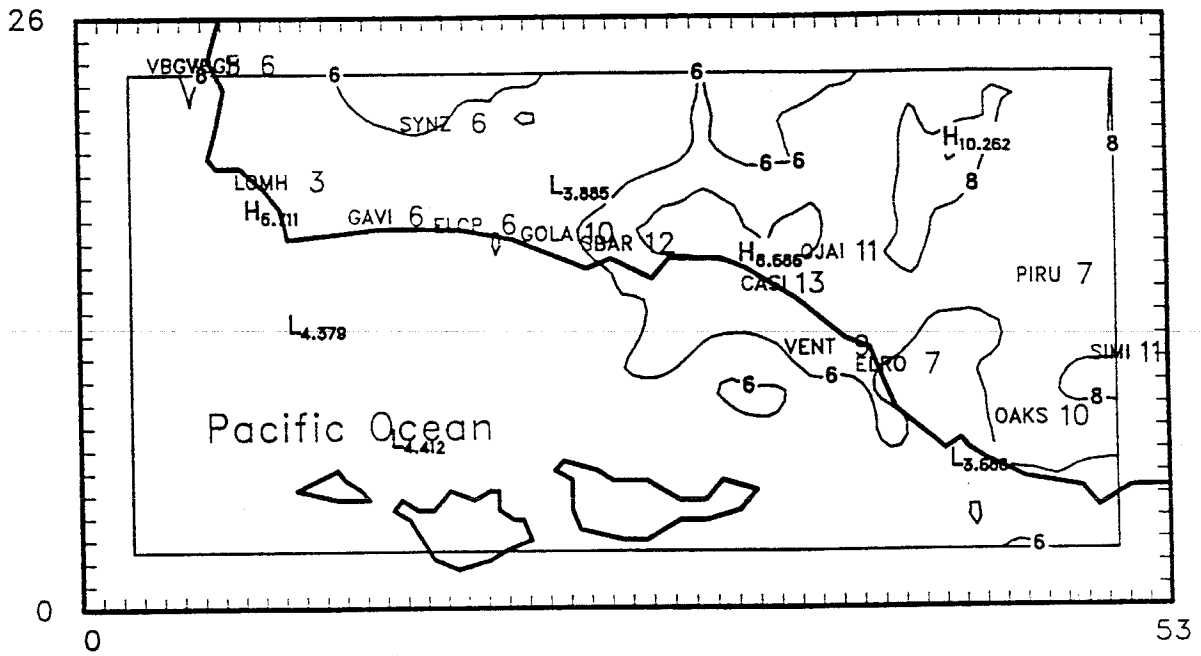


Figure 6-21d. Ground Level Ozone Isopleths of Hourly Ozone Concentrations for the 16-17 September, 1984 Episode – 16 September, 1800 PST.

CALGRID-IV



UAM-IV

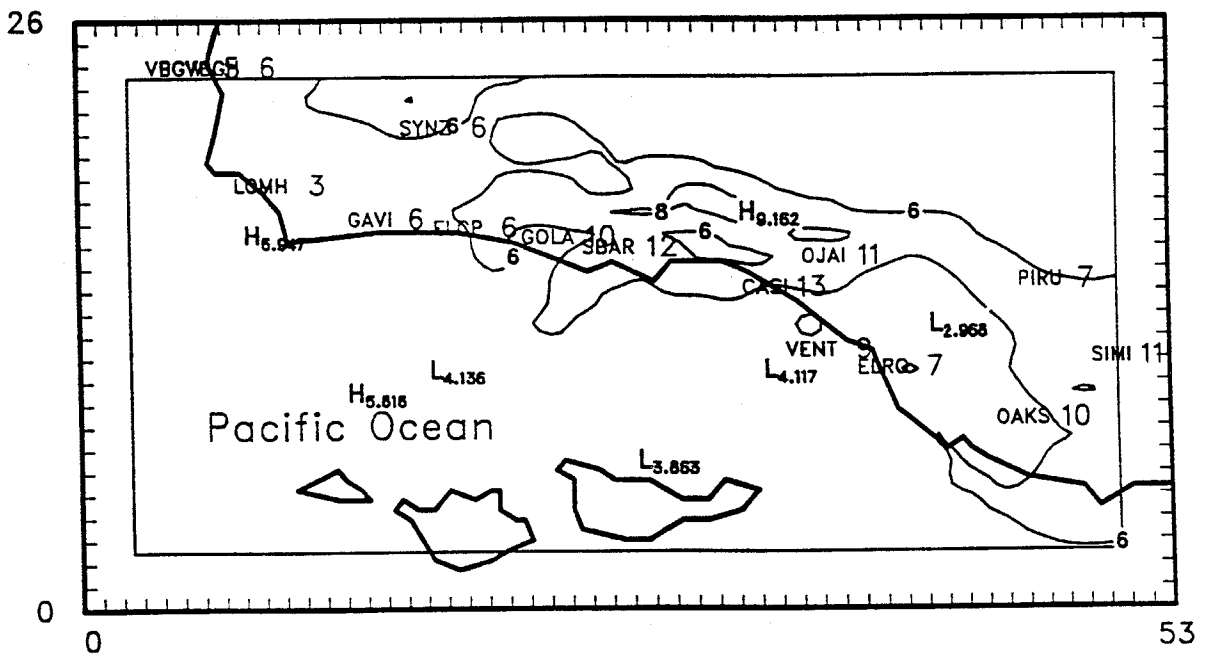


Figure 6-21e. Ground Level Ozone Isopleths of Hourly Ozone Concentrations for the 16-17 September, 1984 Episode – 17 September, 1200 PST.

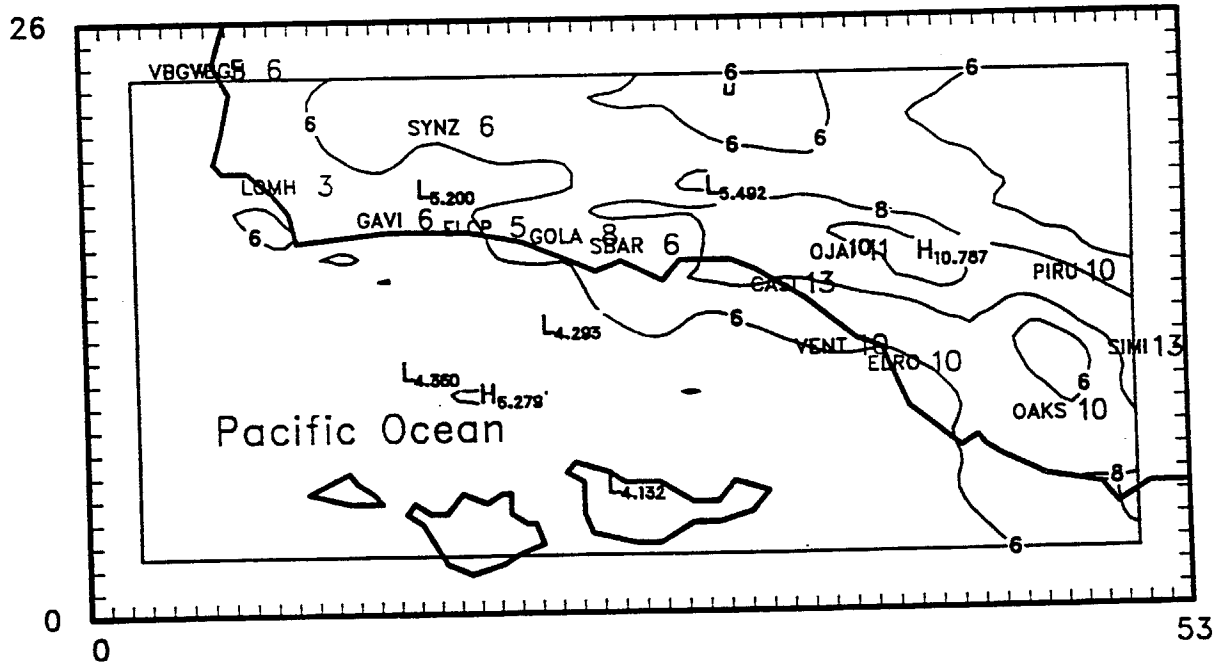
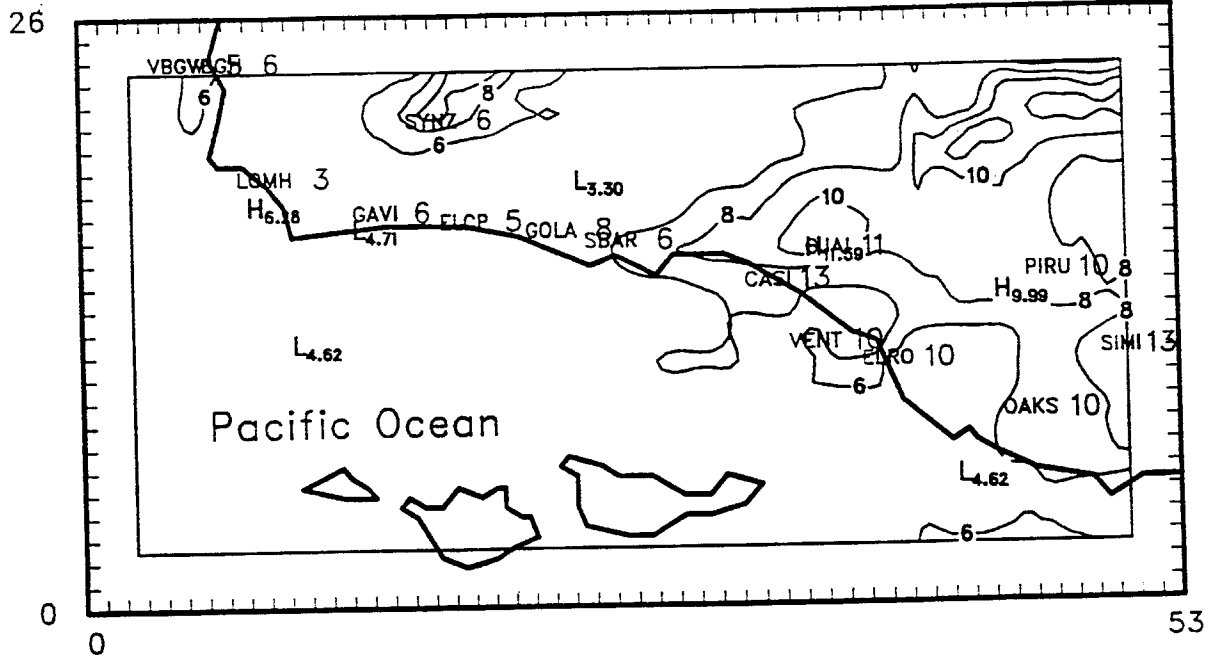
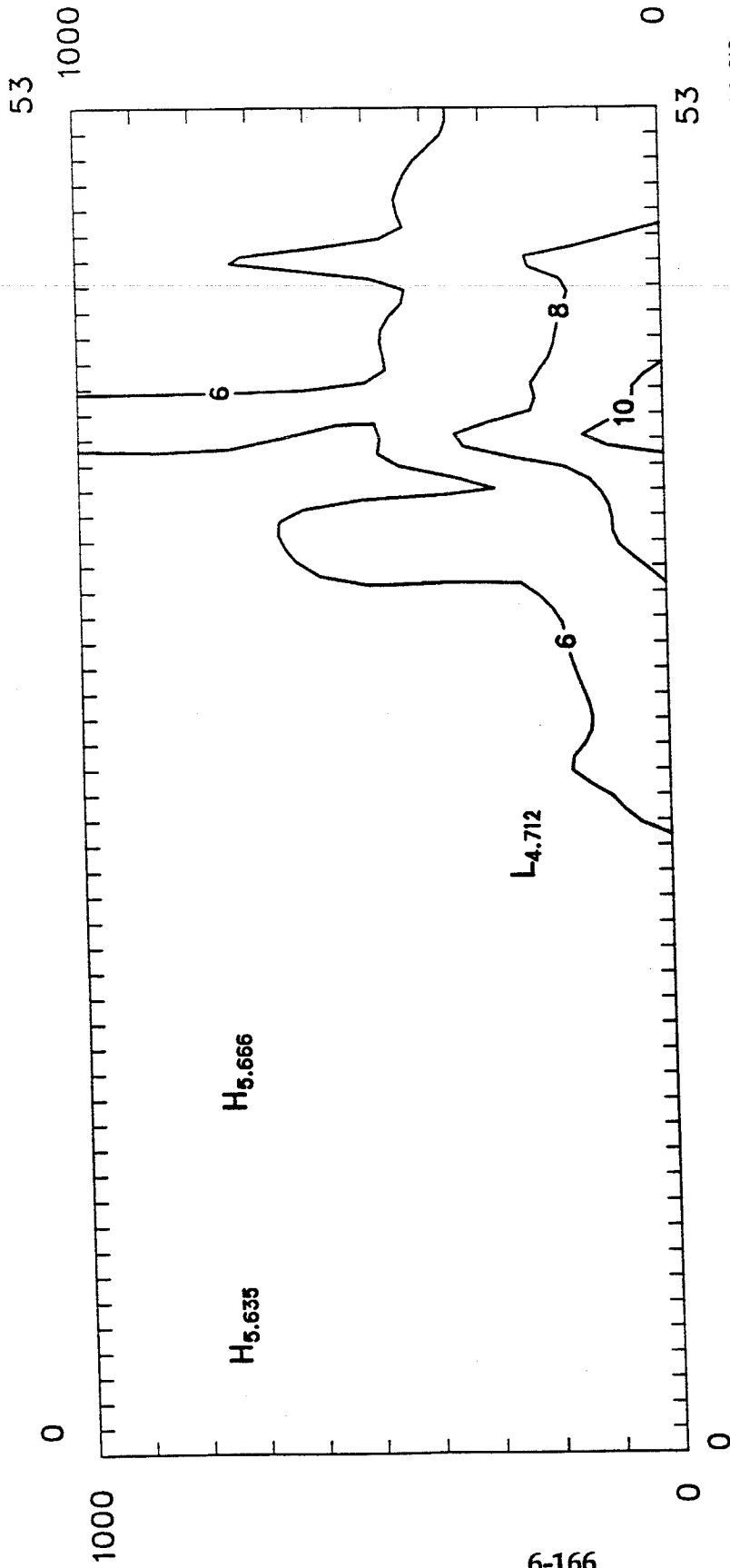


Figure 6-21f. Ground Level Ozone Isopleths of Hourly Ozone Concentrations for the 16-17 September, 1984 Episode - 17 September, 1400 PST.



E-W Slice J = 15 Hour 14 (pst)

Date 9/17/84

O3 140084261AIR001  
CCHT140084261AIR001

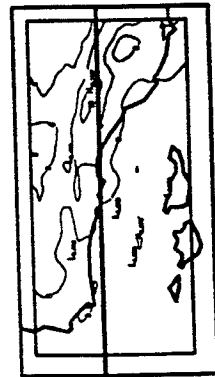
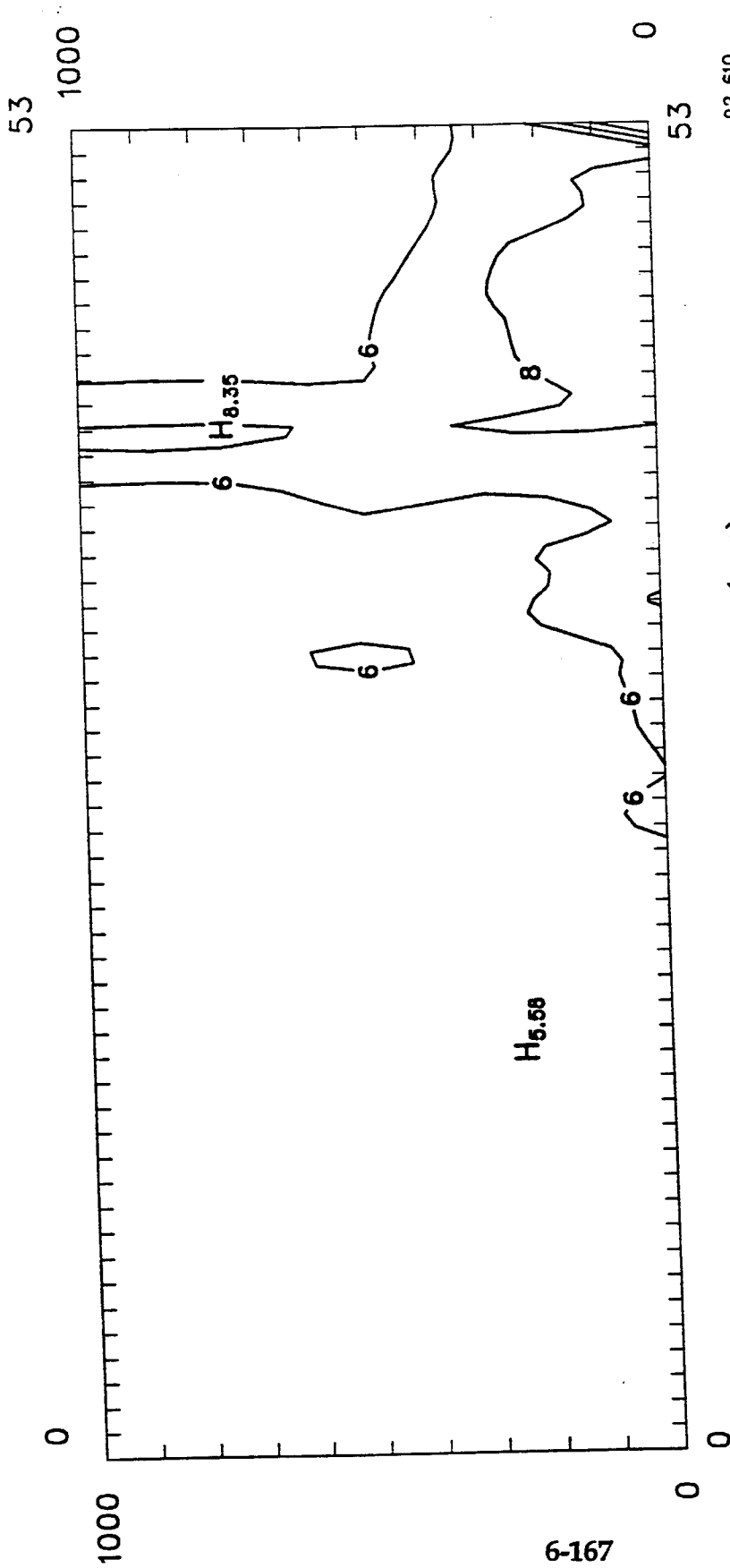


Figure 6-21f-s1. UAM-IV Vertical Ozone Isopleths Along East-West Transect for the 16-17 September, 1984 Episode -- 17 September, 1400 PST.



92 610  
1637  
dem

E-W Slice J = 15 Hour 14 (pst)

Date 9/17/84

03 140084261CG4502  
CCRT140084281CG4001

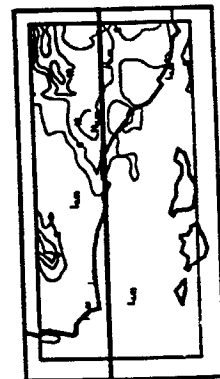
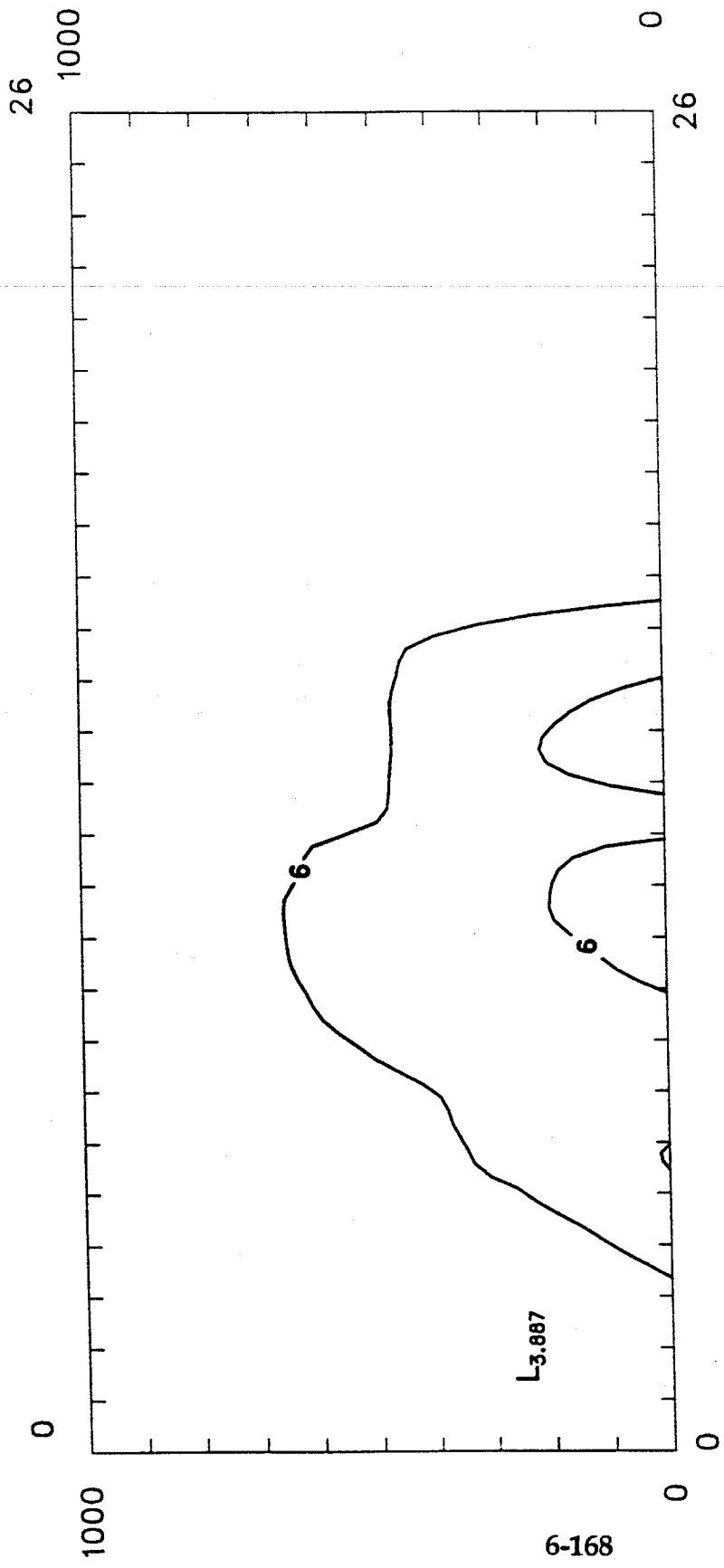


Figure 6-21f-s2. CALGRID-IV Vertical Ozone Isopleths Along East-West Transect for the 16-17 September, 1984 Episode -- 17 September, 1400 PST.



N-S Slice I = 48 Hour 14 (pst)

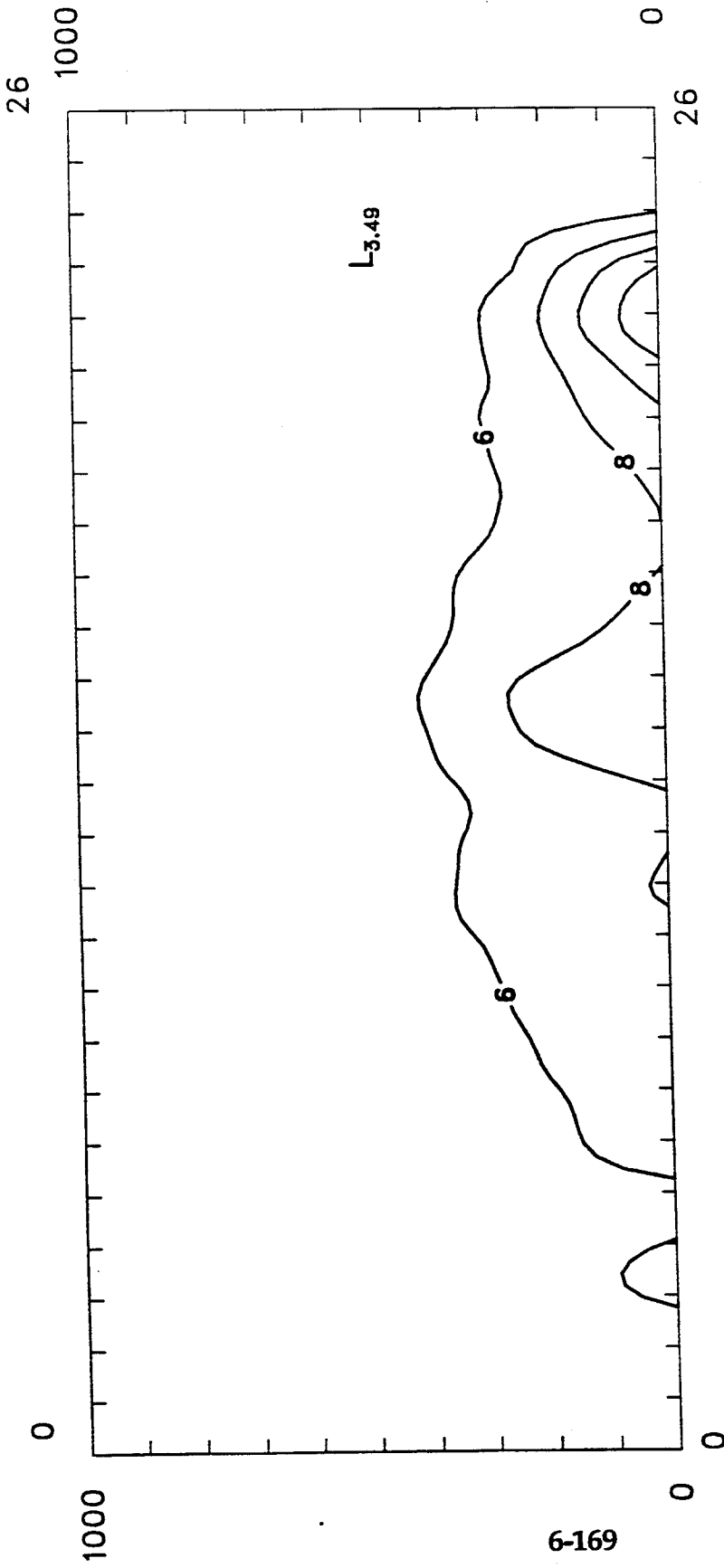
Date 9/17/84



O3 140084281AIR001  
CCHTT140084281AIR001

92 610  
2226  
dem

Figure 6-21f-s3. UAM-IV Vertical Ozone Isopleths Along North-South Transect for the 16-17 September, 1984 Episode -- 17 September, 1400 PST.



N-S Slice I = 48 Hour 14 (pst)

Date 9/17/84

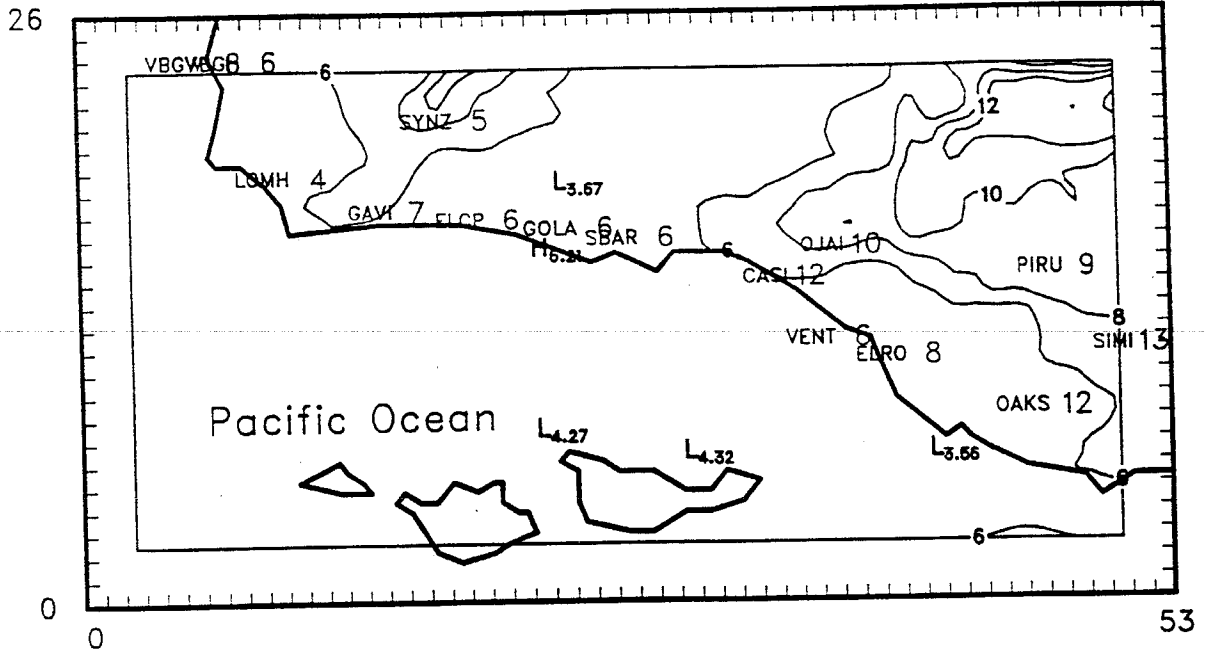
03 140084281CG4502  
 CCHT140084281CG4001

92 610  
 1628  
 dem



Figure 6-21f-s4. CALGRID-IV Vertical Ozone Isopleths Along North-South Transect for the 16-17 September, 1984 Episode -- 17 September, 1400 PST.

CALGRID-IV



UAM-IV

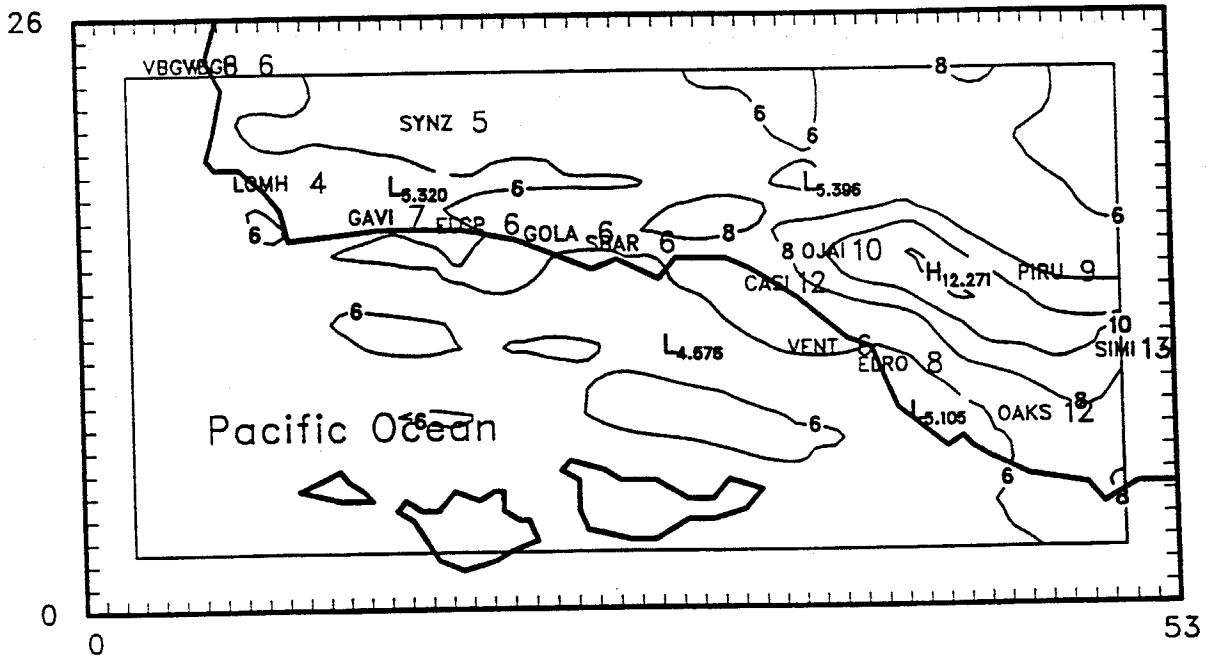


Figure 6-21g. Ground Level Ozone Isopleths of Hourly Ozone Concentrations for the 16-17 September, 1984 Episode – 17 September, 1600 PST.

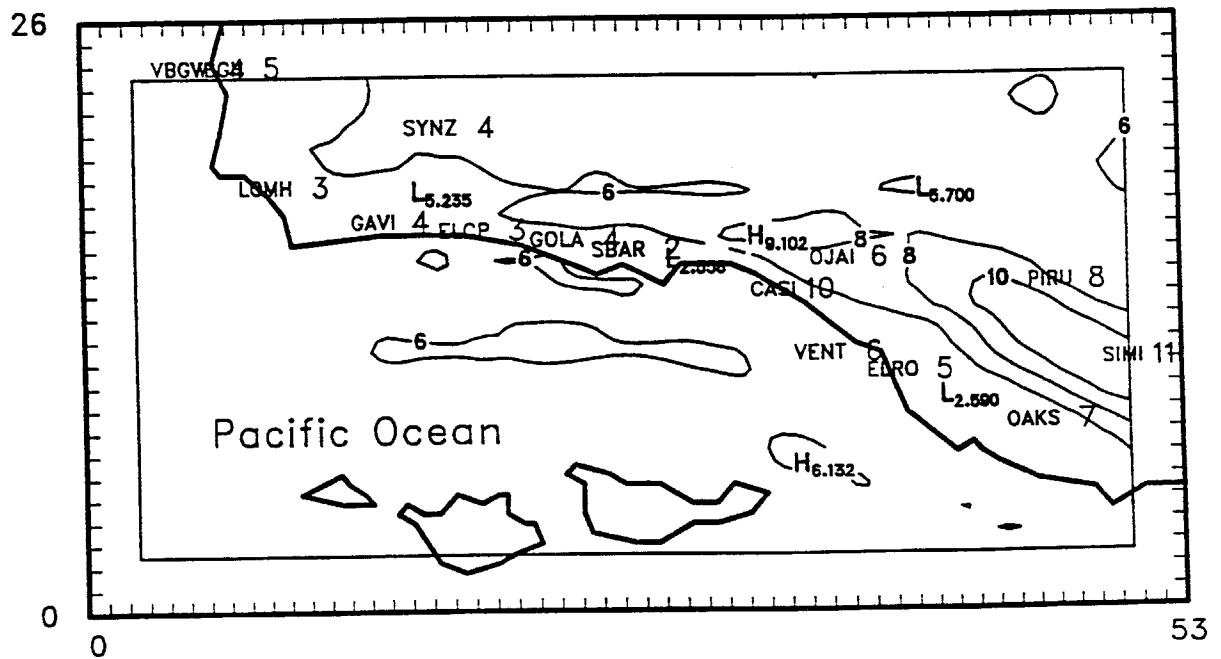
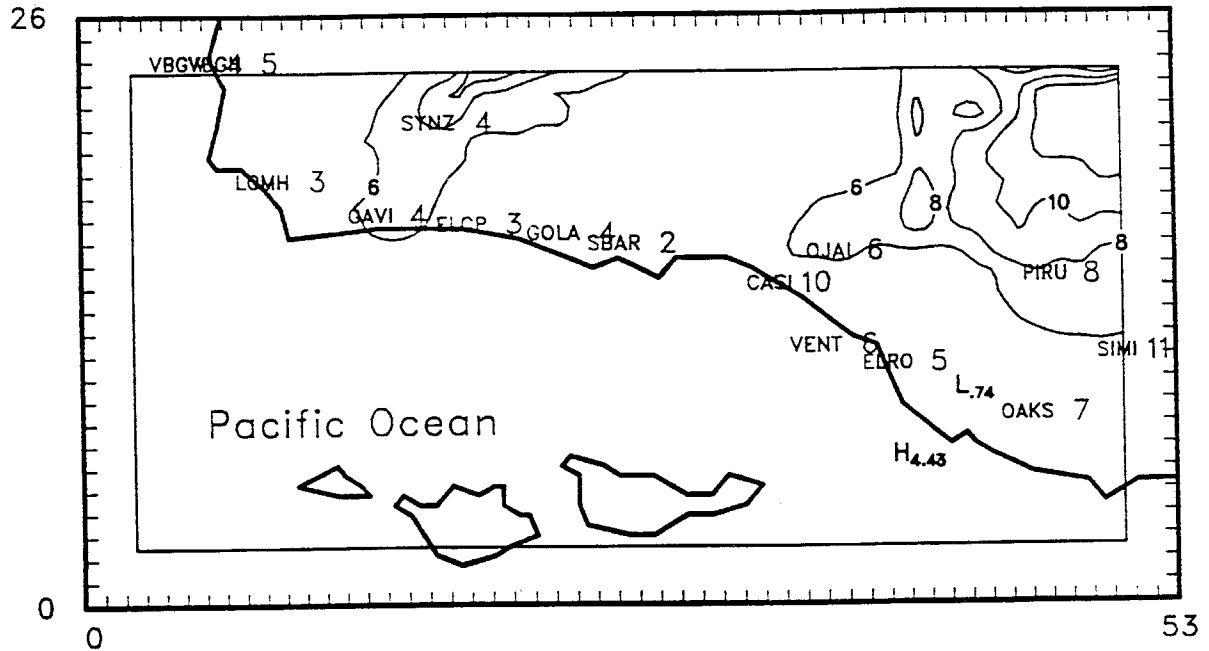
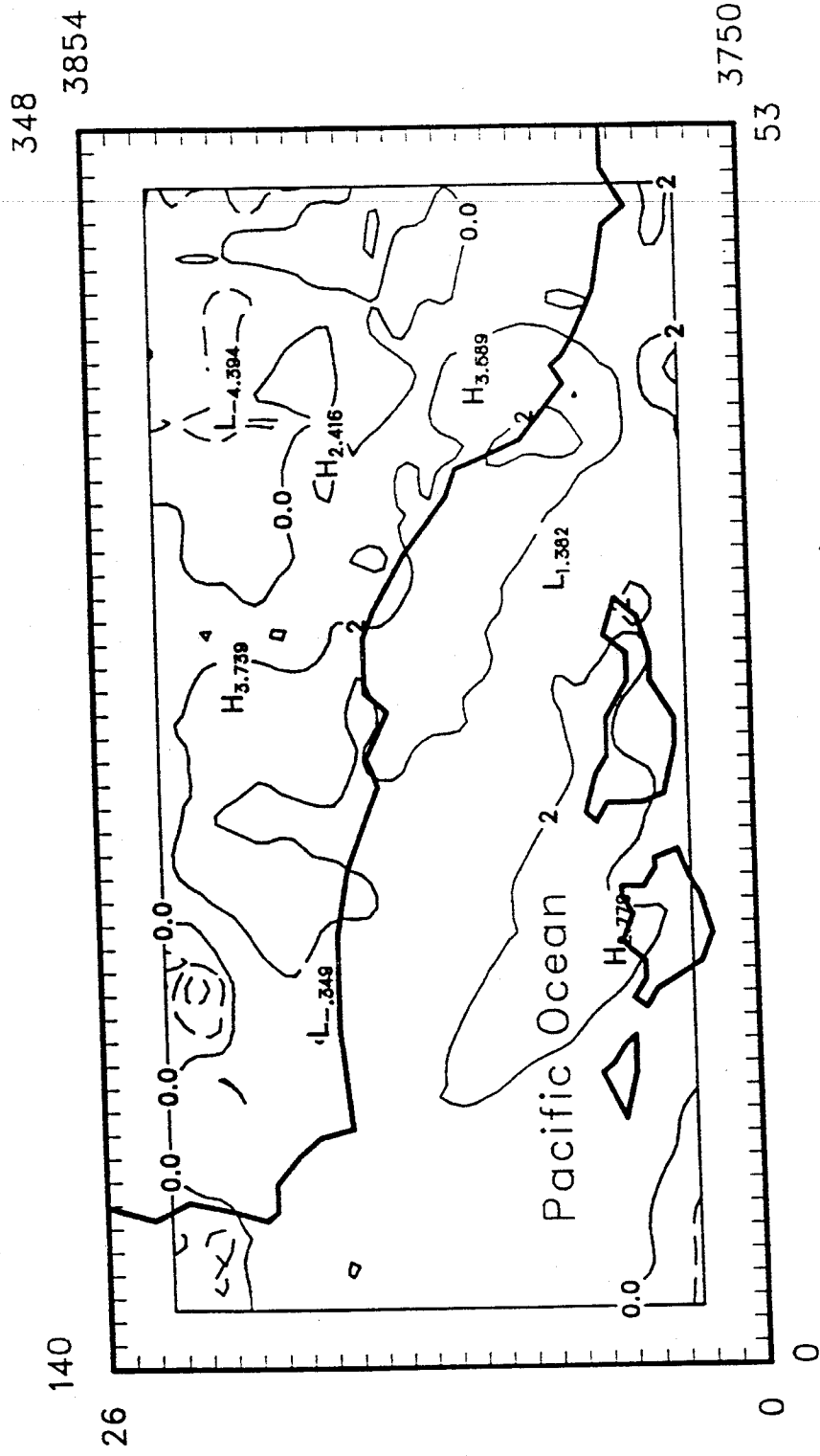


Figure 6-21h. Ground Level Ozone Isopleths of Hourly Ozone Concentrations for the 16-17 September, 1984 Episode - 17 September, 1800 PST.



Level 1 Hour 99 (pst)

Date 9/16/84

Figure 6-22a. Maximum Daily Ozone Residual Plot (UAM-IV Minus CALGRID-IV) for the 16-17 September, 1984 Episode -- 16 September, 1984.

